



HAL
open science

Development of biodegradable polymers and natural fillers-based nanocomposites for potential applications in active food packaging

Abderrahmane Nabgui

► **To cite this version:**

Abderrahmane Nabgui. Development of biodegradable polymers and natural fillers-based nanocomposites for potential applications in active food packaging. Material chemistry. Normandie Université; Université Cadi Ayyad (Marrakech, Maroc), 2022. English. NNT : 2022NORMR107 . tel-04812224

HAL Id: tel-04812224

<https://theses.hal.science/tel-04812224v1>

Submitted on 30 Nov 2024

HAL is a multi-disciplinary open access archive for the deposit and dissemination of scientific research documents, whether they are published or not. The documents may come from teaching and research institutions in France or abroad, or from public or private research centers.

L'archive ouverte pluridisciplinaire **HAL**, est destinée au dépôt et à la diffusion de documents scientifiques de niveau recherche, publiés ou non, émanant des établissements d'enseignement et de recherche français ou étrangers, des laboratoires publics ou privés.



Normandie Université

THÈSE

Pour obtenir le diplôme de doctorat

Spécialité CHIMIE

Préparée au sein de l'Université de Rouen Normandie

En cotutelle internationale avec Université Cadi Ayyad , MAROC

Amélioration des propriétés barrières et antibactériennes de polyesters par formation de matériaux composites à base de produits naturels

**Présentée et soutenue par
ABDERRAHMANE NABGUI**

**Thèse soutenue le 29/11/2022
devant le jury composé de**

M. JULIEN BRAS	MAITRE DE CONFERENCES HDR, INP (Grenoble)	Rapporteur du jury
MME KREMENA MAKASHEVA	DIRECTEUR DE RECHERCHE, UNIVERSITE TOULOUSE 3 PAUL SABATIER	Rapporteur du jury
M. ABDALLAH OUKARROUM	PROFESSEUR DES UNIVERSITES, Université Mohammed VI Polytechnique	Membre du jury
MME ELVIRA VIDOVIC	PROFESSEUR DES UNIVERSITES, UNIVERSITE DE ZAGREB	Membre du jury
M. MUSTAPHA BARAKATE	PROFESSEUR DES UNIVERSITES, Université Cadi Ayyad	Président du jury
M. PASCAL THEBAULT	MAITRE DE CONFERENCES, Université de Rouen Normandie	Directeur de thèse
M. ABDELLATIF EL MEZIANE	PROFESSEUR DES UNIVERSITES, Université Cadi Ayyad	Co-directeur de thèse
M. MOHAMMED LAHCINI	PROFESSEUR DES UNIVERSITES, Université Cadi Ayyad	Co-directeur de thèse

Thèse dirigée par PASCAL THEBAULT (Polymères, biopolymères, surfaces) et MOHAMMED LAHCINI (Laboratoire de Chimie Organométallique et Macromoléculaire -Matériaux composite) et ABDELLATIF EL MEZIANE (Laboratoire de Biotechnologie et bio-ingénierie Moléculaire)

THÈSE EN COTUTELLE

Présentée à la Faculté pour obtenir le grade de :

Docteur

CED : Sciences et Techniques :

Spécialité : Biotechnologie et science des matériaux

Development of biodegradable polymers and natural fillers-based nanocomposites for potential applications in active food packaging

Par:

Abderrahmane NABGUI

(Dernier diplôme : Master Spécialité : Biotechnologie et développement durable des agro-
ressources)

Soutenue le

devant la commission d'examen

Preface:

The research study presented in this manuscript was carried out under a co-direction doctoral thesis between the Cadi Ayyad university in Marrakesh, Morocco and the University of Rouen Normandie in Rouen, France under the financial support of CAMPUS FRANCE: PHC TOUBKAL/18/71. The experimental works was carried out from January 2018 to April 2022 under the supervision of Prof. Abdellatif El Meziane, Prof. Pascal Thébault, and Prof. Mohammed Lahcini. The work was performed at:

- Centre d'Agrobiotechnologie et de Bio-ingénierie, AgroBiotech Center, URL-CNRST-05, Faculty of Sciences and Techniques, Cadi-Ayyad University
- Equipe BRICS du laboratoire Polymères, Biopolymères, Surfaces (PBS, UMR CNRS 6270), Normandie Université
- Innovative Materials, Energy and Development Laboratory (IMED-Lab) at the Faculty of Sciences and Techniques of Marrakech, Cadi Ayyad University).

Besides the above-mentioned laboratories, parts of this work were performed at different research facilities:

- Laboratory of Chemical Engineering, Zagreb University, Zagreb, Croatia
- Center of Analysis and characterization (CAC), Cadi Ayyad University (UCA), Marrakech, Morocco
- Normandie Univ, COBRA UMR 6014, FR 3038, INSA Rouen, CNRS, IRCOF, 76821 Mont-Saint-Aignan, France.
- Normandie Univ, UNIROUEN, INSA Rouen, CNRS, PBS UMR6270, 55 rue Saint-Germain, 27000 Évreux, France
- Instituto de ciencias de los materiales de la universidad de valencia, Calle catedrático josé beltrán, 2, C.P 46980 Paterna Valencia Spain

Scientific production:

Published papers:

- **A. Nabgui**, T. El Assimi, A. El Meziane, G.A. Luinstra, M. Raihane, G. Gouhier, P. Thébault, K. Draoui, M. Lahcini, Synthesis and antibacterial behavior of bio-composite materials-based on poly(ϵ -caprolactone)/bentonite, *European Polymer Journal*. 156 (2021) 110602. <https://doi.org/10.1016/j.eurpolymj.2021.110602>.
- **A. Nabgui**, N. Follain¹, E. Vidović, J. El Haskouri, S. Marais, A. El Meziane, M. Lahcini, P. Thébault. Preparation and study of the thermal, barrier and antibacterial properties of Polylactic acid-Fluorophlogopite-silver nanoparticles nanocomposite films. (Accepted in *Progress in Organic Coating* on July 12th, 2022).

Submitted papers:

- **A. Nabgui**, A. Brik, K. Agayr, G. Gouhier, R. Beniazza, E. Vidović, J. El Haskouri, B. Labat, M. Lahcini, P. Thébault, & A. El Meziane. Long term impact of surfactants on colloidal stability and antibacterial properties of biogenic silver nanoparticle. (Submitted to *Surfaces and interfaces* on October 10th, 2021).

Oral communication:

- **EuroMagh Rouen 2020**: **A. Nabgui**, A. Brik, K. Agayr, G. Gouhier, R. Beniazza, E. Vidović, P. Lahcini, P. Thébault, and A. El Meziane. Biosynthesis of silver nanoparticles by *Rosmarinus officinalis*: Evaluation of their antibacterial activity
- **Journée de l'école doctorale normande de chimie JEDNC 2021**: **A. Nabgui**, T. El Assimi, A. El Meziane, G.A. Luinstra, M. Raihane, G. Gouhier, P. Thébault, K. Draoui, M. Lahcini, Synthesis and antibacterial behavior of bio-composite materials-based on poly(ϵ -caprolactone)/bentonite.

Acknowledgments

First and foremost, I sincerely appreciate the almighty God for His graces, strength, and sustenance from the beginning of my academic life up to this doctoral level. His benevolence has made me excel and be successful in all my academic pursuits.

I would like to express my deep and sincere gratitude to my research supervisors, **Pr. Abdellatif El Meziane**, **Pr. Pascal Thébault**, and **Pr. Mohammed Lahcini**, for giving me the opportunities they gave me, their guidance, expertise, constructive criticism, and all the advice they have provided me throughout this thesis. Their dynamism, vision, sincerity, and motivation have deeply inspired me. They taught me the methodology to carry out the research and to present the research works as clearly as possible. It was a great privilege and honor to work and study under their guidance. I am extremely grateful for what they have offered me. Beyond the scientific and professional scope, I would also like to thank them for their empathy, their understanding, and the enormous kindness they have shown and continue to show me.

I would like also to acknowledge all the jury members, **Pr. Kremena Makasheva**, **Pr. Julien Bras**, **Pr. Mustapha Barakate**, **Pr. Elvira Vidović**, and **Pr. Abdellah Oukarroum** for generously offering their time to examine this work.

I would like to thank **Pr. Géraldine Gouhier** first for hosting me in COBRA, in which many experiments were performed. And secondly, alongside **Pr. Pascal Thébault**, for all the help they provided me when I first come to France, which facilitated my stay in Rouen beyond words. Thank you **Géraldine** and **Pascal**.

I would also like to thank **Pr. Elvira Vidović** for hosting me at the Laboratory of Chemical Engineering and Technology, at the University of Zagreb, Croatia. Professor, I am forever indebted to you for your scientific guidance, your kindness, and hospitality.

All the works in this thesis are the fruit of collaboration with many people for which I am forever grateful. I would like to thank **Pr. Stéphane Marais**, and **Pr. Nadège Follain** for their contribution in the barrier properties of materials, **Pr. Béatrice Labat**, for her experiments in cytotoxicity, **Pr. Jamal El Haskouri**, for the TEM analysis. Moreover, I would like to thank **Pr. Didier Le Cerf**, **Pr. Virginie Dulong**, and **Pr. Kateryna Fatyeyeva** for their help in numerous analyses.

Finally, working at four different laboratories in three countries allowed me to be blessed with knowing many great scientists and colleagues, many of which are friends. I am grateful for your support and friendship with all my colleagues at:

- IMED-Lab: **Taha El Assimi, Oumayma Jennah, Wafae Misrar, Brik Abdelmalik, Jamal Chabbi, Omar Lakbita, Mohammed Ilsouk, Ilyasse Izanzar, Asma Sofyane, Soukaina Ajouguim, Sara Ghazi, Mohja Amou, Salima Lahbabi, Hicham, Ait Bella, Nouamane El Idrissi, El Hassan Boutriouia, Abdelghani Elmouat, Jihad Oumerri, Abir Chekrou, Manal Chaib, and Mustapha El Kadiri,**

- Centre AgroBiotech: **Meriem Ait Ouguinane, Jihane Zeghlouli, Meriem Soufiani, Soukaina Bouissil, Anouar Mouhoub, Hanane Boutaj, Salma Oulad Brahim, and Nouredine Idali.**

- PBS: **Dr. Laurent Coquet, Dr. Annick Schaumann, Pr. Julie Hardouin, Pr. Emmanuelle Dé, Hung Le, Yuzhen Lou, Ben Mlouka Amine, Clément Guillou, Charlotte Roupie, , Mathieu Madau, Brandon Robin, Salomé Sauvage, and Huu Van Le.**

- COBRA : **Sophie Mohamed, Sandra Sembo, Asmaa Bouyahya, and Issam Gaamoussi**

- University of Zagreb: **Roko Blazic, Fabio Faraguna, Marco, Antonia, and Anera.**

Finally, I would like to thank all my family, my mom, **Latifa**, and my sisters, **Kelthoum, Zineb, and Amina**, your love and support overwhelm me and for that, I am forever indebted to you. This thesis is dedicated to you.

I would like to also thank all my friends outside academia for their support, **Youssef, Younes, Anouar, Abdessamad, Asmae, Hasna, and Chaimae.**

Abstract

Bacterial food contaminations are a major challenge to the food industry due to their impact both on the health and economic sectors, causing millions of illnesses and billions of dollars in losses each year. Thus, in an attempt to mitigate and fight against these contaminations, multiple techniques have been developed, including food packaging. Indeed, traditional food packaging using fossil-based polymers is widely used as a physical barrier between the food and the external environment, limiting to some extent microbial contaminations. However, using traditional food packaging materials raises two concerns. First, they are not sufficient to limit bacterial contaminations and second, they use non-biodegradable plastics. In this thesis, we aim to develop new antibacterial nanobiocomposite materials based on biodegradable polymers for potential applications in antibacterial active food packaging.

The first nanocomposites developed are PCL-CTAB-modified bentonite using a grafting from ring opening polymerization by exploiting the hydroxyl groups of bentonite. The second nanocomposites are PLA-Fluorophlogopite-Silver nanoparticles (AgNPs) films prepared using melt extrusion, and the third and last nanocomposites are Chitosan-AgNPs films. All these nanocomposites were characterized using multiple characterization techniques with a special focus on their thermal, mechanical, barrier, and antibacterial properties. The nanocomposites showed excellent properties and exerted important antibacterial activity against both Gram-positive and Gram-negative bacteria. These results demonstrate the potential use of these nanocomposites as antibacterial food packaging materials.

Finally, the excellent potential of AgNPs as nanofillers led us to dedicate a chapter to the optimization and stability of biogenic AgNPs. AgNPs synthesis using rosemary extract as a reducing and a stabilizing agent (R-AgNPs) was optimized in terms of size and production. These R-AgNPs were characterized using multiple techniques, and their stability was monitored and enhanced using three surfactants, CTAB, SDS, and Tween 80. Moreover, these R-AgNPs showed an excellent antibacterial activity against Gram-positive and Gram-negative bacteria at concentrations that are non-cytotoxic to mammalian cells. Finally, the surfactant capping of R-AgNPs enhanced their antibacterial activity without inducing any cytotoxic effect on mammalian fibroblasts.

Résumé

Les contaminations alimentaires constituent l'un des problèmes majeurs de l'industrie alimentaire à cause des pertes énormes qu'elles posent, que ce soit sur le plan sanitaire que sur le plan économique, causant des millions de maladies et des milliards de dollars de pertes chaque année. Ainsi, afin d'atténuer et de lutter contre ces contaminations, de multiples techniques sont développées dont l'emballage alimentaire. En effet, les emballages alimentaires classiques utilisent des polymères d'origine fossile qui sont largement utilisés comme des barrières physiques entre l'aliment et le milieu extérieur. Cependant, ces matériaux soulèvent deux problèmes. Premièrement, ils ne limitent pas les contaminations bactériennes, et deuxièmement, ils sont non biodégradables. Ainsi, dans cette thèse, nous tentons de développer de nouveaux matériaux nanobiocomposites antibactériens à base de polymères biodégradables pour des applications potentielles dans les emballages alimentaires actifs antibactériens.

Les premiers matériaux développés sont des nanocomposites de PCL-Bentonite modifiée par le CTAB préparées *via* une polymérisation par ouverture de cycle en utilisant une approche « *Grafting from* » qui exploitent les groupements hydroxyles de la bentonite qui comportent comme co-initiateurs de la polymérisation. Les deuxièmes nanocomposites sont des films de PLA-Fluorophlogopite-Nanoparticules d'argent (AgNPs) préparés par une simple méthode d'extrusion à l'état fondu, et les troisièmes nanocomposites sont des films de Chitosan-AgNPs. Ces nanocomposites ont été caractérisés en utilisant plusieurs techniques et en focalisant sur leur propriétés thermiques, mécaniques, barrières et antibactériennes. Tous ces systèmes ont montré des propriétés améliorées et ont montré une activité antibactérienne importante contre les bactéries à Gram-positif et à Gram-négatif. Ces résultats montrent le potentiel important de ces matériaux pour des applications en emballage alimentaire actif.

L'excellent potentiel des AgNPs en tant que nanocharges nous a conduit à consacrer un chapitre sur l'optimisation et l'étude de la stabilité des AgNPs préparées biologiquement. A cet égard, la synthèse des AgNPs a été optimisée en termes de taille et de production en utilisant l'extrait du romarin comme agent réducteur et stabilisateur (R-AgNPs). Ces AgNPs ont également été caractérisées par plusieurs techniques et leur stabilité a été suivie et améliorée en utilisant trois tensioactifs, CTAB, SDS et Tween 80. R-AgNPs ont montré une activité antibactérienne importante à des concentrations qui ne sont pas cytotoxiques contre des fibroblastes mammaliens. Finalement, les R-AgNPs stabilisées par les tensioactifs ont montré une activité antibactérienne améliorée sans induire un effet cytotoxique.

ملخص

يعد التلوث البكتيري للغذاء مشكلة كبيرة سواء من الناحية الصحية أو الاقتصادية ، إذ يسبب هذا التلوث ملايين من الحالات المرضية وخسائر بمليارات الدولارات كل عام. وبالتالي، و في محاولة لتخفيف ومكافحة هذا التلوث ، تم تطوير تقنيات متعددة بما في ذلك تغليف المواد الغذائية. تستخدم مواد التغليف الغذائي التقليدية البوليمرات البترولية على نطاق واسع كحاجز مادي بين الطعام والبيئة الخارجية ، مما يحد إلى حد ما من التلوث الميكروبي. ومع ذلك ، فإن استخدام مواد تغليف المواد الغذائية التقليدية يثير مشكلتين أساسيتين. أولاً، الفعالية المحدودة للحد من التلوث البكتيري ، وثانياً ، استخدام مواد بلاستيكية غير قابلة للتحلل. في هذه الأطروحة ، نحاول تطوير مواد مركبات نانوية حيوية جديدة مضادة للبكتيريا تعتمد على البوليمرات القابلة للتحلل لتطبيقات محتملة كمواد تغليف المواد الغذائية المضادة للبكتيريا.

المواد الأولى التي تم تطويرها هي المركبات النانوية PCL-Bentonite والتي تم تحضيرها عن طريق بلورة فتح الحلقة باستخدام نهج "Grafting from". المركبات النانوية الثانية هي مواد PLA-Fluorophlogopite-Silver Nanoparticles (AgNPs) المحضرة بطريقة Melt extrusion ، أخيراً، المركبات النانوية الثالثة هي مواد Chitosan-AgNPs. تم تحديد خصائص هذه المركبات النانوية باستخدام عدة تقنيات مع التركيز خصوصاً على خصائصها الحرارية والميكانيكية والحاجزية والمضادة للبكتيريا. أظهرت كل هذه الأنظمة خصائص محسنة وأظهرت نشاطاً مهماً مضاداً للبكتيريا. تظهر هذه النتائج الإمكانيات الكبيرة لهذه المواد لتطبيقات محتملة في تغليف المواد الغذائية.

دفعتنا الإمكانيات الممتازة لجزيئات الفضة النانوية إلى تخصيص فصل عن تحسين إنتاجها بطريقة بيولوجية صديقة للبيئة ودراسة استقرارها. في هذا الصدد ، تم تحسين تركيب جزيئات الفضة النانوية باستخدام مستخلص إكليل الجبل (R-AgNPs). تم تحديد مميزات هذه الجزيئات باستعمال العديد من التقنيات كما تم تحسين استقرارها باستخدام ثلاثة فواعل بالسطح، CTAB و SDS و Tween 80. وقد أظهرت R-AgNPs نشاطاً كبيراً مضاداً للبكتيريا بتركيزات غير سامة ضد خلايا الثدييات الليفية. أخيراً ، أظهرت R-AgNPs المستقرة بالسطح نشاطاً مضاداً للبكتيريا محسناً دون إحداث تأثير سام للخلايا.

Content

General Introduction	1
Chapter I:	4
Bibliographic overview on antimicrobial food packaging materials based on Polycaprolactone, Polylactic acid, Chitosan, Clay, and Silver nanoparticle	4
I.1) Antibacterial food packaging nanocomposites	5
I.1.1) General context on polymeric nanocomposites	5
I.1.2) An overview of the structure, properties, and synthesis of PLA, PCL, and chitosan.....	6
I.1.3) Antimicrobial Polymers in active food packaging: Emphasis on PLA, PCL, and Chitosan-based materials	10
I.1.4) Fillers: clay MMT/BNT, Mica, and silver nanoparticles	16
I.1.5) Preparation methods of polymer nanocomposites	21
I.2) Silver nanoparticles as antibacterial nanofiller	22
I.2.1) General context	22
I.2.2) Synthesis methods of silver nanoparticles	23
I.2.3) Important Silver nanoparticles parameters	32
I.2.4) Stability of silver nanoparticles	34
I.2.5) Factors influencing plant-mediated AgNPs synthesis	35
I.2.6) Antibacterial activity of silver nanoparticles	40
I.2.7) conclusion.....	42
Chapter II :	61
Synthesis and antibacterial behavior of bio-composite materials-based on poly(ϵ -caprolactone)/bentonite	61
Chapter overview	62
II.1) Introduction.....	64
II.2) Material and methods	66
II.2.1) Materials.....	66
II.2.2) Organo-modification of bentonite	66
II.2.3) Synthesis of tetra(phenylethynyl) tin as a catalyst for the ring-opening polymerization	67
II.2.4) Synthesis of the PCL bio-composites (in-situ polymerization of ϵ -CL)	67
II.2.5) Films preparation	68

II.3)	Characterization techniques.....	68
II.3.1)	Size exclusion chromatography (SEC).....	68
II.3.2)	Suspension stability.....	69
II.3.3)	X-ray diffraction (XRD).....	69
II.3.4)	Fourier transform-infrared spectroscopy (FTIR)	69
II.3.5)	Dynamical scanning calorimetry (DSC).....	69
II.3.6)	Thermogravimetric analysis (TGA)	69
II.3.7)	Contact angle measurement	69
II.3.8)	Mechanical properties.....	69
II.3.9)	Scanning electron microscopy (SEM)	70
II.3.10)	Antimicrobial tests on PCL-g-OBnt bio-composite films	70
II.4)	Results and discussion.....	71
II.4.1)	PCL-OBnt synthesis.....	71
II.4.2)	Characterization of the prepared bio-composites (PCL-OBnt).....	73
II.4.3)	Antimicrobial tests on PCL-OBnt bio-composite films	79
II.5)	Conclusion	81
II.6)	Supporting information.....	82
Chapter III:	87
Synthesis and antibacterial behavior of bio-composite materials-based on poly(ϵ -caprolactone)/bentonite		87
Chapter overview		88
III.1)	Introduction.....	91
III.2)	Materials and Methods	94
III.2.1)	Materials.....	94
III.2.2)	PLA composites preparation	94
III.2.3)	Characterization	95
III.2.4)	Mechanical properties.....	95
III.2.5)	Barrier properties	96
III.2.6)	Antibacterial activity of PLA composites	100
III.2.7)	Statistical analysis.....	100
III.3)	Results and Discussion	101
III.3.1)	Optimization of fluorphlogopite content	101
III.3.2)	Characterization of PLA-Fluorphlogopite-AgNPs nanocomposites.....	102
III.3.3)	Mechanical properties.....	109
III.3.4)	Barrier properties of PLA composites	110

III.3.5) Antibacterial activity of Neat PLA and PLA blends	120
III.4) Conclusion	123
III.5) Supporting information	125
Chapter V:.....	137
Chitosan/Green Silver nanoparticles nanobiocomposites: an efficient dual functionality as antibacterial materials and 4-Nitroaniline reduction catalysts	137
Chapter overview	138
V.1) Introduction.....	141
V.2) Materials and Methods	144
V.2.1) Materials.....	144
V.2.2) Rosemary extract preparation	145
V.2.3) Silver nanoparticles preparation and purification.....	145
V.2.4) Silver nanoparticles characterization	145
V.2.5) Stabilization of Silver nanoparticles using surfactants.....	145
V.2.6) Assessment of silver nanoparticles antibacterial activity	146
V.2.7) Assessment of silver nanoparticles cytotoxicity.....	146
V.3) Results and discussion.....	147
V.3.1) Silver nanoparticles preparation using Rosemary extracts.....	147
V.3.2) Effect of temperature on R-AgNPs production and sizes.....	149
V.3.3) Determination of R-AgNPs size using direct measures and approximations	150
V.3.4) Silver nanoparticles-Rosemary extract interaction and characterization	153
V.3.5) Stabilization of silver nanoparticles using surfactants	154
V.3.6) Evaluation of the antibacterial activity of silver nanoparticles.....	158
V.3.7) Cytotoxicity of pristine and surfactants-capped R-AgNPs.....	161
V.4) Conclusion	162
V.5) Supporting information.....	164
V.6) Supplementary information	168
Chapter V:.....	178
Chitosan/Green Silver nanoparticles nanobiocomposites: an efficient dual functionality as antibacterial materials and 4-Nitroaniline reduction catalysts	178
Chapter overview	179
VI.1) Introduction.....	182
VI.2) Material and methods.....	184
VI.2.1) Materials.....	184
VI.2.2) Silver nanoparticles preparation	184
VI.2.3) Chitosan-AgNPs films preparation	184

VI.2.4)	Characterization of Silver nanoparticles	184
VI.2.5)	Characterization of CS/R-AgNPs films	185
VI.2.6)	Assessment of antibacterial activity of CS and CS/R-AgNPs films.....	185
VI.3)	Results and discussion.....	186
VI.3.1)	Synthesis and Characterization of silver nanoparticles.....	186
VI.3.2)	Preparation and Characterization of CS/AgNPs films.....	187
VI.3.3)	Antibacterial activity of CS and CS/R-AgNPs films.....	191
VI.3.4)	Recyclability of the CS/R-AgNPs catalyst.....	194
VI.4)	Conclusion	195

List of Figures

Figure I.1: Preparation of ϵ -Caprolactone via Baeyer-Villiger oxidation [37].	6
Figure I.2: The Coordination-Insertion mechanism using metal alkoxide species (M-OR) [39].	7
Figure I.3: Lactic acid enantiomers [45].	8
Figure I.4: Synthetic routes of high molecular weight PLA [47].	9
Figure I.5: Structure of Chitosan [55].	10
Figure I.6: Types of nanofillers based on their dimensions in the nanoscale [87].	16
Figure I.7: Crystallographic structure of 2:1 phyllosilicate [87].	17
Figure I.8: The effect of the degree of delamination on the tortuosity factor of nanocomposites (w: thickness of the stack) [96].	18
Figure I.9: Crystallographic structure of Muscovite [107].	19
Figure I.10: schematic representation of intercalation of polymer into the clay nanofiller [119].	21
Figure I.11: Wet chemical reduction of AgNO_3 to prepare AgNPs [143].	25
Figure I.12: Electrochemical synthesis of silver nanoparticles using a sacrificial silver anode in water [155].	27
Figure I.13: The general protocol for the preparation of plant-mediated metal nanoparticles [174].	30
Figure I.14: Schematic representation of the steric, electrostatic, and electrosteric stabilization of silver nanoparticles [201,202].	35
Figure I.15: illustration of the effect of temperature on the biosynthesis of AgNPs under A) sufficient Ag^+ precursors, B) insufficient Ag^+ precursors [226].	39
Figure I.16: The potential antibacterial mechanisms of AgNPs: 1) release of silver 2) AgNPs binding directly to the membrane and membrane protein, 3) Generation of ROS [232].	41
Figure II.1: Proposal of the bio-composites synthesis (PCL-g-OBnt).	67
Figure II.2: Digital pictures of the tablets prepared.	68
Figure II.3: XRD patterns of bentonite (A), bentonite organomodified (A), and prepared biocomposite (B).	72
Figure II.4: Infrared spectrum of neat PCL (a), PCL-OBnt biocomposites 1% (b), 5% (c) and 10% (d).	74
Figure II.5: Suspension in dichloromethane before and after 24 h of OBnt, PCL/OBnt (95:5 wt%) physically mixed, and bio-composite (PCL-OBnt 5%).	75
Figure II.6: TGA curves of the neat PCL and PCL-OBnt nanocomposites.	76
Figure II.7: Contact angle measurement of water drop on the prepared bio-nanocomposites (PCL-OBnt).	77
Figure II.8: Representative compressive stress-strain curves of neat PCL and PCL bio-composites.	78

Figure II.9: SEM images surfaces and cross-sections of the films prepared, the neat PCL (A, B, C) and PCL-OBnt 5% (D, E, F).	79
Figure II.10: Images of diffusion assay of PCL and its bio-composites PCL-OBnt, against <i>S. epidermidis</i> and <i>S. aureus</i>	80
Figure III.1: SEM micrographs on a cross-section of A) Pristine PLA, B) PLA-2% Fluorphlogopite blend	102
Figure III.2: TEM micrographs of A) PLA-2%Fluorphlogopite, B) PLA-1.5%AgNPs, and C) PLA-2%Fluorphlogopite-1.5%AgNPs.....	103
Figure III.3: XRD patterns of fluorphlogopite, PLA-2%Fluorphlogopite and PLA-2%Fluorhplgopite-1.5%AgNPs composites	104
Figure III.4: Water contact angle measurements of neat PLA and PLA-Fluorphlogopite-AgNPs composites	105
Figure III.5: First heating curves of DSC thermograms of neat PLA and PLA-Fluorphlogopite-Silver nanoparticles composites	107
Figure III.6: Weight loss curves and differential weight loss curves of neat PLA and PLA-Fluorphlogopite-AgNPs nanocomposites.....	108
Figure III.7: Young's modulus (MPa) and Elongation at break (%) results of neat PLA and PLA-Fluorphlogopite-AgNPs composites	109
Figure III.8: Water vapor sorption isotherms of the as-received fillers and the neat PLA.....	111
Figure III.9: Water vapor sorption isotherms of the neat PLA and the composite films	112
Figure III.10: Water vapor diffusion coefficients D_1 (a) and D_2 (b) for the neat PLA and the composite films	114
Figure III.11: A) Experimental reduced water flux ($J \cdot L$) and B) normalized water flux (J/J_{st}) as a function of the reduced time (t/L^2) for the neat PLA and the composite films.....	117
Figure III.12. Permeability and diffusion coefficients for the neat PLA film and the composite films. The values are calculated with a standard deviation of about 30% due to the very low obtained values.....	120
Figure 13: Percentages of inhibition of growth on the surface of PLA-Fluorphlogopite-AgNPs composites against <i>S. aureus</i> , <i>E. faecalis</i> , and, <i>E. coli</i> compared to neat PLA	122
Figure III.SI-1: Weight loss curves and differential weight loss curves of neat PLA and PLA-Fluorphlogopite (2, 5, and 10%)	127
Figure III.SI-2: Weight loss curves of melt-extruded PLA and PLA-2% Fluorphlogopite films prepared by the hot press or solvent casting method.....	128
Figure III.SI-3: Results of disc diffusion test on <i>E.coli</i> of PLA and PLA Fluorphlogopite-AgNPs composites	129
Figure III.SI-4: Results of disc diffusion test on <i>S.aureus</i> of PLA and PLA Fluorphlogopite-AgNPs composites	129
Figure IV.1: Schematic representation outlining the experimental setup used in this study	148
Figure IV.2: UV-Vis Extinction spectra of biosynthesized silver nanoparticles R-AgNPs and simulated 35 nm AgNPs A) UV-vis spectra of biosynthesized silver nanoparticles at different temperatures	

depicting blue shift in λ_{max} as the temperature is increased and B) UV-Vis spectrum of R-AgNPs prepared at 80°C and theoretical extinction curve calculated using the Mie Theory of AgNPs of 35 nm	149
Figure IV.3: A) TEM Image of R-AgNPs and B) The size distribution (nm) of R-AgNPs prepared at 80°C determined using TEM	151
Figure IV.4: XRD spectrum of biosynthesized silver nanoparticles at 80°C for 15min	152
Figure IV.5: FTIR spectra of Rosemary leaf Extract and Biosynthesized silver nanoparticles at 80°C for 15 min.....	154
Figure IV.6: The absorbance difference at λ_{max} (%) of non-stabilized and surfactant stabilized silver nanoparticles in function of days. A: SDS stabilized R-AgNPs, B: Tween 80 stabilized R-AgNPs, and C: CTAB stabilized R-AgNPs. The non-stabilized group is depicted in all figures as control (Black line) .	155
Figure IV.7: UV-Vis spectra of A: pristine R-AgNPs (Control), B: 3 μ M CTAB R-AgNPs, C: 7 μ M SDS R-AgNPs and, D: 5 μ M Tween 80 R-AgNPs over time.....	157
Figure IV.8: The effect of surfactant capping on the antibacterial activity of R-AgNPs against <i>E.coli</i> (dark grey) and <i>S.aureus</i> (light grey). C-AgNPs: CTAB-capped R-AgNPs, S-AgNPs: SDS-capped R-AgNPs, and T-AgNPs: Tween 80- capped R-AgNPs.....	160
Figure IV.9: The effect of surfactant capping on the cytotoxic of AgNPs in contact with L929 fibroblasts for 24 hours. The horizontal red line corresponds to the threshold of cell viability set at 70%. Results are presented as mean \pm SD. * correspond to p <0.05 compared to cytotoxicity positive control.	162
Figure IV.SI-1 : a) Rosemary leaves extract, b) 2 mM Silver nitrate , c-h) R-AgNPs prepared at 80°C at different reaction time c: 0.5 min, d: 1 min, e: 3 min, f: 5 min, g: 7 min, h: 9 min.	164
Figure IV.SI-2: UV-vis spectra of biosynthesized silver nanoparticles at, A: 25°C, B: 40°C, C: 60°C and D: 80°C.	164
Figure IV.SI-3: UV-Vis spectra of R-AgNPs prepared at 80°C for different times.	165
Figure IV.SI-4: Theoretical calculation of absorption spectrum of spherical AgNPs of theoretical size of 35 nm using the Mie theory.....	165
Figure IV.SI-5: Thermogravimetric analysis (TGA) profile of R-AgNPs prepared at 80°C.....	166
Figure IV.SI-6: XRD Spectra of biosynthesized silver nanoparticles at 80°C for 15min before (R-AgNPs) and after surfactants capping	166
Figure IV.SI-7: Williamson-Hall plot of A) Pristine R-AgNPs, B: 7 μ M CTAB R-AgNPs, C: 7 μ M SDS R-AgNPs and, D: 7 μ M Tween 80 R-AgNPs	167
Figure IV.SI-8: Optical images of L929 cells at magnification X20. A) Cells treated with pristine R-AgNPs and, B) cells treated with 7 μ M CTAB-AgNPs. Scale bar: 50 μ m.....	168
Figure IV.S1: UV-Vis spectra of synthesized AgNPs at different temperatures and times using A: Rosemary extract and B: Thyme extract	168
Figure IV.S2: Size distribution by volume measured using DLS of A: R-AgNPs prepared at 80°C, B: R-AgNPs prepared at 60°C, C: T-AgNPs prepared at 80°C, and D: T-AgNPs prepared at 60°C.....	169
Figure IV.S3: The effect of CTAB, SDS, and Tween 80 on the stability of R-AgNPs after 24 h at A: 0.1 mM and B: 1 mM.....	170
Figure V.1: UV-Vis Spectrum of Rosemary extract mediated R-AgNPs prepared at 80°C.	187

Figure V.2: TEM result of R-AgNPs prepared at 80°C.....	187
Figure V.3: Protocol of the preparation of CS and CS/AgNPs nanocomposites at different AgNPs loadings.	188
Figure V.4: FTIR spectra of native CS and CS/3% R-AgNPs films.	189
Figure V.5: TGA curves of native CS and CS/R-AgNPs films.....	190
Figure V.6: TEM images of A) Neat CS and B) CS/1.5%R-AgNPs nanocomposites.....	191
Figure V.7: UV-Vis result for the reduction of 4-NA to 4-PD: A) Without catalysts, B) Free 3 μ l of 2.5% R-AgNPs as catalysts, C) CS/3% R-AgNPs film as catalysts, D) The elimination of the catalyst after 7 min.....	193
Figure V.8: The plot of $\ln(A_t/A_0)$ vs time for 4-NA reduction using CS nanocomposites with different R-AgNPs loadings.....	194
Figure V.9: The recyclability of CS/3% R-AgNPs film for the 4-NA reduction.....	195

List of Tables

Table I.1: Examples of antimicrobial food packaging based on PCL, PLA, and Chitosan.....	13
Table I.2: Advantages and drawbacks of silver nanoparticles preparation techniques.....	26
Table II.1: Molecular mass values, DSC results, and contact angle results of neat PCL and PCL-OBnt nanocomposites.	73
Table II.2: Growth of <i>S. epidermidis</i> and <i>S. aureus</i> in the presence of PCL and bio-composites films.	80
Table II.1SI: Texture and cation exchange capacity of bentonite	82
Table II.2SI : Chemical composition.....	82
Table III.1: DSC data of neat PLA and PLA-Fluorophlogopite-Silver nanoparticles composites.....	107
Table III.2: $T_{5\%}$, $T_{50\%}$, and T_{Onset} result of PLA and PLA-Fluorophlogopite composites.	108
Table III.3: Parameters of the Park model for the neat PLA film and the composite films.....	113
Table III.4: Water permeation parameters of the neat PLA film and the composite films.....	118
Table III.SI-1: Comparative table of works on binary of PLA/2D particles composites and antibacterial tertiary PLA/2D/metallic nanoparticles composites.	125
Table III.SI-2: $T_{5\%}$, $T_{50\%}$, and T_{Onset} result of PLA and PLA-Fluorophlogopite composites	128
Table IV.1: The size of R-AgNPs prepared at 80°C for 15 min determined using different techniques.	150
Table IV.2: MICs and MBCs results of biosynthesized silver nanoparticles at 80°C for 15 min (size using TEM = 31nm) and commercial nanoparticles (size = 50-60nm).....	159
Table IV.SI-1: Crystallite size (D), Microstrain (ϵ) obtained from Williamson-Hall plot, and Lattice constant (a) of Pristine and capped R-AgNPs.....	167
Table IV.S1: The approximative hydrodynamic size obtained using DLS of AgNPs prepared using rosemary extract (R-AgNPs) and thyme extract (T-AgNPs) at different temperatures	169
Table V.1: The inhibition percentage of <i>E. coli</i> (Light grey) and <i>S. aureus</i> (Dark grey) adhesion on CS/R-AgNPs nanocomposites compared to native CS films (n=3).	192

General Introduction

General introduction

Bacterial food contaminations are one of the main problems facing the food industry due to the economical and human health risks it poses. Health risk-wise, foodborne pathogens are responsible for an approximation of 600 million illnesses annually with about 420.000 death casualties according to the World Health Organization (WHO) [1]. The economical loss of such illnesses amounts to about 152 billion dollars in the US alone each year [1]. Moreover, the food loss due to spoilage is estimated to be around 1.3 billion tons each year, attributed mainly to microbial contamination [2]. Techniques to prevent food spoilage due to microbial contamination are numerous including freezing, thermal processing, refrigeration, and the use of additives [3]. However, the use of food packaging is still essential to extend the shelf-life of food by acting as a barrier between the food and the external environment, offering thus, protection against external factors such as dust, gases, and moisture [4].

Traditional food packaging materials are usually petroleum-based plastics such as polyethylene (PE), polyamide (PA), and polystyrene (PS), although with excellent mechanical and barrier properties, are extracted from non-renewable sources and are not biodegradable, posing thus, an environmental problem [5]. Moreover, these traditional food packaging materials are not sufficient to provide active protection against foodborne microorganisms [6]. Therefore, it is necessary to develop new alternatives. Indeed, according to the European Union Guidance to the Commission Regulation No 450/2009, active food packaging is defined as packaging that provides functions beyond the inert barrier protection against the external environment [7]. This includes antimicrobial packaging which is a form of active food packaging where the packaging reduces, inhibits, or delays the growth of microorganisms either on the packaged food or the packaging material itself [8].

The need to use ecofriendly antimicrobial food packaging materials is, therefore, a necessity in the pursuit of sustainable development with ecological, economical, and health benefits. In that regard, polymers with inherent antimicrobial activity such as chitosan could be used [9], however, a more common approach is the incorporation of antibacterial agents directly into the packaging material. Antibacterial agents such as organic acids [10], enzymes [11], plant extracts (e.g., essential oils) [12], and metal nanoparticles [13] were used as additives to provide antibacterial activity to polymers for food packaging purposes. Among the additives used in antimicrobial packaging, silver nanoparticles (AgNPs) are considered promising candidates due

to their excellent antibacterial activity against a wide range of foodborne pathogens including *Escherichia coli*, *Pseudomonas aeruginosa*, *Staphylococcus aureus* [14], *Listeria monocytogenes*, and *Salmonella spp.* [15]. Moreover, AgNPs have a low effect on the organoleptic properties of food compared to plant extracts for instance (e.g., essential oils) [16]. Moreover, the migration of silver nanoparticles from the polymer into the food is usually found to be within the authorized legislative limit (0.01 mg/Kg of food) by the commission regulation (EC) No. 450/2009 for “non-authorized substances” [17].

In addition to the antimicrobial activity, an active food packaging has to have good mechanical and barrier properties to oxygen and moisture [3]. Contrary to conventional food packaging, these properties are lacking in most biodegradable polymers such as Poly-caprolactone (PCL), and polysaccharides such as Chitosan (Cs) and therefore, need to be improved. In that regard, multiple approaches are used such as copolymerization [18], and the preparation of microcomposites or nanocomposites through the incorporation of micro or nanofillers such as nanoclay [19,20].

The preparation of nanocomposites remains the preferred choice as they offer a better improvement in the physical properties of polymers using a lower amount of fillers compared to microcomposites [21]. Moreover, they allow better control over the final properties of materials than copolymerization.

In this context, this work is divided into five chapters that explore the preparation of nanocomposites based on different biodegradable polymers and different natural nanofillers in the pursuit of the elaboration of antimicrobial food packaging materials.

The first chapter is a literature overview divided into two parts. The first part deals with polymeric nanocomposites with a special focus on nanocomposites based on PCL, PLA, and Chitosan. We discussed their preparation techniques as well as their potential use in antibacterial food packaging. Afterward, different nanofillers are discussed while focusing on their role in the enhancement of biodegradable polymers' physical properties (Bentonite and Fluorophlogopite) and/or providing an antibacterial activity to the end nanocomposites (Silver nanoparticles). The second part is dedicated to silver nanoparticles, particularly, i) on their preparation techniques; especially via an eco-friendly biological pathway, ii) on the relationship between their properties (Size, charge, and stability) and their antibacterial activity, and iii) on their antibacterial mechanism.

The second chapter deals with the preparation of PCL/Organo-modified Bentonite (OBnt) nanocomposites through a *Grafting from* ring-opening polymerization approach under solvent-free conditions. Bentonite was chosen due to its lamellar structure and its high surface area susceptible to enhancing the physical properties of PCL. The mechanical and thermal properties of nanocomposites were assessed. Finally, due to the CTAB organo-modification, we studied the antibacterial activity by the diffusion test and in solution against *Staphylococcus aureus* and *Staphylococcus epidermidis*.

The third chapter is dedicated to the preparation of PLA/Fluorophlogopite/AgNPs using melt extrusion. We used Fluorophlogopite to enhance PLA physical properties while AgNPs were used to provide the antibacterial activity to the nanocomposites. The thermal, mechanical, and barrier properties of the nanocomposites were assessed and compared to neat PLA. Finally, the inhibition of bacterial adhesion was tested against *E. coli*, *E. faecalis*, and *S. aureus*.

A fourth chapter is dedicated to the optimization of AgNPs synthesis *via* a simple green biological pathway using rosemary leaves extract as a reducing and capping agent. AgNPs were characterized using multiple techniques and their properties were determined (Size, shape, and charge). We assessed their stability over 6 months and we studied the potential of three surfactants (CTAB, SDS, and Tween 80) in the enhancement of the long-term stability of AgNPs. Finally, we evaluated the antibacterial activity of R-AgNPs and surfactant-capped-AgNPs and we determined their cytotoxicity.

The fifth chapter is concerned with the preparation of Chitosan/AgNPs nanobiocomposites using the optimized AgNPs discussed in the previous chapter. Chitosan was chosen due to its inherent antibacterial activity and polysaccharidic nature. The antibacterial activity of CS/AgNPs nanobiocomposites was assessed against *E. coli* and *S. aureus*. Finally, nitroarenes are common water pollutants, their reduction to non-toxic aminoarenes is usually performed via a catalytic pathway using metal nanoparticles. In that regard, we tested CS/AgNPs nanobiocomposites as heterogeneous catalysts for the catalysis of 4-nitroaniline to p-Phenylenediamine. The antibacterial activity combined with the hydrogenation catalytic activity could be exploited in water treatment applications.

Chapter I:

Bibliographic overview on antimicrobial food packaging materials based on Polycaprolactone, Poly-lactic acid, Chitosan, Clay, and Silver nanoparticle

I.1) Antibacterial food packaging nanocomposites

I.1.1) General context on polymeric nanocomposites

Polymers are widely used as materials owing to their lightweight, flexibility, and simple manufacturing process [22,23]. However, they are rarely used in their native form as they have inherent limitations such as low mechanical properties and thermal stability [24]. To bypass these limitations, multiple methods are used to improve these properties such as copolymerization [25], preparation of microcomposites [26], and preparation of nanocomposites [27].

Nanocomposites can be defined as materials composed of multiple phases, in which at least one of them is on a nanometric scale [28]. A filler, at a nanometric size, is incorporated as a reinforcing material into a matrix phase, a polymer, for example, to design Polymer Matrix Nanocomposites (PMCs) [29]. Compared to the other methods, the preparation of nanocomposites is more advantageous. Indeed, compared to microcomposites, nanocomposites could achieve the desired properties at lower filler loadings due to the high surface area of nanofillers [21] while in the case of copolymerization, the preparation is relatively more complicated than that of nanocomposites [30].

Nanofillers used for the preparation of nanocomposites can be classified into three types according to their dimensions: one-dimensional (nanotubes), two-dimensional (clay layers), or zero-dimensional nanofillers (spherical nanoparticles) [31]. The introduction of these nanofillers into polymers results in an enhancement of polymer properties such as mechanical, ionic, and chemical properties [29] or the acquisition of new properties such as antimicrobial activity [32]. This requires a good dispersion and distribution of the filler into the polymer matrix because the agglomeration of nanofillers leads to low improvements or even to the deterioration of materials properties [31,33,34].

Here, we will focus on PLA, PCL, and chitosan nanocomposites as examples of both biodegradable polyesters and polysaccharides. The first section presents an overview of the structure and properties of pristine PLA, PCL, and chitosan, their preparation methods, and a special emphasis on their use in antimicrobial food packaging. The reinforcing agents of nanocomposites will be discussed in the second section of this chapter, with a special focus on the fillers that are used in the research works of this thesis: Mica, Clay, and silver nanoparticles.

Finally, the polymer matrix nanocomposites preparation methods will be presented with a comparison of their advantages and drawbacks.

I.1.2) An overview of the structure, properties, and synthesis of PLA, PCL, and chitosan

I.1.2.1) Polycaprolactone (PCL)

Polycaprolactone (PCL) is a commonly used biodegradable semicrystalline aliphatic polyester with physical, thermal, and mechanical properties proportional to its molecular weight (ranging from 530 to 630.000 g.mol⁻¹). The main advantages of this polymer are, (i) its miscibility with other polymers such as polycarbonates, (ii) its good solubility in common organic solvents such as chloroform and dichloromethane, (iii) its low melting point (58-65°C), and (iv) its blend compatibility with other polymers such as PLA and Polymethylmethacrylate (PMMA), enabling it to have many applications in packaging, medical implants, and drug delivery [35,36].

PCL is usually synthesized by the polymerization of caprolactone (ϵ -CL), a petroleum-based molecule that is usually prepared using the Baeyer-Villiger oxidation of cyclohexanone (Fig. I.1) [37].

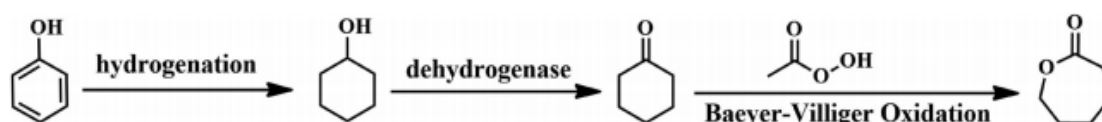


Figure I.1: Preparation of ϵ -Caprolactone via Baeyer-Villiger oxidation [37].

PCL can be synthesized using two approaches, either by polycondensation or ring-opening polymerization. The polycondensation of 6-hydroxyhexanoic acid produces PCL with low molecular weight and broad dispersity [38], whereas high molecular weight PCL can be produced using ROP of ϵ -CL. ROP can be anionic, cationic, or by coordination-insertion in which metals with empty p, d, or f orbitals can be used as coordination catalysts.

The mechanism of the coordination-insertion method is depicted in Fig I.2. The monomer is coordinated to the metal catalyst through the exocyclic oxygen forming an alkoxide bond which makes the carbonyl group of caprolactone susceptible to nucleophilic attacks (pseudo-anionic ROP). This leads to the opening of the caprolactone ring and the growth of the PCL chain following the same mechanism. This method limits side reactions, which occur in the anionic ROP. The coordination-insertion ROP used multiple metal catalysts such as Sn, Al, and Ti.

However, tin(II)2-ethylhexanoate and tin(II) octanoate remain the most commonly used catalyst for both industrial and academic purposes due to their high performance [37,39].

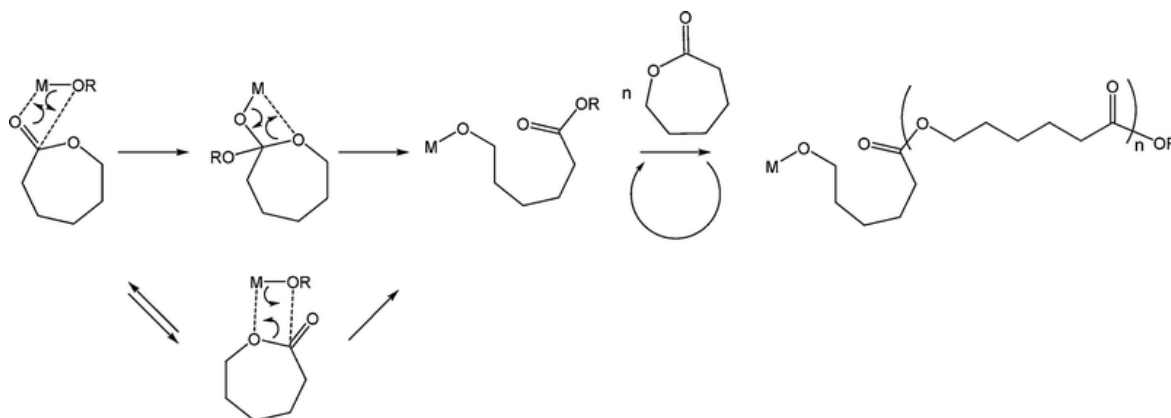


Figure I.2: The Coordination-Insertion mechanism using metal alkoxide species (M-OR) [39].

I.1.2.2) Polylactic acid (PLA)

Poly(lactic acid) is a biodegradable polyester, which has gained a lot of attention in the last two decades. Compared to other aliphatic polyesters, PLA has high mechanical properties, good biocompatibility, and easy processability [40]. In fact, its properties are comparable to that of petrochemical polymers such as polyethylene (PE), polypropylene (PP), and polystyrene (PS), which are the most used polymers for packaging [41]. Indeed, PLA shows higher strength and toughness and lower water vapor and methane permeability than PS [41], but it has a slow degradation rate and lacks reactive side-chain groups [42]. These drawbacks limit its use in some specific applications.

PLA is prepared through the polymerization of lactic acid (LA), which is produced either by fermentation or by the chemical hydrolysis of lactonitrile. The microbial fermentation approach is more advantageous as it is eco-friendly and generates optically pure LA, either L-LA or D-LA, whereas the chemical hydrolysis produces a racemic mixture of DL-LA [43]. Moreover, the LA might be produced by bacterial fermentation of simple sugar such as glucose, but for economical purposes, cheaper alternatives such as sugarcane, corn, and cassava are used [44].

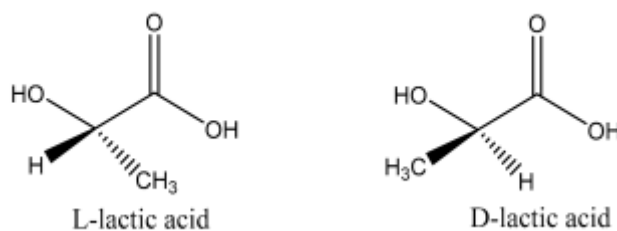


Figure I.3: Lactic acid enantiomers [45].

As mentioned above, lactic acid has a chiral carbon, thus it exists under two enantiomers form, L -LA and D -LA (Fig. I.3). Their polymerization produces PLLA and PDLA, respectively while the polymerization of their racemic mixture produces “PDLLA” which has different properties [46]. Recently, the stereocomplex PLA has attracted increasing attention due to its thermal stability [43]. Indeed, PDLLA shows a higher melting point (50°C) than the T_m of the homopolymers, and a more stable crystal structure [43]. However, it generally has lower mechanical properties than the PLLA homopolymer [30].

PLA can be synthesized through the condensation of lactic acid (Fig. I.4). However, this approach produces low molecular weight PLA with poor mechanical properties (Fig. I.4A). Alternatively, industrialized PLA is prepared using the ring-opening polymerization of lactide (Fig. I.4B). Lactide itself is prepared by the unzipping depolymerization through a back-biting mechanism involving OH terminals of Oligo-LA or low molecular weight PLA. This reaction is catalyzed by metal compounds of Sn, Zn, Al, *etc* [47,48].

Another technique was reported in 1994 by Mitsui Toatsu Chemicals to produce high molecular weight PLA *via* the azeotropic dehydrative condensation of lactide using metal oxides and metal salts of groups II, III, IV, and V as catalysts (Fig. I.4C). The reaction occurs under reduced pressure in refluxing, high boiling conditions using an aprotic solvent [49].

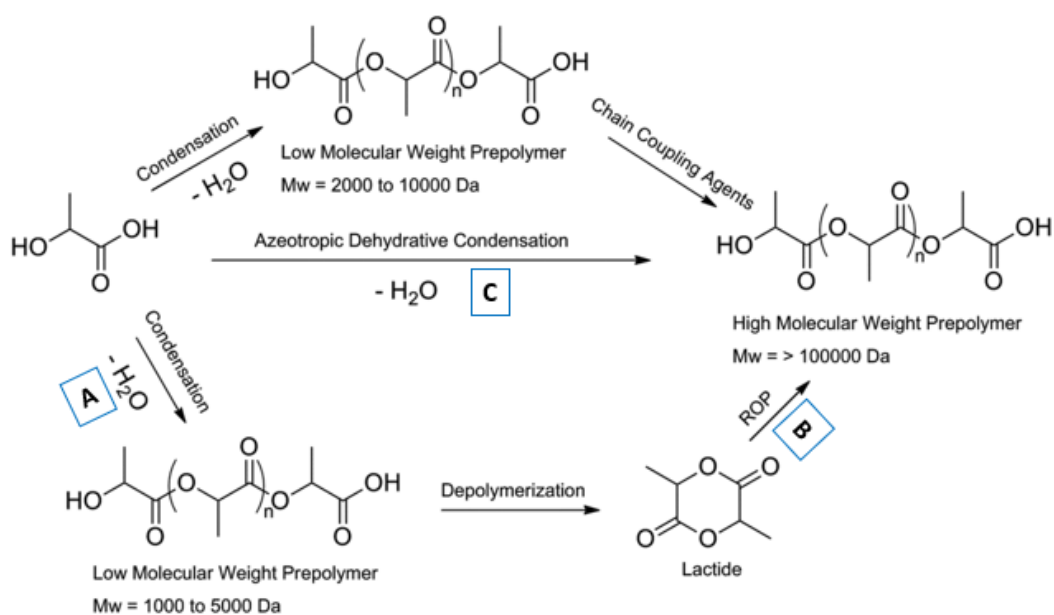


Figure I.4: Synthetic routes of high molecular weight PLA [47].

I.1.2.3) Chitosan

Chitosan is one of the most used polysaccharides as biomaterials. It is widely used in various biomedical and pharmaceutical applications such as tissue engineering, drug delivery, and wound-dressing [50]. It is also used in other fields such as food packaging [25]. The broad applications of chitosan are due to its biocompatibility, biodegradability, and non-toxic character [51]. Furthermore, it exhibits antimicrobial, antifungal, and mucoadhesion properties that are attributed to its unique cationic character, which is due to the presence of primary amino groups [52,53].

Chitosan cannot be extracted directly from natural resources and it is prepared through the deacetylation of chitin, which is the second most abundant polysaccharide in the world. The deacetylation of N-acetyl glucosamine chitin unit is generally carried out by hydrolysis at high temperatures under alkali conditions. As this reaction is incomplete, chitosan is defined by its degree of deacetylation, on which many chitosan properties are dependent such as solubility or antibacterial activity [51,54,55]. Accordingly, chitosan is composed of β -1,4-linked 2-amino-

2-deoxy- β -d-glucose or deacetylated d-glucosamine and N-acetyl-d-glucosamine repeating units (Fig. I.5)

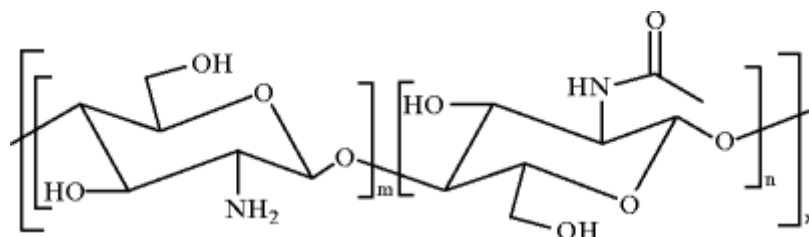


Figure I.5: Structure of Chitosan [55].

The PCL, PLA, and chitosan properties, especially their biodegradability and biocompatibility, make them great candidates for active food packaging, particularly after the enhancement of their limitations. In the next section, the potential use of these polymers in antimicrobial food packaging is discussed.

I.1.3) Antimicrobial Polymers in active food packaging: Emphasis on PLA, PCL, and Chitosan-based materials

I.1.3.1) General context

Food spoilage constitutes a major concern in the food industry due to its impact on human health as well as its economic burden. In fact, foodborne pathogens such as *Bacillus cereus*, *Staphylococcus*, *E. coli*, and *Listeria monocytogenes* cause about 600 million illnesses each year [1] costing about 152 billion dollars in the US alone. Moreover, around 1.3 billion tons of food are wasted every year [2]. In that regard, conventional food packaging has been used to isolate food from the external environment in order to protect it from spoilage, thus preserving its constituents and quality, and extending its shelf life [56]. The requirements for a good traditional food packaging material include good mechanical property, flexibility, and barrier properties to oxygen and moisture [3]. Additionally, active food packaging materials can provide additional features such as oxygen and ethylene scavenging, flavor emission, and antimicrobial activities [57].

Indeed, antimicrobial food packaging is a promising solution to actively preserve food from spoilage and limit its contamination by foodborne pathogens. In that regard, multiple antimicrobial active food packaging materials are developed, either by using polymers with inherent antimicrobial activity such as chitosan or by adding antimicrobial agents into the packaging material such as natural extracts, lysozymes, or silver nanoparticles [58,59].

I.1.3.2) PCL as antimicrobial food packaging material

PCL is mostly used in medical and pharmaceutical packaging due to its high price. Indeed, for food packaging applications, PCL is mostly blended with other polymers such as PLA [60], Polyethylene [61], and starch [62].

PCL does not have any inherent antibacterial activity, thus, developing antimicrobial active food packaging based on PCL requires formulations with other antimicrobial agents or polymers. For that purpose, Wang *et al.*, (2019) [63] developed PCL/Chitosan films loaded with grapefruit seed extract (GFSE) using extrusion and the antibacterial activity against *E. coli* was assessed compared to polyethylene (PE) as classical packaging material. Although a bacterial growth was observed in all tested films, compared to PE films, PCL/Cs films have shown a slower bacterial growth rate after 7 days ($7.77 \log_{10}$ CFU/g Vs $7.4 \log_{10}$ CFU/g), while the addition of 2.5 mL of GFSE per 1 g of Cs slowed *E. coli* growth even more ($5.04 \log_{10}$ CFU/g). In another work, PCL/PLA films were loaded with cinnamaldehyde at different concentrations (0, 3, and 9 wt%) (CNMA) [64] and were tested as packaging materials for button mushrooms. Compared to Low-density PE (LDPE), PCL/PLA/9%CNMA significantly slowed down the total psychotropic bacteria growth.

I.1.3.3) PLA as antimicrobial food packaging material

As discussed above, PLA presents several advantages that are a must for food packaging applications such as biocompatibility, biodegradability, and processability. However, neat PLA does not exhibit any antibacterial activity. Therefore, the design of PLA-based antibacterial active packaging requires the development of PLA-based formulations with antibacterial compounds. Jin and Gurtler (2011) [65] have used allyl isothiocyanate (AIT) as an additive to provide an antibacterial activity to PLA. The resulting PLA-AIT material was used to coat the inside of glass jars that were used for liquid egg white containers. They reported an effective growth inhibition of three strains of *Salmonella* (10^3 to 10^5 CFU. mL⁻¹) in liquid egg albumin samples with PLA containing only 500µl of AIT. However, as the use of essential oils (*i.e.*, AIT) is known to affect the organoleptic properties of food, it is necessary to develop more appropriate systems. Indeed, PLA-based nanocomposites were developed by Yang *et al.*, (2016) [66] through the incorporation of cellulose nanocrystals (CNC) and lignin nanoparticles. These prepared PLA nanocomposites inhibited the growth of *Pseudomonas syringae pv. Tomato* after only 3 hours of its application. Likewise, PLA films embedded with TiO₂ and silver nanoparticles showed good antibacterial activity against *L. monocytogenes* and *E. coli* compared to PLA films [67]. In fact, neat PLA increased bacterial concentrations from $5 \log_{10}$

to 8.94 log₁₀ (*E. coli*) and from 5log₁₀ to 9.12 log₁₀ (*L. monocytogenes*) after 24h, whereas in the presence of 5% TiO₂ and 0.5% Ag nanoparticles, the bacterial concentrations decreased significantly from 5log₁₀ to 3.06 log₁₀ for *E. coli* and from 5log₁₀ to 3.42 log₁₀ for *L. monocytogenes*. Finally, the migration of TiO₂ and Ag nanoparticles was found within the allowed standard limit (1mg.kg⁻¹) according to the commission regulation (EU) No 10/2011.

I.1.3.4) Chitosan as antimicrobial food packaging material

Compared to PCL and PLA, chitosan is an excellent candidate for antimicrobial food packaging due to its film-forming ability, antimicrobial activities, and good barrier to gases [68]. Moreover, chitosan could also be used as an edible coating material due to its polysaccharidic nature [69].

As an antimicrobial food packaging material, chitosan can either be solely used or in blends to increase and broaden its antimicrobial activity. For example, the application of chitosan as an edible coating to fresh-cut Broccoli shows inhibition of the growth of mesophilic aerobic bacteria with a reduction of 1.5-2.5 log CFU/g compared to uncoated Broccoli after 20 days [9]. Similarly, Kanatt *et al.*, (2013) [70] successfully extended the shelf life of meat products using neat chitosan coating. Indeed, the total viable count of uncoated chicken products at day 0 was 4-5 log CFU/g and was reduced to 3.2-3.3 log CFU/g with Cs coating. After 3 days, the uncoated samples had a total viable count in the range of 5-6 log CFU/g compared to 3-4 log CFU/g when Cs coating was applied. Cs coating has improved the shelf-life by 10 days.

In some antimicrobial food packaging, the antimicrobial activity of chitosan has been improved with several antibacterial agents, such as natural extracts and metal nanoparticles. In that sense, chitosan films loaded with cinnamon essential oils (CEO) were tested against *L. monocytogenes*, *Lactobacillus planatum*, *Lactobacillus sakei*, *Pseudomonas fluorescens*, and *E. coli*. Compared to neat Cs films, Cs-CEO films have shown an increasing antibacterial activity with the increase of CEO content against all tested bacteria. Indeed, the addition of 2% (v/v) CEO has demonstrated an inhibition zone of 52.31±2.65 mm² against *L.monocytogenes*, 53.64 ± 3.07 mm² against *L.planatum*, 57.23 ± 1.5 mm² against *L.sakei*, 43.6 ± 1.21 against *P.fluorescens*, and 51.04 ± 2.12 mm² against *E.coli* while Neat Cs have not demonstrated any inhibition zone at all [71]. Other natural extracts, such as apricot kernel essential oils [12], grapefruit seed extract [72], and rosemary essential oils [73] have also been used to enhance the antimicrobial activity of chitosan for food packaging applications.

Metal nanoparticles are considered a better antimicrobial alternative to natural extracts due to their low effect on the organoleptic properties of food (See **General introduction**). Indeed, ZnO nanoparticles (ZnONPs) [74] were added to chitosan using an *ex-situ* approach and were used for polyethylene (PE) coating. PE is widely used for conventional food packaging but it lacks the antibacterial activity. Although neat Cs coating has shown excellent antibacterial activity against *E. coli*, *S. aureus*, and *S. enterica*, the addition of ZnONPs eradicated the growth of these bacteria altogether.

Table I.1 summarizes the works regarding the use of PCL, PLA, and Chitosan in antimicrobial food packaging. Other interesting examples from the literature were also reported by specifying the formulation, the method used for incorporating the antimicrobial agent, and the tested microorganisms.

Table I.1: Examples of antimicrobial food packaging based on PCL, PLA, and Chitosan

	Antimicrobial packaging material	Incorporation technique	Microorganisms	Reference
PCL	PCL-Chitosan-GFSE	Solution mixing then extrusion	<i>E. coli</i> <i>P. aeruginosa</i>	Wang <i>et al.</i> , (2019) [63]
	PCL-PLA-CNMA	Solution mixing	Various mesophilic and psychrophilic microorganisms of mushroom	Qin <i>et al.</i> , (2015) [64]
	PCL-organoclay-Chitosan	Solution mixing	<i>E. coli</i> <i>P. aeruginosa</i> , <i>Candida albicans</i>	Cesur <i>et al.</i> , (2017) [75]
	PLC-ZnO nanoparticles	Solution mixing	<i>S. aureus</i>	Pina <i>et al.</i> , (2020) [76]
	PCL-Starch-Pomegranate rind hybrids	Melt mixing	<i>E. coli</i> , <i>S. aureus</i>	Khalid <i>et al.</i> , (2018) [77]
	PCL-Grapefruit seed extract	Melt mixing	<i>L. monocytogenes</i>	Lyu <i>et al.</i> , (2019) [78]

PLA	PLA-allyl Isothiocyanate (AIT) PLA-AIT-Nisin	Solution mixing	<i>Salmonella enteritidis</i> <i>Salmonella oranienburg</i>	Jin and Gutler (2011) [65]
	PLA-CNC-LNP	Melt mixing	<i>Pseudomonas syringae pv. Tomato</i>	Yang <i>et al.</i> , (2016) [66]
	PLA-Pectin-Nisin	Diffusion coating	<i>Listeria monocytogenes</i>	Jin <i>et al.</i> , (2008) [79]
	PLA-nanoTiO ₂ -nanoAg	Solution mixing	<i>Listeria monocytogenes</i> <i>E. coli</i>	Li <i>et al.</i> , (2017) [67]
	PLA-Chitosan particles	Melt mixing	Total aerobic mesophilic and coliform microorganisms of pork meat	Bonilla <i>et al.</i> (2013) [80]
	PLA-Cinnamaldehyde (w/ or w/o clay) PLA-Thymol (w/ or w/o clay)	Melt mixing	<i>E. coli</i> <i>Staphylococcus aureus</i>	Villegas <i>et al.</i> , (2019) [81]
	PLA-Ag-Vitamine E	Solution mixing	<i>E. coli</i> <i>L. monocytogenes</i> <i>S. typhimurium</i>	Munteanu <i>et al.</i> , (2014) [82]
Chitosan	Chitosan	N/A	<i>E.coli</i> Coliform microorganims	Moreira <i>et al.</i> , (2011) [9]
	Chitosan	N/A	Coliform microorganims	Kanatt <i>et al.</i> , (2013) [70]
	Chitosan- cinnamon essential oils	Solution mixing	<i>L. monocytogenes</i> , <i>Lactobacillus sakei</i> , <i>Pseudomonas fluorescens</i> <i>E. coli</i>	Ojagh <i>et al.</i> , (2010) [71]
	Chitosan-Apricot kernel EO	Solution mixing	<i>E. coli</i> , <i>B. subtilis</i>	Priyadarshi <i>et al.</i> , (2018) [12]
	Chitosan-Grapefruit seed extract	Solution mixing	Fungi	Tan <i>et al.</i> , (2015) [72]

	Chitosan-Rosemary essential oils	Solution mixing	<i>S. agalactiae, E. coli, L. Monocytogenes</i>	Abdollahi <i>et al.</i> , (2012) [73]
	Chitosan-ZnO nanoparticles	Solution mixing	<i>E. coli, S. enterica and S. aureus</i>	Al-Naamani <i>et al.</i> , (2016) [74]
	Chitosan-Gelatin-Silver nanoparticles	Solution mixing	<i>E. coli, S.aureus, S. mutans, P. aeruginosa, C. albicans</i>	Ediyilyam <i>et al.</i> , (2021) [83]

I.1.4) Fillers: clay MMT/BNT, Mica, and silver nanoparticles

I.1.4.1) General context

As discussed above, polymers have many limitations. Thus, it is necessary to enhance their properties in order to use them on a larger scale. Indeed, the preparation of polymer-based composites is one of the most commonly used methods for such purposes. The nature of the filler is dependent on the polymer matrix and the type of the sought-after properties. For instance, silver nanoparticles are widely used to provide antibacterial activity [84], while sheet-like nanoclay are usually used to enhance thermal, mechanical, and barrier properties [85,86].

As discussed in the introduction, nanofillers are divided into three types depending on their dimensions (Fig. I.6): one-dimensional (nanotubes and nanofibers), two-dimensional (nanosheets such as layered silicates), and zero-dimensional nanofillers (nanoparticles) [87]. This section is an overview of multiple nanofillers: Montmorillonite (MMT), a known and a well-studied model of nanoclay fillers, Bentonite and Mica (2D nanofillers), which are nanofillers with a similar structure to MMT, and finally, silver nanoparticles (3D nanofiller), which are widely used for their antibacterial properties. Finally, we discuss their structure and their mechanism in the enhancement of polymer properties in the case of nanoclays, or their role in providing the antibacterial activity in the case of silver nanoparticles.

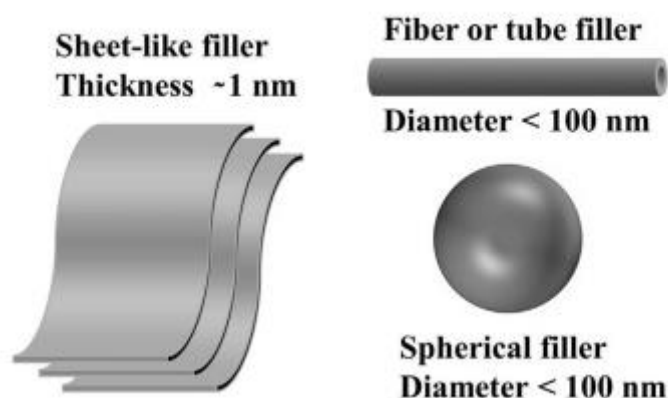


Figure I.6: Types of nanofillers based on their dimensions in the nanoscale [87].

I.1.4.2) Montmorillonite and bentonite

Both montmorillonite (MMT) and bentonite (BNT) are layered silicates belonging to the smectite group of the 2:1 phyllosilicate family. As shown in Fig. I.7, they are composed of one octahedral magnesia or alumina sheet situated between two silica tetrahedral sheets while the oxygen atoms of the octahedral sheet are also shared with the tetrahedral sheets. The 2:1 Phyllosilicates have a layer thickness of 1 nm, while their lateral dimension is ranging from

tens of nanometers to several micrometers [87,88] which provides an extremely high surface area.

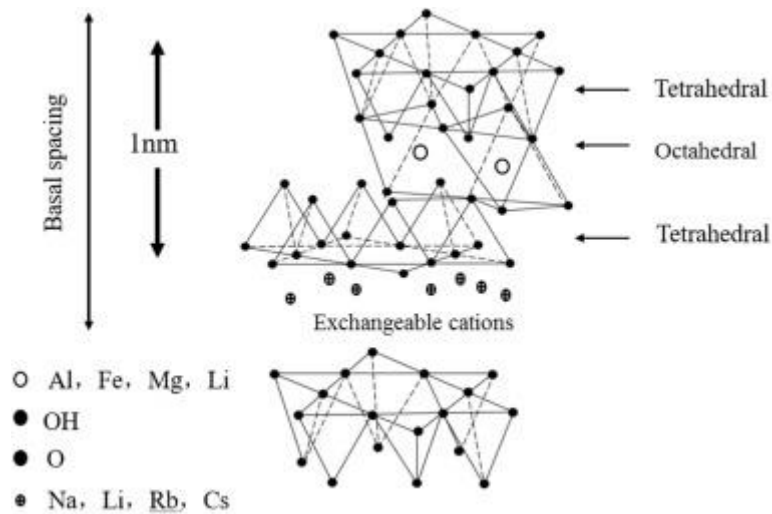


Figure I.7: Crystallographic structure of 2:1 phyllosilicate [87].

MMT was the first clay to be used as a nanofiller by the Toyota group. Indeed, in 1993, they reported the synthesis of Nylon 6/MMT nanocomposites using solution intercalation in an aqueous hydrochloric acid solution (36% HCl). compared to Nylon-6, the nanocomposites have shown an improvement of the physico-mechanical properties such as strength, modulus, and heat-distortion temperature using very low filler content (4.7 – 5.3 wt%) [89,90]. Ever since, MMT is the most used sheet-like nanoclay to improve the mechanical, thermal, and barrier properties of polymers [91]. Similarly, the enhancement potential of BNT is well established in the literature [92–95]. For example, it was reported that the incorporation of BNT enhances the mechanical and barrier properties of polyethylene acrylate (PEA) [92], and the thermal stability of polyvinyl alcohol (PVA) [93]. The mechanism by which sheet-like nanoclays enhance polymer properties is also very known in literature due to the extensive study of these smectite nanoclays, especially MMT. For example, the enhancement of barrier properties of the permeable phase (polymer matrix) originates from the increase of tortuosity that resulted from the introduction of clay nanosheets. Indeed, the degree of improvement is dependent on the ratio of the nanofiller, its shape, and its dispersion. Moreover, the degree of dispersion itself depends on the degree of delamination (exfoliation) of the filler. In that regard, fully delaminated (exfoliated) nanocomposites show a high tortuosity factor, thus, better barrier properties than partially delaminated nanocomposites (Intercalated) (Fig. I.8) [96,97].

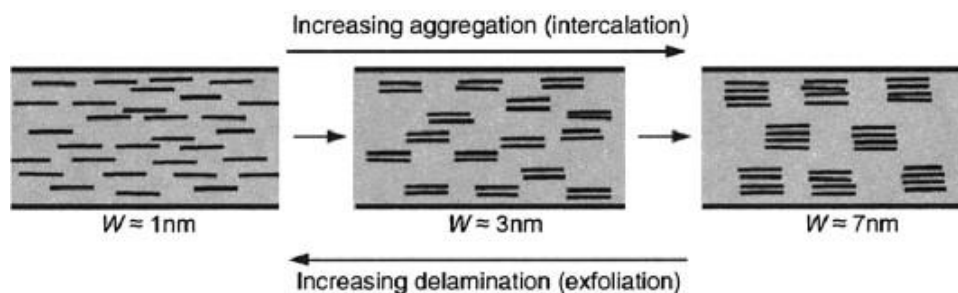


Figure I.8: The effect of the degree of delamination on the tortuosity factor of nanocomposites (w : thickness of the stack) [96].

In the same manner, as the barrier properties, the enhancement of thermal properties, which is another important property of packaging materials, is linked to the increase of the tortuosity factor, which hinders the diffusion of volatile decomposition products. Layered silicates could also act as a char formation promoter by forming a protective char layer on the surface of the polymer phase, and delaying the combustion process [98,99].

The mechanical properties of polymers are another important feature where an enhancement is observed when layered silicates are introduced as nanofillers. Sheet-like clays were used to enhance the tensile strength, Young's modulus, and the storage modulus among other mechanical properties of polymers [100]. These improvements are dependent on the interfacial interaction between the polymer matrix and the nanofiller. As this interaction increases proportionally to the degree of delamination, a better stress transfer from the matrix to the filler occurs [87]. Another factor influencing the degree of improvement by clay is its content. Indeed, the improvement is usually observed in a specific range of clay content, which depends on the interaction between the clay and the polymer. Indeed, Ma *et al.*, (2001) [101] have reported an enhancement of tensile strength and elongation at break of polyurethane in the range of 0 to 8 wt% of clay, but beyond 8%, the enhancement was reduced because of particles aggregation.

As discussed above, the improvement of polymer inherent properties is highly dependent on the interaction between the filler phase and the polymer matrix. Indeed, as the degree of exfoliation is increased, the interaction between clay and polymers increases which results in a better enhancement of the polymer properties. The degree of exfoliation itself is dependent on the nanocomposite preparation method and the compatibility between the clay and the polymer matrix. Phyllosilicates are hydrophilic due to the presence of hydrated ions (Na^+ and Ca^{2+} ions) in their interlayer space. In that sense, phyllosilicates are not very compatible with hydrophobic organic polymers [102,103]. However, due to their high cation exchange capacity (CEC),

phyllosilicates can be organo-modified using a multitude of organic molecules such as quaternary ammonium [104] and organo-silanes [105]. The organo-modification of phyllosilicates enhances both the dispersion of nanoclay in the polymer matrix and the interaction between these two phases. Interestingly, the organomodification of clay could also provide an antibacterial activity to the resulting nanocomposites. Indeed, Mondal *et al.*, (2013) [106] used CTAB to organo-modify MMT for the preparation of poly(butylene adipate-co-terephthalate)/MMT nanocomposites resulting in an antibacterial activity against *Bacillus subtilis* and *Staphylococcus aureus*, which was attributed to the inherent antibacterial activity of CTAB

I.1.4.3) Mica

Mica is another 2:1 phyllosilicate clay mineral used as a nanofiller in the preparation of polymer nanocomposites. It is composed of two tetrahedral sheets and one octahedral sheet [107]. Compared to the smectite family (MMT, BNT), the tetrahedral sheets contain one-third of Al^{3+} ions instead of Si^{4+} ions, rendering mica more negatively charged compared to smectites which influence its CEC. Similar to smectites, the octahedral sheet contains either Al^{3+} or Mg^{2+} ions, which can be also replaced by Fe^{2+} or Fe^{3+} ions depending on the type of mica [108]. Fig. I.9 depicts the structure of muscovite, a type of Mica composed of Al^{3+} ions in the octahedral sheet [107].

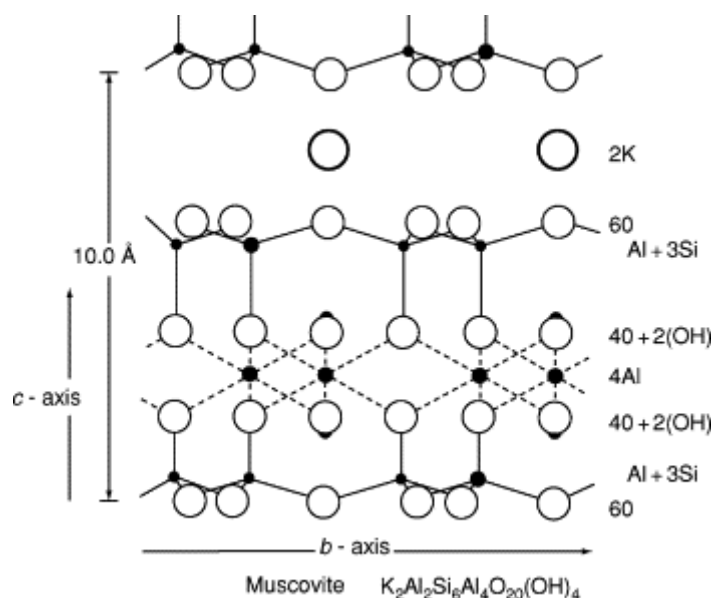


Figure I.9: Crystallographic structure of Muscovite [107].

Mica is not as commonly used as nanofillers such as MMT or BNT. However, its potential for improving polymers' properties is well established. For example, mica was used for the

preparation of PLA-mica nanocomposites through melt extrusion by Maiti *et al.*, (2002) [109]. The nanocomposites enhance the storage modulus by 41.2% and reduce the gas oxygen permeability by 28% using only 3.8 wt% of mica compared to neat PLA. Additionally, mica showed similar enhancement potential as MMT but lower than other smectite nanoclay due to their large size. Likewise, Ojijo *et al.*, (2014) [110] compared mica and MMT in PLA/Poly[(butylenesuccinate)-co-adipate (PBSA)] blends and have shown that both mica and MMT enhanced the thermal, mechanical, and permeability to oxygen and water vapor. Additionally, Mica showed a better enhancement of the oxygen and water vapor barrier properties than MMT, whereas MMT showed a better potential to enhance the toughness of PLA/PBSA blends [96].

Similar to smectites, the organo-modification of mica by replacing the cations in the interlayer enhances the compatibility of mica with the polymer matrix [111,112]. Furthermore, the substitution of hydroxyl groups (OH) in mica by fluorine ions has shown an enormous enhancement in their properties. Indeed, Yano *et al.*, (1997) [113] have reported a substantial reduction in water vapor permeability (about 90%) using fluorine-modified mica compared to MMT (about 55%). Moreover, the introduction of fluorine-modified Mica (Fluorphlogopite) in Polycarbonate enhanced i) the barrier properties to water, N₂, O₂, and CO₂ with increasing fluorphlogopite content (0.7-7.5 wt%) and ii) the E modulus with only 0.7 wt%. An optimal enhancement was obtained at 5 wt% of fluorphlogopite [114].

I.1.4.4) Silver nanoparticles

Various nanofillers are introduced in the polymer matrix in low content for two main reasons: i) the enhancement of polymer properties or ii) the introduction of completely novel properties in order to broaden their domains of application. In the former, classic nanofillers are used such as nanoclay while in the latter, nanofillers with intrinsic properties of interest are used such as metal nanoparticles. Indeed, silver nanoparticles (AgNPs) are among the most used metal nanoparticles in the preparation of polymer nanocomposites due to their excellent properties, particularly the antimicrobial ones [115,116]. Indeed, AgNPs provided an excellent antibacterial activity against a wide range of bacteria when incorporated into a variety of polymers such as LDPE [117] and PLA [67]. A more detailed overview of silver nanoparticles is discussed in part “**I.2.silver nanoparticles as antibacterial filler**”

I.1.5) Preparation methods of polymer nanocomposites

As discussed above, the dispersion of nanofillers into the polymer matrix and their degree of interaction (Intercalation/Exfoliation) is critical to achieving the desired properties. This dispersion is highly dependent on the used preparation method. Indeed, various methods are employed to prepare polymer nanocomposites including solution mixing, melt mixing, and in-situ polymerization.

I.1.5.1) Solution mixing – Intercalation of polymers

Solution mixing is also called intercalation of polymers in the case of layered silicate. It is the simplest method to prepare polymer nanocomposites (Fig. I.10): a polymer is dissolved in a suitable solvent and mixed with a nanofiller. In this process, the dispersion is usually enhanced by ultrasonication for example. In the case of layered silicates, the nanoclays are firstly swollen in a suitable solvent and added to a solution of the polymer, which is prepared in the same solvent or a miscible solvent. Then the solvent is evaporated under controlled conditions to produce the nanocomposite materials using techniques such as solvent casting, spin casting, and electrospinning [87,118]. The major concern about these techniques is the use of organic solvents in the case of non-water-soluble polymers.

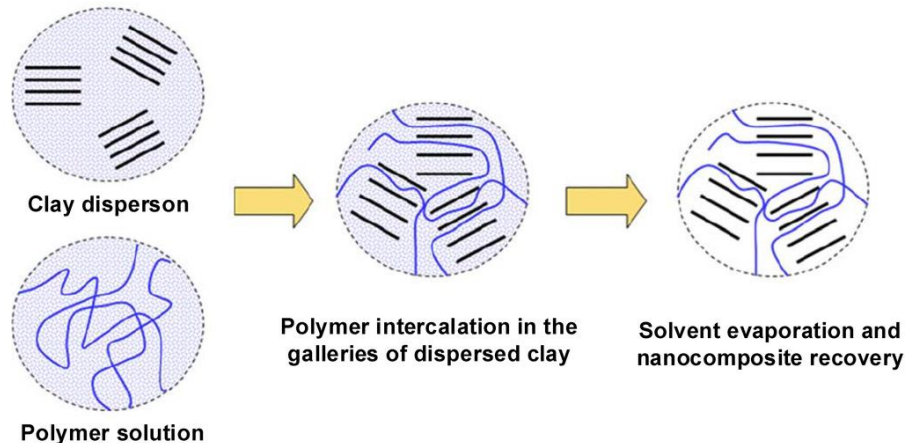


Figure I.10: schematic representation of intercalation of polymer into the clay nanofiller [119].

I.1.5.2) Melt mixing – Melt intercalation

Melt mixing or melt intercalation in the case of layered nanofillers, is a method in which the polymer is melted at high temperatures (Above T_m) and mixed with the nanofiller under shear force. This method is widely used in the preparation of commercial nanocomposites due to its simplicity and the green nature of the process as it does not require the use of toxic solvents. However, the use of high temperatures can lead to the degradation of organic modifiers of

nanofillers or polymeric chains [120]. This method usually produces nanocomposites with intercalated structures. Nevertheless, exfoliation could be achieved by increasing the compatibility of the nanofiller with the polymer. Indeed, Chen *et al.*, (2005) [121] achieved exfoliations using a twice functionalized cloisite 25A (C25A) as a nanofiller. The C25A was modified using an amine compound and was further functionalized using (glycidoxypropyl)trimethoxy silane.

I.1.5.3) *In-situ* polymerization

In this method, a nanofiller is dispersed in a solution of the monomer prior to the polymerization to ensure post-synthesis dispersion. Then the polymerization is induced under suitable conditions, which depend on the nature of the monomer. This method is more advantageous than the other ones because it can be carried out under bulk conditions without the use of solvents and can produce high molecular weight polymers. However, its main advantage is its ability to produce nanocomposites with an exfoliated structure [122,123]. Among the *in-situ* polymerization methods, the *grafting from* coordination insertion polymerization is of great interest as it allows the preparation of nanocomposites with good dispersion between the polymer and the nanofiller. In this method, the catalyst reacts covalently with the hydroxyl group of the nanofiller, thus activating these groups to co-initiate the polymerization [124].

I.2) Silver nanoparticles as antibacterial nanofiller

I.2.1) General context

As it was introduced briefly previously (See **I.1.4.4**), silver nanoparticles are one of the most used nanofillers for the preparation of antimicrobial food packaging nanocomposites due to their excellent antimicrobial activity compared to other metal nanoparticles [125]. Furthermore, AgNPs offer other advantages compared to organic antimicrobial agents as these organic molecules have major drawbacks such as their instability at high temperatures, moisture sensitivity, and the possible modification of the organoleptic properties of food [126].

The unique properties of AgNPs originate from their high surface area and the quantum confinement effect due to their nanoscale. Indeed, AgNPs are widely used in food packaging, medicine, and cosmetics, due to their antibacterial activity and in other domains as catalysts and sensors, *etc* [127,128]. Nevertheless, AgNPs' activities are highly dependent on their size, shape, surface charge, and stability. The latter is of primordial importance as AgNPs aggregation results in the loss of their advantageous properties. In that regard, in this sub-chapter, the preparation methods of AgNPs are discussed with emphasis on plant-mediated

biosynthesis. Moreover, parameters affecting the characteristics of AgNPs are discussed. Finally, the antibacterial activity of AgNPs is reviewed with regard to the mechanism, bacterial resistance, and methods for its enhancement.

I.2.2) Synthesis methods of silver nanoparticles

Multiple methods are used for the synthesis of silver nanoparticles (AgNPs), each one has its own advantages and drawbacks in terms of the procedure simplicity, control of the physico-chemical characteristics, eco-friendliness, *etc.* These methods can be divided into two main categories: top-down and bottom-up approaches [129]. The difference between these two approaches, as their names suggest, is that the top-down method starts with a bulk material which is then broken down into nanoparticles using techniques such as grinding, milling, thermal, or laser ablation, *etc.* [130], whereas the bottom-up approach uses the self-assembly of silver atoms that grow into nanoparticles [131].

A more distinctive and precise way to categorize silver nanoparticles synthesis is to divide them into physical, chemical, or biological methods based on the principle of the method rather than the starting precursors of AgNPs. The physical methods are discussed briefly in this section. More emphasis will be on the chemical methods as they are more commonly employed and the biological methods as they are more eco-friendly. All advantages and drawbacks of each method are gathered in table 1.2.

I.2.2.1) Physical methods

Physical methods include a multitude of techniques such as laser ablation, mechanical ball milling, and inert gas condensation [127].

Laser ablation uses a laser as an extremely high energy source to remove silver species from a solid target, then the growth and nucleation of these species produce the nanoparticles [132]. Depending on the purity of the starting material and the surrounding medium, this method can produce nanoparticles with high purity. Moreover, this technique is more advantageous as it produces “Naked NPs” which would be easier to functionalize if required [133]. However, in addition to the necessity of a laser device, the control of the size distribution is limited and potential agglomeration of nanoparticles is possible as NPs are prepared through random Brownian motion [132].

Concerning mechanical ball milling, it uses high-energy mills to reduce bulk powder to the nanometric size [134]. These high-energy mills are produced using attrition, planetary, or vibrating ball mills. The main advantage of this technique is the large-scale production of

nanoparticles with high purity. Nevertheless, it requires high energy input and presents the risk of contamination caused by steel balls [135].

The inert gas condensation (IGC) uses fast heating at constant inert gas pressure (*e.g.*, He or Ar) to evaporate the solid precursor which generates ultrafine particles that are condensed using a surface cooled by water or liquid nitrogen [136,137]. Although this technique offers good control over the size distribution by varying the procedure parameters (temperature and pressure) [136], it requires high energy input and complex equipment.

The main advantage of these methods is their occurrence in a solvent-free environment.

I.2.2.2) Chemical methods

a. Wet chemical reduction

Wet chemical reduction is widely used for preparing silver nanoparticles [138]. The principle of this technique is very straightforward. A reducing agent is used to reduce silver salt to its neutral form (Ag^0), which grows into nanoparticles by nucleation through Ostwald ripening followed by coalescence. Subsequently, capping agents (*e.g.*, Sodium citrate, Polyethylene glycol, *etc*) are used to stabilize the nanoparticles and protect them from agglomeration (Fig. I.11) [139,140]. The advantages of wet chemical reduction over other techniques are its simplicity because it does not require complicated equipment or high energy input. Nevertheless, the toxicity of the reducing and capping reagents is the main concern of this technique [141,142].

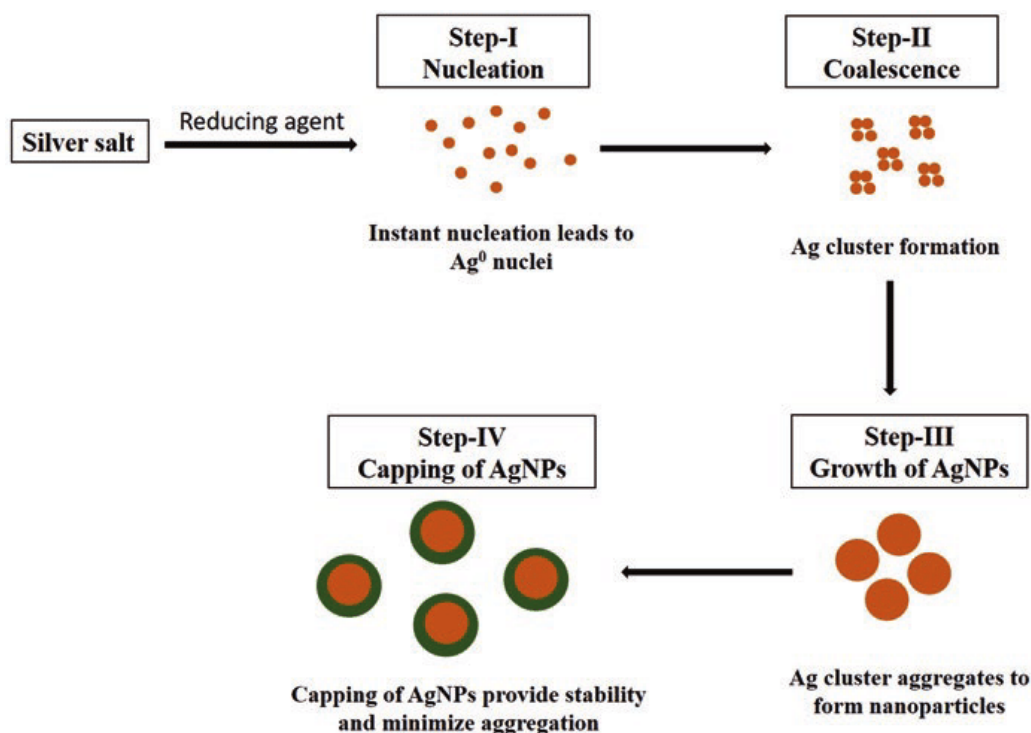


Figure I.11: Wet chemical reduction of AgNO_3 to prepare AgNPs [143].

Thermodynamically, the preparation of metal nanoparticles is only possible when the difference of Gibbs energy (ΔG) is negative. Interchangeably, the difference between values of standard redox potential in the hydrogen scale (E^0) of the metal ions redox system and the reducing molecule redox system must be positive [141,144]. A more detailed explanation of the effect of redox potential on the synthesis of metal nanoparticles can be found in Kvitek *et al.*, (2016) [141]. In the case of silver, the redox system Ag^+/Ag^0 has a relatively large standard redox potential ($E^0 = +0.799$ V), thus it can be reduced by a variety of molecules such as hydrazine ($E^0 = -0.230$ V), sodium citrate ($E^0 = -0.180$ V), sodium borohydride ($E^0 = -0.481$ V) [145–147].

b. Photochemical method

The photo-assisted synthesis of silver nanoparticles uses irradiation from a light source (a laser or a lamp) to prepare silver nanoparticles in the presence of a photo-reducing agent such as graphitic carbon nitride with or without the presence of a stabilizing agent [148,149]. The main advantage of this method is the possibility to prepare nanoparticles directly in matrices such as zeolite crystals, Chitosan/Montmorillonite nanocomposites, and PVA. However, this technique has also drawbacks such as the use of non-ecofriendly photo-reducing agents and the requirement of multiple steps during AgNPs synthesis [150–152].

Table I.2: Advantages and drawbacks of silver nanoparticles preparation techniques

	Technique	Advantages	Drawbacks
PHYSICAL METHODS	Laser ablation	-High purity -Naked NPs for further functionalization	-Necessity of a Laser -Size distribution and agglomeration limited control
	Mechanical ball milling	-High purity -Large production -Absence of the solvent	- High energy input -Risk of contamination
	Inert Gas Condensation	-Size and size distribution control	-High energy input -The necessity of a complex equipment
CHEMICAL METHODS	Chemical reduction	-Simplicity - Low energy requirements	- Non-eco-friendly
	Photochemical method	- Simplicity - In situ synthesis of AgNPs in matrices	- Non-eco-friendly - Multiple steps synthesis
	Electrochemical method	- High purity - Size and homogeneity control by varying the current density - Ecofriendly	-Deposition of silver on the cathode
	Microemulsion technique	-Control of size and shape -Homogeneity	-Non-eco-friendly
Biological methods	Bacteria & fungi synthesis	-Ecofriendly	-Require specific conditions (incubation conditions) -Cost of culture media -Require purification using special conditions in case of intracellular synthesis -Reproducibility
	Plant-mediated synthesis	-Ecofriendly - Low cost	-Reproducibility

c. Electrochemical synthesis

In the electrochemical synthesis of silver nanoparticles, the reduction of silver ions occurs at the cathode, usually in platinum, followed by the formation of nanoclusters, which are then stabilized by polymers or surfactants to prevent their aggregation. The use of “Sacrificial” silver anodes (Fig. I.12) is very interesting because as shown in the reaction below, the silver anode will be dissolved by electrolysis to give silver ions (Equation 1), which are then transferred to the cathode where they get reduced to form neutral Ag^0 (Equation 2) [127,153,154]:

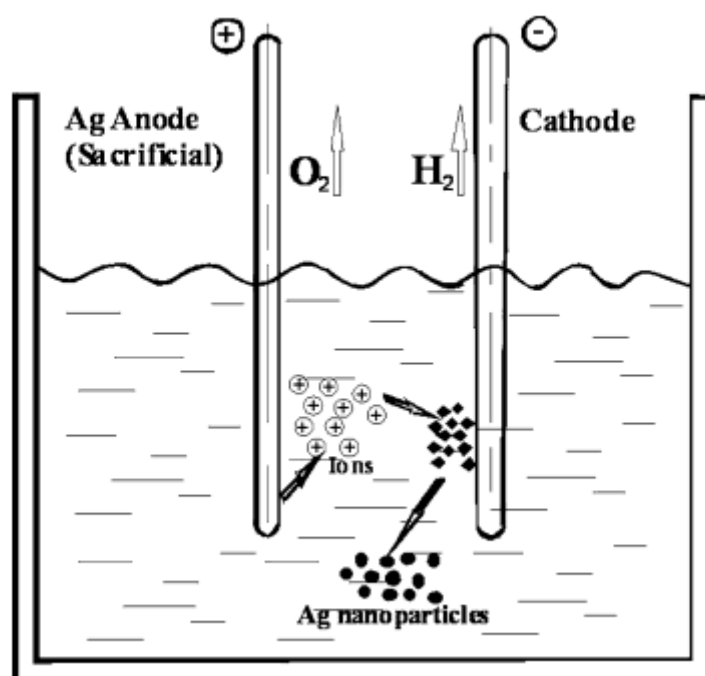


Figure I.12: Electrochemical synthesis of silver nanoparticles using a sacrificial silver anode in water [155].

The advantage of the “Sacrificial technique” is the elimination of the use of expensive metal salts. However, the deposition of silver on the cathode limits its use [153,155].

d. Microemulsion synthesis

Microemulsion synthesis of nanoparticles is another chemical method. The metal precursor and the reducing agent are separated spatially in two immiscible phases, an aqueous and an organic phase such as dodecane. The preparation of AgNPs occurs at the interface between the two

phases and depends on the inter-phase transport intensity mediated by emulsifiers such as quaternary alkylammonium salts. The formed nanoclusters are then stabilized to prevent their agglomeration and are transferred to the organic phase [127]. This technique allows the control over nanoparticles' size and shape by varying the nature and content of the organic phase [156]. However, the main drawback of this technique is the use of organic solvents.

I.2.2.3) Biological “green” methods

As described above and summarized in table I.2, the majority of chemical and physical techniques are non-environmentally friendly and energetically expensive. Thus, the necessity of alternative methods is of primordial importance. In recent years, biological pathways for the synthesis of metal nanoparticles in general, and silver nanoparticles in particular, have gained a lot of attention as promising alternatives. Here, the synthesis of the silver nanoparticles *via* biological approaches is discussed with a particular emphasis on the plants mediated synthesis.

AgNPs are produced using different biological species or systems such as i) microorganisms (Bacteria and Fungi) ii) plants and plant extracts and, iii) templates such as membranes, viruses, DNA, and diatoms [142]. The AgNPs synthesis mediated either by microorganisms, plants, and their extracts is further discussed due to their versatility, simplicity, and cost.

a. Silver nanoparticle synthesis using bacteria or fungi

In 1999, Klaus *et al.*, [157], demonstrated the AgNPs accumulation inside the bacterium *Pseudomonas stutzeri* AG259, which was isolated from silver mines. These bacteria grow in this highly concentrated silver environment by converting toxic silver ions into a less toxic form (AgNPs). Ever since many researchers have reported the synthesis of AgNPs using extracellular and intracellular approaches.

In the intracellular synthesis, silver nanoparticles are synthesized inside the bacterial cell as mentioned for *Pseudomonas stutzeri* AG259. In vitro, the intracellular reduction of Ag^+ can be accomplished by bacteria using a culture medium containing silver salt under the appropriate incubation conditions [158]. The synthesized AgNPs should then be extracted using special treatments such as sonication and/or detergents [159]. This approach requires tolerant bacteria to silver.

The extracellular synthesis is more advantageous and more common compared to its intracellular counterpart. In this method, AgNPs are produced in the culture medium using bacterial excreted molecules as reducing and stabilizing agents. Even though this method does

not require the separation of the cells from the culture medium [160], the more common approach is to use the culture medium supernatant for the reduction of silver ions and the stabilization of AgNPs [161–163].

The use of fungi for AgNPs synthesis is very similar to the bacteriogenic synthesis with similar intracellular and extracellular methods. In addition, fungi can produce more proteins, which could act as reducing and capping agents therefore, fungi are more advantageous than bacteria in the synthesis of AgNPs [164].

In summary, the advantages of microbial synthesis of silver nanoparticles are related to their green nature and simplicity, and to the dual role of their excreted molecules as reducing and capping agents making it possible to synthesize AgNPs in a one-pot reaction. Nevertheless, this method presents some drawbacks such as reproducibility which is mainly due to qualitative and quantitative variations in the composition of microbial excreted molecules. Furthermore, the use of costly culture media and specific incubation conditions are also considered disadvantages of this technique. Finally, in case of the intracellular synthesis, more complicated purification processes are required compared to the chemical methods.

b. Silver nanoparticle synthesis using plants or plants extracts

The first study on the synthesis of silver nanoparticles using plants goes back to 2003 by Gardea-Torresdey *et al.* [165], who have reported the use of Alfalfa sprouts (*Medicago sativa*) to prepare AgNPs internally. However, the applicability of this finding, except from an academic point of view is very limited due to the complexity of the approach, the potential cost, the limited control over AgNPs parameters, and the purification process. Ever since the number of papers reporting the synthesis of AgNPs using plant extracts (and not directly plants) has increased dramatically over the years.

Compared to the microbial-mediated synthesis, the plant-mediated approach does not require the use of expensive culture media nor does it require special treatment for the extraction of AgNPs. Moreover, parameters such as pH and temperature could be controlled as easily as in wet chemical reduction, thus giving more flexibility to control the AgNPs parameters (size, size distribution...). The plants mediated synthesis is based on the same principle as the wet chemical reduction. Indeed, silver ions are reduced to their neutral form Ag⁰, which grows into nanoparticles that would eventually be stabilized by plant biomolecules.

The earliest reports have used extracts from *Azadirachta indica* [166], *Embilica officinalis* [167], *Capsicum annuum* [168], *Cinnamomum camphora* [169], and a variety of other plants. The common denominator between most of these plants is that they are medicinal and aromatic plants (MAPs). Indeed, MAPs are rich in secondary metabolites such as terpenoids and alkaloids, but especially polyphenols, which have excellent reducing properties [170]. Moreover, the phytochemicals of the MAP extracts could synergistically enhance the antimicrobial activity of metallic nanoparticles [171]. Other molecules such as primary metabolites like proteins, amino acids, saccharides, and vitamins are also involved in the reduction of silver ions and the stabilizations of NPs [14].

In summary, the phytogetic synthesis of AgNPs (Fig. I.13) involves the collection of the desired part of the plant, usually leaves, and then the extraction is carried out using the dried material in water. Other studies involving the use of essential oils or organic extracts are also reported in the literature [172,173]. The extract is then used to reduce silver salt and stabilize the nanoparticles. Parameters such as temperature, pH, the plant extract, and the silver salt concentrations can be varied to control the production and characteristics of AgNPs.

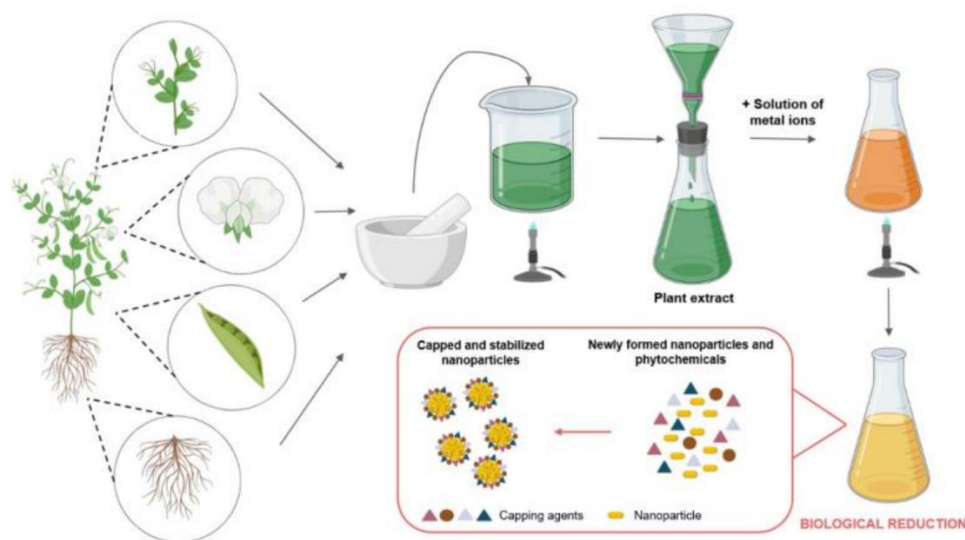


Figure I.13: The general protocol for the preparation of plant-mediated metal nanoparticles [174].

The plant-mediated synthesis of silver nanoparticles has many advantages over classical “chemical” approaches. The approach is eco-friendly, simple, and economically more efficient. But, is it a viable commercial alternative to classical chemical and physical approaches?

I.2.2.4) Comparison of the chemical and biological methods

The silver nanoparticles market is expanding rapidly with its current uses in a variety of consumer products such as antimicrobial coating, textiles, cosmetics, and packaging. The market is in constant growth and even the most skeptical estimates predict a global market of 300 000 tons by 2022 [175]. Syafiuddin *et al.*, (2017) [176] reported a summary of the world's top suppliers of AgNPs. In a search on these suppliers' official websites, a lot of them do not mention the preparation method, but among those who do, none of them uses plant-mediated AgNPs synthesis. The reasons behind the limited commercial use of biogenic AgNPs could be due to the drawbacks of the biological method such as its low reproducibility.

The main advantage of using the chemical synthesis of silver nanoparticles is the reproducibility of the process. In fact, many developed processes give reliable results under a set of fixed parameters such as the Tollens process [177]. AgNPs of various controlled size from 5 to 100 nm were prepared by Agnihotri *et al.*, (2014) [178] by varying the concentrations of sodium borohydride and trisodium citrate in a co-reduction approach.

The plant-mediated synthesis of metal nanoparticles gives different results using the same plant species under the same reaction conditions. For example, *Rosmarinus officinalis* was used by both Farghaly and Nafady (2015) [179] and Fierascu *et al.*, (2014) [180], but they obtained different results. In these reports, the extraction and the synthesis were performed under similar conditions. However, the obtained SPR bands are very different (427 vs 440 nm), which indicates AgNPs with different sizes. In the same context, using the same plant (Rosemary), El-Aziz *et al.*, (2018) [181] and Mohamed *et al.*, (2017) [182] have also obtained AgNPs with different sizes: 10-31.7 Vs 7.55-16.5 nm as shown by TEM. Moreover, using *Azadirachta indica*, the same procedure was used by Shakeel Ahmed *et al.*, (2015) [183] and Roy *et al.*, (2017) [184], but the SPR bands were found to be 436 vs 420 nm, respectively, indicating variability in size. These data variations may be explained mainly by differences in the chemical composition of plant extracts. The methodology and parameters of plant extraction are different for all studies, such as the extraction solvent, temperature, and time. Indeed, these parameters could affect greatly the chemical composition of the extract, and thus, the synthesis of AgNPs. Moreover, the chemical composition of aromatic and non-aromatic plants varies greatly not only between different plant species but within the same species (intraspecific variability). The chemical composition of the same plant species is known to contain different chemotypes and its variation is due to many parameters such as seasonality, humidity, altitude, drying methods, *etc* [185,186]. For all the reasons discussed above, obtaining reproducible results via the plant-

AgNPs synthesis is very difficult as one cannot control the chemical composition of the extract. Moreover, when the effect of the concentration of the extract is discussed in the literature, either the volume or the percentage of the extract is used, which is not a standardized unit and is only useful in comparing the results within the same study. Therefore, a standardized measurement(s) of the plant extract is necessary to control the reproducibility of metal nanoparticles biosynthesis. This standard measurement(s) is needed to characterize the plant extract, but it has to be completely independent of the species, the chemotype, or the seasonal variability.

From a thermodynamic point of view, the wet chemical reduction of Ag^+ is determined by the difference between the metal ions redox system and the reducing molecule redox system which should be positive [141], and the more positive it is, the more spontaneous the reaction is. And as discussed above, the biological pathway (using plants and microorganisms) is technically, a chemical reduction technique that was considered a new approach for the sake of its eco-friendliness and cost-effectiveness. Thus, the use of the “redox potential” of plant extracts instead of the concentration may achieve the required standardization of measurable parameters.

I.2.3) Important Silver nanoparticles parameters

I.2.3.1) Size distribution

The unique properties of silver nanoparticles come mainly from their nanometric size and quantum confinement effect, which enable them to have different properties in comparison to the bulk form, and therefore, allow them to have multiple applications in various domains [187]. Indeed, All AgNPs properties are size-dependent, making size and size distribution the most important factors regarding AgNPs. For example, higher antimicrobial activity has been found for smaller AgNPs nanoparticles [187–189]. Also, the catalytic activity of AgNPs was found to be size-dependent as was reported for the reduction of 4-nitrophenol [190] and methylene Blue [191]. Indeed, Priya and Asharani, (2017) [190] have studied the effect of AgNPs size (20, 35, and 60 nm) in the reduction of 4-nitrophenol and have found that the constant rate is inversely proportional to the size of AgNPs. The size-dependent activity of AgNPs is explained by the larger surface area of small nanoparticles compared to bigger ones, leading to more or better interactions between AgNPs and microorganisms (antibacterial activity) or substrates (catalytic activity). Moreover, in the case of antibacterial activity, there are also more Ag ions released as NPs get smaller [191].

I.2.3.2) Shape

The shape is another important parameter for silver nanoparticles' properties as many of their properties are also shape-dependent. For example, Cheon *et al.*, (2019) [192] have reported the greatest antibacterial activity for spherical AgNPs followed by disk AgNPs and then triangular plate AgNPs. The authors explained this trend by the difference in surface area between the different shapes. Other studies have also demonstrated the shape-dependence for the catalytic activity of AgNPs [193,194]. Interestingly, the effect of the shape can be different not only between catalytic and antibacterial properties but also within different catalytic systems. Indeed, the results found for the catalytic oxidation of hydrazine [194] showed that shapes rich in {111} crystallographic planes (e.g., nanospheres) showed higher catalytic activity than those rich in {100} planes (e.g., nanocubes), which was explained by the presence of the hcp lamellar defects on the {111} crystallographic planes. However, the opposite was found for the catalytic oxidation of styrene [193] and it was explained by the higher surface energy of the different crystallographic planes (*i.e.*, $\gamma\{110\} > \gamma\{100\} > \gamma\{111\}$), suggesting that the effect of shape may also be dependent on the catalytic system.

I.2.3.3) Surface charge

The surface charge of AgNPs is determined by measuring the Zeta Potential, which is the difference in potential between the inner Helmholtz layer near the nanoparticle surface and the liquid surrounding nanoparticles [195]. AgNPs with values far from zero (negative or positive) tend to repel each other, thus, preventing their aggregation. Besides its important role in AgNPs' stability, it was also proven that the functional properties of AgNPs are dependent on their surface charges. Abbaszadegan *et al.*, (2015) demonstrated the impact of the surface charge on the antibacterial activity of AgNPs [196]. Indeed, positively charged AgNPs have shown higher antibacterial activity against both gram-positive (*S. aureus*, *Streptococcus mutans*, and *Streptococcus pyogenes*) and gram-negative (*E. coli* and *Proteus vulgaris*) bacteria, followed by the neutral AgNPs, and finally the negatively charged AgNPs [196]. This is explained by the electrostatic interaction between AgNPs and the negatively-charged bacteria, which decreases as the AgNPs surface charge gets more negative due to repulsions between similar charges.

I.2.4) Stability of silver nanoparticles

AgNPs stability is another important parameter that should be taken into consideration for final AgNPs properties. Stability can be defined as the preservation of nanoparticles' size and dispersion. As the surface area increases in nanoparticles compared to the bulk structure, their surface energy also increases which makes nanostructures, thermodynamically unfavored. Therefore, the stability of nanostructures can only exist for a finite period of time [197]. The instability of silver nanoparticles originates either from aggregation or dissolution. The aggregation of AgNPs is favored by Zeta potential values close to zero [198]. On the other hand, the AgNPs dissolution by oxidizing agents (molecular oxygen or H₂O₂) results in the release of silver ions and the disintegration of AgNPs over time [198].

The preservation of AgNPs dispersion is essential for maintaining the AgNPs' size and shape, and therefore AgNPs' properties such as the antibacterial and catalytic activities. Aggregation can be avoided or limited over a finite period by using electrostatic, steric, or electrosteric stabilization (Fig. I.14) [199]. In that sense, polymers and surfactants were used mainly to increase AgNPs stability over time [199,200]. Indeed, Kvittek *et al.*, (2008) [199] have tested multiple surface stabilizers on the stability of AgNPs such as sodium dodecyl sulfate (SDS), polysorbate 80, and PVP. The anionic surfactant SDS was found to be the most effective stabilizer via both electrostatic (Doubled Zeta potential value) and steric repulsion, whereas the polymer PVP and the non-ionic surfactant (Polysorbate 80) have shown a lesser effect on AgNPs stability. Bae *et al.*, (2011) [200] have also tested multiple surfactants (SDS, sodium dodecylbenzenesulfonate “NaDDBS”, Tween 80, and CTAB) and polymers (PVP, Polyacrylamide “PAA”, polyalkylamine hydrochlorid “PAH” and Carboxymethyl cellulose “CMC”) differing in their charge and molecular weight on the colloidal stability of AgNPs, and have also confirmed that anionic surfactants (SDS and NaDDBS) were more effective compared to other cationic, non-ionic surfactants. Moreover, polymers (ionic and non-ionic) showed the lowest enhancement potential compared to surfactants. This was explained by the viscosity of polymers compared to surfactants.

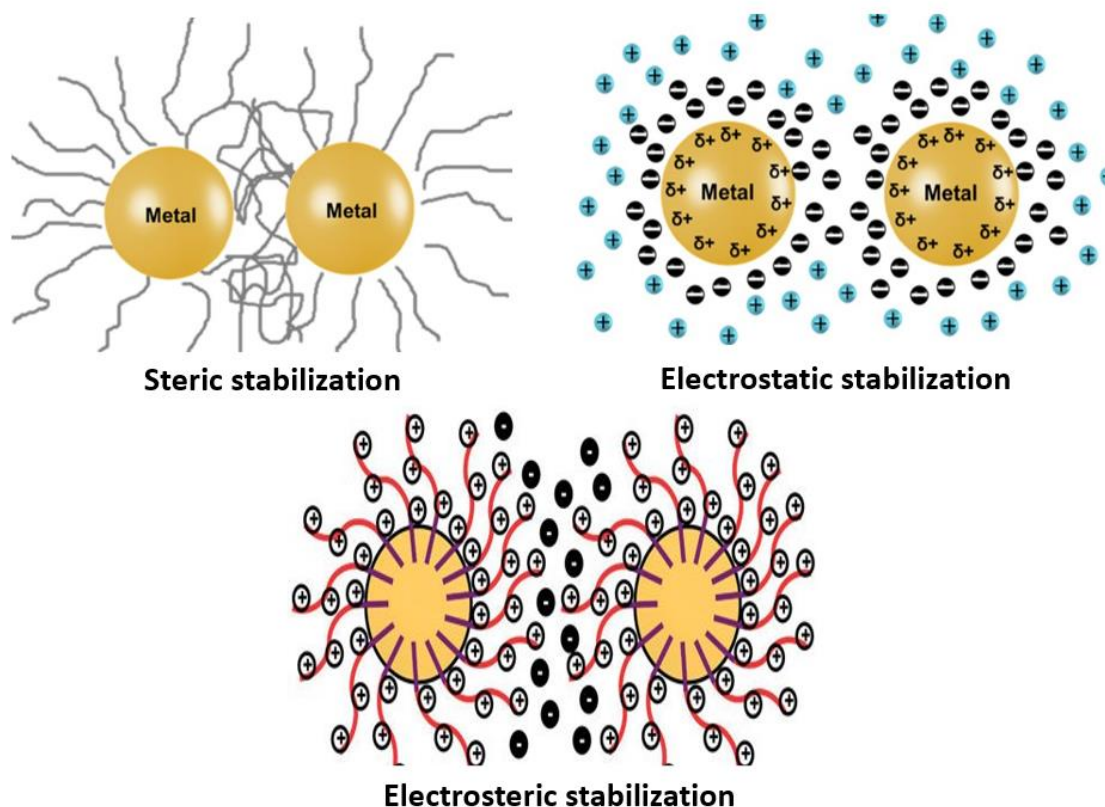


Figure I.14: Schematic representation of the steric, electrostatic, and electrosteric stabilization of silver nanoparticles [201,202].

I.2.5) Factors influencing plant-mediated AgNPs synthesis

Plant-mediated AgNPs synthesis follows the same principle as the wet chemical reduction method, therefore, it is influenced by the same factors such as pH, temperature, and silver salt concentration. Additionally, these syntheses are influenced by specific factors such as the plant nature, the plant part used for the extraction, and the concentration of the plant extract.

I.2.5.1) Temperature

Several studies have assessed the effect of temperature on the plant-mediated synthesis of silver nanoparticles. Kaviya *et al.*, (2011) [203] have reported the synthesis of smaller AgNPs when the temperature was increased from 25°C to 60°C (10 nm vs 35 nm) as indicated by a blue shift of the SPR band. Similarly, Asimuddin *et al.*, (2020) [204] prepared Persimmon-AgNPs at different temperatures in the range of 25°C to 95°C and found that the size decreased from 50 nm (25°C) to 16 nm (95°C). This effect of temperature is explained by an increase in the reaction rate because, generating thus a high number of nuclei, therefore producing smaller NPs [203–205].

The effect of reaction temperature on the stability of silver nanoparticles is reported only in a few studies. Mishra *et al.*, (2015) [206] have reported the instability of AgNPs synthesized using *Averrhoa carambola* extract and reaction temperature above 60°C. This was explained by the degradation of *A. carambola* biomolecules at high temperatures. Other studies have used the Zeta potential values to predict the potential stability of AgNPs. Anbu *et al.*, (2019) [207] noticed an increase in Zeta Potential from -5.23 to 11.25mV when they varied the temperature from 37°C to 50°C, respectively. The authors concluded that the NPs with more negative Zeta potential values are more stable. Nevertheless, this conclusion is erroneous as they ought to compare the absolute values rather than the negativity of Zeta Potential. Moreover, the use of Zeta potential measurement to predict the stability of AgNPs, predict only their aggregation behavior and not the dissolution process.

I.2.5.2) pH

The pH of the AgNPs synthesis reaction influences the charge of biomolecules, which modify their reducing and capping behavior [208]. Yang and Li (2013) [209] have tested the effect of a wide range of pH values on the Mango peel extract mediated AgNPs synthesis. They have shown a decrease in size (from 27 to 15 nm), when pH values were increased (from pH 3 to 11). These data were explained by the possibility of deprotonation of mango peel extract molecules. Similar results were found using Rudanti fruit extract [210] where AgNPs prepared at higher pH values showed a smaller and narrower size distribution. On the other hand, different observations were also reported in the literature [211,212]. Indeed, Krishnaraj *et al.*, (2012) [211] showed the synthesis of smaller AgNPs using *Acalypha indica* extract occurred optimally at neutral pH. At acidic pH, no synthesis was observed due to the protonation of biomolecules, which decreases the interactions between reducing agents and silver ions. On the contrary, at alkaline pH 13, agglomeration was observed immediately due to partial hydrolysis of silver ions forming Bioorganic–Ag(OH)_x or Bioorganic–Ag(NH₃)₂ complex on the surface of the nanoparticles and AgOH/Ag₂O colloid [213,214].

The reports on the effect of pH on the stability of biosynthesized AgNPs are scarce. Saware and Venkataraman (2004) [215] have prepared AgNPs using *Ficus religiosa* extract and they obtained smaller AgNPs as pH was increased. However, their agglomeration for the higher pH values was observed within 24 hours. The opposite data was found in Nalawde *et al.*, (2014) study [216], where the stability has increased in reactions at pH values above 9.5. The Zeta potential values demonstrated that the stability is due to a more negative surface charge, which probably is the result of the deprotonation of *Acacia auriculiformis* molecules at higher pH

values. In summary, the contribution of alkaline pH values to the stability of silver nanoparticles may be due to the deprotonation of biomolecules that are involved in the capping of AgNPs, as indicated by the more negative Zeta Potential values [217].

I.2.5.3) Silver salt concentration

The silver salt concentration has an important role in the characteristics of silver nanoparticles. Yang and Li (2013) [209] have studied the AgNPs synthesis using *Mangifera indica* peel extract at different concentrations of AgNO₃ in the range of 0.5 to 4 mM. They showed an increase in AgNPs size with the increase in silver salt concentration. The authors suggested that at a higher Ag salt concentration, Ag⁺ could be adsorbed on the first formed AgNPs where a second reduction would occur leading to an increase in the size of these AgNPs. Although this conclusion was confirmed in other studies [218,219], some other works have reported opposite observations [220,221]. For example, Seifipour *et al.*, (2020) [221] have tested concentrations ranging from 1 to 20 mM and found that AgNPs size decreases when Ag⁺ concentration is increased up to 2.5 mM. But above this concentration, they observed an increase in AgNPs size due to the continuous growth of AgNPs in excess of silver ions.

I.2.5.4) Plant extract concentration

The effect of plant extract concentration on the synthesis of AgNPs was widely studied, but opposite results were reported. Jain and Mehata (2017) [208] have reported an increase in AgNPs size when the ratio of AgNO₃: Tulsi extract (mL: mL) was increased from 5:0.1 to 5:0.5. This trend was also found in other studies using *A. indica* extract [183] and *Ziziphus jujuba* extract [222]. This could be explained by the extract promoting secondary reduction reactions on the silver ions adsorbed on the already formed nuclei or NPs. On the other hand, other studies have reported a decrease in size with the increase in extract concentration [223–225]. Indeed, Amin *et al.*, (2012) [223] have tested different concentrations of *Solanum xanthocarpum* extract by varying the volume of the extract and reported a decrease in size when 10 mL of the extract was used instead of 2 mL. This could be due to the increase in reducing molecules in the reaction medium.

I.2.5.5) Summary of parameters affecting AgNPs synthesis

The effect of the most important parameters such as temperature, pH, extract concentration, and silver salt concentration has been discussed above. These studies have shown contradictory data for each parameter, therefore making it difficult to draw clear conclusions about the effect of these parameters on AgNPs synthesis, activities, and stability. For instance, alkaline pH was reported to enhance the synthesis of silver nanoparticles in most reports. However, other studies

have observed agglomeration when alkaline pH was tested. Similarly, the effect of the concentration of the extract is obscure as the literature reports contradicting findings. The ambiguity of the effect of silver salt concentration was less apparent, but reported. The main reason is that most studies test these parameters individually (while everything else is being fixed) rather than the interaction between them. For instance, in a study by Liu *et al.*, (2020) [226], the effect of temperature on the *Cinnamomum camphora* mediated AgNPs was studied under both sufficient and insufficient Ag^+ concentrations. The results indicated that under sufficient Ag^+ concentrations, the size increased with temperature due to the increase of growth rate constant K_2 (Fig. I.15A). Under insufficient Ag^+ , the size increased in the range of 70-80°C due to a higher increase in the growth rate constant K_2 compared to the nucleation rate constant. While above 80°C, the size decreased sharply due to the sharp decrease in K_1 between 80 and 90°C (Fig. I.15B).

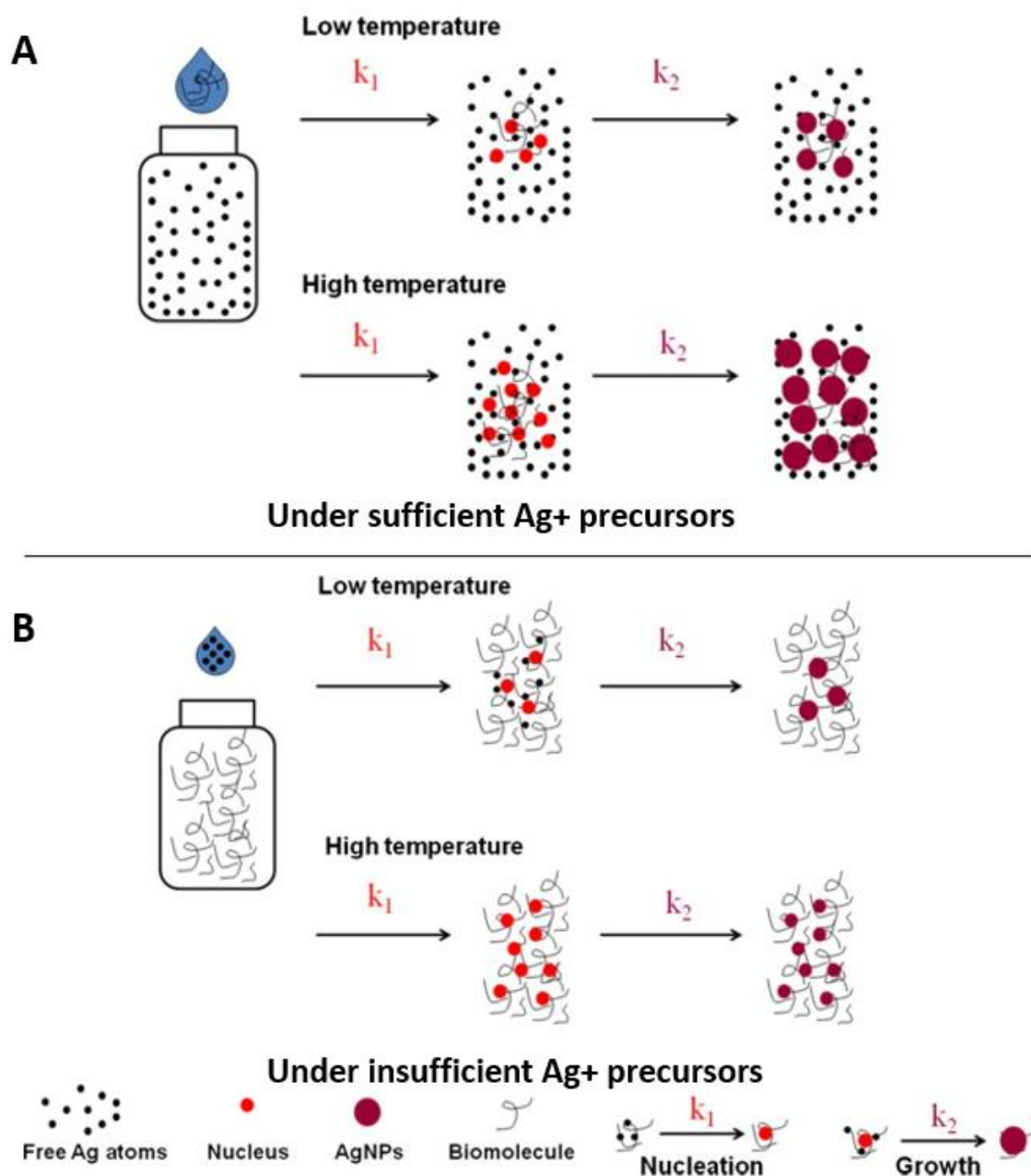


Figure I.15: illustration of the effect of temperature on the biosynthesis of AgNPs under A) sufficient Ag⁺ precursors, B) insufficient Ag⁺ precursors [226].

Similarly, Elemike *et al.*, (2017) [227] studied the interaction between the pH and the ratio concentration of leaf extract from *Lasienthra africanum* to AgNO₃. They found that for a ratio of 1:5, smaller nanoparticles were favored at alkaline pH, but for the ratio of 1:10, the neutral pH was more favorable for the synthesis of smaller AgNPs. The authors explained these observations by the effect of pH on the partial hydrolysis of Ag⁺ (In excess) to form bioorganic-Ag(OH)_x on the surface of the particles.

I.2.6) Antibacterial activity of silver nanoparticles

One of the most exploited properties of AgNPs is their antibacterial activity. Indeed, AgNPs' applications in medical products, medical devices, textiles, and water treatment are primarily owed to their excellent antibacterial activity [143]. AgNPs were found effective against a wide range of bacteria including Multidrug-resistant bacteria (MRBs); such as methicillin-resistant *Staphylococcus aureus* (MRSA), methicillin-resistant *Staphylococcus epidermidis* (MRSE) [228], multidrug-resistant *Pseudomonas aeruginosa* [229], *Klebsiella pneumoniae*, and *Acinetobacter baumannii* at concentrations that are non-toxic to human cells [230]. Thus, these nanoparticles are considered an interesting alternative to antibiotics due to the development of bacterial resistance to antibiotics [143].

I.2.6.1) Mechanism

Even though the exact mechanism of AgNPs antibacterial activity is not entirely elucidated, there are three ways by which AgNPs exert an antibacterial activity (Fig I.16), (i) by liberating silver ions (Ag^+), (ii) by acting directly on the bacterial cell, and (iii) by generating Reactive oxygen species (ROS). AgNPs undergo oxidative dissolution, releasing electronegative Ag ions with high affinity to electrons donating groups that exist on the bacterial membrane and proteins like phosphate, carbonyl, sulfhydryl, and amine groups [231] which leads to the disruption of the bacterial membrane permeability and the deactivation of proteins. Moreover, Ag^+ ions adhere also to other biomolecules such as DNA and RNA, thus disrupting the transcription, protein synthesis, and cell functioning overall [232].

Silver nanoparticles also act directly on bacteria as they can attach and accumulate directly on the cell wall and the bacterial membrane causing several morphological changes. Indeed, AgNPs can attach to membrane proteins, fatty acids, and carbohydrates, thus, interfering with the membrane permeability, the respiratory chain, cell division, and ions transport. Due to the importance of the impact of AgNPs on the bacterial membrane and cell wall, Gram-positive bacteria are less susceptible to AgNPs compared to Gram-negative bacteria because of their thicker cell wall and the presence of more peptidoglycan [232].

AgNPs can also interfere with bacterial survival by generating ROS either directly or via Ag^+ release causing oxidative stress. ROS are generated under normal circumstances but eliminated by natural antioxidant mechanisms of the cell. However, AgNPs and Ag^+ can interfere with the bacterial respiratory chain dehydrogenase leading to an excessive generation of ROS. AgNPs can also interfere with the antioxidant system of the bacteria (catalase, superoxide dismutase,

and Glutathione), thus inhibiting the elimination of ROS. ROS are highly reactive and cause cell lipid peroxidation, DNA damage, and apoptosis [233,234].

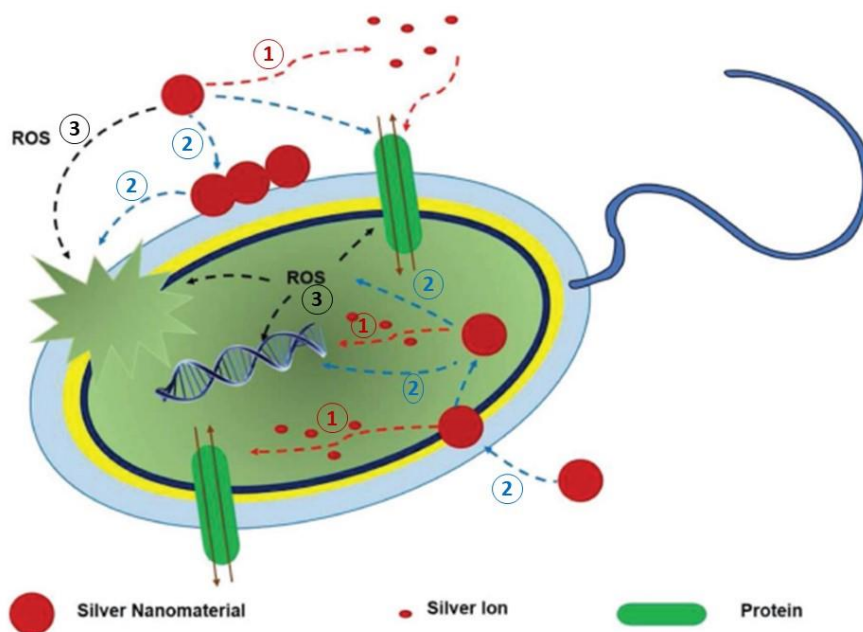


Figure I.16: The potential antibacterial mechanisms of AgNPs: 1) release of silver 2) AgNPs binding directly to the membrane and membrane protein, 3) Generation of ROS [232].

I.2.6.2) Bacterial resistance against AgNPs

The use of AgNPs as antibacterial agents to replace antibiotics is of increasing importance. Even though their antibacterial activity is well established against a wide range of bacteria including MRBs, bacterial resistance to AgNPs is not well studied. As previously shown, AgNPs exhibit a very diverse mechanism of action against multiple components of bacteria, which decreases the bacterial ability to develop resistance [234]. However, few studies reported that bacteria can develop resistance against AgNPs [235,236]. Indeed, Panáček *et al.*, (2018) [235] have tested subinhibitory concentrations of AgNPs against Gram-negative bacteria *E. coli* CCM3954, *E.coli* 013, and *P.aeruginosa* CCM3955 and found a gradual increase of the minimal inhibitory concentration (MIC) by each culture step. All the tested bacteria developed phenotypic resistance at the 13th step at most. This resistance was attributed to the production of flagellin, an adhesive flagellum protein that causes the aggregation of AgNPs.

I.2.6.3) Enhancement of antibacterial activity of AgNPs through functionalization.

The antibacterial activity of silver nanoparticles is dependent on multiple parameters such as AgNPs size and surface charge. Consequently, this antibacterial activity can be enhanced by

decreasing the AgNPs size or increasing their zeta Potential values toward more positive ones (See **I.2.3.1.** and **I.2.3.3.**). Furthermore, the enhancement of antibacterial activity can be attained by using other methods such as functionalization.

Indeed, several molecules have been used to functionalize AgNPs to enhance their antibacterial activity. For example, Ahmed *et al.*, (2017) [237] modified the surface of AgNPs using chitosan which increased their antibacterial activity against *E. coli*. In another study, Bhargava *et al.*, (2018) [238], functionalized AgNPs using L-fucose, a molecule that binds to LecB lectin on the bacterial cell. L-fucose functionalized AgNPs showed higher antibacterial activity against *P. aeruginosa* compared to citrate-capped AgNPs.

Antibiotics are also used to enhance the antibacterial activity of AgNPs *via* functionalization. For instance, tetracycline improved the antibacterial activity of AgNPs against *P. aeruginosa*, *E. coli*, *Klebsiella pneumoniae*, *S. aureus*, and *S. epidermidis* [239]. Finally, surfactants are another class of molecules known for their antibacterial activity, that were used to enhance the antibacterial activity of AgNPs. Indeed, Sodium dodecyl sulfate-capped AgNPs showed a much higher antibacterial activity against *P. aeruginosa* compared to other AgNPs [240].

I.2.7) conclusion

Conventional food packaging materials such as PE, PS, and PA are widely used to protect food by acting as a passive barrier between the external environment and food. However, these petroleum-based polymers are non-biodegradable, thus they raise a huge environmental concern. Moreover, they do not provide antimicrobial protection to packaged food, which is a feature in high demand due to the rising threat that microbial food contaminations pose. For these reasons, finding alternatives is of utmost importance. Such alternatives need to i) be biodegradable and ecofriendly, ii) have comparable thermal, mechanical, and barrier properties to conventional plastics, and iii) exhibit antibacterial activity.

Biodegradable polymers, either petroleum-based (PCL) or natural (PLA, or Chitosan) are excellent alternatives to conventional plastics due to their biodegradability and biocompatibility. However, they usually lack other important features such as thermal, barrier, and mechanical properties. Thus, as a first step, it is necessary to enhance these properties. In that regard, multiple techniques have been used. Among these, the preparation of nanocomposites is an overall more advantageous approach as it allows the enhancement of properties using small content of fillers. Fillers such as MMT, BNT, and mica have, thus, been

widely used to enhance the thermal, mechanical, and barrier properties of biodegradable polymers.

A second step toward the development of antibacterial biodegradable materials is the incorporation of antibacterial agents. Usually, organic extracts with known antibacterial activity are used (*e.g.*, Essential oils). However, these extracts affect the organoleptic properties of packaged food. Thus, wide attention has been paid recently to metal nanoparticles as an alternative to organic extracts. Particularly, silver nanoparticles are excellent antibacterial agents with low migration behavior, thus they are less likely to affect the organoleptic properties of food.

Silver nanoparticles can be prepared through chemical, physical, or biological pathways. However, the chemical and physical methods are usually non-ecofriendly, expensive, and require high energy consumption. Biological methods, especially using plant extracts, are an excellent alternative because they are cheaper, greener, and usually simpler. Moreover, AgNPs' antibacterial activity depends greatly on their size and stability among other parameters. Thus, the optimization of AgNPs synthesis in terms of size and stability is primordial to their use as antibacterial nanofillers.

In this thesis, we aimed to develop biodegradable polymer-based nanocomposites with enhanced properties and antibacterial activity for the potential use in active antibacterial food packaging. In chapter II, petroleum-based PCL was used as a polymeric matrix to prepare PCL-BNT nanocomposites using a “*grafting from*” ring-opening polymerization approach. CTAB-modified BNT was used as a nanofiller to enhance PCL properties and to provide antibacterial activity *via* the CTAB modification. In chapter III, PLA-Mica-AgNPs were prepared using melt extrusion exploiting thus, the potential of mica to enhance PLA properties and commercial AgNPs to provide the antibacterial activity to the resulting nanocomposites. In chapter IV, we aimed to optimize the green synthesis of silver nanoparticles using rosemary extract and to further enhance their stability using surfactants such as CTAB, SDS, and Tween 80. And finally, in chapter V, the optimized AgNPs were used as an additive for the preparation of chitosan nanocomposites for potential applications in antibacterial food packaging.

Reference

- [1] R.L. Scharff, Health-Related Costs from Foodborne Illness in the United States, (2010).
- [2] J. Gustavsson, C. Cederberg, U. Sonesson, R.V. Otterdijk, A. Meybeck, Global food losses and food waste: extent, causes and prevention, Undefined. (2011). <https://www.semanticscholar.org/paper/Global-food-losses-and-food-waste%3A-extent%2C-causes-Gustavsson-Cederberg/19c0065b1ad3f83f5ce7b0b16742d137d0f2125e> (accessed March 8, 2022).
- [3] T. Huang, Y. Qian, J. Wei, C. Zhou, Polymeric Antimicrobial Food Packaging and Its Applications, *Polymers*. 11 (2019) 560. <https://doi.org/10.3390/polym11030560>.
- [4] N.A. Al-Tayyar, A.M. Youssef, R. Al-hindi, Antimicrobial food packaging based on sustainable Bio-based materials for reducing foodborne Pathogens: A review, *Food Chem*. 310 (2020) 125915. <https://doi.org/10.1016/j.foodchem.2019.125915>.
- [5] F. Luzi, L. Torre, J.M. Kenny, D. Puglia, Bio- and Fossil-Based Polymeric Blends and Nanocomposites for Packaging: Structure–Property Relationship, *Materials*. 12 (2019) 471. <https://doi.org/10.3390/ma12030471>.
- [6] E. Drago, R. Campardelli, M. Pettinato, P. Perego, Innovations in Smart Packaging Concepts for Food: An Extensive Review, *Foods*. 9 (2020) 1628. <https://doi.org/10.3390/foods9111628>.
- [7] Commission Regulation (EC) No 450/2009 of 29 May 2009 on act... - EUR-Lex, (n.d.). <https://eur-lex.europa.eu/legal-content/en/LSU/?uri=CELEX%3A32009R0450> (accessed April 3, 2022).
- [8] R. Chawla, S. Sivakumar, H. Kaur, Antimicrobial edible films in food packaging: Current scenario and recent nanotechnological advancements- a review, *Carbohydr. Polym. Technol. Appl*. 2 (2021) 100024. <https://doi.org/10.1016/j.carpta.2020.100024>.
- [9] M. del R. Moreira, S.I. Roura, A. Ponce, Effectiveness of chitosan edible coatings to improve microbiological and sensory quality of fresh cut broccoli, *LWT - Food Sci. Technol*. 44 (2011) 2335–2341. <https://doi.org/10.1016/j.lwt.2011.04.009>.
- [10] M.C. Cruz-Romero, T. Murphy, M. Morris, E. Cummins, J.P. Kerry, Antimicrobial activity of chitosan, organic acids and nano-sized solubilisates for potential use in smart antimicrobially-active packaging for potential food applications, *Food Control*. 34 (2013) 393–397. <https://doi.org/10.1016/j.foodcont.2013.04.042>.
- [11] R. Irkin, O.K. Esmer, Novel food packaging systems with natural antimicrobial agents, *J. Food Sci. Technol*. 52 (2015) 6095–6111. <https://doi.org/10.1007/s13197-015-1780-9>.
- [12] R. Priyadarshi, Sauraj, B. Kumar, F. Deeba, A. Kulshreshtha, Y.S. Negi, Chitosan films incorporated with Apricot (*Prunus armeniaca*) kernel essential oil as active food packaging material, *Food Hydrocoll*. 85 (2018) 158–166. <https://doi.org/10.1016/j.foodhyd.2018.07.003>.
- [13] F. Li, C. Zhang, Y. Weng, Improvement of the Gas Barrier Properties of PLA/OMMT Films by Regulating the Interlayer Spacing of OMMT and the Crystallinity of PLA, *ACS Omega*. 5 (2020) 18675–18684. <https://doi.org/10.1021/acsomega.0c01405>.
- [14] A. Roy, O. Bulut, S. Some, A.K. Mandal, M.D. Yilmaz, Green synthesis of silver nanoparticles: biomolecule-nanoparticle organizations targeting antimicrobial activity, *RSC Adv*. 9 (2019) 2673–2702. <https://doi.org/10.1039/C8RA08982E>.

- [15] Y.Y. Loo, Y. Rukayadi, M.-A.-R. Nor-Khaizura, C.H. Kuan, B.W. Chieng, M. Nishibuchi, S. Radu, In Vitro Antimicrobial Activity of Green Synthesized Silver Nanoparticles Against Selected Gram-negative Foodborne Pathogens, *Front. Microbiol.* 9 (2018). <https://www.frontiersin.org/article/10.3389/fmicb.2018.01555> (accessed June 13, 2022).
- [16] R.K. Dhall, Advances in Edible Coatings for Fresh Fruits and Vegetables: A Review, *Crit. Rev. Food Sci. Nutr.* 53 (2013) 435–450. <https://doi.org/10.1080/10408398.2010.541568>.
- [17] K. Kraśniewska, S. Galus, M. Gniewosz, Biopolymers-Based Materials Containing Silver Nanoparticles as Active Packaging for Food Applications—A Review, *Int. J. Mol. Sci.* 21 (2020) 698. <https://doi.org/10.3390/ijms21030698>.
- [18] L. Genovese, M. Soccio, N. Lotti, M. Gazzano, V. Siracusa, E. Salatelli, F. Balestra, A. Munari, Design of biobased PLLA triblock copolymers for sustainable food packaging: Thermo-mechanical properties, gas barrier ability and compostability, *Eur. Polym. J.* 95 (2017) 289–303. <https://doi.org/10.1016/j.eurpolymj.2017.08.001>.
- [19] N. Rasana, K. Jayanarayanan, Polypropylene/short glass fiber/nanosilica hybrid composites: evaluation of morphology, mechanical, thermal, and transport properties, *Polym. Bull.* 75 (2018) 2587–2605. <https://doi.org/10.1007/s00289-017-2173-1>.
- [20] A. Arora, G. w. Padua, Review: Nanocomposites in Food Packaging, *J. Food Sci.* 75 (2010) R43–R49. <https://doi.org/10.1111/j.1750-3841.2009.01456.x>.
- [21] K. Müller, E. Bugnicourt, M. Latorre, M. Jorda, Y. Echegoyen Sanz, J.M. Lagaron, O. Miesbauer, A. Bianchin, S. Hankin, U. Bölz, G. Pérez, M. Jesdinszki, M. Lindner, Z. Scheuerer, S. Castelló, M. Schmid, Review on the Processing and Properties of Polymer Nanocomposites and Nanocoatings and Their Applications in the Packaging, Automotive and Solar Energy Fields, *Nanomaterials.* 7 (2017) 74. <https://doi.org/10.3390/nano7040074>.
- [22] A. Alateyah, H. Dhakal, Z. Zhang, Processing, properties, and applications of polymer nanocomposites based on layer silicates: a review, *Adv. Polym. Technol.* 32 (2013) 21368. <https://doi.org/10.1002/adv.21368>.
- [23] C. Shuai, G. Liu, Y. Yang, F. Qi, S. Peng, W. Yang, C. He, G. Wang, G. Qian, A strawberry-like Ag-decorated barium titanate enhances piezoelectric and antibacterial activities of polymer scaffold, *Nano Energy.* 74 (2020) 104825. <https://doi.org/10.1016/j.nanoen.2020.104825>.
- [24] S.-L. Bee, M.A.A. Abdullah, S.-T. Bee, L.T. Sin, A.R. Rahmat, Polymer nanocomposites based on silylated-montmorillonite: A review, *Prog. Polym. Sci.* 85 (2018) 57–82. <https://doi.org/10.1016/j.progpolymsci.2018.07.003>.
- [25] S.Y. Hwang, E.S. Yoo, S.S. Im, The synthesis of copolymers, blends and composites based on poly(butylene succinate), *Polym. J.* 44 (2012) 1179–1190. <https://doi.org/10.1038/pj.2012.157>.
- [26] R.T. Thimma, N.S. Reddy, S. Tammishetti, Synthesis and characterization of guar gum-graft-polyacrylonitrile, *Polym. Adv. Technol.* 14 (2003) 663–668. <https://doi.org/10.1002/pat.372>.
- [27] J.-M. Raquez, Y. Habibi, M. Murariu, P. Dubois, Polylactide (PLA)-based nanocomposites, *Prog. Polym. Sci.* 38 (2013) 1504–1542. <https://doi.org/10.1016/j.progpolymsci.2013.05.014>.
- [28] E. Omanović-Miklićanin, A. Badnjević, A. Kazlagić, M. Hajlovac, Nanocomposites: a brief review, *Health Technol.* 10 (2020) 51–59. <https://doi.org/10.1007/s12553-019-00380-x>.

- [29] M. Muhammed Shameem, S.M. Sasikanth, R. Annamalai, R. Ganapathi Raman, A brief review on polymer nanocomposites and its applications, *Mater. Today Proc.* 45 (2021) 2536–2539. <https://doi.org/10.1016/j.matpr.2020.11.254>.
- [30] S. Farah, D.G. Anderson, R. Langer, Physical and mechanical properties of PLA, and their functions in widespread applications — A comprehensive review, *Adv. Drug Deliv. Rev.* 107 (2016) 367–392. <https://doi.org/10.1016/j.addr.2016.06.012>.
- [31] N. Hamadneh, W. Khan, W. Khan, Polymer nanocomposites – synthesis techniques, classification and properties, in: 2016.
- [32] J.H. Lee, D. Jeong, P. Kanmani, Study on physical and mechanical properties of the biopolymer/silver based active nanocomposite films with antimicrobial activity, *Carbohydr. Polym.* 224 (2019) 115159. <https://doi.org/10.1016/j.carbpol.2019.115159>.
- [33] J. Jordan, K.I. Jacob, R. Tannenbaum, M.A. Sharaf, I. Jasiuk, Experimental trends in polymer nanocomposites—a review, *Mater. Sci. Eng. A.* 393 (2005) 1–11. <https://doi.org/10.1016/j.msea.2004.09.044>.
- [34] I.-Y. Jeon, J.-B. Baek, Nanocomposites Derived from Polymers and Inorganic Nanoparticles, *Materials*. 3 (2010) 3654–3674. <https://doi.org/10.3390/ma3063654>.
- [35] M. Labet, W. Thielemans, Synthesis of polycaprolactone: a review, *Chem. Soc. Rev.* 38 (2009) 3484–3504. <https://doi.org/10.1039/B820162P>.
- [36] R.M. Mohamed, K. Yusoh, A Review on the Recent Research of Polycaprolactone (PCL), *Adv. Mater. Res.* 1134 (2016) 249–255. <https://doi.org/10.4028/www.scientific.net/AMR.1134.249>.
- [37] P. Mandal, R. Shunmugam, Polycaprolactone: a biodegradable polymer with its application in the field of self-assembly study, *J. Macromol. Sci. Part A.* 58 (2021) 111–129. <https://doi.org/10.1080/10601325.2020.1831392>.
- [38] T. El Assimi, Roko Blažic, A. El Kadib, M. Raihane, R. Beniazza, G.A. Luinstra, E. Vidović, M. Lahcini, Synthesis of poly(ϵ -caprolactone)-grafted guar gum by surface-initiated ring-opening polymerization, *Carbohydr. Polym.* 220 (2019) 95–102. <https://doi.org/10.1016/j.carbpol.2019.05.049>.
- [39] A. Arbaoui, C. Redshaw, Metal catalysts for ϵ -caprolactone polymerisation, *Polym. Chem.* 1 (2010) 801–826. <https://doi.org/10.1039/B9PY00334G>.
- [40] X. Qi, Y. Ren, X. Wang, New advances in the biodegradation of Poly(lactic) acid, *Int. Biodeterior. Biodegrad.* 117 (2017) 215–223. <https://doi.org/10.1016/j.ibiod.2017.01.010>.
- [41] K. Hamad, M. Kaseem, M. Ayyoob, J. Joo, F. Deri, Polylactic acid blends: The future of green, light and tough, *Prog. Polym. Sci.* 85 (2018) 83–127. <https://doi.org/10.1016/j.progpolymsci.2018.07.001>.
- [42] A. Sharif, S. Mondal, M.E. Hoque, Polylactic Acid (PLA)-Based Nanocomposites: Processing and Properties, in: M.L. Sanyang, M. Jawaid (Eds.), *Bio-Based Polym. Nanocomposites Prep. Process. Prop. Perform.*, Springer International Publishing, Cham, 2019: pp. 233–254. https://doi.org/10.1007/978-3-030-05825-8_11.
- [43] J. Tan, M.A. Abdel-Rahman, K. Sonomoto, Biorefinery-Based Lactic Acid Fermentation: Microbial Production of Pure Monomer Product, in: M.L. Di Lorenzo, R. Androsch (Eds.), *Synth. Struct. Prop. Polylactic Acid*, Springer International Publishing, Cham, 2018: pp. 27–66. https://doi.org/10.1007/12_2016_11.
- [44] M.A. Abdel-Rahman, Y. Tashiro, K. Sonomoto, Recent advances in lactic acid production by microbial fermentation processes, *Biotechnol. Adv.* 31 (2013) 877–902. <https://doi.org/10.1016/j.biotechadv.2013.04.002>.
- [45] G. Li, M. Zhao, F. Xu, B. Yang, X. Li, X. Meng, L. Teng, F. Sun, Y. Li, Synthesis and Biological Application of Polylactic Acid, *Molecules*. 25 (2020) 5023. <https://doi.org/10.3390/molecules25215023>.

- [46] J.A. Byers, A.B. Biernesser, K.R. Delle Chiaie, A. Kaur, J.A. Kehl, Catalytic Systems for the Production of Poly(lactic acid), in: M.L. Di Lorenzo, R. Androsch (Eds.), *Synth. Struct. Prop. Polylactic Acid*, Springer International Publishing, Cham, 2018: pp. 67–118. https://doi.org/10.1007/12_2017_20.
- [47] S. Corneillie, M. Smet, PLA architectures: the role of branching, *Polym. Chem.* 6 (2015) 850–867. <https://doi.org/10.1039/C4PY01572J>.
- [48] K. Masutani, Y. Kimura, Chapter 1:PLA Synthesis. From the Monomer to the Polymer, in: *Polylactic Acid Sci. Technol.*, 2014: pp. 1–36. <https://doi.org/10.1039/9781782624806-00001>.
- [49] K. Enomoto, M. Ajioka, A. Yamaguchi, Polyhydroxycarboxylic acid and preparation process thereof, US5310865A, 1994. <https://patents.google.com/patent/US5310865A/en> (accessed April 3, 2022).
- [50] R. de Sousa Victor, A. Marcelo da Cunha Santos, B. Viana de Sousa, G. de Araújo Neves, L. Navarro de Lima Santana, R. Rodrigues Menezes, A Review on Chitosan's Uses as Biomaterial: Tissue Engineering, Drug Delivery Systems and Cancer Treatment, *Materials.* 13 (2020) 4995. <https://doi.org/10.3390/ma13214995>.
- [51] S.K. Shukla, A.K. Mishra, O.A. Arotiba, B.B. Mamba, Chitosan-based nanomaterials: A state-of-the-art review, *Int. J. Biol. Macromol.* 59 (2013) 46–58. <https://doi.org/10.1016/j.ijbiomac.2013.04.043>.
- [52] A. Ali, S. Ahmed, A review on chitosan and its nanocomposites in drug delivery, *Int. J. Biol. Macromol.* 109 (2018) 273–286. <https://doi.org/10.1016/j.ijbiomac.2017.12.078>.
- [53] V.G.L. Souza, J.R.A. Pires, C. Rodrigues, I.M. Coelho, A.L. Fernando, Chitosan Composites in Packaging Industry—Current Trends and Future Challenges, *Polymers.* 12 (2020) 417. <https://doi.org/10.3390/polym12020417>.
- [54] J. Li, S. Zhuang, Antibacterial activity of chitosan and its derivatives and their interaction mechanism with bacteria: Current state and perspectives, *Eur. Polym. J.* 138 (2020) 109984. <https://doi.org/10.1016/j.eurpolymj.2020.109984>.
- [55] R. Riva, H. Ragelle, A. des Rieux, N. Duhem, C. Jérôme, V. Prétat, Chitosan and Chitosan Derivatives in Drug Delivery and Tissue Engineering, in: R. Jayakumar, M. Prabakaran, R.A.A. Muzzarelli (Eds.), *Chitosan Biomater. II*, Springer, Berlin, Heidelberg, 2011: pp. 19–44. https://doi.org/10.1007/12_2011_137.
- [56] V. García Ibarra, R. Sendón, A. Rodríguez-Bernaldo de Quirós, Chapter 29 - Antimicrobial Food Packaging Based on Biodegradable Materials, in: J. Barros-Velázquez (Ed.), *Antimicrob. Food Packag.*, Academic Press, San Diego, 2016: pp. 363–384. <https://doi.org/10.1016/B978-0-12-800723-5.00029-2>.
- [57] S. Quintavalla, L. Vicini, Antimicrobial food packaging in meat industry, *Meat Sci.* 62 (2002) 373–380. [https://doi.org/10.1016/S0309-1740\(02\)00121-3](https://doi.org/10.1016/S0309-1740(02)00121-3).
- [58] B. Malhotra, A. Keshwani, H. Kharkwal, Antimicrobial food packaging: potential and pitfalls, *Front. Microbiol.* 6 (2015). <https://www.frontiersin.org/article/10.3389/fmicb.2015.00611> (accessed April 3, 2022).
- [59] A. Mousavi Khaneghah, S.M.B. Hashemi, S. Limbo, Antimicrobial agents and packaging systems in antimicrobial active food packaging: An overview of approaches and interactions, *Food Bioprod. Process.* 111 (2018) 1–19. <https://doi.org/10.1016/j.fbp.2018.05.001>.
- [60] I. Lukic, J. Vulic, J. Ivanovic, Antioxidant activity of PLA/PCL films loaded with thymol and/or carvacrol using scCO₂ for active food packaging, *Food Packag. Shelf Life.* 26 (2020) 100578. <https://doi.org/10.1016/j.fpsl.2020.100578>.
- [61] A. Rešček, L. Kratožil Krehula, Z. Katančić, Z. Hrnjak-Murgić, Active Bilayer PE/PCL Films for Food Packaging Modified with Zinc Oxide and Casein, *Croat. Chem. Acta.* 88 (2015) 461–473. <https://doi.org/10.5562/cca2768>.

- [62] I. Arvanitoyannis, E. Psomiadou, C.G. Biliaderis, H. Ogawa, N. Kawasaki, A. Nakayama, Biodegradable Films Made from Low Density Polyethylene (LDPE), Ethylene Acrylic Acid (EAA), PolyCaprolactone (PCL) and Wheat Starch for Food Packaging Applications: Part 3, *Starch - Stärke*. 49 (1997) 306–322. <https://doi.org/10.1002/star.19970490712>.
- [63] K. Wang, P.N. Lim, S.Y. Tong, E.S. Thian, Development of grapefruit seed extract-loaded poly(ϵ -caprolactone)/chitosan films for antimicrobial food packaging, *Food Packag. Shelf Life*. 22 (2019) 100396. <https://doi.org/10.1016/j.fpsl.2019.100396>.
- [64] Y. Qin, D. Liu, Y. Wu, M. Yuan, L. Li, J. Yang, Effect of PLA/PCL/cinnamaldehyde antimicrobial packaging on physicochemical and microbial quality of button mushroom (*Agaricus bisporus*), *Postharvest Biol. Technol.* 99 (2015) 73–79. <https://doi.org/10.1016/j.postharvbio.2014.07.018>.
- [65] T. Jin, J. b. Gurtler, Inactivation of Salmonella in liquid egg albumen by antimicrobial bottle coatings infused with allyl isothiocyanate, nisin and zinc oxide nanoparticles, *J. Appl. Microbiol.* 110 (2011) 704–712. <https://doi.org/10.1111/j.1365-2672.2011.04938.x>.
- [66] W. Yang, E. Fortunati, F. Dominici, G. Giovanale, A. Mazzaglia, G.M. Balestra, J.M. Kenny, D. Puglia, Synergic effect of cellulose and lignin nanostructures in PLA based systems for food antibacterial packaging, *Eur. Polym. J.* 79 (2016) 1–12. <https://doi.org/10.1016/j.eurpolymj.2016.04.003>.
- [67] W. Li, C. Zhang, H. Chi, L. Li, T. Lan, P. Han, H. Chen, Y. Qin, Development of Antimicrobial Packaging Film Made from Poly(Lactic Acid) Incorporating Titanium Dioxide and Silver Nanoparticles, *Molecules*. 22 (2017) 1170. <https://doi.org/10.3390/molecules22071170>.
- [68] S. Kumar, A. Mukherjee, J. Dutta, Chitosan based nanocomposite films and coatings: Emerging antimicrobial food packaging alternatives, *Trends Food Sci. Technol.* 97 (2020) 196–209. <https://doi.org/10.1016/j.tifs.2020.01.002>.
- [69] M.Z. Elsabee, E.S. Abdou, Chitosan based edible films and coatings: A review, *Mater. Sci. Eng. C*. 33 (2013) 1819–1841. <https://doi.org/10.1016/j.msec.2013.01.010>.
- [70] S.R. Kanatt, M.S. Rao, S.P. Chawla, A. Sharma, Effects of chitosan coating on shelf-life of ready-to-cook meat products during chilled storage, *LWT - Food Sci. Technol.* 53 (2013) 321–326. <https://doi.org/10.1016/j.lwt.2013.01.019>.
- [71] S.M. Ojagh, M. Rezaei, S.H. Razavi, S.M.H. Hosseini, Effect of chitosan coatings enriched with cinnamon oil on the quality of refrigerated rainbow trout, *Food Chem.* 120 (2010) 193–198. <https://doi.org/10.1016/j.foodchem.2009.10.006>.
- [72] Y.M. Tan, S.H. Lim, B.Y. Tay, M.W. Lee, E.S. Thian, Functional chitosan-based grapefruit seed extract composite films for applications in food packaging technology, *Mater. Res. Bull.* 69 (2015) 142–146. <https://doi.org/10.1016/j.materresbull.2014.11.041>.
- [73] M. Abdollahi, M. Rezaei, G. Farzi, Improvement of active chitosan film properties with rosemary essential oil for food packaging, *Int. J. Food Sci. Technol.* 47 (2012) 847–853. <https://doi.org/10.1111/j.1365-2621.2011.02917.x>.
- [74] L. Al-Naamani, S. Dobretsov, J. Dutta, Chitosan-zinc oxide nanoparticle composite coating for active food packaging applications, *Innov. Food Sci. Emerg. Technol.* 38 (2016) 231–237. <https://doi.org/10.1016/j.ifset.2016.10.010>.
- [75] S. Cesur, C. Koroğlu, H.T. Yalçın, Antimicrobial and biodegradable food packaging applications of polycaprolactone/organo nanoclay/chitosan polymeric composite films, *J. Vinyl Addit. Technol.* 24 (2018) 376–387. <https://doi.org/10.1002/vnl.21607>.
- [76] H. de V. Pina, A.J.A. de Farias, F.C. Barbosa, J.W. de L. Souza, A.B. de S. Barros, M.J.B. Cardoso, M.V.L. Fook, R.M.R. Wellen, Microbiological and cytotoxic perspectives of

- active PCL/ZnO film for food packaging, *Mater. Res. Express.* 7 (2020) 025312. <https://doi.org/10.1088/2053-1591/ab7569>.
- [77] S. Khalid, L. Yu, M. Feng, L. Meng, Y. Bai, A. Ali, H. Liu, L. Chen, Development and characterization of biodegradable antimicrobial packaging films based on polycaprolactone, starch and pomegranate rind hybrids, *Food Packag. Shelf Life.* 18 (2018) 71–79. <https://doi.org/10.1016/j.fpsl.2018.08.008>.
- [78] J.S. Lyu, J.-S. Lee, J. Han, Development of a biodegradable polycaprolactone film incorporated with an antimicrobial agent via an extrusion process, *Sci. Rep.* 9 (2019) 20236. <https://doi.org/10.1038/s41598-019-56757-5>.
- [79] T. Jin, L. Liu, H. Zhang, K. Hicks, Antimicrobial activity of nisin incorporated in pectin and polylactic acid composite films against *Listeria monocytogenes*, *Int. J. Food Sci. Technol.* 44 (2009) 322–329. <https://doi.org/10.1111/j.1365-2621.2008.01719.x>.
- [80] J. Bonilla, E. Fortunati, M. Vargas, A. Chiralt, J.M. Kenny, Effects of chitosan on the physicochemical and antimicrobial properties of PLA films, *J. Food Eng.* 119 (2013) 236–243. <https://doi.org/10.1016/j.jfoodeng.2013.05.026>.
- [81] C. Villegas, M.P. Arrieta, A. Rojas, A. Torres, S. Faba, M.J. Toledo, M.A. Gutierrez, E. Zavalla, J. Romero, M.J. Galotto, X. Valenzuela, PLA/organoclay bionanocomposites impregnated with thymol and cinnamaldehyde by supercritical impregnation for active and sustainable food packaging, *Compos. Part B Eng.* 176 (2019) 107336. <https://doi.org/10.1016/j.compositesb.2019.107336>.
- [82] B.S. Munteanu, Z. Aytac, G.M. Pricope, T. Uyar, C. Vasile, Polylactic acid (PLA)/Silver-NP/VitaminE bionanocomposite electrospun nanofibers with antibacterial and antioxidant activity, *J. Nanoparticle Res.* 16 (2014) 2643. <https://doi.org/10.1007/s11051-014-2643-4>.
- [83] S. Ediyilyam, B. George, S.S. Shankar, T.T. Dennis, S. Waclawek, M. Černík, V.V.T. Padil, Chitosan/Gelatin/Silver Nanoparticles Composites Films for Biodegradable Food Packaging Applications, *Polymers.* 13 (2021) 1680. <https://doi.org/10.3390/polym13111680>.
- [84] K. Shameli, M.B. Ahmad, W.M.Z. Yunus, N.A. Ibrahim, R.A. Rahman, M. Jokar, M. Darroudi, Silver/poly (lactic acid) nanocomposites: preparation, characterization, and antibacterial activity, *Int. J. Nanomedicine.* 5 (2010) 573–579. <https://doi.org/10.2147/IJN.S12007>.
- [85] E. Picard, E. Espuche, R. Fulchiron, Effect of an organo-modified montmorillonite on PLA crystallization and gas barrier properties, *Appl. Clay Sci.* 53 (2011) 58–65. <https://doi.org/10.1016/j.clay.2011.04.023>.
- [86] R. Salehyan, A.A. Yussuf, N.F. Hanani, A. Hassan, A. Akbari, Polylactic acid/polycaprolactone nanocomposite: Influence of montmorillonite and impact modifier on mechanical, thermal, and morphological properties, *J. Elastomers Plast.* 47 (2015) 69–87. <https://doi.org/10.1177/0095244313489906>.
- [87] S. Fu, Z. Sun, P. Huang, Y. Li, N. Hu, Some basic aspects of polymer nanocomposites: A critical review, *Nano Mater. Sci.* 1 (2019) 2–30. <https://doi.org/10.1016/j.nanoms.2019.02.006>.
- [88] R. Rafiee, R. Shahzadi, Mechanical Properties of Nanoclay and Nanoclay Reinforced Polymers: A Review, *Polym. Compos.* 40 (2019) 431–445. <https://doi.org/10.1002/pc.24725>.
- [89] A. Usuki, M. Kawasumi, Y. Kojima, A. Okada, T. Kurauchi, O. Kamigaito, Swelling behavior of montmorillonite cation exchanged for ω -amino acids by ϵ -caprolactam, *J. Mater. Res.* 8 (1993) 1174–1178. <https://doi.org/10.1557/JMR.1993.1174>.

- [90] Y. Kojima, A. Usuki, M. Kawasumi, A. Okada, T. Kurauchi, O. Kamigaito, Synthesis of nylon 6–clay hybrid by montmorillonite intercalated with ϵ -caprolactam, *J. Polym. Sci. Part Polym. Chem.* 31 (1993) 983–986. <https://doi.org/10.1002/pola.1993.080310418>.
- [91] F. Guo, S. Aryana, Y. Han, Y. Jiao, A Review of the Synthesis and Applications of Polymer–Nanoclay Composites, *Appl. Sci.* 8 (2018) 1696. <https://doi.org/10.3390/app8091696>.
- [92] T. Tang, X. Tong, Z. Feng, B. Huang, 6 - Poly(ethyl acrylate)/bentonite nanocomposites, in: Y.-W. Mai, Z.-Z. Yu (Eds.), *Polym. Nanocomposites*, Woodhead Publishing, 2006: pp. 172–187. <https://doi.org/10.1533/9781845691127.1.172>.
- [93] A.A. Sapalidis, F.K. Katsaros, Th.A. Steriotis, N.K. Kanellopoulos, Properties of poly(vinyl alcohol)—Bentonite clay nanocomposite films in relation to polymer–clay interactions, *J. Appl. Polym. Sci.* 123 (2012) 1812–1821. <https://doi.org/10.1002/app.34651>.
- [94] Y. Turhan, Z.G. Alp, M. Alkan, M. Doğan, Preparation and characterization of poly(vinylalcohol)/modified bentonite nanocomposites, *Microporous Mesoporous Mater.* 174 (2013) 144–153. <https://doi.org/10.1016/j.micromeso.2013.03.002>.
- [95] A.M. Motawie, M. Madani, E.A. Esmail, A.Z. Dacorry, H.M. Othman, M.M. Badr, D.E. Abulyazied, Electrophysical characteristics of polyurethane/organo-bentonite nanocomposites, *Egypt. J. Pet.* 23 (2014) 379–387. <https://doi.org/10.1016/j.ejpe.2014.09.005>.
- [96] G. Choudalakis, A.D. Gotsis, Permeability of polymer/clay nanocomposites: A review, *Eur. Polym. J.* 45 (2009) 967–984. <https://doi.org/10.1016/j.eurpolymj.2009.01.027>.
- [97] R.K. Bharadwaj, Modeling the Barrier Properties of Polymer-Layered Silicate Nanocomposites, *Macromolecules.* 34 (2001) 9189–9192. <https://doi.org/10.1021/ma010780b>.
- [98] C.C. Eng, N.A. Ibrahim, N. Zainuddin, H. Ariffin, W.M.Z.W. Yunus, Y.Y. Then, C.C. Teh, Enhancement of Mechanical and Thermal Properties of Polylactic Acid/Polycaprolactone Blends by Hydrophilic Nanoclay, *Indian J. Mater. Sci.* 2013 (2013) e816503. <https://doi.org/10.1155/2013/816503>.
- [99] S.-T. Bee, A. Hassan, C.T. Ratnam, T.-T. Tee, L.T. Sin, D. Hui, Dispersion and roles of montmorillonite on structural, flammability, thermal and mechanical behaviours of electron beam irradiated flame retarded nanocomposite, *Compos. Part B Eng.* 61 (2014) 41–48. <https://doi.org/10.1016/j.compositesb.2014.01.035>.
- [100] S. Puggal, N. Dhall, N.S. and M.S. Litt, A Review on Polymer Nanocomposites: Synthesis, Characterization and Mechanical Properties, *Indian J. Sci. Technol.* 9 (2016) 1–6. <https://doi.org/10.17485/ijst/2016/v9i4/81100>.
- [101] J. Ma, S. Zhang, Z. Qi, Synthesis and characterization of elastomeric polyurethane/clay nanocomposites, *J. Appl. Polym. Sci.* 82 (2001) 1444–1448. <https://doi.org/10.1002/app.1982>.
- [102] B.K.G. Theng, Chapter 7 - Polymer–Clay Nanocomposites, in: B.K.G. Theng (Ed.), *Dev. Clay Sci.*, Elsevier, 2012: pp. 201–241. <https://doi.org/10.1016/B978-0-444-53354-8.00007-4>.
- [103] P. Anadão, *Polymer/ Clay Nanocomposites: Concepts, Researches, Applications and Trends for The Future*, IntechOpen, 2012. <https://doi.org/10.5772/50407>.
- [104] Z. Wu, X. Yuan, H. Zhong, H. Wang, G. Zeng, X. Chen, H. Wang, L. Zhang, J. Shao, Enhanced adsorptive removal of p-nitrophenol from water by aluminum metal–organic framework/reduced graphene oxide composite, *Sci. Rep.* 6 (2016) 25638. <https://doi.org/10.1038/srep25638>.
- [105] V. Sabatini, H. Farina, L. Basilissi, G. Di Silvestro, M.A. Ortenzi, The Use of Epoxy Silanes on Montmorillonite: An Effective Way to Improve Thermal and Rheological

- Properties of PLA/MMT Nanocomposites Obtained via “In Situ” Polymerization, *J. Nanomater.* 2015 (2015) e418418. <https://doi.org/10.1155/2015/418418>.
- [106] D. Mondal, B. Bhowmick, Md.M.R. Mollick, D. Maity, N. Ranjan Saha, V. Rangarajan, D. Rana, R. Sen, D. Chattopadhyay, Antimicrobial activity and biodegradation behavior of poly(butylene adipate-co-terephthalate)/clay nanocomposites, *J. Appl. Polym. Sci.* 131 (2014). <https://doi.org/10.1002/app.40079>.
- [107] P.M. Huang, M.K. Wang, MINERALS, PRIMARY, in: D. Hillel (Ed.), *Encycl. Soils Environ.*, Elsevier, Oxford, 2005: pp. 500–510. <https://doi.org/10.1016/B0-12-348530-4/00464-1>.
- [108] D.G. Schulze, CLAY MINERALS, in: D. Hillel (Ed.), *Encycl. Soils Environ.*, Elsevier, Oxford, 2005: pp. 246–254. <https://doi.org/10.1016/B0-12-348530-4/00189-2>.
- [109] P. Maiti, K. Yamada, M. Okamoto, K. Ueda, K. Okamoto, New Poly(lactide)/Layered Silicate Nanocomposites: Role of Organoclay, *Chem. Mater.* 14 (2002) 4654–4661. <https://doi.org/10.1021/cm020391b>.
- [110] V. Ojijo, S. Sinha Ray, R. Sadiku, Concurrent Enhancement of Multiple Properties in Reactively Processed Nanocomposites of Poly(lactide)/Poly[(butylene succinate)-co-adipate] Blend and Organoclay, *Macromol. Mater. Eng.* 299 (2014) 596–608. <https://doi.org/10.1002/mame.201300306>.
- [111] Y. Fukushima, T. Yamada, K. Tamura, K. Shibata, Dynamic of organic species in organo-clay/polypropylene composite by quasi-elastic neutron scattering, *Appl. Clay Sci.* 155 (2018) 15–19. <https://doi.org/10.1016/j.clay.2017.12.041>.
- [112] D.H.S. Souza, C.T. Andrade, M.L. Dias, Isothermal crystallization kinetics of poly(lactic acid)/synthetic mica nanocomposites, *J. Appl. Polym. Sci.* 131 (2014). <https://doi.org/10.1002/app.40322>.
- [113] K. Yano, A. Usuki, A. Okada, Synthesis and properties of polyimide-clay hybrid films, *J. Polym. Sci. Part Polym. Chem.* 35 (1997) 2289–2294. [https://doi.org/10.1002/\(SICI\)1099-0518\(199708\)35:11<2289::AID-POLA20>3.0.CO;2-9](https://doi.org/10.1002/(SICI)1099-0518(199708)35:11<2289::AID-POLA20>3.0.CO;2-9).
- [114] B. Diawara, K. Fatyeyeva, J. Ortiz, S. Marais, Polycarbonate/mica extrusion using mixing elements: Improvement of transparency and thermal, mechanical and water and gas barrier properties, *Polymer.* 230 (2021) 124030. <https://doi.org/10.1016/j.polymer.2021.124030>.
- [115] M. Gangarapu, S. Sarangapany, K.K. Veerabhali, S.P. Devipriya, V.B.R. Arava, A High-Performance Catalytic and Recyclability of Phyto-Synthesized Silver Nanoparticles Embedded in Natural Polymer, *J. Clust. Sci.* 28 (2017) 3127–3138. <https://doi.org/10.1007/s10876-017-1280-3>.
- [116] N. Salam, B. Banerjee, A.S. Roy, P. Mondal, S. Roy, A. Bhaumik, Sk.M. Islam, Silver nanoparticles embedded over mesoporous organic polymer as highly efficient and reusable nanocatalyst for the reduction of nitroarenes and aerobic oxidative esterification of alcohols, *Appl. Catal. Gen.* 477 (2014) 184–194. <https://doi.org/10.1016/j.apcata.2014.03.014>.
- [117] A. Emamifar, M. Kadivar, M. Shahedi, S. Soleimanian-Zad, Evaluation of nanocomposite packaging containing Ag and ZnO on shelf life of fresh orange juice, *Innov. Food Sci. Emerg. Technol.* 11 (2010) 742–748. <https://doi.org/10.1016/j.ifset.2010.06.003>.
- [118] C.B. Giller, D.B. Chase, J.F. Rabolt, C.M. Snively, Effect of solvent evaporation rate on the crystalline state of electrospun Nylon 6, *Polymer.* 51 (2010) 4225–4230. <https://doi.org/10.1016/j.polymer.2010.06.057>.

- [119] S. Pavlidou, C.D. Papaspyrides, A review on polymer-layered silicate nanocomposites, *Prog. Polym. Sci.* 33 (2008) 1119–1198. <https://doi.org/10.1016/j.progpolymsci.2008.07.008>.
- [120] V. Mittal, Polymer Layered Silicate Nanocomposites: A Review, *Materials*. 2 (2009) 992–1057. <https://doi.org/10.3390/ma2030992>.
- [121] G.-X. Chen, H.-S. Kim, J.-H. Shim, J.-S. Yoon, Role of Epoxy Groups on Clay Surface in the Improvement of Morphology of Poly(l-lactide)/Clay Composites, *Macromolecules*. 38 (2005) 3738–3744. <https://doi.org/10.1021/ma0488515>.
- [122] S. Singha, M.S. Hedenqvist, A Review on Barrier Properties of Poly(Lactic Acid)/Clay Nanocomposites, *Polymers*. 12 (2020) 1095. <https://doi.org/10.3390/polym12051095>.
- [123] D. Bikiaris, Microstructure and Properties of Polypropylene/Carbon Nanotube Nanocomposites, *Materials*. 3 (2010) 2884–2946. <https://doi.org/10.3390/ma3042884>.
- [124] M.-A. Paul, C. Delcourt, M. Alexandre, P. Degée, F. Monteverde, A. Rulmont, P. Dubois, (Plasticized) Polylactide/(Organo-)Clay Nanocomposites by in situ Intercalative Polymerization, *Macromol. Chem. Phys.* 206 (2005) 484–498. <https://doi.org/10.1002/macp.200400324>.
- [125] M. Carbone, D.T. Donia, G. Sabbatella, R. Antiochia, Silver nanoparticles in polymeric matrices for fresh food packaging, *J. King Saud Univ. - Sci.* 28 (2016) 273–279. <https://doi.org/10.1016/j.jksus.2016.05.004>.
- [126] A. Istiqola, A. Syafiuddin, A review of silver nanoparticles in food packaging technologies: Regulation, methods, properties, migration, and future challenges, *J. Chin. Chem. Soc.* 67 (2020) 1942–1956. <https://doi.org/10.1002/jccs.202000179>.
- [127] S. Iravani, H. Korbekandi, S.V. Mirmohammadi, B. Zolfaghari, Synthesis of silver nanoparticles: chemical, physical and biological methods, *Res. Pharm. Sci.* 9 (2014) 385.
- [128] N. Chouhan, Silver Nanoparticles: Synthesis, Characterization and Applications, IntechOpen, 2018. <https://doi.org/10.5772/intechopen.75611>.
- [129] P. Slepíčka, N. Slepíčková Kasálková, J. Siegel, Z. Kolská, V. Švorčík, Methods of Gold and Silver Nanoparticles Preparation, *Materials*. 13 (2020) 1. <https://doi.org/10.3390/ma13010001>.
- [130] P. Mathur, S. Jha, S. Ramteke, N.K. Jain, Pharmaceutical aspects of silver nanoparticles, *Artif. Cells Nanomedicine Biotechnol.* 46 (2018) 115–126. <https://doi.org/10.1080/21691401.2017.1414825>.
- [131] S. Ahmed, M. Ahmad, B.L. Swami, S. Ikram, A review on plants extract mediated synthesis of silver nanoparticles for antimicrobial applications: A green expertise, *J. Adv. Res.* 7 (2016) 17–28. <https://doi.org/10.1016/j.jare.2015.02.007>.
- [132] M. Kim, S. Osone, T. Kim, H. Higashi, T. Seto, Synthesis of Nanoparticles by Laser Ablation: A Review, *KONA Powder Part. J.* 34 (2017) 80–90. <https://doi.org/10.14356/kona.2017009>.
- [133] N.G. Semaltianos, Nanoparticles by Laser Ablation, *Crit. Rev. Solid State Mater. Sci.* 35 (2010) 105–124. <https://doi.org/10.1080/10408431003788233>.
- [134] T.P. Yadav, R.M. Yadav, D.P. Singh, Mechanical Milling: a Top Down Approach for the Synthesis of Nanomaterials and Nanocomposites, *Nanosci. Nanotechnol.* 2 (2012) 22–48.
- [135] P.G. Jamkhande, N.W. Ghule, A.H. Bamer, M.G. Kalaskar, Metal nanoparticles synthesis: An overview on methods of preparation, advantages and disadvantages, and applications, *J. Drug Deliv. Sci. Technol.* 53 (2019) 101174. <https://doi.org/10.1016/j.jddst.2019.101174>.
- [136] C. Suryanarayana, B. Prabhu, 2 - Synthesis of Nanostructured Materials by Inert-Gas Condensation Methods, in: C.C. Koch (Ed.), *Nanostructured Mater. Second Ed.*, William

- Andrew Publishing, Norwich, NY, 2007: pp. 47–90. <https://doi.org/10.1016/B978-081551534-0.50004-X>.
- [137] C. Dhand, N. Dwivedi, X.J. Loh, A.N.J. Ying, N.K. Verma, R.W. Beuerman, R. Lakshminarayanan, S. Ramakrishna, Methods and strategies for the synthesis of diverse nanoparticles and their applications: a comprehensive overview, *RSC Adv.* 5 (2015) 105003–105037. <https://doi.org/10.1039/C5RA19388E>.
- [138] M.G. Guzmán, J. Dille, S. Godet, Synthesis of Silver Nanoparticles by Chemical Reduction Method and Their Antibacterial Activity, (2008). <https://doi.org/10.5281/zenodo.1062628>.
- [139] C. Quintero-Quiroz, N. Acevedo, J. Zapata-Giraldo, L.E. Botero, J. Quintero, D. Zárate-Triviño, J. Saldarriaga, V.Z. Pérez, Optimization of silver nanoparticle synthesis by chemical reduction and evaluation of its antimicrobial and toxic activity, *Biomater. Res.* 23 (2019) 27. <https://doi.org/10.1186/s40824-019-0173-y>.
- [140] S. Mukherji, S. Bharti, G. Shukla, S. Mukherji, Synthesis and characterization of size- and shape-controlled silver nanoparticles, *Phys. Sci. Rev.* 4 (2019). <https://doi.org/10.1515/psr-2017-0082>.
- [141] L. Kvitek, R. Prucek, A. Panacek, J. Soukupova, Physicochemical Aspects of Metal Nanoparticle Preparation, *IntechOpen*, 2019. <https://doi.org/10.5772/intechopen.89954>.
- [142] M. Rafique, I. Sadaf, M.S. Rafique, M.B. Tahir, A review on green synthesis of silver nanoparticles and their applications, *Artif. Cells Nanomedicine Biotechnol.* 45 (2017) 1272–1291. <https://doi.org/10.1080/21691401.2016.1241792>.
- [143] G. Arya, N. Sharma, R. Mankamna, S. Nimesh, Antimicrobial Silver Nanoparticles: Future of Nanomaterials, in: R. Prasad (Ed.), *Microb. Nanobionics Vol. 2 Basic Res. Appl.*, Springer International Publishing, Cham, 2019: pp. 89–119. https://doi.org/10.1007/978-3-030-16534-5_6.
- [144] N.L. Pacioni, C.D. Borsarelli, V. Rey, A.V. Veglia, Synthetic Routes for the Preparation of Silver Nanoparticles, in: E.I. Alarcon, M. Griffith, K.I. Udekwu (Eds.), *Silver Nanoparticle Appl. Fabr. Des. Med. Biosensing Devices*, Springer International Publishing, Cham, 2015: pp. 13–46. https://doi.org/10.1007/978-3-319-11262-6_2.
- [145] B.L. Cushing, V.L. Kolesnichenko, C.J. O'Connor, Recent Advances in the Liquid-Phase Syntheses of Inorganic Nanoparticles, *Chem. Rev.* 104 (2004) 3893–3946. <https://doi.org/10.1021/cr030027b>.
- [146] P. Vanýsek, ELECTROCHEMICAL SERIES, in: 2010. <https://doi.org/10.31399/asm.hb.v13b.a0006542>.
- [147] A.V. Hoonacker, P. Englebienne, Revisiting Silver Nanoparticle Chemical Synthesis and Stability by Optical Spectroscopy, *Curr. Nanosci.* 2 (n.d.) 359–371.
- [148] M. Yusuf, Silver Nanoparticles: Synthesis and Applications, in: L.M.T. Martínez, O.V. Kharissova, B.I. Kharisov (Eds.), *Handb. Ecomater.*, Springer International Publishing, Cham, 2019: pp. 2343–2356. https://doi.org/10.1007/978-3-319-68255-6_16.
- [149] P. Fageria, S. Uppala, R. Nazir, S. Gangopadhyay, C.-H. Chang, M. Basu, S. Pande, Synthesis of Monometallic (Au and Pd) and Bimetallic (AuPd) Nanoparticles Using Carbon Nitride (C₃N₄) Quantum Dots via the Photochemical Route for Nitrophenol Reduction, *Langmuir.* 32 (2016) 10054–10064. <https://doi.org/10.1021/acs.langmuir.6b02375>.
- [150] M. Zaarour, M. El Roz, B. Dong, R. Retoux, R. Aad, J. Cardin, C. Dufour, F. Gourbilleau, J.-P. Gilson, S. Mintova, Photochemical Preparation of Silver Nanoparticles Supported on Zeolite Crystals, *Langmuir.* 30 (2014) 6250–6256. <https://doi.org/10.1021/la5006743>.
- [151] J.S. Gabriel, V.A.M. Gonzaga, A.L. Poli, C.C. Schmitt, Photochemical synthesis of silver nanoparticles on chitosans/montmorillonite nanocomposite films and antibacterial

- activity, *Carbohydr. Polym.* 171 (2017) 202–210. <https://doi.org/10.1016/j.carbpol.2017.05.021>.
- [152] S.H. Lee, B.-H. Jun, Silver Nanoparticles: Synthesis and Application for Nanomedicine, *Int. J. Mol. Sci.* 20 (2019) 865. <https://doi.org/10.3390/ijms20040865>.
- [153] O.I. Kuntiyi, A.R. Kytsya, I.P. Mertsalo, A.S. Mazur, G.I. Zozula, L.I. Bazylyak, R.V. Topchak, Electrochemical synthesis of silver nanoparticles by reversible current in solutions of sodium polyacrylate, *Colloid Polym. Sci.* 297 (2019) 689–695. <https://doi.org/10.1007/s00396-019-04488-4>.
- [154] V.V. Yanilkin, G.R. Nasretdinova, V.A. Kokorekin, Mediated electrochemical synthesis of metal nanoparticles, *Russ. Chem. Rev.* 87 (2018) 1080–1110. <https://doi.org/10.1070/RCR4827>.
- [155] R.A. Khaydarov, R.R. Khaydarov, O. Gapurova, Y. Estrin, T. Scheper, Electrochemical method for the synthesis of silver nanoparticles, *J. Nanoparticle Res.* 11 (2009) 1193–1200. <https://doi.org/10.1007/s11051-008-9513-x>.
- [156] M.A. Malik, M.Y. Wani, M.A. Hashim, Microemulsion method: A novel route to synthesize organic and inorganic nanomaterials: 1st Nano Update, *Arab. J. Chem.* 5 (2012) 397–417. <https://doi.org/10.1016/j.arabjc.2010.09.027>.
- [157] T. Klaus, R. Joerger, E. Olsson, C.-G. Granqvist, Silver-based crystalline nanoparticles, microbially fabricated, *Proc. Natl. Acad. Sci.* 96 (1999) 13611–13614. <https://doi.org/10.1073/pnas.96.24.13611>.
- [158] R. Singh, U.U. Shedbalkar, S.A. Wadhvani, B.A. Chopade, Bacteriogenic silver nanoparticles: synthesis, mechanism, and applications, *Appl. Microbiol. Biotechnol.* 99 (2015) 4579–4593. <https://doi.org/10.1007/s00253-015-6622-1>.
- [159] K.S. Siddiqi, A. Husen, R.A.K. Rao, A review on biosynthesis of silver nanoparticles and their biocidal properties, *J. Nanobiotechnology.* 16 (2018) 14. <https://doi.org/10.1186/s12951-018-0334-5>.
- [160] N. Samadi, D. Golkaran, A. Eslamifar, H. Jamalifar, M.R. Fazeli, F.A. Mohseni, Intra/Extracellular Biosynthesis of Silver Nanoparticles by an Autochthonous Strain of *Proteus mirabilis* Isolated from Photographic Waste, *J. Biomed. Nanotechnol.* 5 (2009) 247–253. <https://doi.org/10.1166/jbn.2009.1029>.
- [161] N. Saifuddin, C.W. Wong, A.A.N. Yasumira, Rapid Biosynthesis of Silver Nanoparticles Using Culture Supernatant of Bacteria with Microwave Irradiation, *E-J. Chem.* 6 (2009) 61–70. <https://doi.org/10.1155/2009/734264>.
- [162] A.H. Mondal, D. Yadav, A. Ali, N. Khan, J.O. Jin, Q.M.R. Haq, Anti-Bacterial and Anti-Candidal Activity of Silver Nanoparticles Biosynthesized Using *Citrobacter* spp. MS5 Culture Supernatant, *Biomolecules.* 10 (2020) 944. <https://doi.org/10.3390/biom10060944>.
- [163] B. Momin, S. Rahman, N. Jha, U.S. Annapure, Valorization of mutant *Bacillus licheniformis* M09 supernatant for green synthesis of silver nanoparticles: photocatalytic dye degradation, antibacterial activity, and cytotoxicity, *Bioprocess Biosyst. Eng.* 42 (2019) 541–553. <https://doi.org/10.1007/s00449-018-2057-2>.
- [164] J. Osorio-Echavarría, J. Osorio-Echavarría, C.P. Ossa-Orozco, N.A. Gómez-Vanegas, Synthesis of silver nanoparticles using white-rot fungus *Anamorphous Bjerkandera* sp. R1: influence of silver nitrate concentration and fungus growth time, *Sci. Rep.* 11 (2021) 3842. <https://doi.org/10.1038/s41598-021-82514-8>.
- [165] J.L. Gardea-Torresdey, E. Gomez, J.R. Peralta-Videa, J.G. Parsons, H. Troiani, M. Jose-Yacaman, Alfalfa Sprouts: A Natural Source for the Synthesis of Silver Nanoparticles, *Langmuir.* 19 (2003) 1357–1361. <https://doi.org/10.1021/la020835i>.

- [166] S.S. Shankar, A. Rai, A. Ahmad, M. Sastry, Rapid synthesis of Au, Ag, and bimetallic Au core–Ag shell nanoparticles using Neem (*Azadirachta indica*) leaf broth, *J. Colloid Interface Sci.* 275 (2004) 496–502. <https://doi.org/10.1016/j.jcis.2004.03.003>.
- [167] B. Ankamwar, C. Damle, A. Ahmad, M. Sastry, Biosynthesis of Gold and Silver Nanoparticles Using *Emblica Officinalis* Fruit Extract, Their Phase Transfer and Transmetallation in an Organic Solution, *J. Nanosci. Nanotechnol.* 5 (2005) 1665–1671. <https://doi.org/10.1166/jnn.2005.184>.
- [168] S. Li, Y. Shen, A. Xie, X. Yu, L. Qiu, L. Zhang, Q. Zhang, Green synthesis of silver nanoparticles using *Capsicum annuum* L. extract, *Green Chem.* 9 (2007) 852–858. <https://doi.org/10.1039/B615357G>.
- [169] J. Huang, Q. Li, D. Sun, Y. Lu, Y. Su, X. Yang, H. Wang, Y. Wang, W. Shao, N. He, J. Hong, C. Chen, Biosynthesis of silver and gold nanoparticles by novel sundried *Cinnamomum camphora* leaf, *Nanotechnology.* 18 (2007) 105104. <https://doi.org/10.1088/0957-4484/18/10/105104>.
- [170] N. Swilam, K.A. Nematallah, Polyphenols profile of pomegranate leaves and their role in green synthesis of silver nanoparticles, *Sci. Rep.* 10 (2020) 14851. <https://doi.org/10.1038/s41598-020-71847-5>.
- [171] H. Chandra, P. Kumari, E. Bontempi, S. Yadav, Medicinal plants: Treasure trove for green synthesis of metallic nanoparticles and their biomedical applications, *Biocatal. Agric. Biotechnol.* 24 (2020) 101518. <https://doi.org/10.1016/j.bcab.2020.101518>.
- [172] M. Vinicius de Oliveira Brisola Maciel, A. da Rosa Almeida, M.H. Machado, W.C. Elias, C. Gonçalves da Rosa, G.L. Teixeira, C.M. Noronha, F.C. Bertoldi, M.R. Nunes, R. Dutra de Armas, P.L. Manique Barreto, Green synthesis, characteristics and antimicrobial activity of silver nanoparticles mediated by essential oils as reducing agents, *Biocatal. Agric. Biotechnol.* 28 (2020) 101746. <https://doi.org/10.1016/j.bcab.2020.101746>.
- [173] Y. Rout, S. Behera, A.K. Ojha, P.L. Nayak, Green synthesis of silver nanoparticles using *Ocimum sanctum* (Tulashi) and study of their antibacterial and antifungal activities, *J. Microbiol. Antimicrob.* 4 (2012) 103–109. <https://doi.org/10.5897/JMA11.060>.
- [174] A. Rónavári, N. Igaz, D.I. Adamecz, B. Szerencsés, C. Molnar, Z. Kónya, I. Pfeiffer, M. Kiricsi, Green Silver and Gold Nanoparticles: Biological Synthesis Approaches and Potentials for Biomedical Applications, *Molecules.* 26 (2021) 844. <https://doi.org/10.3390/molecules26040844>.
- [175] J. Pulit-Prociak, M. Banach, Silver nanoparticles – a material of the future...?, *Open Chem.* 14 (2016) 76–91. <https://doi.org/10.1515/chem-2016-0005>.
- [176] A. Syafiuddin, Salmiati, M.R. Salim, A. Beng Hong Kueh, T. Hadibarata, H. Nur, A Review of Silver Nanoparticles: Research Trends, Global Consumption, Synthesis, Properties, and Future Challenges, *J. Chin. Chem. Soc.* 64 (2017) 732–756. <https://doi.org/10.1002/jccs.201700067>.
- [177] R. Dondi, W. Su, G.A. Griffith, G. Clark, G.A. Burley, Highly Size- and Shape-Controlled Synthesis of Silver Nanoparticles via a Templated Tollens Reaction, *Small.* 8 (2012) 770–776. <https://doi.org/10.1002/sml.201101474>.
- [178] S. Agnihotri, S. Mukherji, S. Mukherji, Size-controlled silver nanoparticles synthesized over the range 5–100 nm using the same protocol and their antibacterial efficacy, *RSC Adv.* 4 (2013) 3974–3983. <https://doi.org/10.1039/C3RA44507K>.
- [179] F. Farghaly, N. Nafady, Green Synthesis of Silver Nanoparticles Using Leaf Extract of *Rosmarinus officinalis* and Its Effect on Tomato and Wheat Plants, *J. Agric. Sci.* 7 (2015) p277. <https://doi.org/10.5539/jas.v7n11p277>.
- [180] R.C. Fierascu, I.R. Bunghez, R. Somoghi, I. Fierascu, R.M. Ion, CHARACTERIZATION OF SILVER NANOPARTICLES OBTAINED BY USING

ROSMARINUS OFFICINALIS EXTRACT AND THEIR ANTIOXIDANT ACTIVITY, Silver Nanoparticles. (n.d.) 6.

- [181] D. Abdel-Aziz, N. Yousef, Enhancement of antimicrobial effect of some spices extract by using biosynthesized silver nanoparticles, *Int. Food Res. J.* 25 (2018) 589–596.
- [182] M. Mohamed, F.M. Mohamed, W.A. El-Said, Enhancement of Antimicrobial Sensitivity of Salmonella and Escherichia coli Strains Isolated from Chickens Using Silver Nanoparticles in Assiut Governorate, *Zagazig Vet. J.* 45 (2017) 273–282. <https://doi.org/10.21608/zvjz.2017.7952>.
- [183] S. Ahmed, Saifullah, M. Ahmad, B.L. Swami, S. Ikram, Green synthesis of silver nanoparticles using *Azadirachta indica* aqueous leaf extract, *J. Radiat. Res. Appl. Sci.* 9 (2016) 1–7. <https://doi.org/10.1016/j.jrras.2015.06.006>.
- [184] P. Roy, B. Das, A. Mohanty, S. Mohapatra, Green synthesis of silver nanoparticles using *Azadirachta indica* leaf extract and its antimicrobial study, *Appl. Nanosci.* 7 (2017) 843–850. <https://doi.org/10.1007/s13204-017-0621-8>.
- [185] S. Kleine, C. Müller, Intraspecific plant chemical diversity and its relation to herbivory, *Oecologia.* 166 (2011) 175–186. <https://doi.org/10.1007/s00442-010-1827-6>.
- [186] A.F. Gomes, M.P. Almeida, M.F. Leite, S. Schwaiger, H. Stuppner, M. Halabalaki, J.G. Amaral, J.M. David, Seasonal variation in the chemical composition of two chemotypes of *Lippia alba*, *Food Chem.* 273 (2019) 186–193. <https://doi.org/10.1016/j.foodchem.2017.11.089>.
- [187] M.A. Raza, Z. Kanwal, A. Rauf, A.N. Sabri, S. Riaz, S. Naseem, Size- and Shape-Dependent Antibacterial Studies of Silver Nanoparticles Synthesized by Wet Chemical Routes, *Nanomaterials.* 6 (2016) 74. <https://doi.org/10.3390/nano6040074>.
- [188] G.A. Martínez-Castañón, N. Niño-Martínez, F. Martínez-Gutierrez, J.R. Martínez-Mendoza, F. Ruiz, Synthesis and antibacterial activity of silver nanoparticles with different sizes, *J. Nanoparticle Res.* 10 (2008) 1343–1348. <https://doi.org/10.1007/s11051-008-9428-6>.
- [189] B. Szerencsés, N. Igaz, Á. Tóbiás, Z. Prucsi, A. Rónavári, P. Béteky, D. Madarász, C. Papp, I. Makra, C. Vágvölgyi, Z. Kónya, I. Pfeiffer, M. Kiricsi, Size-dependent activity of silver nanoparticles on the morphological switch and biofilm formation of opportunistic pathogenic yeasts, *BMC Microbiol.* 20 (2020) 176. <https://doi.org/10.1186/s12866-020-01858-9>.
- [190] D. Badma Priya, I.V. Asharani, Size Dependent Catalytic Activity of *Actinodaphne madraspatana* Bedd Leaves Mediated Silver Nanoparticles, *J. Clust. Sci.* 28 (2017) 1837–1856. <https://doi.org/10.1007/s10876-017-1185-1>.
- [191] V.S. Suvith, D. Philip, Catalytic degradation of methylene blue using biosynthesized gold and silver nanoparticles, *Spectrochim. Acta. A. Mol. Biomol. Spectrosc.* 118 (2014) 526–532. <https://doi.org/10.1016/j.saa.2013.09.016>.
- [192] J.Y. Cheon, S.J. Kim, Y.H. Rhee, O.H. Kwon, W.H. Park, <p>Shape-dependent antimicrobial activities of silver nanoparticles</p>, *Int. J. Nanomedicine.* 14 (2019) 2773–2780. <https://doi.org/10.2147/IJN.S196472>.
- [193] R. Xu, D. Wang, J. Zhang, Y. Li, Shape-Dependent Catalytic Activity of Silver Nanoparticles for the Oxidation of Styrene, *Chem. – Asian J.* 1 (2006) 888–893. <https://doi.org/10.1002/asia.200600260>.
- [194] V. Bansal, V. Li, A.P. O’Mullane, S.K. Bhargava, Shape dependent electrocatalytic behaviour of silver nanoparticles, *CrystEngComm.* 12 (2010) 4280–4286. <https://doi.org/10.1039/C0CE00215A>.
- [195] S. Singh, A. Bharti, V.K. Meena, Structural, thermal, zeta potential and electrical properties of disaccharide reduced silver nanoparticles, *J. Mater. Sci. Mater. Electron.* 25 (2014) 3747–3752. <https://doi.org/10.1007/s10854-014-2085-x>.

- [196] A. Abbaszadegan, Y. Ghahramani, A. Gholami, B. Hemmateenejad, S. Dorostkar, M. Nabavizadeh, H. Sharghi, The Effect of Charge at the Surface of Silver Nanoparticles on Antimicrobial Activity against Gram-Positive and Gram-Negative Bacteria: A Preliminary Study, *J. Nanomater.* 2015 (2015) e720654. <https://doi.org/10.1155/2015/720654>.
- [197] H.T. Phan, A.J. Haes, What Does Nanoparticle Stability Mean?, *J. Phys. Chem. C.* 123 (2019) 16495–16507. <https://doi.org/10.1021/acs.jpcc.9b00913>.
- [198] S.M. Lee, K.C. Song, B.S. Lee, Antibacterial activity of silver nanoparticles prepared by a chemical reduction method, *Korean J. Chem. Eng.* 27 (2010) 688–692. <https://doi.org/10.1007/s11814-010-0067-0>.
- [199] L. Kvítek, A. Panáček, J. Soukupová, M. Kolář, R. Večeřová, R. Prucek, M. Holecová, R. Zbořil, Effect of Surfactants and Polymers on Stability and Antibacterial Activity of Silver Nanoparticles (NPs), *J. Phys. Chem. C.* 112 (2008) 5825–5834. <https://doi.org/10.1021/jp711616v>.
- [200] E. Bae, H.-J. Park, J. Park, J. Yoon, Y. Kim, K. Choi, J. Yi, Effect of Chemical Stabilizers in Silver Nanoparticle Suspensions on Nanotoxicity, *Bull. Korean Chem. Soc.* 32 (2011). <https://doi.org/10.5012/bkcs.2011.32.2.613>.
- [201] M. Navlani-García, D. Salinas-Torres, K. Mori, Y. Kuwahara, H. Yamashita, Tailoring the Size and Shape of Colloidal Noble Metal Nanocrystals as a Valuable Tool in Catalysis, *Catal. Surv. Asia.* 23 (2019). <https://doi.org/10.1007/s10563-019-09271-7>.
- [202] E. Piacenza, A. Presentato, R. Turner, Stability of biogenic metal(loid) nanomaterials related to the colloidal stabilization theory of chemical nanostructures, *Crit. Rev. Biotechnol.* 38 (2018). <https://doi.org/10.1080/07388551.2018.1440525>.
- [203] S. Kaviya, J. Santhanalakshmi, B. Viswanathan, J. Muthumary, K. Srinivasan, Biosynthesis of silver nanoparticles using citrus sinensis peel extract and its antibacterial activity, *Spectrochim. Acta. A. Mol. Biomol. Spectrosc.* 79 (2011) 594–598. <https://doi.org/10.1016/j.saa.2011.03.040>.
- [204] M. Asimuddin, M.R. Shaik, S.F. Adil, M.R.H. Siddiqui, A. Alwarthan, K. Jamil, M. Khan, Azadirachta indica based biosynthesis of silver nanoparticles and evaluation of their antibacterial and cytotoxic effects, *J. King Saud Univ. - Sci.* 32 (2020) 648–656. <https://doi.org/10.1016/j.jksus.2018.09.014>.
- [205] J.Y. Song, B.S. Kim, Rapid biological synthesis of silver nanoparticles using plant leaf extracts, *Bioprocess Biosyst. Eng.* 32 (2008) 79. <https://doi.org/10.1007/s00449-008-0224-6>.
- [206] P. Manjari Mishra, S. Kumar Sahoo, G. Kumar Naik, K. Parida, Biomimetic synthesis, characterization and mechanism of formation of stable silver nanoparticles using Averrhoa carambola L. leaf extract, *Mater. Lett.* 160 (2015) 566–571. <https://doi.org/10.1016/j.matlet.2015.08.048>.
- [207] P. Anbu, S.C.B. Gopinath, H.S. Yun, C.-G. Lee, Temperature-dependent green biosynthesis and characterization of silver nanoparticles using balloon flower plants and their antibacterial potential, *J. Mol. Struct.* 1177 (2019) 302–309. <https://doi.org/10.1016/j.molstruc.2018.09.075>.
- [208] S. Jain, M.S. Mehata, Medicinal Plant Leaf Extract and Pure Flavonoid Mediated Green Synthesis of Silver Nanoparticles and their Enhanced Antibacterial Property, *Sci. Rep.* 7 (2017) 15867. <https://doi.org/10.1038/s41598-017-15724-8>.
- [209] N. Yang, W.-H. Li, Mango peel extract mediated novel route for synthesis of silver nanoparticles and antibacterial application of silver nanoparticles loaded onto non-woven fabrics, *Ind. Crops Prod.* 48 (2013) 81–88. <https://doi.org/10.1016/j.indcrop.2013.04.001>.

- [210] L.B. Anigol, J.S. Charantimath, P.M. Gurubasavaraj, Effect of Concentration and pH on the Size of Silver Nanoparticles Synthesized by Green Chemistry, *Org. Med. Chem. Int. J.* 3 (2017) 124–128.
- [211] C. Krishnaraj, R. Ramachandran, K. Mohan, P.T. Kalaichelvan, Optimization for rapid synthesis of silver nanoparticles and its effect on phytopathogenic fungi, *Spectrochim. Acta. A. Mol. Biomol. Spectrosc.* 93 (2012) 95–99. <https://doi.org/10.1016/j.saa.2012.03.002>.
- [212] M. Ghaffari-Moghaddam, R. Hadi-Dabanlou, Plant mediated green synthesis and antibacterial activity of silver nanoparticles using *Crataegus douglasii* fruit extract, *J. Ind. Eng. Chem.* 20 (2014) 739–744. <https://doi.org/10.1016/j.jiec.2013.09.005>.
- [213] B. Pascu, A. Negrea, M. Ciopec, N. Duteanu, P. Negrea, N.S. Nemeş, C. Seiman, E. Marian, O. Micle, A Green, Simple and Facile Way to Synthesize Silver Nanoparticles Using Soluble Starch. pH Studies and Antimicrobial Applications, *Materials.* 14 (2021) 4765. <https://doi.org/10.3390/ma14164765>.
- [214] P. Jakinala, N. Lingampally, B. Hameeda, R.Z. Sayyed, Y.K. M, E.A. Elsayed, H.E. Enshasy, Silver nanoparticles from insect wing extract: Biosynthesis and evaluation for antioxidant and antimicrobial potential, *PLOS ONE.* 16 (2021) e0241729. <https://doi.org/10.1371/journal.pone.0241729>.
- [215] K. Saware, A. Venkataraman, Biosynthesis and Characterization of Stable Silver Nanoparticles Using *Ficus religiosa* Leaf Extract: A Mechanism Perspective, *J. Clust. Sci.* 25 (2014) 1157–1171. <https://doi.org/10.1007/s10876-014-0697-1>.
- [216] P. Nalawade, P. Mukherjee, S. Kapoor, Biosynthesis, characterization and antibacterial studies of silver nanoparticles using pods extract of *Acacia auriculiformis*, *Spectrochim. Acta. A. Mol. Biomol. Spectrosc.* 129 (2014) 121–124. <https://doi.org/10.1016/j.saa.2014.03.032>.
- [217] D.-Y. Kim, R.G. Saratale, S. Shinde, A. Syed, F. Ameen, G. Ghodake, Green synthesis of silver nanoparticles using *Laminaria japonica* extract: Characterization and seedling growth assessment, *J. Clean. Prod.* 172 (2018) 2910–2918. <https://doi.org/10.1016/j.jclepro.2017.11.123>.
- [218] N.S. Jalani, W. Michell, W.E. Lin, S.Z.H. Syed Zuber, U. Hashim, R. Abdullah, Biosynthesis of silver nanoparticles using *Citrus grandis* peel extract, *Malays. J. Anal. Sci.* 22 (2018) 676–683. <https://doi.org/10.17576/mjas-2018-2204-14>.
- [219] M. Vanaja, K. Paulkumar, G. Gnanajobitha, S. Rajeshkumar, C. Malarkodi, G. Annadurai, Herbal Plant Synthesis of Antibacterial Silver Nanoparticles by *Solanum trilobatum* and Its Characterization, *Int. J. Met.* 2014 (2014) e692461. <https://doi.org/10.1155/2014/692461>.
- [220] R. kumar, G. Ghoshal, M. Goyal, Rapid Green Synthesis of Silver Nanoparticles (AgNPs) Using (*Prunus persica*) Plants extract: Exploring its Antimicrobial and Catalytic Activities, *J. Nanomedicine Nanotechnol.* 8 (2017) 452.
- [221] R. Seifipour, M. Nozari, L. Pishkar, Green Synthesis of Silver Nanoparticles using *Tragopogon Collinus* Leaf Extract and Study of Their Antibacterial Effects, *J. Inorg. Organomet. Polym. Mater.* 30 (2020) 2926–2936. <https://doi.org/10.1007/s10904-020-01441-9>.
- [222] N.L. Gavade, A.N. Kadam, M.B. Suwarnkar, V.P. Ghodake, K.M. Garadkar, Biogenic synthesis of multi-applicative silver nanoparticles by using *Ziziphus Jujuba* leaf extract, *Spectrochim. Acta. A. Mol. Biomol. Spectrosc.* 136 (2015) 953–960. <https://doi.org/10.1016/j.saa.2014.09.118>.
- [223] M. Amin, F. Anwar, M.R.S.A. Janjua, M.A. Iqbal, U. Rashid, Green Synthesis of Silver Nanoparticles through Reduction with *Solanum xanthocarpum* L. Berry Extract:

- Characterization, Antimicrobial and Urease Inhibitory Activities against *Helicobacter pylori*, *Int. J. Mol. Sci.* 13 (2012) 9923–9941. <https://doi.org/10.3390/ijms13089923>.
- [224] T.C. Prathna, N. Chandrasekaran, A.M. Raichur, A. Mukherjee, Biomimetic synthesis of silver nanoparticles by Citrus limon (lemon) aqueous extract and theoretical prediction of particle size, *Colloids Surf. B Biointerfaces.* 82 (2011) 152–159. <https://doi.org/10.1016/j.colsurfb.2010.08.036>.
- [225] M.R. Bindhu, M. Umadevi, Synthesis of monodispersed silver nanoparticles using Hibiscus cannabinus leaf extract and its antimicrobial activity, *Spectrochim. Acta. A. Mol. Biomol. Spectrosc.* 101 (2013) 184–190. <https://doi.org/10.1016/j.saa.2012.09.031>.
- [226] H. Liu, H. Zhang, J. Wang, J. Wei, Effect of temperature on the size of biosynthesized silver nanoparticle: Deep insight into microscopic kinetics analysis, *Arab. J. Chem.* 13 (2020) 1011–1019. <https://doi.org/10.1016/j.arabjc.2017.09.004>.
- [227] E.E. ELEMIKE, D.C. ONWUDIWE, O. ARIJEH, H.U. NWANKWO, Plant-mediated biosynthesis of silver nanoparticles by leaf extracts of *Lasienthra africanum* and a study of the influence of kinetic parameters, *Bull. Mater. Sci.* 40 (2017) 129–137. <https://doi.org/10.1007/s12034-017-1362-8>.
- [228] A. Nanda, M. Saravanan, Biosynthesis of silver nanoparticles from *Staphylococcus aureus* and its antimicrobial activity against MRSA and MRSE, *Nanomedicine Nanotechnol. Biol. Med.* 5 (2009) 452–456. <https://doi.org/10.1016/j.nano.2009.01.012>.
- [229] S. Liao, Y. Zhang, X. Pan, F. Zhu, C. Jiang, Q. Liu, Z. Cheng, G. Dai, G. Wu, L. Wang, L. Chen, <p>Antibacterial activity and mechanism of silver nanoparticles against multidrug-resistant Pseudomonas aeruginosa</p>, *Int. J. Nanomedicine.* 14 (2019) 1469–1487. <https://doi.org/10.2147/IJN.S191340>.
- [230] Y.N. Slavin, K. Ivanova, J. Hoyo, I. Perelshtein, G. Owen, A. Haegert, Y.-Y. Lin, S. LeBihan, A. Gedanken, U.O. Häfeli, T. Tzanov, H. Bach, Novel Lignin-Capped Silver Nanoparticles against Multidrug-Resistant Bacteria, *ACS Appl. Mater. Interfaces.* 13 (2021) 22098–22109. <https://doi.org/10.1021/acsami.0c16921>.
- [231] R.S. Patil, M.R. Kokate, S.S. Kolekar, Bioinspired synthesis of highly stabilized silver nanoparticles using *Ocimum tenuiflorum* leaf extract and their antibacterial activity, *Spectrochim. Acta. A. Mol. Biomol. Spectrosc.* 91 (2012) 234–238. <https://doi.org/10.1016/j.saa.2012.02.009>.
- [232] S. Tang, J. Zheng, Antibacterial Activity of Silver Nanoparticles: Structural Effects, *Adv. Healthc. Mater.* 7 (2018) 1701503. <https://doi.org/10.1002/adhm.201701503>.
- [233] L. Zhang, L. Wu, Y. Mi, Y. Si, Silver Nanoparticles Induced Cell Apoptosis, Membrane Damage of *Azotobacter vinelandii* and *Nitrosomonas europaea* via Generation of Reactive Oxygen Species, *Bull. Environ. Contam. Toxicol.* 103 (2019) 181–186. <https://doi.org/10.1007/s00128-019-02622-0>.
- [234] F. Amaro, Á. Morón, S. Díaz, A. Martín-González, J.C. Gutiérrez, Metallic Nanoparticles—Friends or Foes in the Battle against Antibiotic-Resistant Bacteria?, *Microorganisms.* 9 (2021) 364. <https://doi.org/10.3390/microorganisms9020364>.
- [235] A. Panáček, L. Kvítek, M. Smékalová, R. Večeřová, M. Kolář, M. Röderová, F. Dyčka, M. Šebela, R. Prucek, O. Tomanec, R. Zbořil, Bacterial resistance to silver nanoparticles and how to overcome it, *Nat. Nanotechnol.* 13 (2018) 65–71. <https://doi.org/10.1038/s41565-017-0013-y>.
- [236] L.M. Stabryla, K.A. Johnston, N.A. Diemler, V.S. Cooper, J.E. Millstone, S.-J. Haig, L.M. Gilbertson, Role of bacterial motility in differential resistance mechanisms of silver nanoparticles and silver ions, *Nat. Nanotechnol.* 16 (2021) 996–1003. <https://doi.org/10.1038/s41565-021-00929-w>.
- [237] A. Ahmad, Y. Wei, F. Syed, K. Tahir, A.U. Rehman, A. Khan, S. Ullah, Q. Yuan, The effects of bacteria-nanoparticles interface on the antibacterial activity of green

- synthesized silver nanoparticles, *Microb. Pathog.* 102 (2017) 133–142. <https://doi.org/10.1016/j.micpath.2016.11.030>.
- [238] A. Bhargava, V. Pareek, S. Roy Choudhury, J. Panwar, S. Karmakar, Superior Bactericidal Efficacy of Fucose-Functionalized Silver Nanoparticles against *Pseudomonas aeruginosa* PAO1 and Prevention of Its Colonization on Urinary Catheters, *ACS Appl. Mater. Interfaces.* 10 (2018) 29325–29337. <https://doi.org/10.1021/acsami.8b09475>.
- [239] B. Buszewski, K. Rafińska, P. Pomastowski, J. Walczak, A. Rogowska, Novel aspects of silver nanoparticles functionalization, *Colloids Surf. Physicochem. Eng. Asp.* 506 (2016) 170–178. <https://doi.org/10.1016/j.colsurfa.2016.05.058>.
- [240] A.J. Kora, R. Manjusha, J. Arunachalam, Superior bactericidal activity of SDS capped silver nanoparticles: Synthesis and characterization, *Mater. Sci. Eng. C.* 29 (2009) 2104–2109. <https://doi.org/10.1016/j.msec.2009.04.010>.

Chapter II :

Synthesis and antibacterial behavior of bio-composite materials-based on poly(ϵ -caprolactone)/bentonite

Chapter overview

As discussed in the bibliographic overview, polycaprolactone (PCL) is a biodegradable and biocompatible polyester that could be used in a lot of domains, including food packaging. However, it presents many drawbacks including poor thermal and mechanical properties and the lack of antibacterial activity. In that regard, in this chapter, we aimed to prepare PCL nanocomposites with improved properties and antibacterial activity.

Various types of nanofillers are used for that aim, but phyllosilicates present many advantages such as their higher surface area and their sheet-like structure. Accordingly, we choose Bentonite (Bnt), a natural nanoclay of Moroccan origin, as a nanofiller. Moreover, the OH-groups could be exploited to co-initiate the “grafting from” ring-opening polymerization of ϵ -CL. However, due to the incompatibility between the hydrophilic clay and hydrophobic polymer, the potential of enhancing PCL properties is limited. Consequently, it is necessary to increase the compatibility between these two phases. For that reason, Bnt was organo-modified using CTAB to increase its hydrophobicity, thus increasing its compatibility with PCL. We choose CTAB as an organic modifier due to i) its potential in increasing the hydrophobicity and the interlamellar spacing of Bnt thanks to its long alkyl chain and ii) its inherent antibacterial activity susceptible to providing the end nanocomposites with the antibacterial activity necessary for applications in food packaging.

In this chapter, we report the synthesis of antibacterial bio-composite materials based on Poly(ϵ -Caprolactone) and bentonite (Bnt) *via* a “grafting from” ring-opening polymerization of ϵ -Caprolactone (ϵ -CL) using a tin-based catalyst for final potential applications in active food packaging.

The results of this chapter are presented in the form of a published paper: **A. Nabgui**, T. El Assimi, A. El Meziane, G.A. Luinstra, M. Raihane, G. Gouhier, P. Thébault, K. Draoui, M. Lahcini, Synthesis and antibacterial behavior of bio-composite materials-based on poly(ϵ -caprolactone)/bentonite, *European Polymer Journal*. 156 (2021) 110602. <https://doi.org/10.1016/j.eurpolymj.2021.110602>.

Synthesis and antibacterial behavior of Bio-composite materials based on Poly(ϵ -caprolactone)/Bentonite

Abderrahmane Nabgui^{1,2,5}, Taha El Assimi⁶, Abdellatif El Meziane², Gerrit A Luinstra³, Mustapha Raihane¹, Géraldine Gouhier⁴, Pascal Thébault⁵, Khalid Draoui⁷, Mohammed Lahcini^{1,6*}.

¹ IMED-Lab, Faculty of Sciences and Techniques, Cadi Ayyad University, Avenue Abdelkrim Elkhatabi, B.P 549, 40000, Marrakech, Morocco.

² Laboratory of Agrobiotechnology and Bio-engineering, Department of Biology. Cadi Ayyad University, Avenue Abdelkrim Elkhatabi, B.P 549, 40000, Marrakech, Morocco.

³ Institute of Technical and Macromolecular Chemistry – University of Hamburg, Bundesstr. 45, D-20146 Hamburg, Germany

⁴ Normandie Université, COBRA, UMR 6014, FR 3038, INSA Rouen, CNRS, IRCOF 1 rue Tesnière 76821 Mont-Saint-Aignan, France.

⁵ Normandie Université, PBS UMR 6270, UNIROUEN, INSA Rouen, CNRS, 76821 Mont-Saint-Aignan, France.

⁶ Mohammed VI Polytechnic University, 43150 Ben Guerir, Morocco.

⁷ Department of Chemistry, Faculty of Sciences, University Abdelmalek Essaâdi, 93002 Tetouan, Morocco.

Abstract

Several clay minerals as inorganic fillers were incorporated into aliphatic polyester by various procedures. The target of enhancing the physicochemical properties of the resulting composite material leads thereby to overcoming the limitations of neat polyesters. Still, bentonite (Bnt) as a clay mineral has been relatively unexplored as a reinforcing agent of the poly(ϵ -caprolactone) (PCL). In this study, a bio-nanocomposite based on poly(ϵ -caprolactone) & bentonite nanofiller was prepared by in-situ ring-opening polymerization (ROP) of ϵ -caprolactone (ϵ -CL) under open air using a tin-based catalyst. The obtained bio-composites (PCL-OBnt) were fully characterized to examine their structural interactions, thermal stability, mechanical, and morphological properties. Finally, the antimicrobial activity against *S. epidermidis* and *S. aureus* of the prepared bio-composites materials was evaluated.

Keywords

Polycaprolactone, Ring-opening polymerization, *In-situ* polymerization, Bentonite, Antimicrobial activity

coordination insertion mechanism is operative when an organometallic catalyst is used. The propagation step is based on the coordination of the carbonyl function of the monomer to the catalyst, followed by the ring-opening of the cyclic monomer by an internal nucleophilic attack of an alkoxide chain end, also bonded to the catalyst [7]. The metal catalyst complexes mostly used in the ring-opening polymerization are tin(II) and tin(IV) alkoxide or salt precursors [8], [9], [10], [11]. These tin ROP initiators have a high reactivity towards moisture. Consequently, the ring-opening polymerization is best performed under an inert-gas medium to have control over the polymerization rate and to avoid the dramatic decline of the molecular weight build-up [12], [13]. In the perspective of the ROP accomplishment in open air with high efficiency, our previous findings were that the tetra(phenylethylenyl) tin catalyst could ensure the ring-opening polymerization of ϵ -CL at a higher [monomer]/[initiator] ratio without the need for inert atmosphere, thus considerably reducing the efforts for preparing high molecular weight PCL [14-16]. Moreover, the hydrolysis of tetra(phenylethynyl)tin catalyst at the end of the ROP generates tin oxide, which is a non-toxic compound and has been approved by FDA for internal use in biomedical applications [17].

The major limitation of PCL applications was associated with the hydrophobic character of the polymer (relative to water) and the low mechanical properties and melting point. The last two decades have seen improvements in the properties profile of biopolymers by blending with clay minerals as natural fillers [18]. Indeed, the combination of PCL and inorganic/organic fillers leads to the upgrade of its thermal and mechanical properties, which has increased the applicability of such biopolymers. Despite the fact that the physical blending of biopolymer with fillers produces nanocomposite materials with improved properties [19-20], the weak adhesion between the two components on account of their diverting hydrophobic/hydrophilic characters negatively affects the dispersion, and thus, the targeted property enhancement. Thus, the in-situ polymerization through grafting approach is considered a good strategy to associate covalently biopolymer and filler in order to produce new hybrid materials with original characteristics [21]. In that regard, our team has successfully prepared PCL-based nanocomposites by the in-situ polymerization of ϵ -caprolactone grafted from cellulose and guar gum polysaccharides as organic fillers and Halloysites clay nanotubes and Beidellite clay as inorganic fillers [22-25].

Bentonite is an abundant natural clay mineral. It has a large surface area, which is highly useful when combined with biopolymers in bio-nanocomposites. It has a 2:1 layered structure consisting of two silicon-oxygen tetrahedral sheets and one aluminum-oxygen-hydroxyl

octahedral sheet [26]. This clay is also interesting for its environmental remediation properties as an absorbent of heavy metals, dyes, and organic pollutants [27-29]. In terms of filled polymers, an antimicrobial film based on starch and bentonite was prepared with enhanced mechanical properties for applications in food packaging [30]. Similar properties were reported for Nano-cellulose (NFC) and Bentonite clay nanocomposites obtained by mixing the NFC with exfoliated bentonite [31]. However, the preparation of bentonite/PCL nanocomposites has been reported in two articles, in both the materials were obtained by physical mixing [32-33].

As mentioned earlier, the low compatibility between PCL and bentonite tends to lead to filler aggregates in the prepared composites, and consequently restricts the improvement of its properties. Therefore, this study was undertaken to evaluate the covalent bonding between PCL and bentonite clay with avoidance of the limitations. The bio-composites material was prepared by *in-situ* ring-opening polymerization of ϵ -CL by generation and thus immobilizing PCL at the surface of bentonite using tetra(phenylethynyl)tin as a catalyst. After the synthesis step, the bio-composite (PCL-OBnt) obtained was fully characterized before carrying out its antimicrobial activity against *S. epidermidis* and *S. aureus* bacteria.

II.2) Material and methods

II.2.1) Materials

ϵ -Caprolactone (liquid), ethanol, chloroform, dichloromethane, hexadecyltrimethylammonium bromide (CTAB), and tetrahydrofuran were purchased from Sigma Aldrich and were used as received. Sodium-bentonite (Na-Bentonite) was collected from Segangane-Nador (Morocco) (57.4%, 24.7%, and 12.3% of clay, silt, and sand, respectively) [34] and its raw characteristics were summarized in Table II.1SI/II.2SI.

II.2.2) Organo-modification of bentonite

The clay mineral used in this study was organo-modified using CTAB as a surfactant. 1 g of bentonite was dispersed into 400 mL of distilled water to which an amount of CTAB equivalent to 0.5 and 1 cation exchange capacity (CEC) of the neat bentonite clay was added. The blending was stirred for 2 h at 25 °C, then the resulted product was filtrated, and washed with distilled water to remove bromine ions. The organo-modified bentonite (OBnt) obtained was dried at 50 °C for 24 h and stored at room temperature [29].

II.2.3) Synthesis of tetra(phenylethynyl) tin as a catalyst for the ring-opening polymerization

The synthesis of tin-based catalyst was carried out following a previously published procedure. Under argon, a three-necked flask was charged with 9 g of phenylacetylene. Toluene (20 mL) at 78 °C was gradually added to 32 mL of a solution of butyllithium in hexane. 5 Grams of Sn(IV)chloride in dry toluene were added to the solution under stirring at 70 °C for 16 h. The obtained solution was filtered and the solvent was evaporated in a vacuum oven to obtain a yellow solid residue, which was recrystallized from toluene [35].

II.2.4) Synthesis of the PCL bio-composites (in-situ polymerization of ϵ -CL)

The organo-modified clay (OBnt) was then used as nanofillers in the preparation of poly(ϵ -caprolactone) based bio-composites. For this, ϵ -CL was weighed into 50 mL Erlenmeyer flasks. 1 wt%, 5 wt%, and 10 wt% of modified Bentonite (OBnt) were added and the suspension was dispersed using ultrasound equipment for 10 min. The catalyst (tetra(phenylethynyl)tin) with a ratio of (ϵ -CL)/(Sn(C \equiv CPh)₄ = 500 was then injected and stirred at room temperature for 2 h. The closed reaction vessel was placed into an oil bath preheated at 120 °C and then stirred for over 15 min in which the total conversion was achieved (see Fig. II.1).

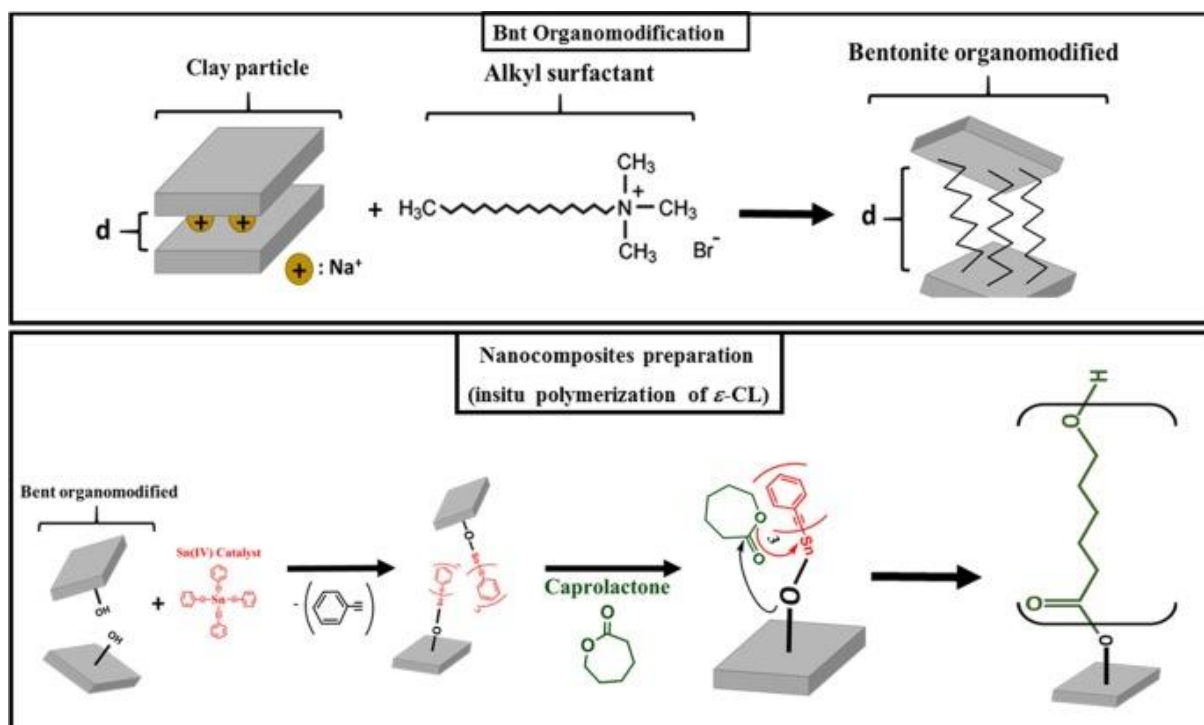


Figure II.11: Proposal of the bio-composites synthesis (PCL-g-OBnt).

II.2.5) Films preparation

PCL and PCL-g-OBnt bio-composites film with different concentrations of modified Bentonite (1, 5, and 10%) were prepared using a solution casting method. Briefly, the nanocomposites of PCL-g-OBnt were dispersed in 2 mL of dichloromethane and stirred for an hour until complete dissolution. The films were cast and allowed to dry for about 24 h at room temperature. The dried films were peeled off from the casting plates (Teflon mold) and pressed using a hot hydraulic press. The tablets obtained (Fig. II.2) were conditioned in a constant temperature humidity chamber. A reference film of neat PCL was also prepared using the same method.

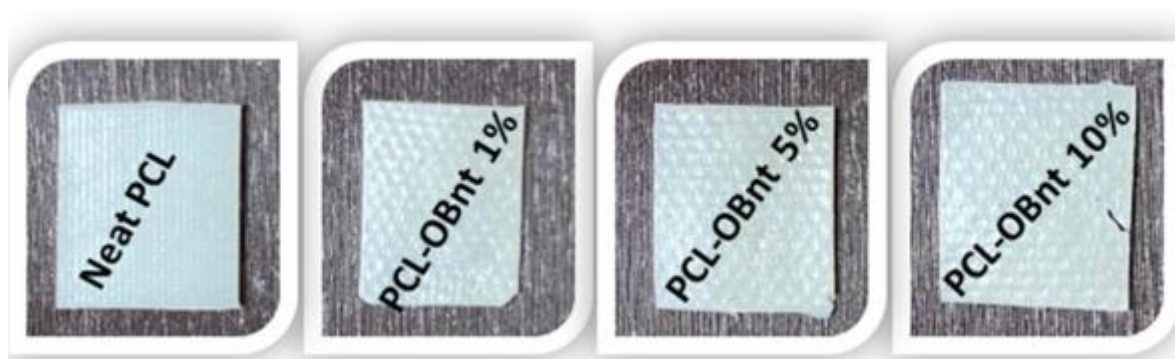


Figure II.12: Digital pictures of the tablets prepared.

II.3) Characterization techniques

II.3.1) Size exclusion chromatography (SEC)

The distribution of the polymer molecular weight (M_n) was carried out by the SEC analysis. The measurements were carried out in a PL-GPC (Polymer laboratory) chromatography equipped with an RI sensor ($\lambda = 264$ nm) and two serially connected columns PLgel Mixed-B (styrene-co-divinylbenzene copolymer gel with 3–100 μm of particle size). THF was used as solvent and eluent wherein the flow rate was 1 mL min^{-1} . The calibration of molecular weight was performed by poly(styrene) (certified reference material EasiCal-PS1B).

PCL extraction was carried out following a published procedure [22]. In order to liberate the chains from the bentonite, the bio-composites prepared were dispersed in chloroform/tetrahydrofuran mixture (20:80) and kept under stirring for 24 h at room temperature. LiCl in THF (2%) was added and the stirring was maintained for an additional 24 h. The last step was the separation of the filler using centrifugation (4000 rpm) of the obtained colloidal aggregates. The polymer (PCL) containing residue was subsequently precipitated in methanol, filtered, and dried in vacuum at 60 °C.

II.3.2) Suspension stability

The success of the grafting was investigated by suspending the physical blending of PCL/OBnt (95:5 wt%) and the prepared bio-composites PCL-g-OBnt in dichloromethane, then the stability of the resulting suspension was compared. The technique involves comparing the dispersity of the PCL-OBnt prepared by in-situ ring-opening polymerization and the physical blending of PCL and the organomodified bentonite (OBnt) [23].

II.3.3) X-ray diffraction (XRD)

The X-ray diffraction of the bentonite (Bnt) and organomodified bentonite (OBnt) powders were analyzed on a D8 Advanced Brüker diffractometer with CuK α radiation ($\lambda = 1.5418 \text{ \AA}$). The XRD analysis indicated a degree of layer intercalation of Bnt after the organo-modification.

II.3.4) Fourier transform-infrared spectroscopy (FTIR)

Infrared spectroscopy was carried out using a PERKIN-ELMER spectrum 1000 Fourier Transform Spectrometer, 32 acquisitions at room temperature at a resolution of 4 cm^{-1} .

II.3.5) Dynamical scanning calorimetry (DSC)

The tests were carried out using a Perkin Elmer Jade DSC under a stream of nitrogen and argon to be able to work under an inert atmosphere. 15 mg of samples were analyzed in a temperature range of 0–100 $^{\circ}\text{C}$ at a rate of 10 $^{\circ}\text{C min}^{-1}$. The crystallization temperatures T_c were determined from the first cooling scan and the melting temperature T_m from the second heating scan.

II.3.6) Thermogravimetric analysis (TGA)

TGA was used to compare the thermal stability of PCL-g-OBnt bio-composites with neat PCL; it was performed using a TGA 55 Discovery instrument at a rate of 10 $^{\circ}\text{C min}^{-1}$ under nitrogen (60 $\text{cm}^3 \text{ min}^{-1}$) from 25 $^{\circ}\text{C}$ to 600 $^{\circ}\text{C}$.

II.3.7) Contact angle measurement

Contact angle was measured by a droplet of water on the surface of the bio-composites (tablets) at room temperature using EASY DROP equipment.

II.3.8) Mechanical properties

The tensile strength of the prepared tablets (PCL-OBnt) was measured and compared to that of neat PCL tablet using an Instron Universal Testing Machine (Model 3369, Instron). Experiments were performed at room temperature, with a crosshead speed of 5 mm/min . The

sample dimensions were $100 \times 20 \times 0.6$ mm³ and the results were averaged on three measurements. The tensile strength and the elongation at break of the prepared film were calculated and compared.

II.3.9) Scanning electron microscopy (SEM)

The morphology of neat PCL and PCL-g-OBnt bio-composite film was examined using Vega 3 TESCAN with conventional tungsten, heated cathode intended both for high vacuum and low vacuum operations. All the samples were previously coated with Au-Pd in argon plasma to enhance their conductivity.

II.3.10) Antimicrobial tests on PCL-g-OBnt bio-composite films

II.3.10.1) Bacterial strains and cultural conditions

The following bacteria were used: *S. epidermidis* (ATCC 35984) and *S. aureus* (ATCC 29213). All materials were previously autoclaved at 121 °C for 15 min. Bacteria were maintained at -20 °C in 30% glycerol. Staphylococcus species were precultured under aerobic conditions in BHI (Brain Heart Infusion) broth (From Difco) for 24 h at 37 °C on a shaker. Cells were harvested by centrifugation (5000 rpm for 15 min at 20–25 °C) and finally resuspended in sterilized PBS solution. The Optical Density (O.D) of the suspension was then measured at 595 nm. If necessary, additional PBS solution was added to the suspension to adjust the O.D to 1 corresponding to 10^7 – 8×10^8 Colony Forming Units (CFU)/mL. Colonies of bacteria were counted on BHI agar plates, after incubation for 24 h at 37 °C.

II.3.10.2) Agar diffusion assay

Bio-composites films (PCL-g-OBnt) and neat PCL films of around 2.6 cm in diameter were placed on the top of BHI agar plates previously inoculated with 10^6 CFU/mL of either *S. epidermidis* or *S. aureus*. The plates were incubated at 5 °C for 2 h to allow pre-diffusion of active molecules, then at 37 °C for 24 h. The inhibition diameter (mm) was then measured for each film. Each test was performed in triplicate.

II.3.10.3) Antibacterial activity of bio-composites films in solution

Bio-composites films (PCL-g-OBnt) and neat PCL films were introduced in test tubes containing 15 mL of PBS solution. Each tube was inoculated by 1 mL of a bacterial culture containing approximately 10^{7-8} CFU/mL to obtain 10^6 CFU/mL as the final concentration of bacteria. All tubes were incubated on a shaker (140 rpm) at 37 °C for 24 h. Then, they were sonicated for 3 min and decimal dilutions of the bacterial culture were spread on BHI agar plates. After incubation for 24 h at 37 °C, the colonies were counted and their concentrations

(CFU/mL) were calculated considering the dilutions. These experiments were repeated 3 times for each film. The percentage of inhibition was determined using the following formula:

$$\% \textit{Inhibition} = \left(\frac{A-B}{A} \right) \times 100 \quad (1)$$

where A is the CFU/mL of the control test (neat PCL film) and B is the CFU/mL in experiments using each Bio-composites film.

II.4) Results and discussion

II.4.1) PCL-OBnt synthesis

The acquired Na-Bentonite used as a filler precursor in this study was initially organo-modified through the exchange of the sodium cations localized into the interlayer space for the cationic surfactant hexadecyl trimethyl ammonium bromide (CTAB). To characterize the intercalation of the cationic surfactant in the organo-modified bentonite (OBnt), X-ray diffraction characterization was carried out. Fig. II.3A gives the XRD diffractograms of the Na-Bentonite before and after the organo-modification of the 001 basal reflection. A significant shift to lower angles value (2θ) was assigned to the interlayer space intercalating effect of the surfactant (CTAB). The expansion of the organo-modified bentonite (OBnt) interlayer spaces occurs by the intercalation of CTAB. Similar results were reported in a previous study [36]. On the other hand, the diffractogram of OBnt was compared to those of the prepared bio-composites (PCL-OBnt). As revealed in Fig. II.3B, the shifting of the basal diffraction peak (0 0 1) from 4° to lower 2θ values (around 1°) suggests the insertion/intercalation of the PCL chains between the clay layers. Indeed, the hydroxyl groups as co-initiators were more accessible for the catalyst after the organomodification of bentonite whereas the in-situ ring-opening polymerization occur following the grafting from approach leading to the expansion of the interplanar distance (d). In fact, the polymer/clay good adhesion may lead to physico-chemical improvement of the biocomposites prepared compared to the neat PCL.

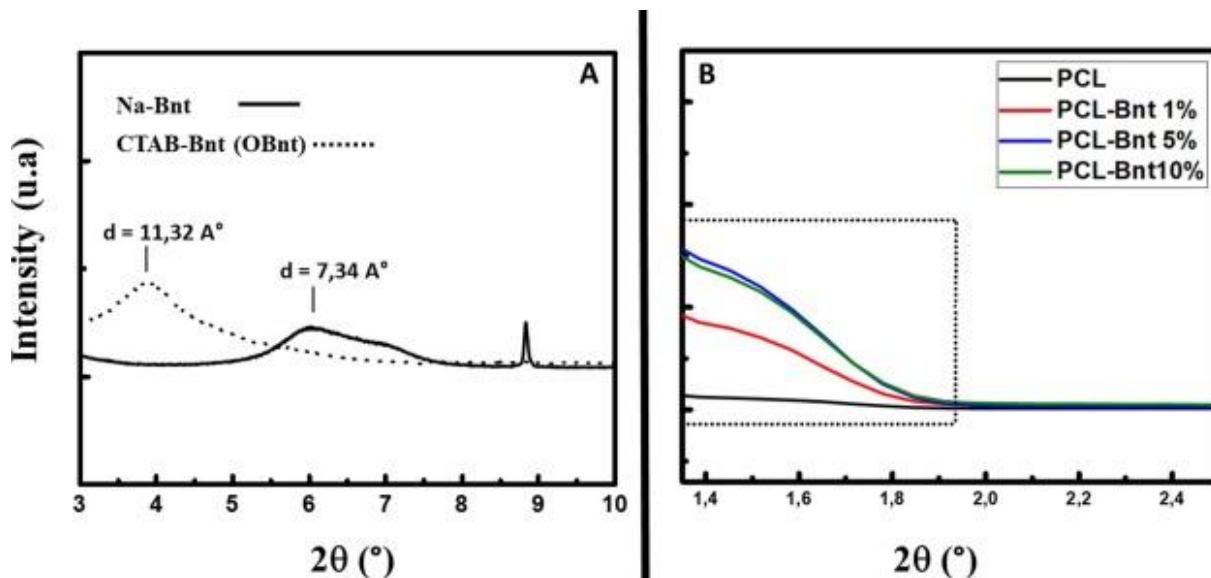


Figure II.13: XRD patterns of bentonite (A), bentonite organomodified (A), and prepared biocomposite (B).

After the organo-modification of the bentonite using CTAB as a surfactant, the poly(ϵ -caprolactone (PCL) was grafted from the organo-modified Bnt (OBnt) by in-situ ring-opening polymerization (ROP). The polymerization was conducted at 120 °C under solvent-free conditions using tetra(phenylethynyl) tin ($\text{Sn}(\text{C}\equiv\text{CPh})_4$) as a catalyst. Bio-composites with various weight percentages of the organomodified bentonite (OBnt) were prepared (1%, 5%, and 10%) to investigate the effect of such a filler on the resulting material properties. The synthesis method involved the dispersion of OBnt in the liquid monomer (ϵ -CL) using an ultrasonic impact for 30 min at 0 °C. The tin initiator ($\text{Sn}(\text{C}\equiv\text{CPh})_4$) was subsequently added to the dispersion after reaching room temperature under stirring. It is envisioned that the hydroxyl groups inside the lamellar galleries of the OBnt react with the tetra(phenylethynyl)tin. As illustrated in suggestion (Fig. II.1), the first step of reaching an active polymerization catalyst consists of generating -Sn-O-Bnt centers inside the organomodified bentonite (OBnt) [37]. The polymerization (ROP) process starts after heating the reaction mixture (to 120 °C), where the mechanism implies the coordination of the monomer (ϵ -CL) next to the alkoxide groups (Bnt-O-Sn) by the carbonyl function followed by an arrangement leading to the cleavage of the O-acyl bond and the insertion of the monomer into the Bnt-O-Sn bond. It is worth noting that the presence of water traces induces the formation of HO-Sn which leads to some free PCL synthesis (HO-PCL-OH). For that, the free polymer (HO-PCL-OH) was extracted by solubilizing the obtained product (PCL-OBnt and HO-PCL-OH) in THF, and by using centrifugation at 6000 rpm the supernatant phase was removed (around 10% of free PCL was

recovered after evaporation of solvent) and only the bio-composites (PCL-OBnt) were characterized.

II.4.2) Characterization of the prepared bio-composites (PCL-OBnt)

The Mn of the free PCL extracted from the prepared PCL biocomposites is summarized in Table II.1. It is found that the Mn of grafted PCL is significantly lower in preparations with a high OBnt (filler) content. In that respect, the lowest value of Mn was obtained with 10% of clay filler (OBnt), while PCL molar mass of 65,973 g.mol⁻¹ was reached when only 1% of OBnt was introduced. The remarkable decrease of the Mn by the increase of the filler amount was the major finding of previous grafting experiments of PCL from organic and inorganic substrates [22], [23], [25]. The main explanation of such results is that the increase of polymerization sites (hydroxyl co-initiator) was related to the increase of the filler (containing OH groups) which leads to more active centers of the polymerization leading to shorter polymer chains [6], [14]. Furthermore, the dispersity of the PCL chains synthesized was as low as 1.91 in all prepared bio-composites (PCL-OBnt) suggesting that the polymerization occurs at least partly by a controlled mechanism with limited contributions of trans-esterification reactions.

Table II.1: Molecular mass values, DSC results, and contact angle results of neat PCL and PCL-OBnt nanocomposites.

	<i>SEC results</i>			<i>DSC results</i>			Contact angle values (°)
	<i>M_w (g mol⁻¹)</i>	<i>M_n (g mol⁻¹)</i>	<i>Đ</i>	<i>T_m (°C)</i>	<i>T_c (°C)</i>	<i>χ_c (ΔH_f^o = 134,6 J/g)</i>	
Neat PCL	97416	45100	2.16	55.3	27.40	32.0 %	91°
PCL-OBnt 1%	136572	65973	2.07	67.6	33.34	37.1 %	87°
PCL-OBnt 5%	64314	33665	1.91	66.6	33.45	38.8 %	84°
PCL-OBnt 10%	39297	20092	1.95	65.8	32.03	34.2 %	69°

The superposition of FTIR spectra of the neat PCL (a) and PCL-OBnt 1%, 5%, and 10% (Fig. II.4, resp. b, c, d) give evidence of the successful grafting through in-situ polymerization. Characteristic signals of the carbonyl groups were clearly identified at 1720 cm⁻¹ with two other vibration signals at around 2850–2940 cm⁻¹ assigned to C-H stretching vibrations [23], [25]. The PCL-OBnt biocomposites spectra show, contrary to those of neat PCL, a broad vibration mode around 3400 cm⁻¹ which is related to the free OH groups in the organomodified bentonite clay.

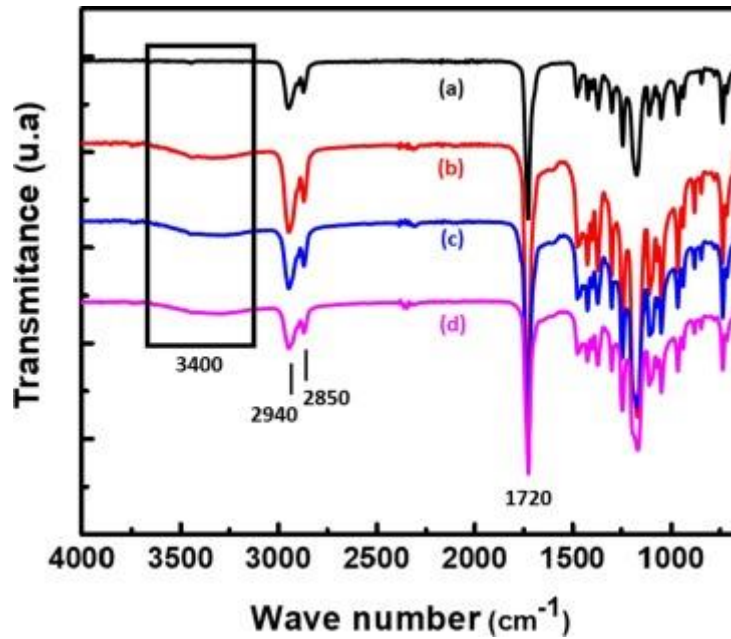


Figure II.14: Infrared spectrum of neat PCL (a), PCL-OBnt biocomposites 1% (b), 5% (c) and 10% (d).

Evidence for grafting of PCL to the OBnt (grafting success) was found in a comparative study of the stability of dichloromethane suspensions of the neat bentonite (Bnt), the synthesized biocomposite (PCL-g-OBnt 5%), and the physical mixture of PCL and bentonite (PCL/OBnt). As shown in Fig. II.5, OBnt and the physically blended PCL/OBnt readily precipitate. A sediment deposition was clearly observed after 24 h in those cases. In contrast, mixtures of dichloromethane and the PCL grafted from bentonite (PCL-g-OBnt) remain stable and appear homogeneous even after 24 h. Apparently, the PCL chains are able to keep the hydrophilic bentonite clay particles in suspension. The PCL does not diffuse out of the bentonite within the time frame of the experiment. The low dynamic of the process is in accordance with a tight binding (chemical bond) between the polymer and the filler.

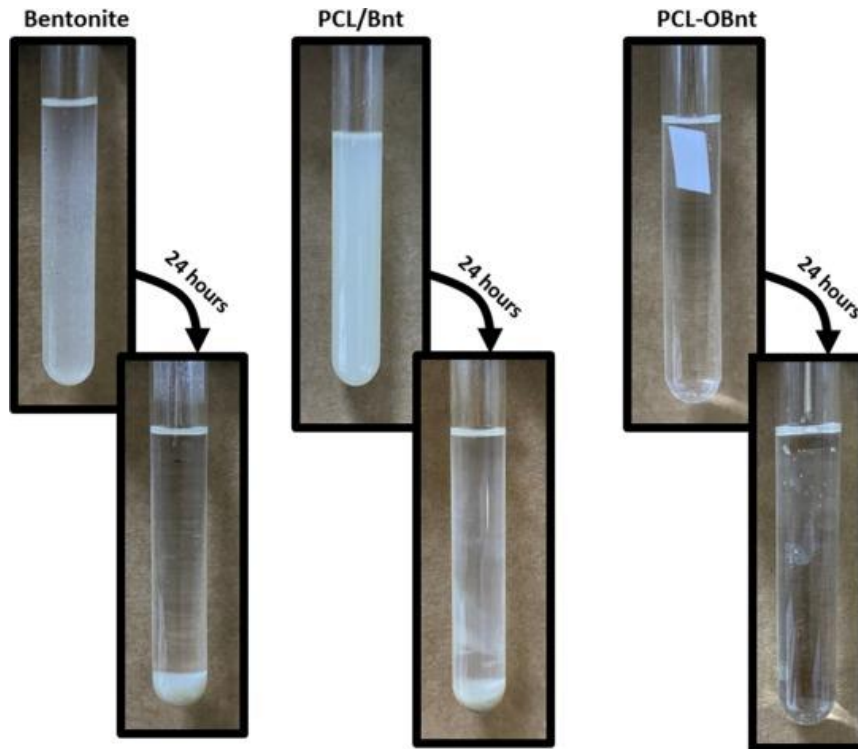


Figure II.15: Suspension in dichloromethane before and after 24 h of OBnt, PCL/OBnt (95:5 wt%) physically mixed, and bio-composite (PCL-OBnt 5%).

The thermal characterization using DSC analysis had a focus on the melting temperature (T_m), crystallization temperature (T_c), and associated degree of crystallinity (χ_c) (Table II.1). The melting point (T_m) and the peak temperature of crystallization (T_c) of the PCL-OBnt bio-composites were considerably higher than neat PCL. These changes might indicate an alteration in the structure of the grafted PCL chains in which a crystalline brush structure could be formed from the filler (OBnt) (substrate). The latter supposition was in concordance with the reported values of the degree of crystallinity (χ_c), where the brush structures could generate an additional small crystalline zone in the biocomposites (PCL-OBnt). Furthermore, the increase in T_c could also be attributed to the difference in molecular weight between native PCL and PCL-OBnt composites. Indeed, Jana et Cho, found that the T_c and the crystallinity of PCL grafted onto multi-walled nanotube (MWNTs) increased with the content of MWNTs [38]. However, the difference in molecular weight cannot be the sole explanation for such phenomena, as we also observed, no significant change in T_c values when the content of OBnt beyond 1% induces a decline in M_n but not in T_c . For the melting point (T_m), the values increased from 55.3 °C for the neat PCL to 67.6 °C for the PCL-based bio-composites (PCL-OBnt). This was also recently observed for PCL/graphene composites [39].

A thermographic analysis was carried out to investigate the effect of the organo-modified bentonite (OBnt) on the bio-composites thermal stability. Fig. II.6 depicts representative thermograms of neat PCL and the prepared PCL-OBnt bio-composites with various amounts of OBnt. The thermal degradation of neat PCL starts at 315 °C, while the thermal degradation of the PCL bio-composites (PCL-OBnt) occurs at a slightly higher temperature (320 °C). In the second stage (up to 330 °C), the shift to higher temperatures of thermal degradation was more significant for the bio-composites material (PCL-OBnt) compared to the neat polymer (PCL). Indeed, the presence of clay as a filler (PCL-OBnt) must be the cause of such thermal stability improvement. Moreover, the good dispersion of the filler (clay mineral) in the polymeric matrix enhances the composite stability by the formation of protecting layers and char [23], [25], [40].

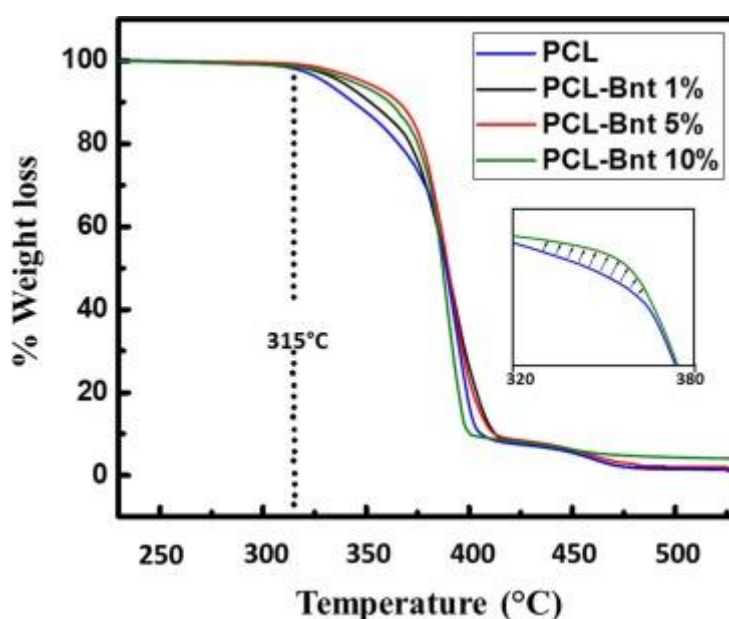


Figure II.16: TGA curves of the neat PCL and PCL-OBnt nanocomposites.

As is well known, the neat PCL is rather hydrophobic in character, which restricts its uses in specific applications such as surface-engineered, antifouling, or repelling material. The OBnt content influences the hydrophobic property of the PCL. As expected, the bio-composites prepared revealed a low contact angle values compared to the homopolymer (Fig. II.7; neat PCL/**91°**, PCL-OBnt 1%/**87°**, 5%/**84°**, and 10%/**69°**). In fact, when PCL was grafted from a high amount of hydrophilic filler, the hydrophobic character decreases considerably. The main explication of such behavior could be related to the polar nature of clay mineral used as a substrate of the polymer “grafting from”. Furthermore, the hydroxyl groups situated in the filler could decrease the hydrophobic character of such bio-composite. Similar changes in the contact angle values were reported previously in PCL grafted from Halloysites clay nanotube [41].

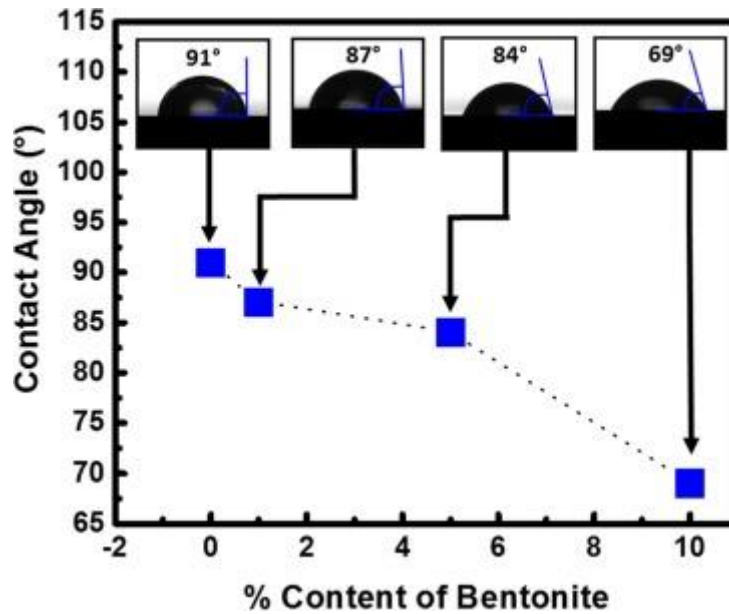


Figure II.17: Contact angle measurement of water drop on the prepared bio-nanocomposites (PCL-OBnt).

The mechanical properties of the prepared bio-composites (PCL-OBnt) were assessed by comparing their tensile at break and the elongation at break with those of neat PCL. As exposed in Fig. II.8, the neat PCL shows the highest value of elongation at break (18%) instead of around only 5% related to the PCL bio-composite based (PCL-OBnt 5%). The usual decrease of the elongation at break by introducing the filler is understandable by the reduced mobility of the chains, leading to higher local tensions, resulting in bond breaking. Consequently, higher filler content leads to lower elongation at break. The differences in the maximum tension between the composites with different filler contents may be related to the concomitant lower molecular weights. This also explains the difference between the neat matrix polymer. The resistance of such biofilms under mechanical stress highlights the great utility of such material in packaging applications.

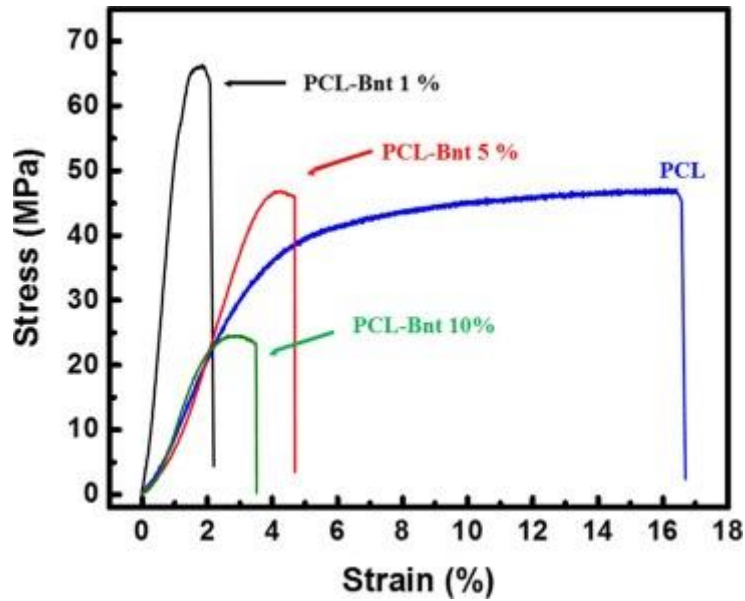


Figure II.18: Representative compressive stress-strain curves of neat PCL and PCL bio-composites.

The morphology and the structure of the surface and cross-section of cryo-broken films of the neat PCL and PCL-OBnt 5% films were explored (Fig. II.9). The neat PCL as a reference shows a smooth surface (Fig. II.9A) with some voids related to the solvent evaporation, which is quite similar to the bio-composite surface (Fig. 9D). Furthermore, a uniform structure was revealed from the cross-section in Fig. II.9B and II.9C while clay particles of organo-modified bentonite could be seen surrounded by polymer from the composite cross-section image represented in Fig. II.9F. From Fig. II.9E, the good dispersion of clay particles in the polymeric matrix could be observed, also the absence of cavity and phase separation confirm the substantial interaction between PCL and OBnt.

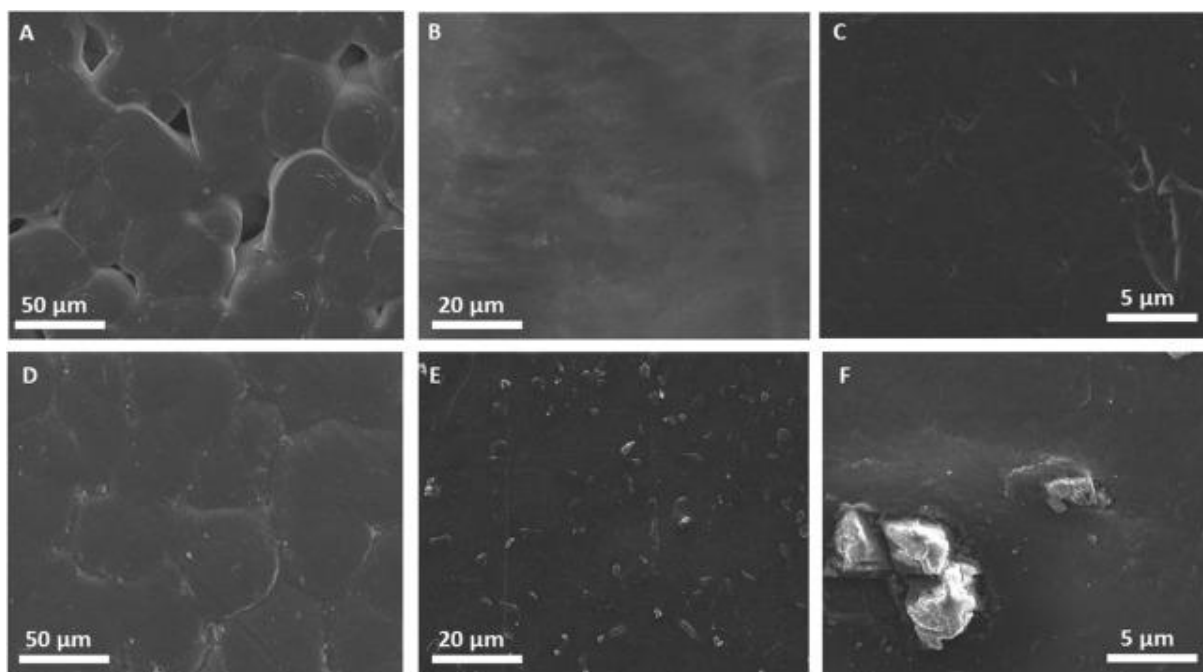


Figure II.19: SEM images surfaces and cross-sections of the films prepared, the neat PCL (A, B, C) and PCL-OBnt 5% (D, E, F).

II.4.3) Antimicrobial tests on PCL-OBnt bio-composite films

Antibacterial activity of bio-composite films was evaluated against *S. epidermis* and *S. aureus* by diffusion experiments. The neat PCL film has not shown any inhibition zone (Fig. II.10), demonstrating that no antimicrobial activity was displayed by the PCL films. On the other hand, the PCL-OBnt bio-composite films clearly inhibited the growth of both species. Moreover, the inhibition zone increased proportionally with the amount of modified bentonite introduced in bio-composite. For *S. epidermidis*, the inhibition zone increased from 2.8 cm for the PCL-OBnt 1% film to 3.25 cm for the PCL-OBnt 10% film. The inhibition zones were slightly lower against *S. aureus* compared to *S. epidermidis*, showing a higher sensitivity of *S. epidermidis* toward the composite films based on PCL grafted from the organo-modified bentonite (PCL-OBnt).

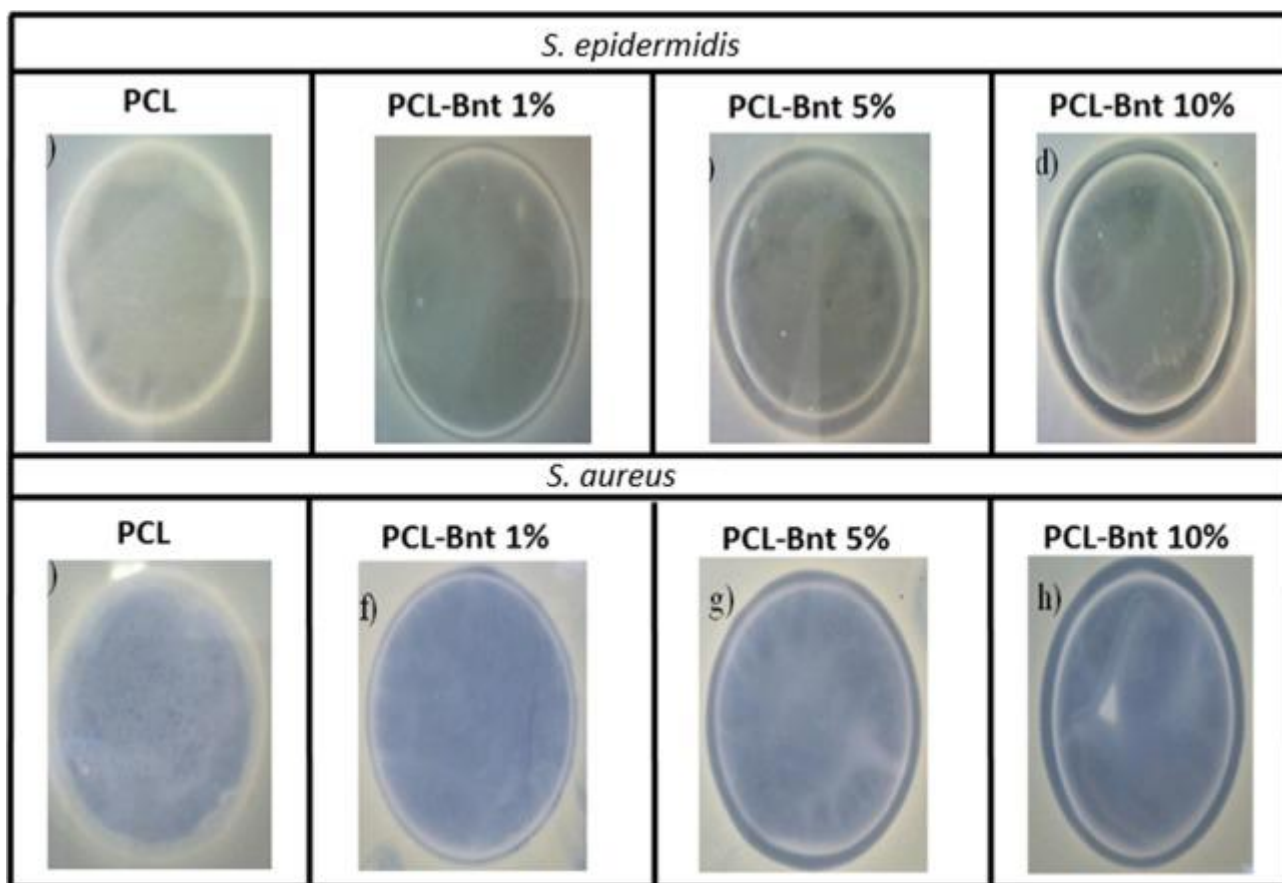


Figure II.20: Images of diffusion assay of PCL and its bio-composites PCL-OBnt, against *S. epidermidis* and *S. aureus*.

In order to evaluate quantitatively the antibacterial effect of the prepared bio-composite films, antibacterial activity experiments were carried out in solution and the bacterial concentrations (CFU/mL) and the inhibition percentages were calculated by counting method (Table II.2).

Table II.2: Growth of *S. epidermidis* and *S. aureus* in the presence of PCL and bio-composites films.

Tested Material	<i>S. epidermidis</i>		<i>S. aureus</i>	
	CFU/ml	% of inhibition	CFU/ml	% of inhibition
PCL		-		-
PCL-OBnt 1%	4.0×10^4	96.3%	2.1×10^5	97.9%
PCL-OBnt 5%	1.3×10^4	99.8%	8.5×10^4	99.2%
PCL-OBnt 10%	4.9×10^3	99.9%	1.6×10^4	99.8%

However, the organo-modified bentonite decreased significantly the bacterial growth with a concentration of OBnt as little as 1% (96.3% and 97.9% against *S. epidermidis* and *S. aureus*, respectively). Furthermore, the inhibition of bacterial growth increased with the content of OBnt against both species and reached up to 99.9% against *S. epidermidis* for bio-composite

film with 10% of OBnt. This trend was also observed in the diffusion assay and can be explained by the higher amount of CTAB in the clay. It is worth mentioning that the antimicrobial activity of bio-composite films is higher against *S. epidermidis* than *S. aureus*. This difference in activity against staphylococci species could be due to a higher sensitivity of *S. epidermidis* towards CTAB than *S. aureus*. Furthermore, a total inhibition of bacteria could occur with a slightly higher percentage of modified bentonite in the bio-composites (PCL-OBnt 10%).

II.5) Conclusion

The Bentonite as clay mineral was successfully organo-modified by exchanging the sodium cations localized into the interlayer space with hexadecyltrimethylammonium bromide (CTAB) as cationic surfactant as proved by the XRD pattern. Moreover, the grafting of PCL on the organo-modified bentonite clay (OBnt) as a filler was achieved for the first time, following the in-situ ring-opening polymerization of ϵ -CL using a nontoxic tin catalyst. Indeed, the grafting from success was validated by comparing the FTIR spectra of neat PCL with those of the prepared biocomposites (PCL-OBnt) where hydroxyl vibrations were slightly visible, the grafting from was also approved by comparing the stability of the physical blending of PCL/OBnt and the prepared bio-composites material in dichloromethane after 24 h. Thus, the prepared bio-composites (PCL-OBnt) presented better thermal stability regardless of the content of OBnt as a reinforcing filler. In fact, the melting point and the PCL-OBnt degree of crystallinity determined by TGA and DSC analysis, increased by increasing the amount of the filler (OBnt). In addition, a significant decrease of the hydrophobicity, from the neat PCL to the PCL grafted from OBnt was perceived. Furthermore, the fractured surfaces of the neat polymer (PCL) and the bio-composites (PCL-OBnt) were compared using scanning electron microscopy (SEM) in which the adhesion between clay particles and the polymer was clearly exposed as well as the dispersion of the OBnt filler in the polymeric matrix. Additionally, the bio-composites with 5% of OBnt (PCL-OBnt 5%) display the highest resistance under stress with 66 MPa instead of 46 MPa only for the neat PCL. Finally, the bio-composites PCL-OBnt have shown excellent antibacterial activity against two bacteria species with an inhibition percentage of more than 96% with only 1% of OBnt content.

II.6) Supporting information

Table II.1SI: Texture and cation exchange capacity of bentonite

pH	CO %	MO %	CEC meq/100g	Sandy %	Loam %	Clay %
7.4	0.71	1.22	84.7	12.3	24.7	57.4

Table II.2SI : Chemical composition

Elemental oxides	wt. %
SiO₂	57.32
Al₂O₃	24.87
Fe₂O₃	3.90
MnO	0.00
MgO	2.42
CaO	1.10
Na₂O	1.90
K₂O	0.65
TiO₂	0.27
P₂O₅	0.04
SO₃	0.12
SrO	0.02

Reference

- [1] M. Murariu, P. Dubois, PLA composites : From production to properties ☆, *Adv. Drug Deliv. Rev.* 107 (2016) 17–46. <https://doi.org/10.1016/j.addr.2016.04.003>.
- [2] F. Chivrac, E. Pollet, L. Avérous, Progress in nano-biocomposites based on polysaccharides and nanoclays, *Mater. Sci. Eng. R Reports.* 67 (2009) 1–17. <https://doi.org/10.1016/j.mser.2009.09.002>.
- [3] L. Peponi, I. Navarro-baena, J.E. Báez, J.M. Kenny, A. Marcos-fernández, Effect of the molecular weight on the crystallinity of PCL-b-PLLA di-block copolymers, *Polymer (Guildf).* 53 (2012) 4561–4568. <https://doi.org/10.1016/j.polymer.2012.07.066>.
- [4] J.E. Mark, *Polymer Data Handbook*, J.E. Mark, Oxford University Press, New York, 1999. <https://books.google.co.ma/books?id=ZCYCPwAACAAJ>.
- [5] Y. Guo, X. Wang, Z. Shen, X. Shu, R. Sun, Preparation of cellulose-graft-poly(ϵ -caprolactone) nanomicelles by homogeneous ROP in ionic liquid, *Carbohydr. Polym.* 92 (2013) 77–83. <https://doi.org/10.1016/j.carbpol.2012.09.058>.
- [6] M. Labet, W. Thielemans, Synthesis of polycaprolactone: a review, *Chem. Soc. Rev.* 38 (2009) 3484. <https://doi.org/10.1039/b820162p>.
- [7] M. Ryner, K. Stridsberg, A.C. Albertsson, H. Von Schenck, M. Svensson, Mechanism of ring-opening polymerization of 1,5-dioxepan-2-one and L-lactide with stannous 2-ethylhexanoate. A theoretical study, *Macromolecules.* 34 (2001) 3877–3881. <https://doi.org/10.1021/ma002096n>.
- [8] A.C.S. Alcântara, M. Darder, P. Aranda, E. Ruiz-Hitzky, Polysaccharide-fibrous clay bionanocomposites, *Appl. Clay Sci.* 96 (2014) 2–8. <https://doi.org/10.1016/j.clay.2014.02.018>.
- [9] N.M. Barkoula, B. Alcock, N.O. Cabrera, T. Peijs, Fatigue properties of highly oriented polypropylene tapes and all-polypropylene composites, *Polym. Polym. Compos.* 16 (2008) 101–113. <https://doi.org/10.1002/pc>.
- [10] C. Jérôme, P. Lecomte, Recent advances in the synthesis of aliphatic polyesters by ring-opening polymerization, *Adv. Drug Deliv. Rev.* 60 (2008) 1056–1076. <https://doi.org/10.1016/j.addr.2008.02.008>.
- [11] L. Najemi, T. Jeanmaire, A. Zerroukhi, M. Raihane, Organic catalyst for ring opening polymerization of ϵ -caprolactone in bulk. Route to starch-graft-polycaprolactone, *Starch/Staerke.* 62 (2010) 147–154. <https://doi.org/10.1002/star.200900198>.
- [12] J.L. Robert, K.B. Aubrecht, Ring-Opening Polymerization of Lactide To Form a Biodegradable Polymer, *J. Chem. Educ.* 85 (2008) 258. <https://doi.org/10.1021/ed085p258>.
- [13] M.C. Tanzi, P. Verderio, M.G. Lampugnani, M. Resnati, E. Dejana, E. Sturani, Cytotoxicity of some catalysts commonly used in the synthesis of copolymers for biomedical use, *J. Mater. Sci. Mater. Med.* 5 (1994) 393–396. <https://doi.org/10.1007/BF00058971>.
- [14] M. Kalmi, M. Lahcini, P. Castro, O. Lehtonen, A. Belfkira, M. Leskelä, T. Repo, Tetrakis Sn(IV) Alkoxides as Novel Initiators for Living Ring-Opening Polymerization of Lactides, *J. Polym. Sci. Part A Polym. Chem.* 42 (2004) 1901–1911. <https://doi.org/10.1002/pola.20028>.

- [15] M. Lahcini, S. Elhakioui, D. Szopinski, B. Neuer, A. El Kadib, F. Scheliga, M. Raihane, Harnessing synergies in tin-clay catalyst for the preparation of poly (ϵ -caprolactone) / halloysite nanocomposites, *Eur. Polym. J.* 81 (2016) 1–11. <https://doi.org/10.1016/j.eurpolymj.2016.05.014>.
- [16] T. ElAssimi, RokoBlažic, A. El Kadib, M. Raihane, R. Beniazza, G.A. Luinstra, E. Vidović, M. Lahcini, Synthesis of poly(ϵ -caprolactone)-grafted guar gum by surface-initiated ring-opening polymerization, *Carbohydr. Polym.* 220 (2019) 95–102. <https://doi.org/10.1016/j.carbpol.2019.05.049>.
- [17] Agency for Toxic Substances and Disease Registry (ATSDR). Toxicological Profile for Tin;, U.S. Department of Health and Human Services, Public Health Service, Atlanta, 2003.
- [18] R.M. Mohamed, K. Yusoh, A Review on the Recent Research of Polycaprolactone (PCL), *Adv. Mater. Res.* 1134 (2015) 249–255. <https://doi.org/10.4028/www.scientific.net/amr.1134.249>.
- [19] T. El, R. Bla, E. Vidovi, M. Raihane, A. El, M. Hassen, V. Baouab, M. Khoulood, R. Beniazza, H. Kricheldorf, M. Lahcini, Progress in Organic Coatings Polylactide / cellulose acetate biocomposites as potential coating membranes for controlled and slow nutrients release from water-soluble fertilizers, 156 (2021). <https://doi.org/10.1016/j.porgcoat.2021.106255>.
- [20] H.S. Cho, H.S. Moon, M. Kim, K. Nam, J.Y. Kim, Biodegradability and biodegradation rate of poly(caprolactone)-starch blend and poly(butylene succinate) biodegradable polymer under aerobic and anaerobic environment, *Waste Manag.* 31 (2011) 475–480. <https://doi.org/10.1016/j.wasman.2010.10.029>.
- [21] H. Lönnberg, Q. Zhou, H. Brumer, T.T. Teeri, E. Malmström, A. Hult, Grafting of cellulose fibers with poly(ϵ -caprolactone) and poly(L-lactic acid) via ring-opening polymerization, *Biomacromolecules.* 7 (2006) 2178–2185. <https://doi.org/10.1021/bm060178z>.
- [22] A. Boujemaoui, L. Carlsson, E. Malmstro, M. Lahcini, L. Berglund, H. Sehaqui, A. Carlmark, Facile Preparation Route for Nanostructured Composites: Surface- Initiated Ring-Opening Polymerization of ϵ -Caprolactone from High- Surface-Area Nanopaper, *ACS Appl. Mater. Interfaces.* 4 (2012) 3191–3198.
- [23] M. Lahcini, S. Elhakioui, D. Szopinski, B. Neuer, A. El Kadib, F. Scheliga, M. Raihane, F.J. Baltá Calleja, G.A. Luinstra, Harnessing synergies in tin-clay catalyst for the preparation of poly(ϵ -caprolactone)/halloysite nanocomposites, *Eur. Polym. J.* 81 (2016) 1–11. <https://doi.org/10.1016/j.eurpolymj.2016.05.014>.
- [24] M. Ilsouk, M. Raihane, M. Lahcini, R.M. Meri, J. Zicāns, L.B. Cimdina, G.B. Kharas, Organomodified Moroccan beidellite clay prepared by in situ ring opening polymerization : Characterizations and properties, *J. Macromol. Sci. Part A Pure Appl. Chem.* 54 (2017) 201–210. <https://doi.org/10.1080/10601325.2017.1282229>.
- [25] T. El, R. Bla, A. El, M. Raihane, R. Beniazza, G.A. Luinstra, E. Vidovi, M. Lahcini, Synthesis of poly (ϵ -caprolactone) -grafted guar gum by surface-initiated ring- opening polymerization, *Carbohydr. Polym.* 220 (2019) 95–102. <https://doi.org/10.1016/j.carbpol.2019.05.049>.
- [26] T.S. Anirudhan, M. Ramachandran, Adsorptive removal of tannin from aqueous solutions by cationic surfactant-modified bentonite clay, *J. Colloid Interface Sci.* 299 (2006) 116–124. <https://doi.org/10.1016/j.jcis.2006.01.056>.

- [27] J. Guo, S. Chen, L. Liu, B. Li, P. Yang, L. Zhang, Y. Feng, Adsorption of dye from wastewater using chitosan-CTAB modified bentonites, *J. Colloid Interface Sci.* 382 (2012) 61–66. <https://doi.org/10.1016/j.jcis.2012.05.044>.
- [28] X. Xin, W. Si, Z. Yao, R. Feng, B. Du, L. Yan, Q. Wei, Adsorption of benzoic acid from aqueous solution by three kinds of modified bentonites, *J. Colloid Interface Sci.* 359 (2011) 499–504. <https://doi.org/10.1016/j.jcis.2011.04.044>.
- [29] L. Bounab, K. Draoui, M. Ahrouch, M. Hadri, D. Bouchta, A. Barhoun, An effective functionalized moroccan bentonite: Application for a green remediation of m-cresol, *J. Mater. Environ. Sci.* 8 (2017) 244–256.
- [30] B. Iamareerat, M. Singh, M.B. Sadiq, A.K. Anal, Reinforced cassava starch based edible film incorporated with essential oil and sodium bentonite nanoclay as food packaging material, *J. Food Sci. Technol.* 55 (2018) 1953–1959. <https://doi.org/10.1007/s13197-018-3100-7>.
- [31] M. Zheng, M. Tajvidi, A.H. Tayeb, N.M. Stark, Effects of bentonite on physical , mechanical and barrier properties of cellulose nanofibril hybrid films for packaging applications, *Cellulose.* 26 (2019) 5363–5379. <https://doi.org/10.1007/s10570-019-02473-2>.
- [32] T.R. Ridwan, Basuki Wirjosentono, Tamrin, Mechanical Properties , Morphology and Thermal Degradation of PCL (Poly ϵ - Caprolactone) Biodegradable Polymer Blended Nanocomposites with Aceh Bentonite as Filler Mechanical Properties , Morphology and Thermal Degradation of PCL (Poly ϵ - Caprolacton, *Mater. Sci. Eng.* 536 (2019). <https://doi.org/10.1088/1757-899X/536/1/012040>.
- [33] Ridwan, B. Wirjosentono, R. Siburian, T. Rihayat, Modification of PLA / PCL / Aceh ' s bentonite nanocomposites as biomedical materials Modification of PLA / Bentonite Nanocomposites as Biomedical Materials, in: *AIP Conf Proc.*, 2018.
- [34] S. Azarkan, A. Peña, K. Draoui, C.I. Sainz-Díaz, Adsorption of two fungicides on natural clays of Morocco, *Appl. Clay Sci.* 123 (2016) 37–46. <https://doi.org/10.1016/j.clay.2015.12.036>.
- [35] B. Jousseume, H. Riague, T. Toupance, M. Lahcini, P. Mountford, B.R. Tyrrell, A general route to alkylene-, arylene-, or benzylene-bridged ditin hexachlorides and hexaalkynides, *Organometallics.* 21 (2002) 4590–4594. <https://doi.org/10.1021/om0202468>.
- [36] T. El, O. Lakbita, A. El, M. Khoulood, A. Dahchour, R. Beniazza, R. Boulif, M. Raihane, M. Lahcini, Sustainable coating material based on chitosan-clay composite and paraffin wax for slow-release DAP fertilizer, *Int. J. Biol. Macromol.* 161 (2020) 492–502. <https://doi.org/10.1016/j.ijbiomac.2020.06.074>.
- [37] P. Jaumier, B. Jousseume, M. Lahcini, F. Ribot, C. Sanchez, New route to monoorganotin oxides and alkoxides from trialkynylorganotins, *Chem. Commun.* 2 (1998) 369–370. <https://doi.org/10.1039/a707298h>.
- [38] R.N. Jana, J.W. Cho, Thermal Stability , Crystallization Behavior , and Phase Morphology of Poly (ϵ -caprolactone) diol- grafted - Multiwalled Carbon Nanotubes, *J. Appl. Polym. Sci.* 110 (2008) 1550–1558. <https://doi.org/10.1002/app>.
- [39] M. Bagheri, A. Mahmoodzadeh, Polycaprolactone / Graphene Nanocomposites : Synthesis , Characterization and Mechanical Properties of Electrospun Nanofibers, *J. Inorg. Organomet. Polym. Mater.* 30 (2020) 1566–1577. <https://doi.org/10.1007/s10904-019-01340-8>.

[40] T. Žukas, V. Jankauskaitė, K. Žukienė, A. Baltušnikas, The Influence of Nanofillers on the Mechanical Properties of Carbon Fibre Reinforced Methyl Methacrylate Composite, 18 (2012) 250–255.

[41] T. El, A. Manal, M. Raihane, A. El, M. Mehdi, K. Rachid, Poly (ϵ - caprolactone)- g - Guar Gum and Poly (ϵ - caprolactone)- g - Halloysite Nanotubes as Coatings for Slow - Release DAP Fertilizer, J. Polym. Environ. (2020). <https://doi.org/10.1007/s10924-020-01750-7>.

Chapter III:

Synthesis and antibacterial behavior of bio-composite materials-based on poly(ϵ -caprolactone)/bentonite

Chapter overview

In the previous chapter, PCL-OBnt nanocomposites showed enhanced thermal and mechanical properties as well as excellent antibacterial activity through diffusion. These results prove the potential of these nanocomposites as food packaging materials. However, PCL is prepared through the polymerization of ϵ -CL, a fossil-based monomer, thus raising environmental concerns. Additionally, the antibacterial activity exhibited by these nanocomposites is due to the diffusion of CTAB from PCL-OBnt nanocomposites which could contaminate the packaged food as well as impact its organoleptic properties.

As a solution, in this chapter, PCL was replaced by PLA, which is another biodegradable and biocompatible but is more advantageous as it's prepared through the polymerization of lactide, a monomer prepared from lactic acid. Moreover, PLA presents higher mechanical properties compared to PCL.

As for the diffusion of the antibacterial agent which is usually the case with organic antibacterial molecules (*e.g.*, CTAB). In these new composites, silver nanoparticles, known to have a low migration, were used to provide antibacterial activity. Therefore, the organomodification to enhance the compatibility between Bnt and the polymer was no longer an option. To bypass this problem, Bnt was replaced by fluorphlogopite, a synthetic mica with a sheet-like structure in which -OH groups were replaced by fluorine ions, thus making it more hydrophobic and potentially more compatible with PLA. This also means that the “grafting from” *in-situ* ring-opening polymerization using -OH groups as co-initiators is no longer possible. Thus, in this chapter, melt extrusion was used to prepare PLA-fluorphlogopite-AgNPs nanocomposites instead of ROP. This technique also offers the advantage of being simpler and easily scaled up making it the technique of choice in industrial processes.

The results of this chapter are presented in the form of a published paper entitled “Preparation and study of the thermal, barrier and antibacterial properties of Polylactic acid-Fluorphlogopite-Silver nanoparticles nanocomposite films” in “*Progress in organic coating*”, DOI is yet to be available.

The preparation and study of the thermal, barrier and antibacterial properties of Polylactic acid-Fluorophlogopite-silver nanoparticles nanocomposite films

Abderrahmane Nabgui^{1,2,3}, Nadège Follain¹, Elvira Vidović⁴, Jamal El Haskouri⁵, Stéphane Marais¹, Abdellatif El Meziane², Mohamed Lahcini^{3,6}, Pascal Thébault^{1*}

¹Normandie Univ, UNIROUEN, INSA Rouen, CNRS, PBS UMR6270, Bd Maurice de Broglie, 76821 Mont Saint Aignan Cedex, France.

²Center of Agrobiotechnology and Bio-engineering (Centre AgroBiotech, URL-CNRST 05), Department of Biology. Faculty of Sciences and Techniques, Cadi-Ayyad University, 40000, Marrakech, Morocco.

³IMED-Lab, Faculty of Sciences and Techniques, Cadi-Ayyad University, 40000, Marrakech, Morocco

⁴University of Zagreb, Faculty of Chemical Engineering and Technology, HR-10000, Croatia

⁵Instituto de ciencias de los materiales de la universidad de valencia, Calle catedrático José Beltrán, 2, C.P 46980 Paterna Valencia Spain

⁶Mohammed VI Polytechnic University, Ben Guerir, 43150, Morocco

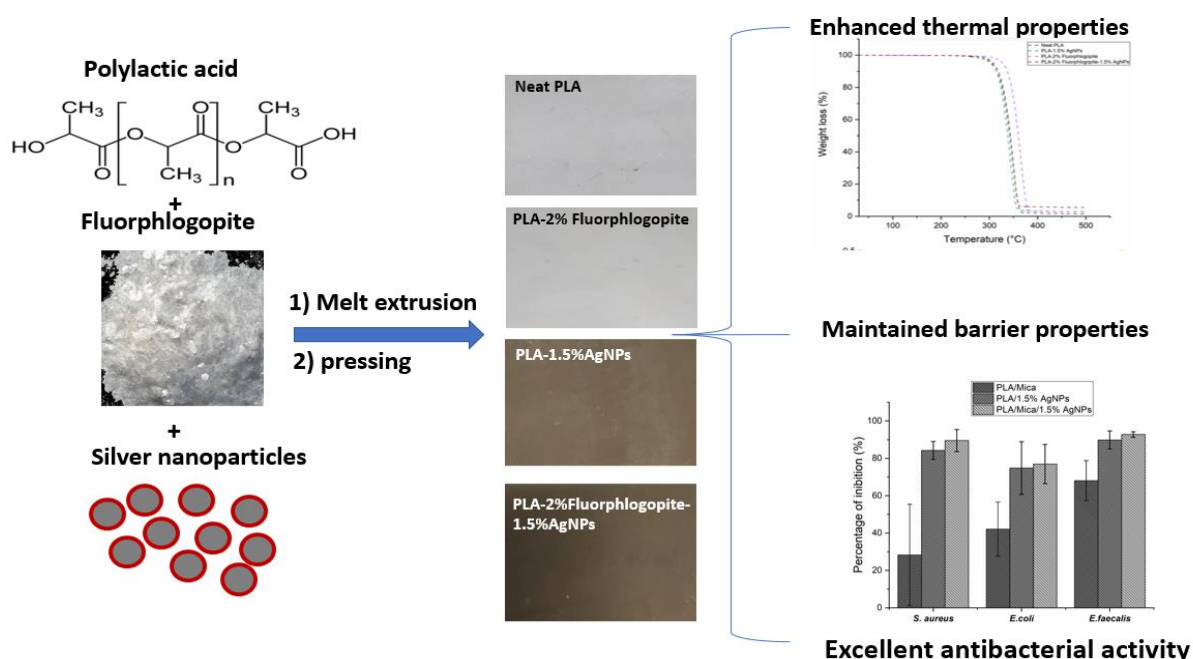
* Corresponding author at : Normandie Univ, UNIROUEN, INSA Rouen, CNRS, PBS UMR6270, Bd Maurice de Broglie, 76821 Mont Saint Aignan Cedex, France.
pascal.thebault@univ-rouen.fr

Abstract

Nowadays, there is an increasing need to develop new green biodegradable materials for active antimicrobial food packaging applications. In this work, polylactic acid-2% Fluorophlogopite-1.5% silver nanoparticles (AgNPs) composites were prepared using melt extrusion. Films were characterized using Scanning Electron Microscopy, Transmission Electron Microscopy, X-Ray Diffraction, Differential Scanning Calorimetry, and Water Contact Angle measurements. Results showed a good dispersion of both fluorophlogopite and AgNPs in PLA which increased the surface roughness and hydrophobicity of PLA. Subsequently, the thermal, mechanical, and barrier properties of PLA nanocomposites were assessed. PLA-2%Fluorophlogopite-1.5%AgNPs showed higher thermal stability than neat PLA while the mechanical properties remained unchanged. Furthermore, the excellent barrier properties of PLA were also unaffected by the introduction of fluorophlogopite and AgNPs. Finally, the antibacterial activity of the nanocomposites was assessed against three bacteria, *S. aureus*, *E. faecalis*, and *E. coli* and PLA-2%Fluorophlogopite-1.5%AgNPs inhibited almost completely the bacterial adhesion on the surface of the films.

Keywords: Antimicrobial food packaging, Polylactic acid, Fluorophlogopite, Silver nanoparticles, Antibacterial activity, Barrier properties, Thermal properties

Graphical abstract



III.1) Introduction

Food contamination due to foodborne pathogens constitutes a major health concern leading, according to the World Health Organization, to about 600 million sick and 420,000 dead each year. Furthermore, these contaminations have also an economic impact with, for example, an annual cost of about 152 billion dollars in the US [1]. Additionally, the food loss due to spoilage by microorganisms is estimated to be ~ 1.3 billion tons annually [2]. In that regard, multiple techniques are used to prevent food spoilage and contamination such as freezing, thermal processing, and refrigeration [3]. However, the need for fresh and minimally-processed food requires other alternatives. Food packaging is one such alternative used to extend the shelf-life of food by acting as a physical barrier to the external environment [4].

In that regard, petroleum-based plastics such as polyethylene (PE), polystyrene (PS), polyvinylchloride (PVC) and polyethylene terephthalate (PET) are usually used owing to their excellent mechanical and barrier properties, abundance, and cost-effectiveness [5]. However, from an ecological standpoint, fossil-based plastics constitute a major environmental concern due to their non-biodegradability [6]. To address this issue, special attention is given to biodegradable polymers prepared from renewable resources. Polylactic acid (PLA) is one such polymer and has been widely used in numerous applications, e.g., medicine and textiles due to their mechanical properties, visual transparency, simple processability, availability, biocompatibility, and biodegradability [7]. Moreover, PLA shows inherent good water vapor and humidity barrier properties, comparable even to petroleum-based polymers such as PET or PS [8], commonly used as food packaging [9]. Additionally, PLA shows even lower CO₂ and O₂ permeability coefficients compared to PS [10]. For food packaging applications, good barrier properties to water and gases are crucial for maintaining the food quality and extending its shelf-life [9].

In an attempt to further increase PLA properties, inorganic fillers such as sheet-like nanoclays are widely used as potential fillers due to their high aspect ratio and abundance [11]. For example, Sinha Ray et al., [11] have prepared PLA/MMT nanocomposites and have demonstrated a decrease of permeability by about 14% and 50% to gases and water respectively at very low MMT content (i.e., 4 wt%) compared to neat PLA. Similar results were obtained by other groups [12–14]. Mica is another phyllosilicate clay with a structure very similar to MMT. However, only a few works studied the effect of Mica as a filler. In regard to PLA, Maiti

et al., [15] have reported the enhancement of both PLA barrier properties to oxygen gas using Mica, at only 3.8 wt%, by 28% ($144 \times 10^3 \text{ mL } \mu\text{m m}^{-2} \text{ day}^{-1} \text{ MPa}^{-1}$ compared to $200 \times 10^3 \text{ mL } \mu\text{m m}^{-2} \text{ day}^{-1} \text{ MPa}^{-1}$) and storage modulus (2.33 GPa compared to 1.65 GPa of neat PLA). These results were explained by the increase of tortuosity when Mica was added. However, due to the difference in hydrophobicity between the hydrophilic PLA and hydrophobic Mica, the chemical modification of Mica, using, for example, n-hexadecyl tri-n-butyl phosphonium bromide, was necessary to increase the compatibility between the polymeric matrix and the filler. However, besides their toxicity [16], which may highly limit its applications in food packaging, organic modifiers are prone to degradation at high temperature during melt extrusion [17] which is necessary for material processing. An alternative is to substitute the hydroxyl groups of native Mica with fluorine ions (F⁻) (i.e., fluorphlogopite) which increase the hydrophobicity of Mica; thus, eliminate the necessity to use toxic organic modifiers.

Furthermore, the passive protection offered by conventional food packaging materials is often not sufficient to limit bacterial growth; thus, preventing food contamination. In that sense, antimicrobial food packaging has been developed either by using polymers with inherent antimicrobial activity like pristine Chitosan [18], diisocyanate-modified chitosan [19], or by adding antimicrobial agents into polymer matrices. One interesting approach that is used to combine the benefits of clay to improve polymers properties as well as to provide antibacterial activity to the resulting composites is the modification of clay using organic modifiers with inherent antibacterial activity. Indeed, using such an approach, Wang et al., [20] modified saponite using quaternary fulvic acid (QFA) in order to increase the compatibility between the hydrophilic saponite and the hydrophobic PLA. The resulting nanocomposites showed improved thermal and mechanical properties at 1% loading of QFA-saponite. Moreover, the organomodification of saponite using QFA provided the resulting nanocomposites with important antibacterial activity. Lei et al., [21] modified layered double hydroxides (LDH) using phytic acid-Cu(II) (PA-Cu(II)) which enhanced the tensile strength, the elongation at break of PLA by 18.9% and 53%, respectively, and reduced the oxygen relative permeability by 28% using only 1wt% of the filler. Furthermore, 1 wt% LDHs@PA-Cu(II)/PLA nanocomposites showed an antibacterial rate of 99.9% against *Escherichia coli* which is attributed mainly due to PA-Cu(II) modification. Similarly, Nabgui *et al.*, [22] used CTAB-modified bentonite (Bnt) to improve the thermal and mechanical properties of polycaprolactone at loadings as low as 1 wt% of Bnt. The organomodification using CTAB provided the resulting nanocomposites with high antibacterial activity against *Staphylococcus aureus* and

Staphylococcus epidermidis. Works on the preparation of PLA nanocomposites with improved properties and antibacterial activity using 2D and metallic nanoparticles fillers are summarized in table III.SI-1.

Alternatively, antibacterial agents can be added directly to provide/enhance the antibacterial activity of biodegradable polymers. However, using organic antibacterial agents raises concerns over their migration from the polymers to the external environment. Indeed, in all the above-mentioned works, the antibacterial activity was the result of the diffusion of the antibacterial agent.

In that regard, other antibacterial agents have gained wide attention such as metal nanoparticles due to their important activity and low migration rates such as Zinc oxide nanoparticles [23] and Copper nanoparticles [24]. Particularly silver nanoparticles (AgNPs) are of great interest due to their antibacterial activity against a wide range of food-borne pathogens compared to other metal nanoparticles [25–27] and their low effect on the organoleptic properties of food compared to organic antimicrobial agents (e.g., essential oils and other plant extracts) [28,29]. Indeed, in a study [30] the antibacterial activity of PLA films with only 1wt% AgNPs prepared using solution mixing has been evaluated in solution. The nanocomposites showed excellent antibacterial activity against *Escherichia coli* (inhibition of 95.85% compared to 4.91% for the neat PLA) and *Staphylococcus aureus* (inhibition of 97.04% compared to 4.26% for the neat PLA). Moreover, inorganic fillers, including phyllosilicates are known to modify the surface characteristics of the resulting polymers (*i.e.*, hydrophobicity, roughness) [31,32], which may influence the bacterial adhesion to the surface of the resulting nanocomposites [33].

Additionally, PLA is one of the most suitable polymers for biomedical applications such as the preparation of scaffolds and drug delivery. Such applications are highly related to PLA thermomechanical and barrier properties (prolonging drug release) [34]. As such, PLA nanocomposites with enhanced properties could be of high interest for biomedical applications. Furthermore, the antibacterial activity of materials used for biomedical applications is of primordial interest due to the risk associated with bacterial infections [35]. Indeed, Liu *et al.*, [36] prepared PLA nanocomposites mats using Graphene oxide and AgNPs as fillers. These nanocomposites showed enhanced thermomechanical properties as well as excellent antibacterial activity. The authors concluded that such nanocomposites are promising antibacterial materials for biomedical applications.

In our study, we report, for the first time, the combination of PLA as the matrix, Fluorine-modified mica (fluorophlogopite) as the fillers, and the antibacterial AgNPs via a simple process of melt extrusion. The effect of fluorophlogopite and AgNPs contents on the thermal, mechanical, and barrier properties of PLA nanocomposites (Water vapor permeability, Water sorption behavior, and Gas permeability) were investigated and compared to native PLA. Finally, the antibacterial activity of PLA nanocomposites was assessed against three model bacteria, *Escherichia coli* (Gram-negative bacteria) and *Staphylococcus aureus*, and *Enterococcus faecalis* (Gram-positive bacteria) and compared to neat PLA.

III.2) Materials and Methods

III.2.1) Materials

PLA Ingeo 4043D characterized (D-isomer content = 4.3%; melting point (T_m)=145-160 °C, and glass transition temperature T_g = 55-60 °C was purchased from NatureWorks (United States)) and was used as a polymeric matrix in the preparation of nanocomposites. Two fillers were used, silver nanoparticles (size= 30-50 nm) were purchased from US Research Nanomaterials Inc (United States) and Fluorophlogopite ($KMg_3(AlSiO_3O_{10})F_2$) was obtained from Continental Trade (Poland). All chemicals were used as received without further modification.

III.2.2) PLA composites preparation

PLA composites with different percentages of fluorophlogopite (2, 5, and, 10 wt%) and 1.5 wt% silver nanoparticles were prepared by melt mixing using a Brabender at 200 °C at a constant rotation speed of 60 rpm for 5 min. The ratio of AgNPs was chosen based on percentages reported in the literature [37,38]. Initially, a 3g masterbatch was prepared using the solvent casting method. Briefly, PLA was dissolved in dichloromethane (DCM), then the amount of AgNPs and/or fluorophlogopite particles corresponding to the target percentage with respect to 40g was added and the mixture was stirred for 2 h (*e.g.*, for PLA/2%Mica films, 2.2 g of PLA was dissolved in DCM then 0.8 g of Mica was added). The solution was ultrasonicated for 15 min and poured into Teflon molds and dried at 100 °C overnight to ensure the complete evaporation of the solvent. The masterbatch films were then cut and mixed with the remained quantity of PLA pellets (Total quantity = 40 g) in the Brabender.

The obtained materials were preheated to 200 °C and then pressed for 4 min followed by quenching for 2 min, in order to produce films with a fixed thickness of 200 μ m using a hydraulic press. Films used for barrier properties were prepared by dissolving the melt-extruded

materials in chloroform. The solution was poured onto Petri dishes and evaporated at ambient temperature overnight. The films were then peeled off and dried at 90 °C to remove the residual solvent.

III.2.3) Characterization

Thermogravimetric analysis (TGA) was carried out to evaluate the thermal stability of neat PLA and PLA composites using a TGA 55 Discovery device in a range of 25 °C to 500 °C at 20 °C/min in N₂ atmosphere. 5 wt% loss temperature was determined ($T_{5\%}$), peak temperature (T_d) and onset temperature (T_{Ons}) were determined from TGA graphs.

Differential scanning calorimetry (DSC) analysis was performed using a Mettler Toledo DSC 823e device. Samples were heated from 0 to 200 °C with a scanning rate of 10 °C/min with two heating and cooling cycles. DSC thermal parameters of neat PLA and PLA composites in terms of crystallization temperature (T_c), melting point (T_m), the enthalpy of crystallization (ΔH_c) and the enthalpy of melting (ΔH_m) were determined from the first heating scan. The degree of crystallinity χ_c was determined following the formula:

$$\chi_c = \frac{\Delta H_m - \Delta H_c}{\Delta H_m^0 (1 - \alpha)} \quad (1)$$

Where ΔH_m^0 is the melt enthalpy of 100% crystalline PLA (93.7 J/g) [39] and α is the mass fraction of fillers within the nanocomposites.

X-ray diffraction measurements were performed using a D8 Advanced Brüker Diffractometer using Cu K α radiation ($\lambda = 1.5418 \text{ \AA}$) operating at 20 Kv and 10 mA. The measurements were collected at 2θ in the range of 5-80° at 5°/min with a resolution of 0.02°.

Films surface morphology was studied using Scanning Electron Microscopy (SEM) using a Vega3 Tescan device. To determine the morphology and the dispersion of AgNPs nanofillers in PLA, Transmission Electron Microscopy (TEM) images were obtained using a Hitachi HT7800 operating at an accelerating voltage of 100Kv.

The hydrophobic/hydrophilic surface characterization was investigated by means of Water Contact angle measurements using DGD Fast/60 contact angle meter and Windrop++ software (Digidrop, DGD, Fast/60, GBX). The measurements were performed after 60 seconds, at the equilibrium state of the deposited drop.

III.2.4) Mechanical properties

The mechanical properties of PLA and the different PLA composites measurements were performed on a Zwick Roell apparatus following DIN 53455 standard. The specimen gauge length was 50 mm and the crosshead speed was 10 mm/min. Samples were 10x120 mm with a thickness of about 200 μm . Results were presented as the mean of 5 measurements \pm standard deviation.

III.2.5) Barrier properties

III.2.5.1) Water permeation measurement

Water permeation measurements at 25°C were conducted on a lab-built device constituted by a temperature-regulated measurement cell containing two compartments separated by the film sample [40]. A sweep of the permeation cell with dry nitrogen was initially carried out until reaching a low constant dew point (indicating a very low water content < 2.5 ppmV) measured by a chilled mirror hygrometer (Elcowa[®], France, General Eastern Instruments). Then, the upstream compartment was filled with liquid water (Milli-Q water system with a resistivity of 18 $\text{M}\Omega\text{-cm}^{-1}$). The water permeation flux J , leading by the water transfer through the film thickness, was recorded at downstream compartment by the monitoring of the increase of the dew point temperature as a function of time. The permeability coefficient P , with the unity in Barrer (1 Barrer = 10^{-10} $\text{cm}^3_{(\text{STP})} \text{cm cm}^{-2} \text{s}^{-1} \text{cmHg}^{-1}$), was calculated from the steady-state of the water flux J_{st} by:

$$P = \frac{J_{st} \times L}{\Delta a_w} \quad (2)$$

with J_{st} is the stationary flux, L is the film thickness and Δa_w is the difference in water activity between the two faces of the tested film. In this study, the water permeability is the mean value of two measurements on different specimens per film.

The diffusion coefficient D was calculated from the transient regime of the water flux curves, *i.e.* from the plot of the dimensionless flux J/J_{st} as a function of the reduced time τ ($= D \times t/L^2$). By assuming a Fickian mechanism of diffusion, two diffusion coefficients can be determined at two specific times of the permeation process that corresponds to the inflexion point I ($j_I = J/J_{st} = 0.24$, $\tau_I = 0.091$) and the time-lag point L ($j_L = J/J_{st} = 0.6167$, $\tau_L = 1/6$) [41]. The first diffusion coefficient, noted D_I ($D_I = L^2 \times 0.091/t_I$), is calculated at the time t_I of the theoretical flux curve [42] where the flux J is at 24% of the stationary flux J_{st} . and the second diffusion coefficient, noted D_L ($D_L = L^2/6.t_L$), is calculated at the time t_L (named the time-lag point L) of the theoretical flux curve [43] where the flux J is at 62% of the stationary flux J_{st} . When D_I is

practically equal to D_L , the diffusion coefficient D is assumed to be constant. However, the D_T coefficient is generally found to be smaller than the D_L coefficient, which highlights a dependence of the diffusion coefficient with the water concentration owing to the water plasticization effect [44]. This dependence is usually expressed under the exponential law:

$$D = D_0 \times e^{\gamma C} \quad (3)$$

where D_0 ($\text{cm}^2 \cdot \text{s}^{-1}$) is the limit diffusion coefficient, γ ($\text{cm}^3 \cdot \text{mmol}^{-1}$) is the plasticization coefficient and C is the local concentration of sorbed water.

III.2.5.2) Water vapour sorption measurement

Water vapor sorption measurements were performed at 25 °C using a regulated dynamic sorption Cahn D200 microbalance (Dynamic Vapour Sorption from Surface Measurement Systems Ltd., U.K.) with a mass resolution of 0.1 µg. Kinetic data were recorded by following the mass evolution versus time as a function of water activity. The initial mass of film samples (films with a thickness of 200 µm and diameter of 8 mm) was ~12 mg. The film sample was also taken as a plane sheet in which water vapour transfer was considered as one-dimensional flux in the axial direction. Initially, a dry nitrogen flux was flushed until a constant sample mass was reached indicating that the dry mass was obtained. Then, water vapour was flushed at controlled pressure and the mass uptake was measured as a function of time. The sorption kinetic at each relative humidity was followed step by step until reaching sorption equilibrium as the change in mass with time was below a predefined threshold value. Water activity a_w ranging from 0 to 0.95 was adjusted by mixing dry and saturated nitrogen gases using electronic mass flow controllers. At pressures close to saturation point, a special attention is paid to avoid vapour condensation.

The water mass gain at sorption equilibrium (ΔM_{eq} expressed in % or g of water per 100 g of sample) was calculated for each water activity by:

$$\Delta M_{eq} = \frac{m_{eq} - m_d}{m_d} \times 100 \quad (4)$$

where m_d and m_{eq} are the dry mass and the mass at equilibrium state of sample, respectively.

Water vapour sorption isotherms representing the equilibrium water mass gain versus water activity were plotted. Sorption behaviour of samples was analysed from a thermodynamic and kinetic point of view by means of methodologies described hereafter. The accuracy of mass gain values at sorption equilibrium was estimated to be better than 3%.

III.2.5.3) Sorption isotherm modelling.

Usually, sorption isotherm curves are fitted with the help of well-known mechanistic models to describe solvent-solvent and solvent-polymer interactions occurring during the sorption process. In the literature, it is commonly reported several phenomenological models suitable for sigmoidal sorption features and classified according to theoretical isotherm types referenced in the IUPAC recommendations. Among them, the BET II model describes water vapor sorption isotherm in hydrophilic polymers and also in polymeric matrices having polar groups. The BET II isotherm represents unrestricted monolayer-multilayer adsorption highlighting as a combination of Langmuir (first part of the curve, *i.e.*, concave to the activity axis) and Flory-Huggins isotherms (the second part, *i.e.*, convex to the activity axis). In particular, the GAB (Guggenheim-Anderson-De Boer) model which comes from the BET theory is often used to fit water sorption isotherms (concave and convex curve), more especially in the field of food products [45]. However, the Park model allows better fitting for water sorption in polymer more or less hydrophilic and such as PLA [46]. This model combines the dual-mode (Henry and Langmuir sorption modes) and the clustering formation and the equation is as follows:

$$C = \frac{C_L \cdot b_L \cdot a}{1 + b_L \cdot a} + k_D \cdot a + n \cdot K_a k_D^n \cdot a^n \quad (5)$$

where C_L and b_L are the mean concentration and affinity constant of Langmuir sites (microvoids and polar groups), k_D (Henry's constant) is the constant related to dissolution of solvent in the polymer matrix, K_a is the equilibrium constant associated with the water aggregation reaction and n is the mean number of water molecules constituting the aggregates.

The widely-adopted mean relative deviation modulus [47], noted MRD (in %), is used to evaluate the quality of the fitting and so the relevance of the mathematical description of sorption isotherms and is calculated by the root sum square method (RSS method):

$$MRD = \frac{100}{N} \cdot \sum_{i=1}^N \frac{|m_i - m_{pi}|}{m_i} \quad (6)$$

where m_i is the experimental mass at sorption equilibrium, m_{pi} the theoretical mass resulting from isotherm modelling and N is the number of experimental points. A value below 10% is an indication of a good fitting [48]. A non-linear regression analysis of model parameters by Table Curve 2D software was carried out.

III.2.5.4) Water vapor diffusion coefficient determination.

From kinetic data, the two diffusion coefficients D_1 and D_2 were determined at short and long times from the mass gain versus time curve in order to highlight the variation of the water diffusivity and its dependence with the water concentration (*i.e.* water activity). By applying the Fick's diffusion law, the first diffusion coefficient, noted D_1 , was calculated for a short time of sorption (Eq. (7)) (that is when mass gain lower than 50%, referred to as the first-half sorption). The second diffusion coefficient, noted D_2 , was determined for a longer time (Eq. (8)) (that is when mass gain higher than 50%, referred to as the second-half sorption).

$$\frac{M(t)}{M_{eq}} = \frac{4}{\sqrt{\pi}} \times \sqrt{\frac{D_1 t}{L^2}} \quad (7)$$

$$\ln \left[1 - \frac{M(t)}{M_{eq}} \right] = -\pi^2 \times \frac{D_2 t}{L^2} + \ln \left(\frac{8}{\pi^2} \right) \quad (8)$$

where $M(t)$ is the mass gain of the sample at time t of the experiment and M_{eq} the mass gain at equilibrium state. L corresponds to the thickness of the film.

III.2.5.5) Gas permeation measurement

Gas permeation measurements were conducted at 25 °C by using a barometric method based on the time-lag method with the help of a lab-built apparatus. This peculiar apparatus was previously detailed [49]. A high vacuum desorption step for 15 h was initially applied to the permeation cell in which the film sample is placed. The monitoring of the increase of pressure in the downstream side of the film was followed with a pressure sensor as soon as a 3 bars-pressure of gas (Messer, France) was sent into the upstream of the permeation cell. Reaching a constant value has indicated the setting of the stationary state of the permeation process. The permeability coefficient P (usually expressed in Barrer unit, 1 Barrer = $10^{-10} \text{ cm}^3_{(\text{STP})} \text{ cm cm}^{-2} \text{ s}^{-1} \text{ cmHg}^{-1}$) was determined from the steady state of the experimental permeation process by the equation:

$$P = \frac{J_{st} \times L}{\Delta p} \quad (9)$$

where J_{st} is the stationary flux, L is the film thickness and Δp is the difference of pressure between the two sides of the sample. The reproducibility of measurements was checked from at least two specimens per film.

III.2.6) Antibacterial activity of PLA composites

III.2.6.1) Bacterial strains

Three bacterial strains, *Staphylococcus aureus* (ATCC 29213), *Enterococcus faecalis* (ATCC29212), and *Escherichia coli* (K12 MG1655) were used to assess the antibacterial activity of neat PLA and filled PLA films. All materials were previously autoclaved at 121 °C for 15 min. Bacteria were maintained at -20 °C in 30% glycerol. Bacterial strains were precultured under aerobic conditions in “Brain Heart Infusion” nutritive medium (BHI, Bacto™) at 37 °C and 140 rpm for 16 h then the optical density was then adjusted to 0.05 at 600 nm corresponding to a bacterial concentration around $5 \cdot 10^6$ Colony Forming Units (CFU) · mL⁻¹.

III.2.6.2) Bacterial growth on the surface of the films assay

In order to quantify the bacterial growth on the surface of the films, 100 µl of the prepared bacterial preculture was added to 2.9 mL of BHI broth. 1 cm² ethanol-sterilized squared film was then put in the medium and incubated for 16 h at 37 °C and 140 rpm. The films were gently washed with sterile MilliQ water and then put in 3 mL of a sterile PBS solution followed by sonication for 3 min to remove adhered bacteria from the surface of the films. Bacteria in solution were diluted with serial 10-fold dilutions, spread on BHI agar plates, and enumerated after incubation for 16 h at 37 °C. Each sample was tested in triplicate and the percentage of inhibition was determined compared to neat PLA films.

III.2.6.3) Film diffusion method assay

The antibacterial activity of the film was evaluated qualitatively using the diffusion method assay. Sterile plates of BHI agar were prepared and inoculated with 1% (v/v) of the prepared bacterial preculture. Then, 1 cm² squared films were put on the surface of the plate and kept at 4 °C for 1 hour, and incubated at 37 °C for 24 h. Diffusion of the antibacterial compounds was characterized by a zone of bacterial growth inhibition around the film. Each sample was tested in triplicate.

III.2.7) Statistical analysis

Statistical significance was evaluated using a one-way ANOVA test in IBM SPSS statistics 20. Differences between groups were considered statistically significant at $P < 0.05$.

III.3) Results and Discussion

III.3.1) Optimization of fluorphlogopite content

One of the problems of nanocomposites preparation with several fillers (*i.e.*, fluorphlogopite and AgNPs in our case), each with different contents, is the high number of combinations which limits the feasibility to study multiple parameters. In our work, we firstly optimized the content of fluorphlogopite before adding AgNPs. PLA composites containing 2, 5, or 10 wt% of fluorphlogopite were prepared and their thermal stability and degradation behavior compared to neat PLA were studied. Fig. III.SI-1 and Table III.SI-2 show the TGA mass loss curves and TGA parameters of PLA and PLA-Fluorphlogopite composites respectively. All films exhibited a single mass loss that takes place around 300 °C corresponding to polyester chains degradation. The lower fluorphlogopite ratio of 2% showed the best enhancement in thermal stability. Fluorphlogopite is a modified Mica belonging to the phyllosilicate family with enhanced thermal resistance and insulation properties compared to natural Mica. Fluorphlogopite is a filler with a lamellar structure [50], which can explain the enhancement of the thermal properties of PLA. This improvement in thermal stability as evidenced by the increase of $T_{5\%}$, $T_{50\%}$, and T_{Onset} is generally attributed to the barrier effect induced by the dispersed fluorphlogopite layers in the PLA matrix. This provides heat insulation by reducing the transfer of volatile degradation products. Surprisingly, as fluorphlogopite ratio increased to 5%, no improvement in TGA results was observed compared to neat PLA. On the contrary, a slight decrease in $T_{5\%}$ was noticed. Moreover, a huge decrease in TGA calculated values was observed when compared to PLA-2% fluorphlogopite. This behavior was reported in the case of organoclay and was explained by the flocculation of filler at higher content [51]. However, for 10% of fluorphlogopite, an improvement in PLA thermal stability appeared, even though, still less than the improvement provided by 2% of Fluorphlogopite. This can be explained by the higher probability of limitation of diffusion of volatile degradation products and reduction of polymeric chains movement that limits the effect of flocculation. Similar results were obtained by Diawara *et al.*, [50] using fluorphlogopite as a filler in the preparation of Polycarbonate nanocomposites, in which they reported a substantial and non-linear enhancement of thermal stability of PC when fluorphlogopite was added with an optimum ratio of 2.5% of fluorphlogopite.

As 2% of fluorphlogopite gave the best result for the enhancement of thermal properties of PLA, which may be indicative of a better dispersion of the filler within the PLA matrix, this ratio was used for the preparation of PLA-Fluorphlogopite-AgNPs nanocomposites.

Finally, as the experiments to study the barrier properties were performed on films prepared by solvent casting method of the extruded PLA and PLA nanocomposites for convenience, the thermal degradation profile of PLA-2% Fluorophlogopite prepared by both methods were compared to ensure that the same results were obtained. From Fig. III.SI-2, identical TGA curves of PLA-2% Fluorophlogopite were obtained confirming the possibility to use both methods for the preparation of PLA films.

III.3.2) Characterization of PLA-Fluorophlogopite-AgNPs nanocomposites

III.3.2.1) Morphology analysis

The effect of fluorophlogopite and AgNPs on the morphological properties of PLA was assessed using multiple techniques. The SEM micrographs performed on cross-sections of PLA and PLA-2%Fluorophlogopite shown in Fig. III.1A and III.1B respectively, demonstrates a good dispersion of the fluorophlogopite filler with an apparent increase in the roughness of PLA. The apparent roughness is similar along the cross section evidencing a uniform distribution of fluorphlogopite on the nanocomposites films and not only on the surface. This behavior is a common result in the case well distributed inorganic filler in PLA [52,53].

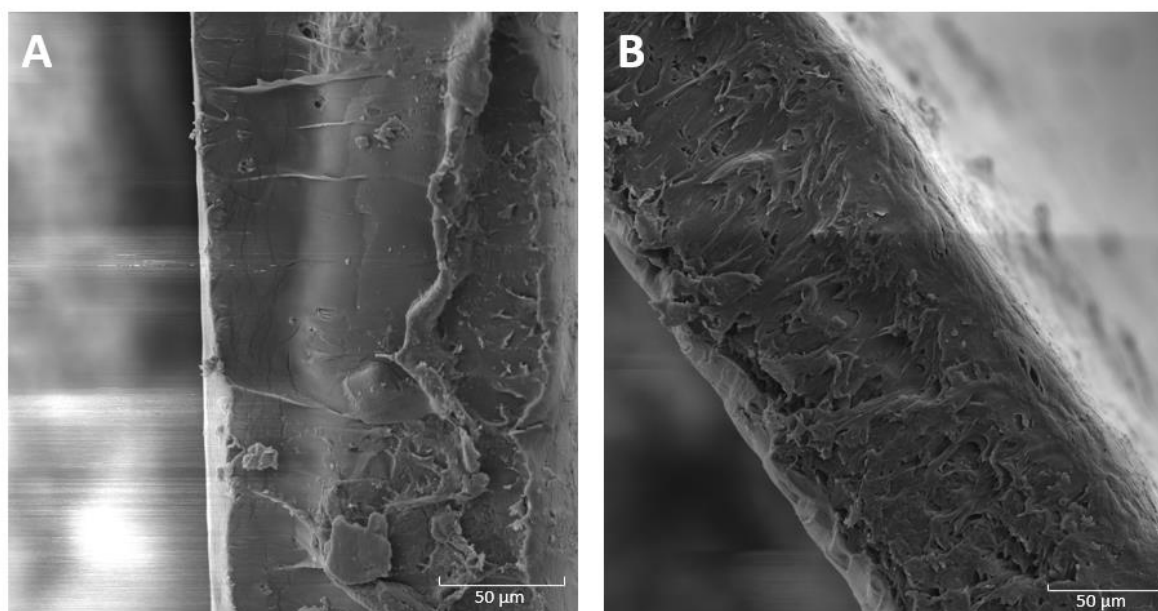


Figure III.1: SEM micrographs on a cross-section of A) Pristine PLA, B) PLA-2% Fluorophlogopite blend

Furthermore, in order to verify the distribution and agglomeration states of both fluorphlogopite and AgNPs, TEM analysis was performed. TEM images of PLA-Fluorphlogopite-AgNPs nanocomposites are presented in Fig. III.2A-C. Fig. III.2A-B show the dispersion of 2% fluorphlogopite and 1.5% AgNPs in the PLA matrix, respectively while figure III.2C shows TEM micrographs of PLA-2%Fluorphlogopite-1.5%AgNPs tertiary nanocomposites. As can be seen, a good and random dispersion of 2% fluorphlogopite (green circles) in the PLA matrix with very few aggregates were obtained. These results are consistent with the SEM results. The micrographs showed also aggregates of AgNPs (red circles) leading to an increase in AgNPs size, however, at the scale of the micrograph, only AgNPs aggregates can be detected. The results were similar to those found by Demchenko *et al.*, [54] for silver nanoparticles and Diawara *et al.*, [50] for fluorphlogopite.

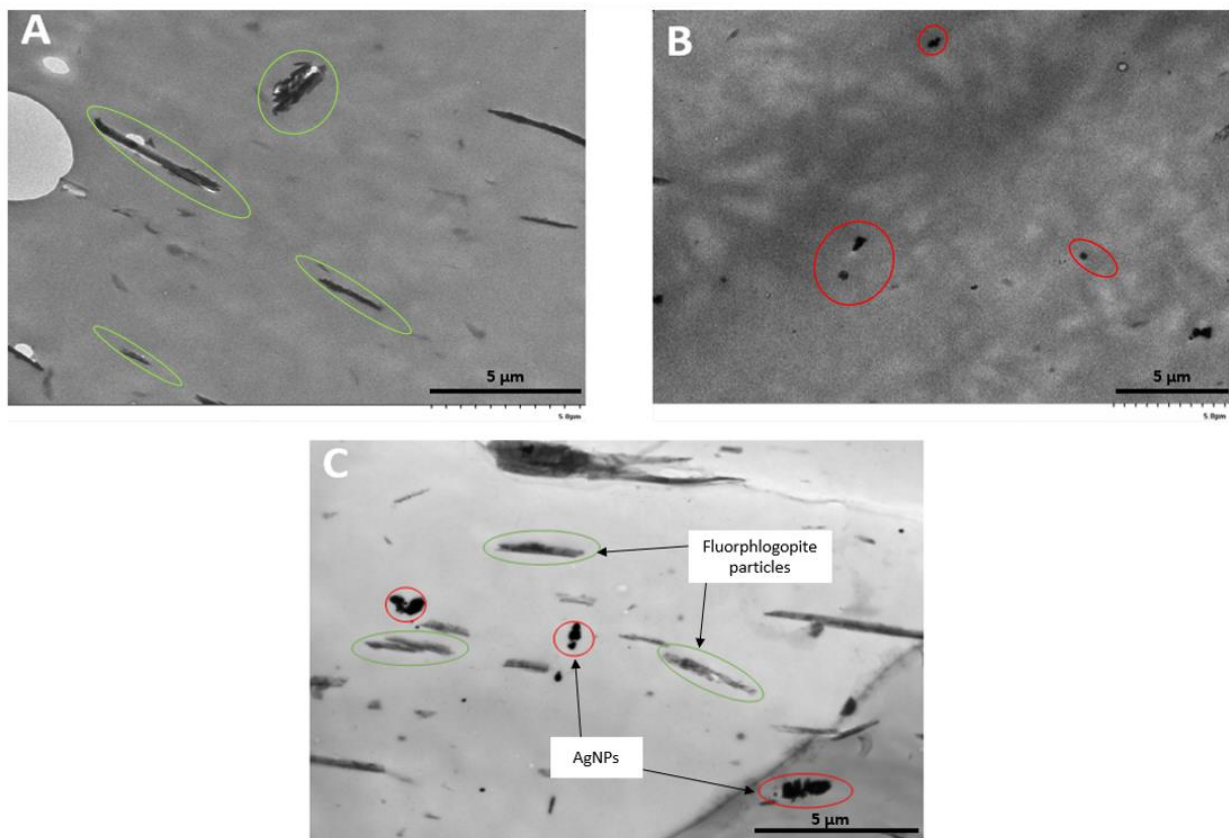


Figure III.2: TEM micrographs of A) PLA-2%Fluorphlogopite, B) PLA-1.5%AgNPs, and C) PLA-2%Fluorphlogopite-1.5%AgNPs

Furthermore, the effect of blending PLA with fluorphlogopite particles was studied using XRD. Fig. III.3 shows the XRD patterns focusing on the region that shows the 001 crystallographic plane of fluorphlogopite. From Fig. III.3, a shift of the 001 plane to lower angles was observed indicating an increase of the d_{001} spacing as calculated by Bragg's law ($d = \lambda / (2 \sin \theta)$) from 9.91 for fluorphlogopite sheets to 10.18 Å in PLA nanocomposites. The results indicate the

successful intercalation of the PLA chains in the fluorphlogopite sheets. The further addition of AgNPs did not induce any changes to the d spacing of fluorphlogopite. This could be due to the much larger size of AgNPs (30-50 nm) compared to the interlayer spacing of fluorphlogopite which could prevent their intercalation. Similar results were found by Rhim and Wang [55]

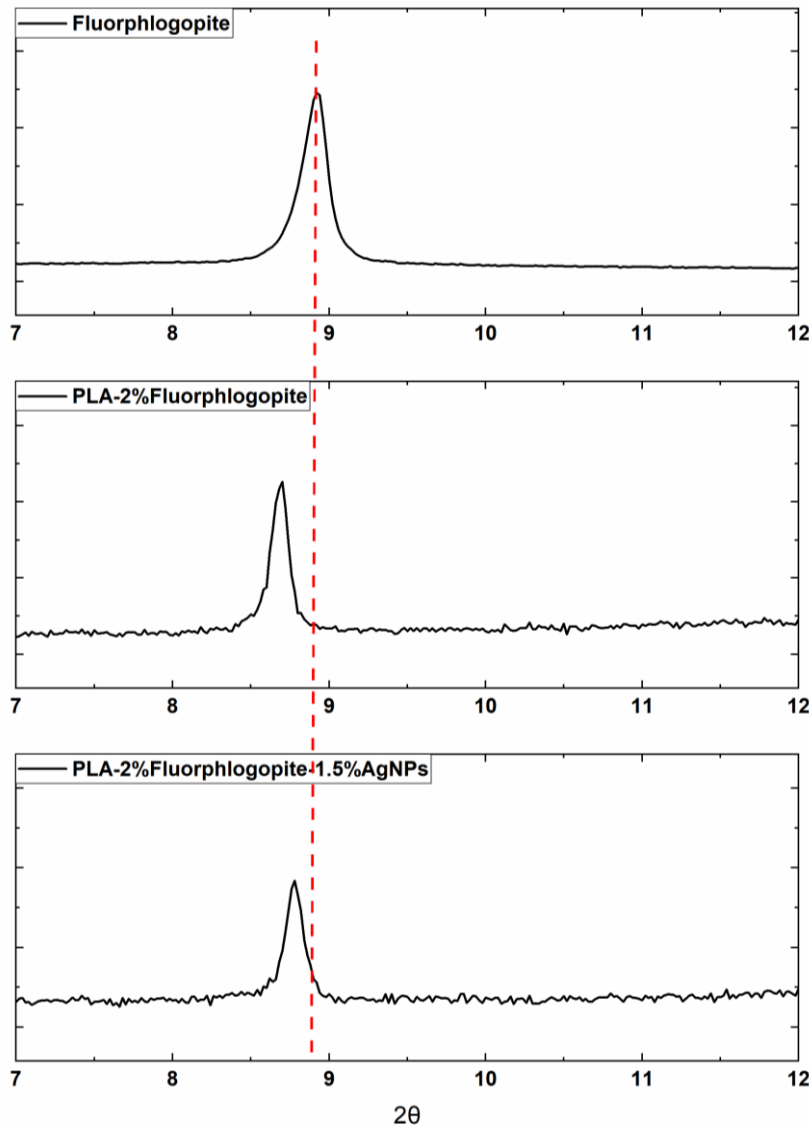


Figure III.3: XRD patterns of fluorphlogopite, PLA-2%Fluorphlogopite and PLA-2%Fluorphlogopite-1.5%AgNPs composites

III.3.2.2) Water contact angle measurements

Water contact angle values were determined in order to evaluate the hydrophilic/ hydrophobic character of PLA and PLA nanocomposites films. Hydrophobicity is a desired property in materials with food packaging applications [56] as it limits the transfer of moisture by limiting the water vapor permeability which may create a favorable environment for microorganisms development [57]. As shown in Fig. III.4, the addition of fluorphlogopite particles caused a

shift towards higher angle values (from $48^{\circ} \pm 2^{\circ}$ for neat PLA to $73^{\circ} \pm 2^{\circ}$ for PLA-2% Fluorophlogopite), thus making PLA more hydrophobic. This increase was expected as fluorophlogopite is hydrophobic. The addition of silver nanoparticles to neat PLA has also caused, to a much lesser extent, a slight increase in hydrophobicity ($55^{\circ} \pm 1^{\circ}$). This behavior could probably be due to the increase of roughness of the PLA surface as found by Armentano *et al.*, [58] in the case of Poly(lactide-*co*-Glycolide)/AgNPs nanocomposites. Finally, the addition of both 2% fluorophlogopite and 1.5% AgNPs have similarly induced, as expected, an increase in PLA hydrophobicity due to the effect of the fillers.

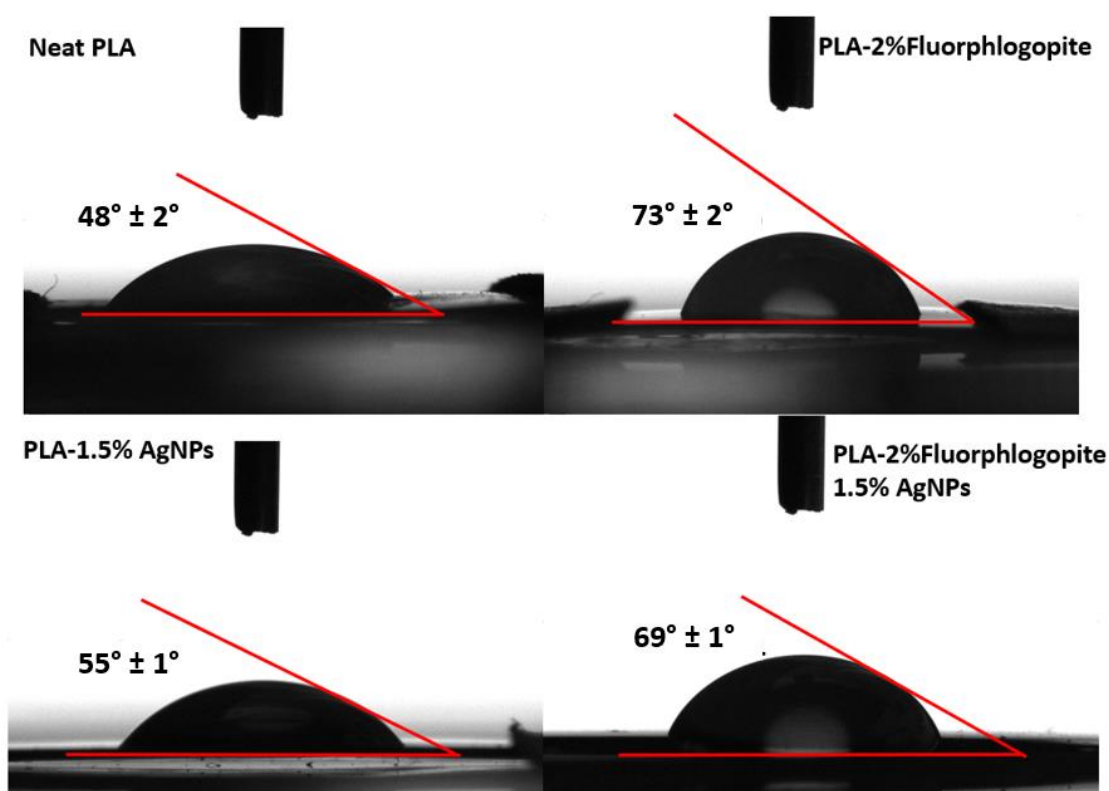


Figure III.4: Water contact angle measurements of neat PLA and PLA-Fluorophlogopite-AgNPs composites

III.3.2.3) Differential scanning calorimetry analysis

The crystallization and melting behavior of PLA and PLA nanocomposites were studied using DSC. Usually, DSC parameters are obtained from the second heating curve after erasing the thermal history of the materials. However, in our study, the thermal events were calculated from the first heating curve as materials are assumed to be in the same thermal and structural states as for the experiments of the evaluation of the barrier and antibacterial properties. Fig. III.5

shows the DSC thermograms of the first heating and Table III.1 summarizes the DSC values deduced from these curves.

DSC thermograms show an endothermic relaxation peak at about 65°C for all the tested materials superposed on the glass transition temperature (T_g), thus, preventing its determination. This peak corresponds to the structural relaxation caused by the physical aging effect of the polymer processing [10,46]. Erasing the thermal history of the materials enables us to determine the T_g values to be around 60 °C for all the tested materials.

Moreover, an exothermic crystallization peak was observed at 112 °C associated with two endothermic melting peaks for neat PLA at 146 °C and 152 °C corresponding to the melting of different crystal forms with different lamellae thicknesses or perfections. This phenomenon was already observed in the case of PLA 4043D [59]. The addition of fillers, either 2% of fluorphlogopite or 1.5% of AgNPs, induced a slight shift in the crystallization peak to higher temperatures indicating that the fillers acted as nucleating agents [60]. The addition of both fluorphlogopite and AgNPs further increases the T_c . To determine the degree of crystallinity (χ_c), equation (1), described in 2.3 section, was used. Interestingly, a decrease of χ_c was observed (Table III.1) when the fillers were added, either alone, or in combination. Both phenomena together (*i.e.*, fillers acting both as a nucleation agent and decreasing the degree of crystallinity) have rarely been reported in the literature as it is usually expected that nucleating agents promote crystallization. Lai *et al.*, [61] also reported similar findings with PLA-Organomodified Montmorillonite and it was explained by the existence of some possible exfoliated filler particles. Moreover, Vidović *et al.*, [62] reported similar findings where the PLA degree of crystallinity decreased in PLA/Mica nanocomposites prepared via melting processing and it was explained by the possibility of filler creating free volume between the polymer chains in order to accommodate.

Interestingly, the bimodal endotherm corresponding to the melting process of PLA appeared to be less pronounced when either of the fillers was added and disappeared completely for the tertiary film. This could be explained by a higher level of perfections of PLA crystals induced by the nucleating role of fillers. This was also found by Rezaei *et al.*, [63] with PLA 4043D and Titanium dioxide nanoparticles as fillers.

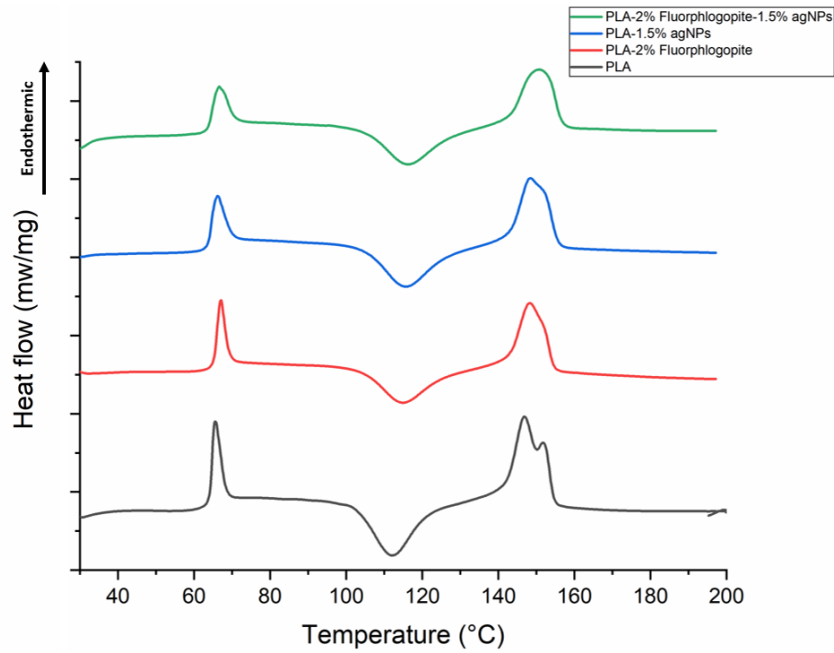


Figure III.5: First heating curves of DSC thermograms of neat PLA and PLA-Fluorphlogopite-Silver nanoparticles composites

Table III.1: DSC data of neat PLA and PLA-Fluorphlogopite-Silver nanoparticles composites

Sample	T_c (°C)	T_m (°C)	ΔH_m (J/g)	ΔH_c (J/g)	χ_c (%)
Neat PLA	112	146 152	33.4	26.7	7.15
PLA-2% Fluorphlogopite	114	148 -	26	24.1	2.06
PLA-1.5%AgNPs	115	148 -	22.1	20.4	1.84
PLA-2% Fluorphlogopite-1.5% AgNPs	116	151 -	23	23.6	0

III.3.2.4) Thermal stability

The effect of fluorphlogopite and silver nanoparticles on the thermal properties of PLA was assessed. The results were depicted in Fig. III.6 and summarized in Table III.2. In the optimization process discussed above, we reported a substantial increase in the thermal stability of PLA when 2% of fluorphlogopite was added. On the contrary, the addition of AgNPs alone in the PLA matrix resulted in a slight decrease in the thermal stability of PLA which was also found by Ramos *et al.*, [64]. A plausible explanation for this result could be the thermal conductivity of AgNPs which can speed up the degradation process of the polymer. Furthermore, the PLA-2%Fluorphlogopite-1.5%AgNPs showed a lower thermal stability

compared to PLA-2%Fluorphlogopite, but still slightly higher than neat PLA, which could also be due to the thermal conductivity of AgNPs.

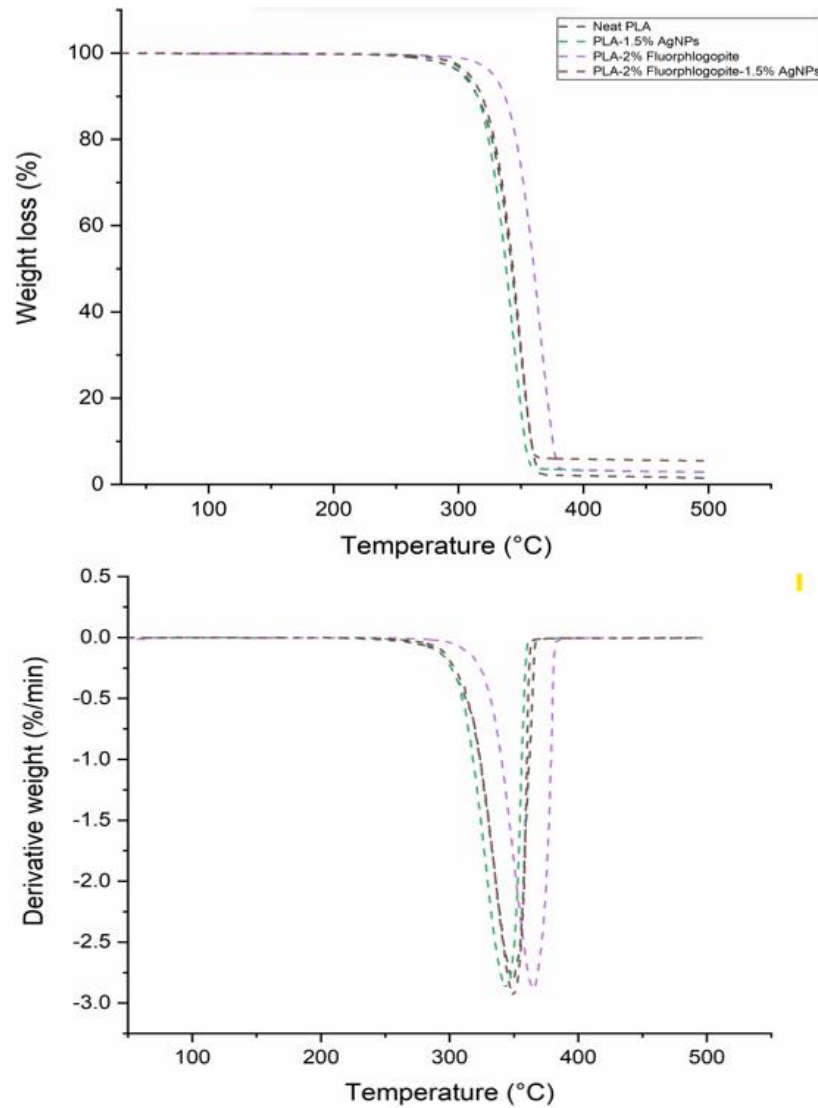


Figure III.6: Weight loss curves and differential weight loss curves of neat PLA and PLA-Fluorphlogopite-AgNPs nanocomposites.

Table III.2: $T_{5\%}$, $T_{50\%}$, and T_{Onset} result of PLA and PLA-Fluorphlogopite composites.

	$T_{5\%}$	$T_{50\%}$	T_{Onset}
PLA	300	342	315
PLA-1.5% AgNPs	303	339	314
PLA-2% Fluorphlogopite	326	360	338
PLA-2%Fluorphlogopite-1.5%AgNPs	307	342	319

III.3.3) Mechanical properties

Young Modulus (or elastic modulus) and Elongation at break are two parameters widely used to assess the effect of fillers on the mechanical performances of materials. As shown in Fig. III.7, the incorporation of fluorphlogopite particles and AgNPs did not affect neither the stiffness (Young modulus) nor the elongation at break, taking into account measurement errors. To the best of our knowledge, there was no previous study on the effect of fluorphlogopite on the mechanical properties of PLA. However, a study on the effect of natural Mica on PVC has found a similar result for the same mica content [65].

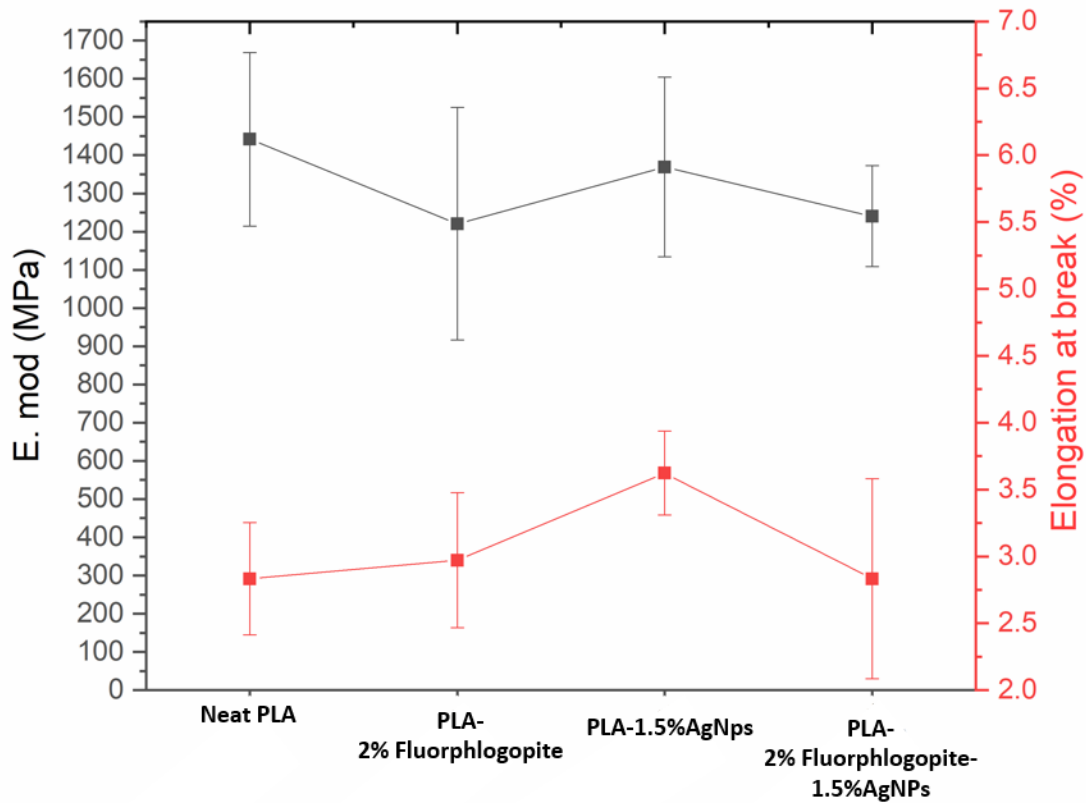


Figure III.7: Young's modulus (MPa) and Elongation at break (%) results of neat PLA and PLA-Fluorphlogopite-AgNPs composites

III.3.4) Barrier properties of PLA composites

III.3.4.1) Water vapor sorption

Water vapor sorption measurements were performed on the neat PLA film, the as-received fillers, and the resulting composite films. First, one can indicate that the size and the thickness of the tested films are unchanged after sorption measurements. The water vapor sorption isotherms were deduced from the equilibrium state of the kinetic curves and are plotted in the following Figs. III.8-10.

Water sorption isotherms of the neat PLA film and the as-received fillers are presented in Fig. III.8. As shown, it can be stated that the fluorophlogopite sorbs a larger water content than the neat PLA film within the whole water activity range due to the presence of water-sensitive groups, such as magnesium aluminum silicate groups. The shape of the isotherm curve is thus sigmoidal, as usually obtained for lamellar fillers such as montmorillonite [66] presenting water sensitivity. This isotherm shape means that three main contributions to sorption coexist successively with an upswing of water mass gain concave to the activity axis followed by a linear and then sharp rise (convex curve) of mass gain as water activity increases. For the silver nanoparticles, the water uptake is very low for the whole range of water activities, meaning that AgNPs did not display a water affinity due to the absence of polar functions. PLA polymer can be seen as a polymer of low affinity for water in the light of its very low water uptake. This was already reported in the literature [45]. This low water sorption capacity (<1% at the highest water activity), similar to hydrophobic glassy polymer such as PET [67], can be surprising because of the hydrophilic character of the PLA surface.

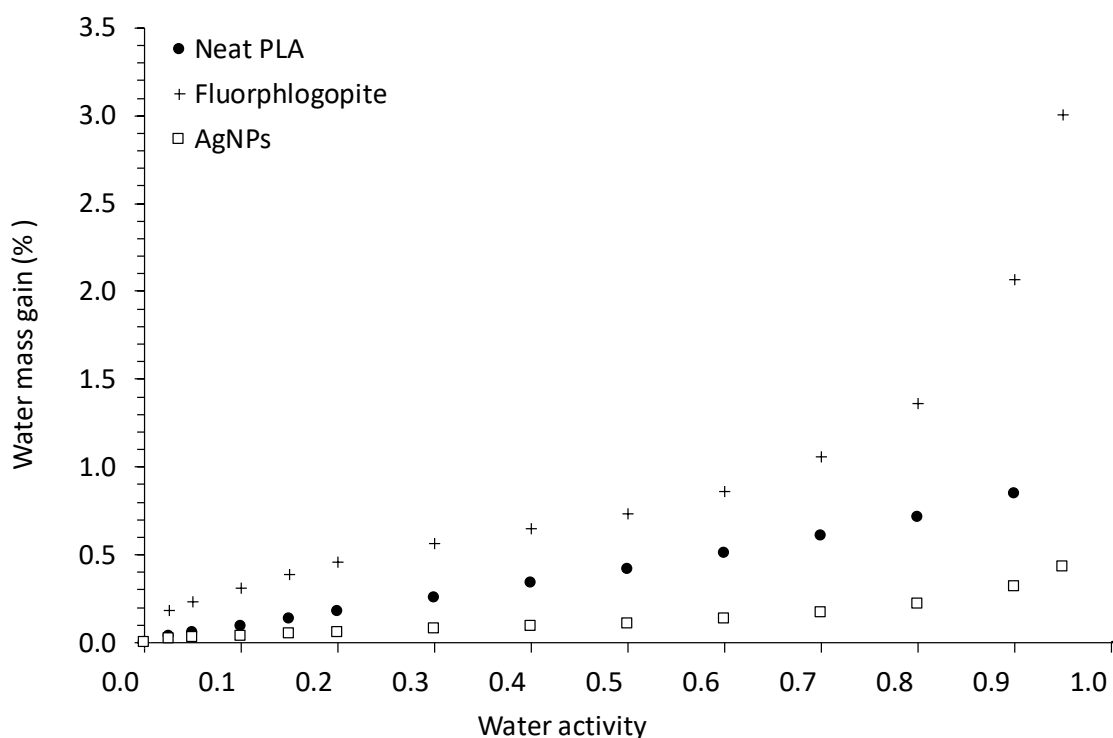


Figure III.8: Water vapor sorption isotherms of the as-received fillers and the neat PLA

In Fig. III.9 are reported the water vapor sorption isotherms of the composite films. Obviously, the water vapor sorption isotherms of the composite films show a shift towards lower water mass gain at given water activities, especially at high water activities ($a_w > 0.7$), which seems not to be in relation with the water capacity of the fluorphlogopite. The composite films followed the same behavior than the PLA matrix showing a linear increase of mass gain with the water activity. It is however not surprising considering that PLA is the main component of the composites and hence, the water sorption capacity of the composite films is governed by the major phase of the film.

Regarding the impact of the fillers within the films, one can indicate that the incorporation of fluorphlogopite presenting a certain water affinity induced a little decrease in water mass gain. In fact, the sorption curve profiles indicate a slight reduction in water clustering, especially at high water activities ($0.6 < a_w < 0.9$) and to a lesser extent from $a_w = 0.2$. We can infer that the filler acts as obstacles to water diffusion by tortuosity effects, even at 2 wt% which can be estimated as a very low loading. It is likely that only 2 wt% of filler in PLA is sufficient to ensure the setup of tortuosity effects within the polymeric matrix in terms of water uptake. fluorphlogopite is also sufficiently embedded into PLA to hinder its inherent water affinity. In

addition, the incorporation of the fluorphlogopite + AgNPs has further contributed to this decrease due to the addition of a non-polar filler to fluorphlogopite. Nevertheless, at water activity higher than 0.9, the trend is reversed: the films containing the fluorphlogopite present a larger water mass gain. It seems that at this high level of hydration the water affinity of fluorphlogopite counterbalanced the small effect induced by the setup of tortuosity effects.

Nevertheless, in a general point of view, and taking into account the uncertainty of measurements, it can be concluded that the presence of AgNPs and fluorphlogopite did not drastically modify the water sorption capacity of the PLA polymer matrix.

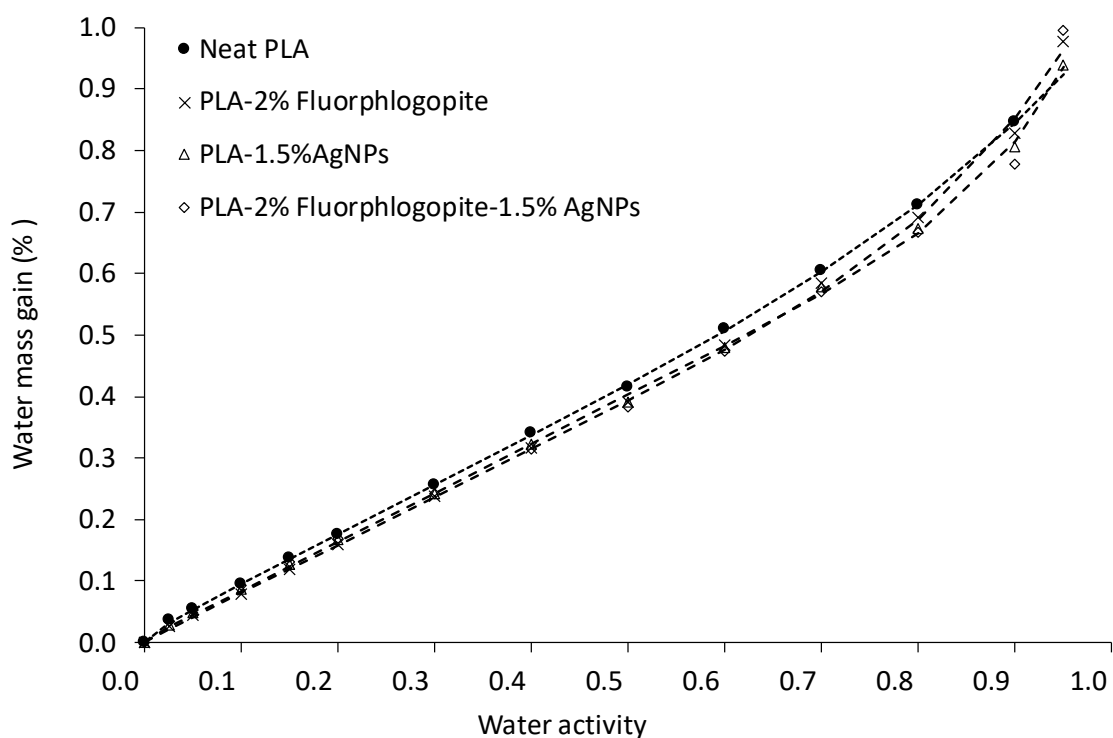


Figure III.9: Water vapor sorption isotherms of the neat PLA and the composite films

To describe the water sorption mechanisms involved in PLA and PLA composite films, the isotherm curves are modeled by the Park model (eq. 5) [68] which refers to the combination of dual-mode and aggregation sorption modes, as shown by the fitted curves reported in Fig. III.9.

The fitted values (C_L , b_L , K_D , K_a and n) and the accuracy of the fit, based on the average deviation modulus MDM lower than 10% as reviewed [48], are gathered in Table III.3. Note that a nonlinear regression was carried out using Table Curve 2D software. It should be noted

that the lack of experimental points for water activity below 0.1 prevents the parameter b_L being appropriately determined

Table III.3: Parameters of the Park model for the neat PLA film and the composite films.

	C_L $\text{g}\cdot\text{g}^{-1}$	b_L	k_D $\text{g}\cdot\text{g}^{-1}$	n	K_a
Neat PLA	$15.1 \cdot 10^{-5}$	200	0.0080	6	$2.1 \cdot 10^8$
PLA - 2% Fluorophlogopite	$3.3 \cdot 10^{-5}$	96	0.0078	8	$8.8 \cdot 10^{12}$
PLA - 1.5% AgNPs	$4.5 \cdot 10^{-5}$	100	0.0080	12	$3.0 \cdot 10^{20}$
PLA - 2% Fluorophlogopite - 1.5% AgNPs	$14.9 \cdot 10^{-5}$	90	0.0085	25	$3.5 \cdot 10^{48}$

The analysis of the Park model parameters points out some differences existing between the composite films in comparison with the neat PLA film. At a low water activity range ($a_w < 0.2$), the Langmuir-concentrations C_L are very low, which agrees with the very low water affinity of PLA matrix. In addition, at these very low sorbed water concentration, an “antiplasticization” effect of water is regularly noted, as a result of a strong cohesion through water-polyester hydrogen bondings [46] reducing free volumes, and hence the water mobility, as thereafter highlighted from the evaluation of the kinetic behavior. The fact that the C_L values remains low with filled PLA films is not surprising insofar as one can imagine that the amount of fluorophlogopite or AgNPs of relatively low sorption capacity is not sufficient to change the water uptake in PLA, especially when the water vapor pressure is low. At the intermediate water activity range ($0.2 < a_w < 0.6$), the k_D term for the composite films is found similar to that of the neat PLA film. This Henry coefficient is an indication that the dissolution of the water as a solvent in the polymer matrix occurs identically. This can be related to the similarity in the degree of crystallinity of PLA in composite films. In fact, an increase in crystallinity of PLA could limit the access of microvoids in matrix, and hence a decrease of the k_D term is obtained, whereas additional microvoids or changes in free volume could induce an increase in the k_D term. In the present case, it seems that the PLA matrix is not impacted by the incorporation of fillers in terms of sorption properties. At a high water activity range ($a_w > 0.7$), a change in the access of water molecules is noted since the K_a and n parameters are affected with the incorporation of fillers. As the K_a increases, the water cluster formation would be favored and this by the presence of fillers which can enhance water interactions because of better affinity for fluorophlogopite particles and probably because of an increase of free volumes at the vicinity of AgNPs. This can be related to the increase in n parameter, showing that the mean size of water clusters is increased with the addition of fillers. It seems that a certain disruption in

conformational structure of polyester chains can explain such result, with the presence of some filler aggregation as shown by microscopic observation.

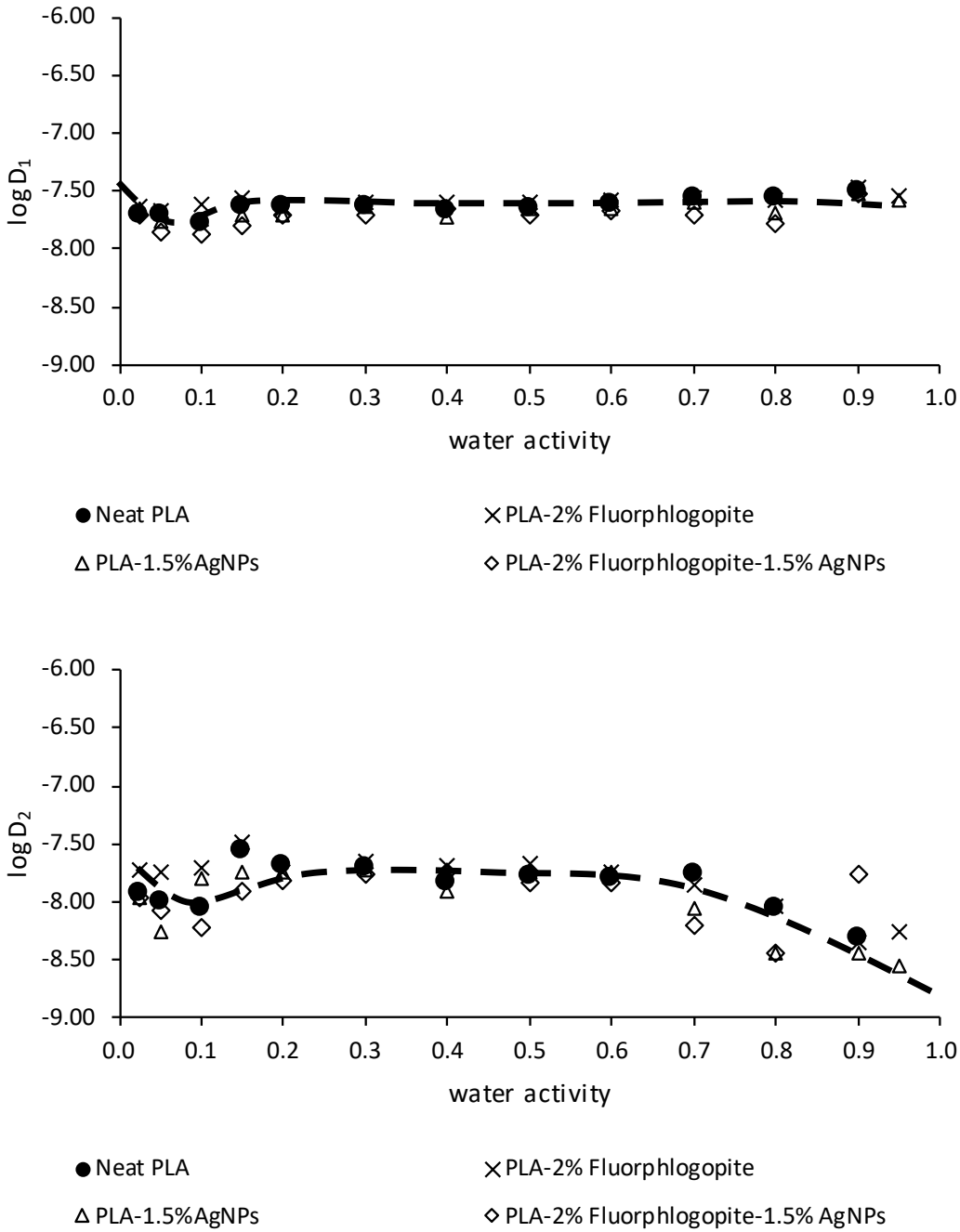


Figure III.10: Water vapor diffusion coefficients D_1 (a) and D_2 (b) for the neat PLA and the composite films

The kinetic behavior of water sorption in the neat PLA and composite films was evaluated through diffusivity coefficients D_1 and D_2 in a semi-logarithmic scale ($\log D$ as a function of water activity), as presented in Fig. III.10. The water diffusion coefficients for the first-half

sorption, D_1 , and for the second-half sorption, D_2 , are plotted as a function of water activity. The diffusion profiles are rather similar for all the films, indicating that the water diffusivity is not really impacted by the filler incorporation. The general trend of diffusivity can be highlighted as follows: a short decrease in diffusion is observed at low water activity due to the antiplasticization effect of sorbed water molecules followed by a constant diffusivity as water activity increases and then a decrease in diffusion is observed at high water activities due to the water clustering phenomenon initiated by the accumulated sorbed water molecules. This last trend is clearly shown by the variation of D_2 coefficient values as a function of water activity. In a way, it is likely that the diffusion in the core of films, associated to the D_2 coefficient since referred to as the coefficient of the second-half sorption, leads in the present case to a better observation of the diffusivity phenomenon owing to a larger water sorption capacity since the second-half sorption is calculated when the mass gain is higher than 50% (*i.e.* at longer extent of water sorption, higher water concentration).

It is surprising to observe that, whatever the film, the D_2 values remains lower than the D_1 ones in the whole water activity range since the inverse trend is commonly reported due to water plasticization effects. However, such a behavior has been recently mentioned in the literature for PLA-based and PBSA-based composites [45]. Two antagonist effects occurred for longer time balancing each effect to give similar coefficients ultimately. The first effect increases water diffusion due to plasticization effects of water molecules while the second effect decrease the water diffusion due to the formation of water aggregates restricting their mobility and as a result their diffusivity within the films. The general curve profile depicts a majority linear portion and a reduction of diffusion at higher water activities. This profile evidences thus that diffusion coefficient is rather constant and is then reduced by water aggregation phenomenon related to the increase in water cluster size which makes water molecules less mobile [69]. It is interesting to see that there is no predominant effect, except at high water activity for clustering phenomenon. The more or less hydrophobic character of PLA clearly explain a such behavior.

III.3.4.2) Water permeation

The water permeation flux J through the film (of thickness noted L), was measured in function of time t . The water barrier performance of a polymeric film depends both on the water solubility and the water diffusivity in the film. Water permeation parameters (Permeability and diffusivity coefficients) of the neat PLA film and the composite films are gathered in Table III.4.

Considering the same driving force ($\Delta a=1$) for all tested films, the water permeation flux curves were compared by plotting the product $J \cdot L$ as function of the reduced time (t/L^2) to overcome the film thickness effect (Fig. III.11A). The permeation curve is usually divided in three steps. When starting measurement, no water molecule has diffused through the entire film and $J \cdot L$ is found to be equal to 0. Then, with the water diffusion through the film, a strong increase of the water flux is measured showing the transient regime of the permeation process from which the diffusion coefficient D is determined. When the water flux is obtained practically constant, indicating that the steady state of permeation is reached, in that case J becomes J_{st} and the water permeability P can be then calculated (Eq. 2).

The incorporation of fillers affects differently the water barrier properties of the neat PLA film, but a general trend can be observed: a low increase in permeability is measured with the fillers. This finding seems to be in contradiction with the sorption measurement results where a reduction of water sorption capacity is found. From permeation measurement, the tortuosity effects can be highlighted more finely, whereas from sorption measurement the change in water affinity of a substrate is evidenced. From the present results, one can infer that the tortuosity effects expected by the incorporation of fillers did not occur. This testifies to an inhomogeneous dispersion and distribution of filler with filler aggregates into the matrix, which favors the water permeation in the unfilled domains of the composite films, resulting in the rise in the permeability. Probably the lack of compatibility between fillers and the polyester chains leads to weak filler-PLA interface, inducing an increase of free volume at this interface and thus favoring as a consequence the water permeation. The incorporation of non-polar and non-crystalline filler such AgNPs, initially used for obtaining antibacterial activity, did not have an impact on the water barrier properties of the composite films. Again, this result evidences the absence of a strong interface between these particles and the polymer matrix. In a way, the tortuosity effects what can be expected is counterbalanced by the weak interfaces and the microstructure.

In terms of diffusivity, the water diffusion coefficient is determined from the slope of the permeation curve by plotting the normalized water flux (J/J_{st}) as a function of the reduced time (t/L^2), as presented in Fig. III.11B. For all the composite films, the curves are superimposed on the neat PLA film one, reflecting any clear delay time in diffusion. Only, a small shift can be detected indicating the presence of fillers within the films, and hence to setup of low filler tortuosity effects.

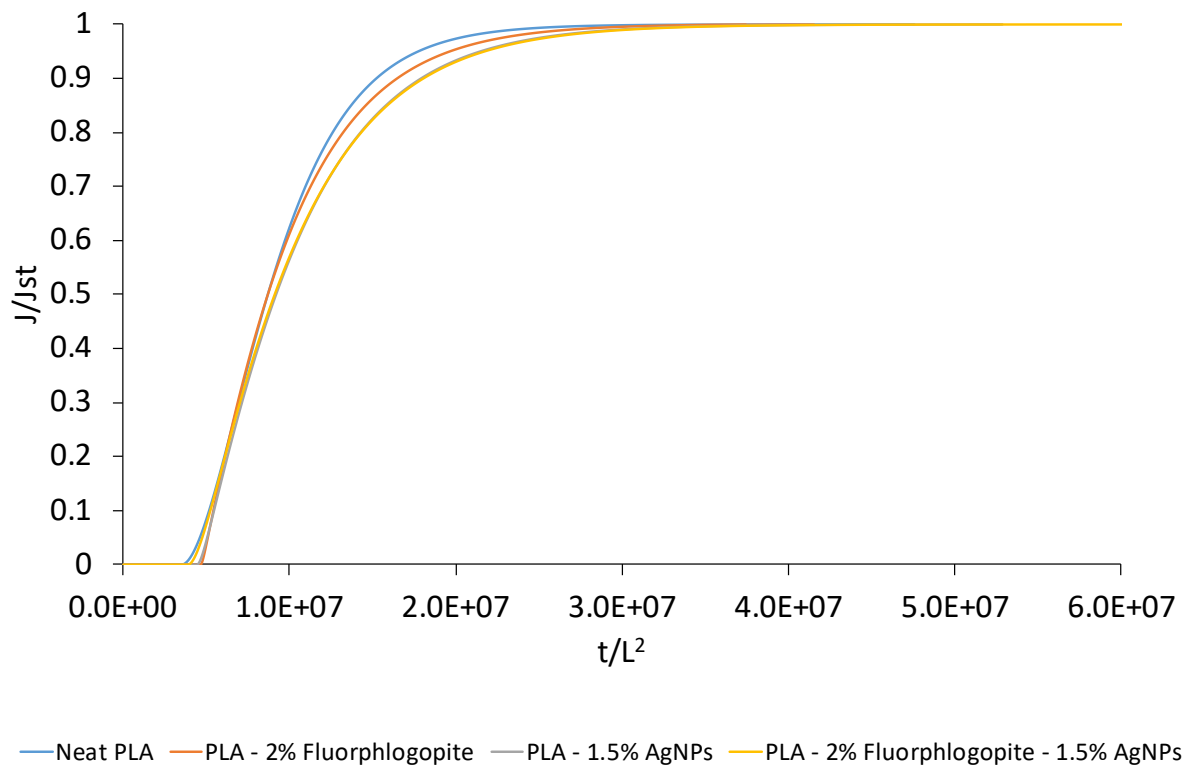
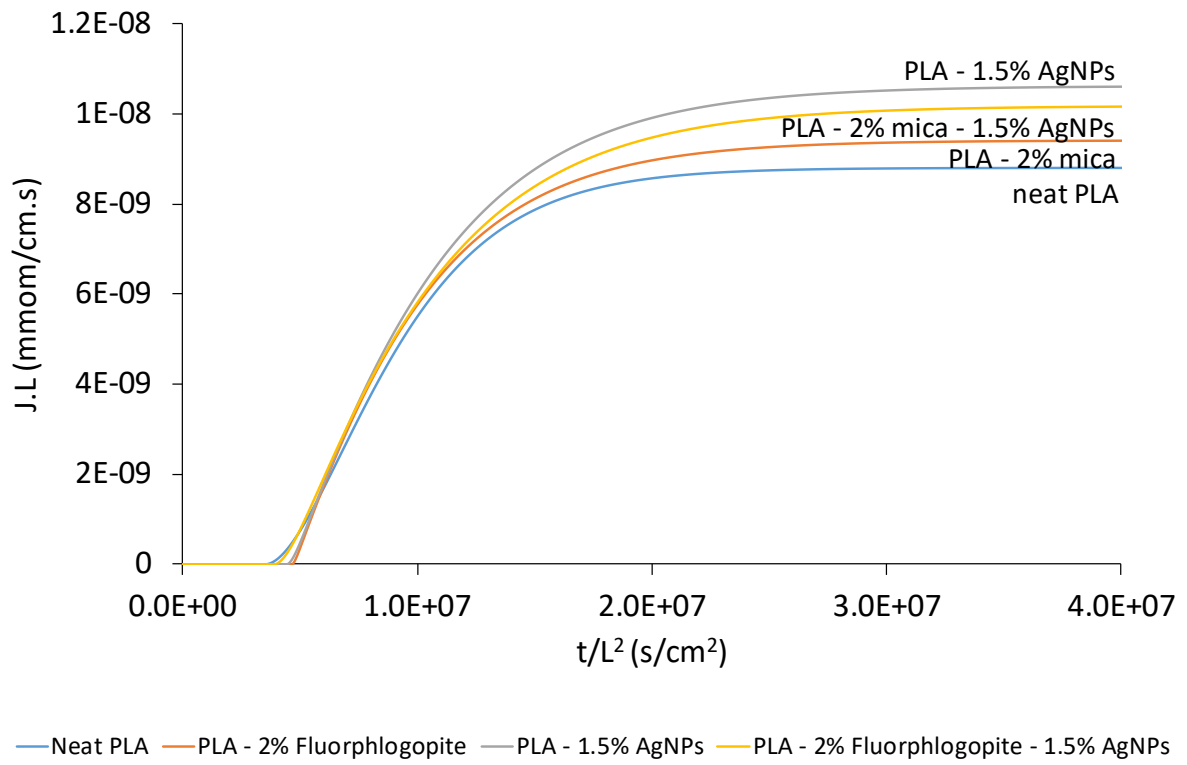


Figure III.11: A) Experimental reduced water flux ($J.L$) and B) normalized water flux (J/J_{st}) as a function of the reduced time (t/L^2) for the neat PLA and the composite films

Table III.4: Water permeation parameters of the neat PLA film and the composite films

	P Barrer	D_0 $\times 10^9 \text{ cm}^2\text{s}^{-1}$	D_I and D_L $\times 10^8 \text{ cm}^2\text{s}^{-1}$	γC_{eq}	γ cm^3 mmol^{-1}	C_{eq} mmol cm^{-3}
Neat PLA	833	9.9	1.4 / 1.7	1.7	4.7	0.35
PLA - 2%	910	8.7	1.4 / 1.7	2.0	6.0	0.34
Fluorophlogopite						
PLA - 1.5% AgNPs	1064	9.5	1.4 / 1.4	1.7	3.9	0.43
PLA - 2%	1026	10.3	1.4 / 1.6	1.5	3.4	0.43
Fluorophlogopite - 1.5% AgNPs						

Thus, from water permeation results, the calculated diffusion coefficients D_0 , D_I and D_L (Table 5) indicate that the low presence of fillers has practically no effect on the water diffusion through PLA, and that agrees well with the water vapor sorption results for which the diffusion coefficient values were close ($\sim 1.7 \cdot 10^{-8} \text{ cm}^2\cdot\text{s}^{-1}$) and not really changed by the presence of fillers.

III.3.4.3) Water plasticization effect

Using Fick's diffusion law equations, for which D coefficient is assumed to be a constant parameter, the diffusion coefficient can be calculated at two specific times of the extent of water permeation process, as already described [43]. Briefly, the coefficient D_I is determined at $J/J_{st} = 0.24$, while the coefficient D_L is calculated at $J/J_{st} = 0.62$. The values are presented in Table 5. The D_I coefficients are found lower than the D_L coefficients, meaning that the water diffusion mechanism increases during permeation process, *i.e.*, when the water concentration increases. Such water concentration-dependence of the diffusion coefficient indicates a water plasticization effect which can be expressed by the well-known exponential law of diffusivity D with the local water concentration C (eq. (3)), (from the free volume theory). According to the procedure described in [44], the diffusion coefficient at nil concentration D_0 , the plasticization factor γC_{eq} and the water concentration at steady state C_{eq} were determined.

The low increase of D_0 values in presence of fillers suggests a low increased water diffusion during permeation process, mainly rather in the numerous areas free of fillers. This observation agrees with XRD results and TEM observations. In contrast, a low decrease of D_0 value with the incorporation of fluorophlogopite confirms low tortuosity effects, which is not maintained when adding AgNPs. The positive values of γC_{eq} , reported in Table 5, testify to the plasticization effect of water [44] in PLA, which is maintained despite the presence of fillers. From the calculated values of water concentration C_{eq} , it seems that the presence of Ag

nanoparticles increases slightly the water solubility in PLA while fluorophlogopite particles have no effect. This result would be consistent with water sorption results obtained at high water activity showing that the water mass at equilibrium state is increased especially with the presence of AgNPs.

III.3.4.4) Gas permeation

In addition to water, the transfer of gas molecules across the neat PLA and the composite films was investigated through gas permeation measurements to evaluate how the barrier properties of the PLA film can be affected by the presence of fillers. Three diffusing gas molecules, nitrogen N_2 , dioxygen O_2 and carbon dioxide CO_2 , differing in van der Waals molar volume [70], were selected because they are known not to interact (or only very weakly) with organic materials. The permeation behaviour for the neat PLA and the composite films conforms to a linear Henry's sorption law, which involves a constant diffusion coefficient. The diffusion coefficient is usually determined from the time-lag t_L given by the intercept of the steady-state asymptote on the time axis via the time-lag method. Permeability and diffusion coefficients (Fig. III.12) are calculated from permeation kinetic curves and thus reflect the film resistance towards small molecules.

In the present study, all the films globally showed the same tendency: $P(N_2) < P(O_2) < P(CO_2)$, as reported by Van Krevelen [71]. In most cases, small gas molecules diffuse more easily than larger molecules, as the permeability increases, even though, with their low critical temperature, the solubility of these diffusing molecules is reduced. The higher critical temperature of CO_2 (31.15 °C) led to a greater permeability to carbon dioxide. In contrast, the low critical temperature (-146.94 °C) associated to the higher dynamic diameter of N_2 (3.64 Å), in comparison with the two other gases, explains the lower permeability of nitrogen.

Because of the small gap for permeability values and for diffusion coefficient values, and considering the measurement errors, very few changes are obtained with the addition of fillers compared to coefficients of the neat PLA film. This result reveals that there is very few tortuosity induced by fluorophlogopite and silver nanoparticles within the PLA matrix. Besides, the small reduction of diffusion coefficients measured with the incorporation of fluorophlogopite tends to show that fluorophlogopite particles act as obstacles to gas diffusion, as highlighted with the water sorption behavior. This finding reflects thus a moderate tortuosity effect initiated by the filler and which seems to be maintained with the co-incorporation of silver nanoparticles. One can conclude that the gas barrier properties of the PLA film are thus maintained even in presence of fillers.

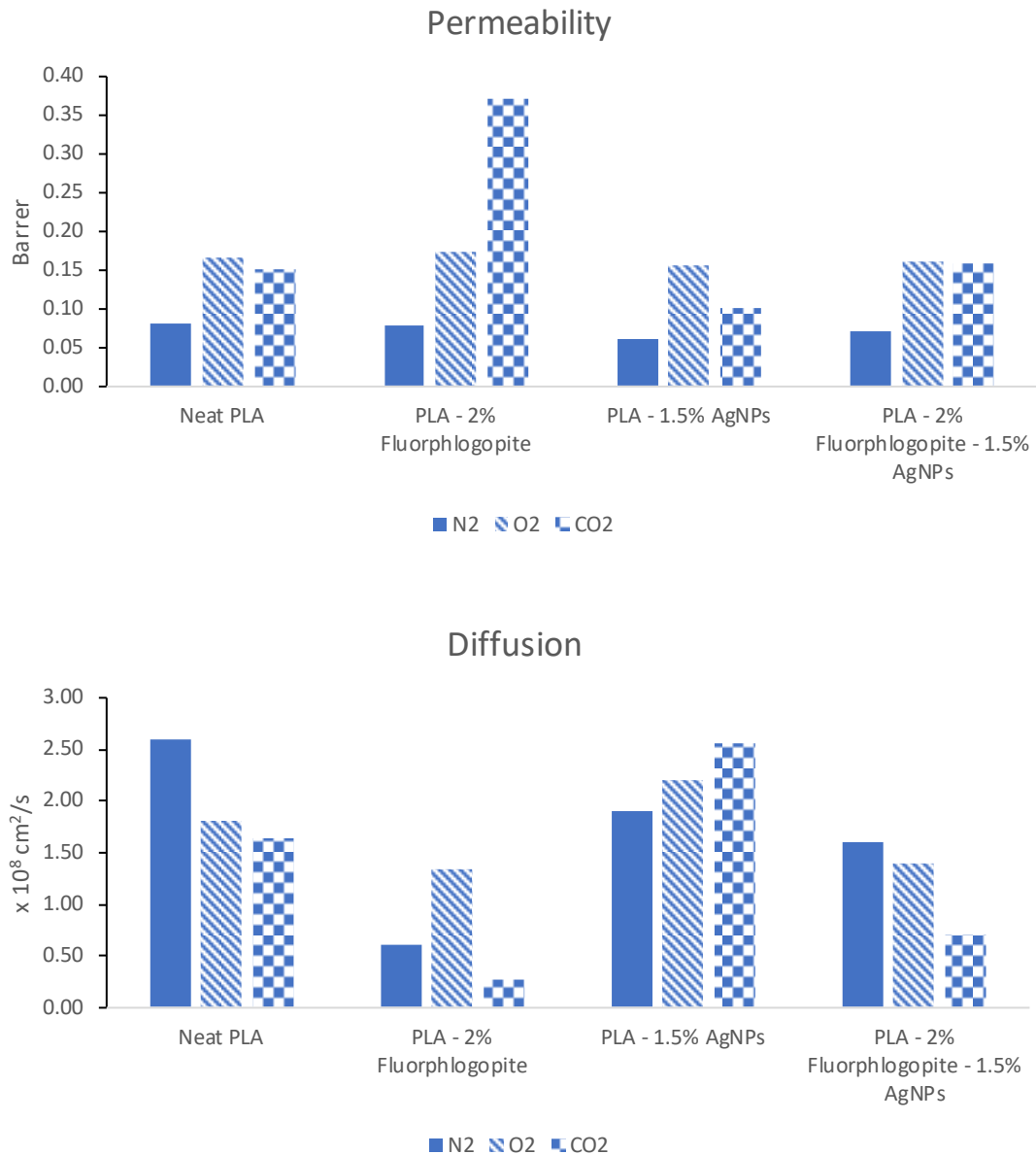


Figure III.12. Permeability and diffusion coefficients for the neat PLA film and the composite films. The values are calculated with a standard deviation of about 30% due to the very low obtained values

Overall, from all these sorption and permeation results, it can be stated that the incorporation of fluorphlogopite and AgNPs has very little effect on the water and gas transport properties of PLA. In other words, the gas and water barrier properties of PLA are kept with the presence of both fillers.

III.3.5) Antibacterial activity of Neat PLA and PLA blends

The antibacterial activity was firstly assessed by evaluating the percentage of inhibition of bacterial adhesion on the surface of the modified PLA films compared to neat PLA film (Fig. III.13). Three bacterial strains were used, 2 Gram-positive bacteria, *S. aureus*, and *E. faecalis*

and one Gram-negative bacteria, *E. coli*. These bacteria are usually connected to food poisoning but are also widely used in microbiology tests as model bacteria. All the films have demonstrated an inhibition of bacterial adhesion for the three bacteria. However, PLA-2% Fluorophlogopite films exhibited the lowest inhibition. On the other hand, PLA-1.5% AgNPs and PLA-2% Fluorophlogopite-1.5% AgNPs have shown a substantial significant inhibition of bacterial adhesion of 84% and 89% against *S. aureus*; 89% and 92% against *E. faecalis* and, 74% and 76% against *E. coli*, respectively.

The slight inhibition exhibited by the PLA films modified only by fluorophlogopite is probably due to a limitation of adhesion by an antiadhesive property and not a bacteriostatic/bactericidal activity as fluorophlogopite does not have this type of activity. The limitation of adhesion could be due to the change of physico-chemical characteristics of PLA when fluorophlogopite was added. Indeed Mica is known to increase the polymer roughness which was confirmed by the SEM micrographs in Fig. III.1 and was also found by Wang *et al.*, [72]. However, the surface roughness is generally associated with an increase in bacterial adhesion with few reports demonstrating otherwise [73]. Another possibility is the increase in the hydrophobicity of PLA as was evidenced by water contact angle result. Indeed, Kyun Oh *et al.*, [74] have found that bacterial adhesion is more favored on hydrophilic surfaces than on hydrophobic surfaces [73]. In the case of silver nanoparticles, the inhibition was expected due to the potent antibacterial activity of silver nanoparticles as demonstrated by the measurement of MIC values of AgNPs in solution (*i.e.*, 150 $\mu\text{g. mL}^{-1}$ against *S. aureus* and *E. coli* and 75 $\mu\text{g. mL}^{-1}$ against *E. faecalis*). AgNPs inhibit the growth of bacteria by interacting directly, or indirectly via the release of Ag^+ , with vital bacterial components such as DNA, proteins, and cell membrane, compromising, thus, bacterial survival [75]. Finally, tertiary films containing fluorophlogopite and AgNPs showed the best inhibition of bacterial adhesion which is expected due to the combined effect of these fillers. In a similar work, Cai *et al.*, [76] found a similar combined effect of a nanoclay and AgNPs against the growth of *E.coli* and *S.aureus* at PLA interface. Similarly, the effect of nanoclay on the bacterial adhesion was explained by the possible effect of the filler on the physical interaction between the bacterial and the material surface Other works on the preparation of antibacterial PLA nanocomposites using antibacterial fillers such as AgNPs are summarized in Table SI-1.

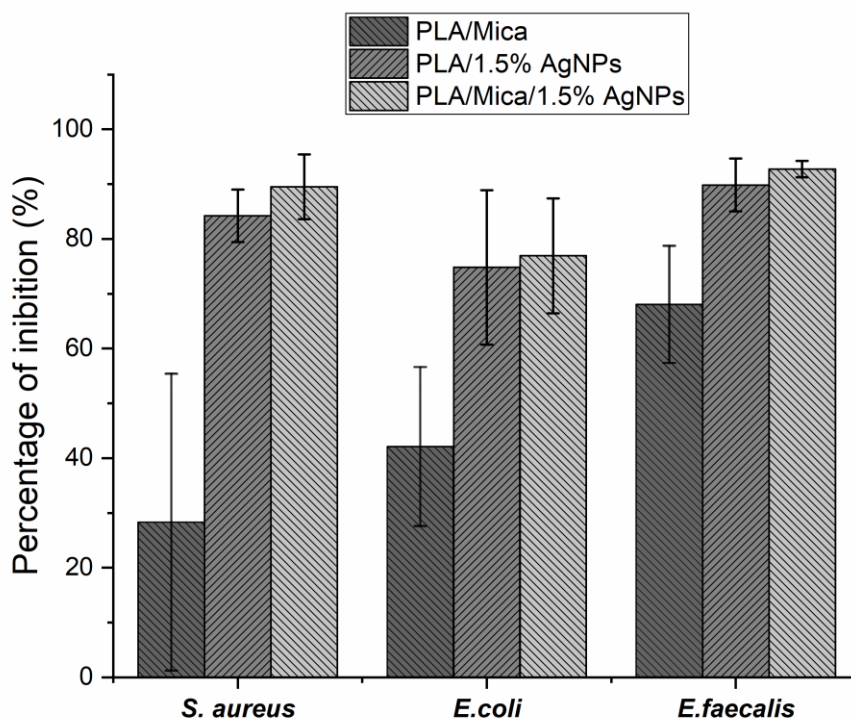


Figure 13: Percentages of inhibition of growth on the surface of PLA-Fluorophlogopite-AgNPs composites against *S. aureus*, *E. faecalis*, and *E. coli* compared to neat PLA

In order to assess if PLA nanocomposites exhibit an antibacterial activity by diffusion of AgNPs or by contact of bacteria with the film, a disc diffusion method was performed. Square discs of neat PLA and different PLA blends with 2% fluorophlogopite or/and 1.5% AgNPs content were tested against *E. coli* and *S. aureus* and the inhibition zone around the films was observed. As seen in Figs. III.SI-3 and III.SI-4 no film has shown any antibacterial activity against either bacteria through diffusion characterized by an absence of inhibition halo around the films. This result for PLA films that contain AgNPs is therefore probably due to the non or very low diffusion of AgNPs in the agar leading to a bactericidal activity only by contact. This mode of action makes this film suitable for applications in antimicrobial food packaging as well as in biomedical applications by avoiding (i) the loss of activity over time with the decrease of the AgNPs concentration and (ii) the contact of active agents with the packaged food. Indeed, biomedical device-related infections are a huge concern in the medical field. To limit such infections, using antibacterial coatings with antibacterial activity through contact is preferable due to their long-term effectiveness and the avoidance of concerns over the release and accumulation of antibacterial agents in the body [77].

III.4) Conclusion

PLA-based nanocomposites were prepared using melt mixing for potential antimicrobial food packaging applications. For this purpose, fluorphlogopite and silver nanoparticles were used as fillers, and the nanocomposites morphological, thermal, mechanical, barrier, and antibacterial properties were determined. A substantial enhancement of thermal stability of PLA was observed when 2wt% of fluorphlogopite was added while the mechanical properties of PLA remained unchanged. The barrier properties (*i.e.*, water permeation, water sorption, and gas permeation to O₂, CO₂, and N₂) are important properties of food packaging materials. PLA barrier properties, which are already excellent, comparable even to conventional food packaging plastics, were not affected by the introduction of fluorphlogopite and AgNPs.

Finally, the antibacterial activity of the nanocomposites was assessed against three bacteria, *S. aureus*, *E. faecalis*, and *E. coli*. The introduction of fluorphlogopite caused a slight inhibition of bacterial adhesion on the surface of the films, probably through changes in the surface morphology rather than through surface killing. However, the introduction of 1.5 wt% AgNPs alone has exhibited a bacterial adhesion inhibition of 84% *S. aureus*; 89% against *E. faecalis*, and, 74% against *E. coli*. PLA tertiary films containing 1.5% AgNPs and 2% fluorphlogopite have further increased the antibacterial potency of the nanocomposites.

Furthermore, as discussed in the introduction section, PLA is considered a suitable material for potential biomedical applications such as the preparation of scaffolds and drug delivery. Thus, the enhancement of PLA thermal properties and maintaining its mechanical and barrier properties as well as the excellent antibacterial activity through contact rather than diffusion could make of PLA-Fluorphlogopite-AgNPs nanocomposites a promising candidate for the preparation of biomedical scaffolds or the coating of biomedical implants in order to limit implant-associated infections.

The results presented in this paper showed, to the best of our knowledge, the very first report on the successful preparation of antibacterial PLA-Fluorphlogopite-AgNPs films with an enhancement of the PLA thermal properties while maintaining the intrinsic barrier properties of PLA. All these properties make this material a promising candidate for food packaging and biomedical applications.

Acknowledgment

This project was financially supported by French-Morocco bilateral programs by CAMPUS FRANCE: PHC TOUBKAL/18/71 and APUR 2019.

This work was also performed with the support of the Erasmus+ program of the European Union (Mobility at the University of Zagreb (HRZAGREB01))

CRedit authorship contribution statement

A. Nabgui: Conceptualization, Methodology, Validation, Investigation, Writing – original draft, **N. Follain:** Resources, Investigation, Writing - Review & Editing, **E. Vidović:** Resources, **J. El Haskouri:** Resources, Investigation, **S. Marais:** Resources, Investigation, Writing - Review & Editing, **A. El Meziane:** Conceptualization, Resources, Writing - Review & Editing, Supervision, Funding acquisition **M. Lahcini:** Conceptualization, Resources, Writing - Review & Editing, Supervision, Funding acquisition, **P. Thébault:** Conceptualization, Resources, Writing - Review & Editing, Supervision, Funding acquisition.

Data availability

All raw and processed data are available upon request to the authors

III.5) Supporting information

Table III.SI-1: Comparative table of works on binary of PLA/2D particles composites and antibacterial tertiary PLA/2D/metallic nanoparticles composites.

Materials	Processing methods	2D fillers modification	Materials morphology	Key results	Reference
PLA/Cloisite 30	Melt extrusion/ Flat film extrusion	MT2EtOH	Films	-Reduction in Oxygen permeability -Reduction in Water Vapor permeability	[SI-1]
PLA/OMt	Melt extrusion	Gemini surfactants	Films	-Enhanced tensile strength and Young's modulus but a lower elongation at break -Reduced water vapor permeability by 38 to 49.6% depending on the loadings (1 or 3%) and the hydrophobic chain length of the surfactants	[SI-2]
PLA/Mica	-Melt extrusion/Pressing -Solution mixing/Solvent casting	None	Films	-Enhanced thermal properties	[62]
PLA/GO/AgNPs	Solution mixing/ Electrospinning	None	Electrospun mats	-Substantial enhancement of the elastic modulus and tensile strength -Enhancement of thermal stability - Excellent antibacterial activity against <i>E. coli</i> and <i>S. aureus</i>	[36]
PLA/PA-Cu(II)-LDH	Solution mixing/ Solvent casting	PA-Cu(II)	Films	-Enhancement of elongation at break and tensile strength increase by 53.0% and 18.9% -Reducing oxygen relative permeability by 28% -Antibacterial rate against <i>E. coli</i> >99.9%	[21]
PLA/Saponite	Solution mixing/ Solvent casting	Quaternary fulvic acid	Films	- Enhancement of elongation at break and tensile strength -Enhancement of thermal stability - Excellent antimicrobial activity against <i>E. coli</i> , <i>Bacillus subtilis</i> , <i>Aspergillus</i> , and <i>Penicillium</i>	[20]
PLA/GO/ZnONps	Solution mixing/ Solvent casting	None	Films	-Enhanced tensile strength and storage modulus -Antibacterial rate of 99.2% against <i>E. coli</i> and 97.6% against <i>S. aureus</i> under light and 83% against <i>E. coli</i> and 52.3% against <i>S. aureus</i> in dark conditions	[SI-3]
PLA/Nanoclay/ AgNPs	Melt extrusion	None	Fibrous meshes	- Lower affinity for bacterial adhesion - Antibacterial activity at the materials surface	[76]

PCL/PLA/Ag-MMT	Melt extrusion/ compression molding	Ag	Films	- Enhanced thermal stability - Enhanced tensile strength, elongation at break, and E modulus - Total inhibition of the growth of <i>E. coli</i> , <i>S. aureus</i> , <i>Salmonella</i> , and <i>Pseudomonas aeruginosa</i>	[SI-4]
PLA/Fluorophlogopite/ AgNPs	Melt extrusion/Pressing/ Solvent casting	None	Films	-Enhanced thermal stability -Maintained mechanical and barrier properties -Extensive study of barrier properties -Excellent antibacterial activity against <i>E.coli</i> , <i>S. aureus</i> , and <i>E.faecalis</i> through contact	Our study

IV) OMt: Organomodified montmorillonite; GO : Graphene oxide; AgNPs: Silver nanoparticles; PA : Phytic acid; LDH: Layered double hydroxides; ZnONPs: Zinc oxide nanoparticles;

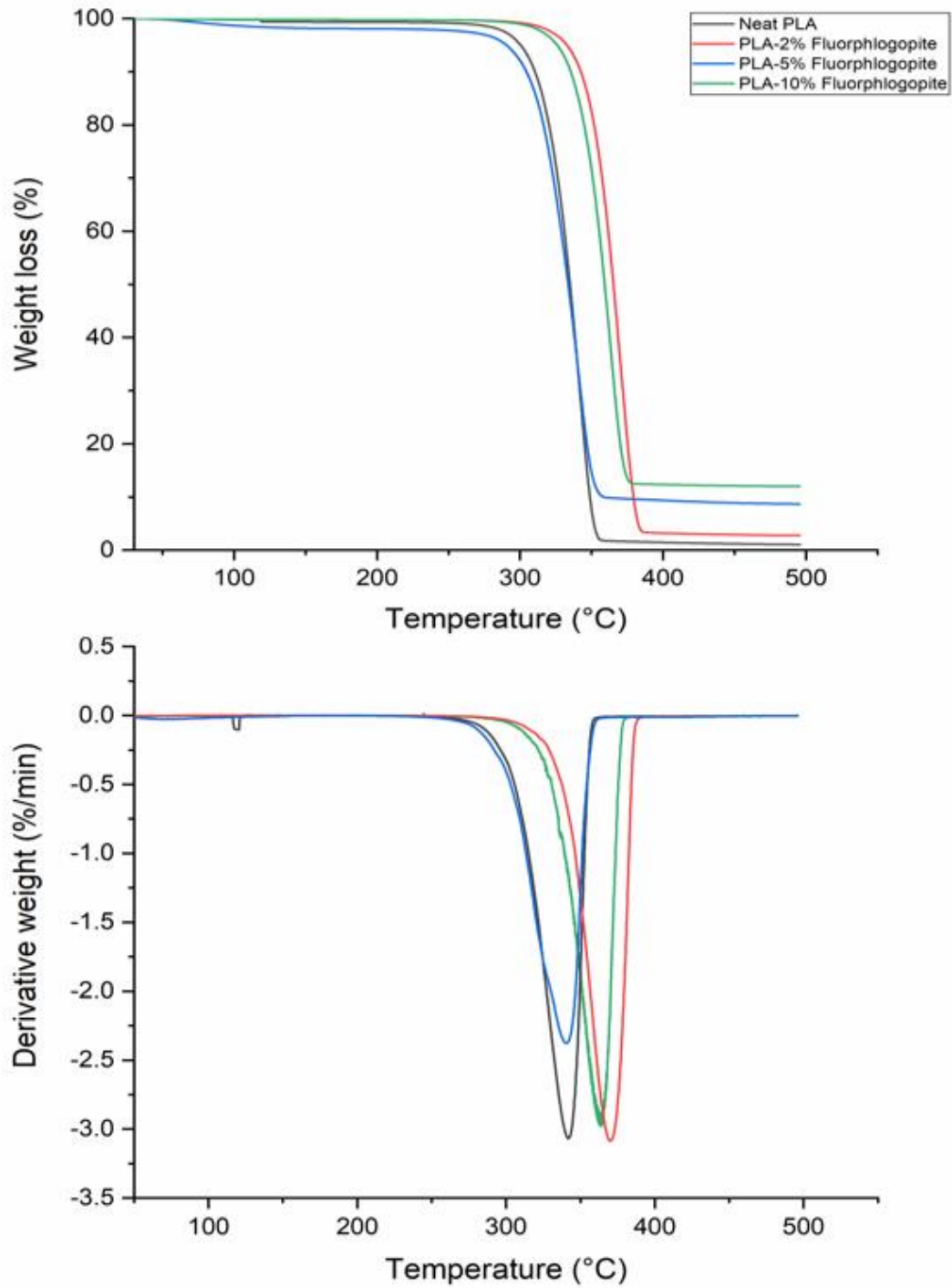


Figure III.SI-1: Weight loss curves and differential weight loss curves of neat PLA and PLA-Fluorophlogopite (2, 5, and 10%)

Table III.SI-2: $T_{5\%}$, $T_{50\%}$, and T_{Onset} result of PLA and PLA-Fluorophlogopite composites

	$T_{5\%}$	$T_{50\%}$	T_{Onset}
PLA	300	334	306
PLA-2% Fluorophlogopite	335	365	337
PLA-5% Fluorophlogopite	290	334	303
PLA-10% Fluorophlogopite	326	359	329

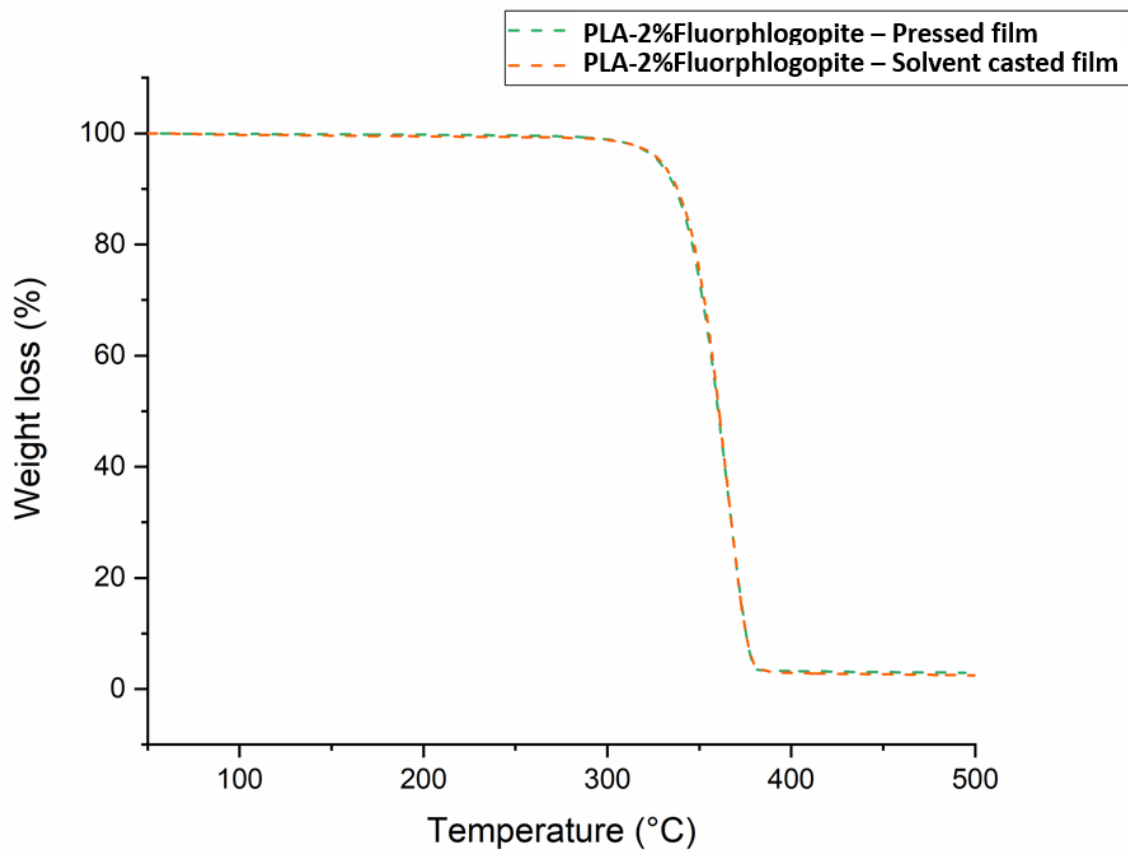


Figure III.SI-2: Weight loss curves of melt-extruded PLA and PLA-2% Fluorophlogopite films prepared by the hot press or solvent casting method

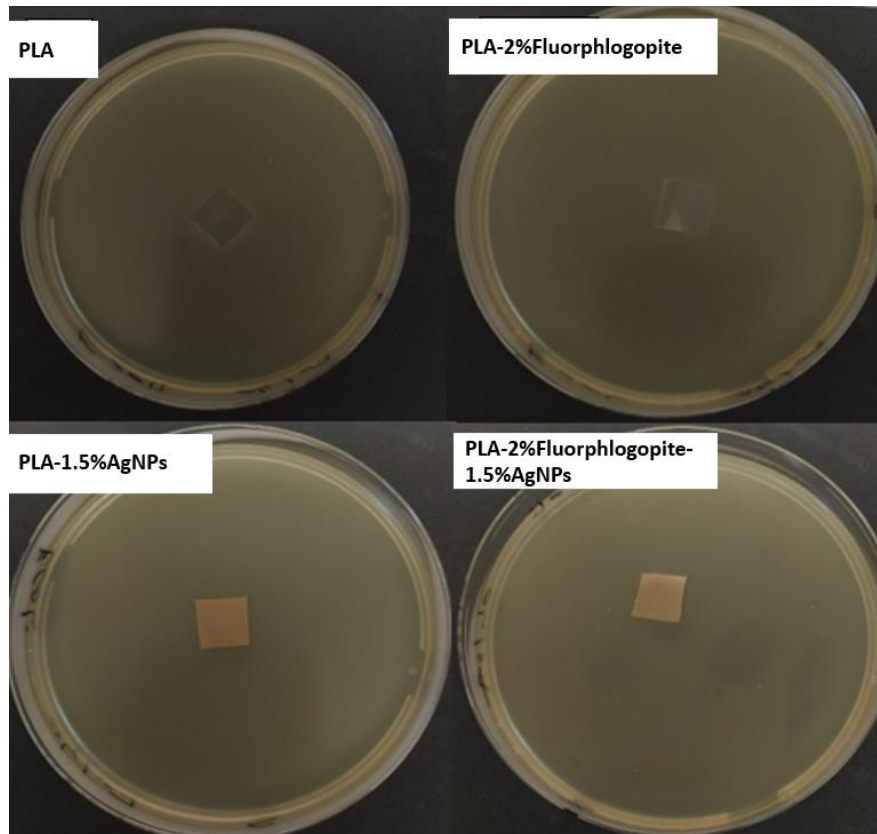


Figure III.SI-3: Results of disc diffusion test on E.coli of PLA and PLA Fluorphlogopite-AgNPs composites

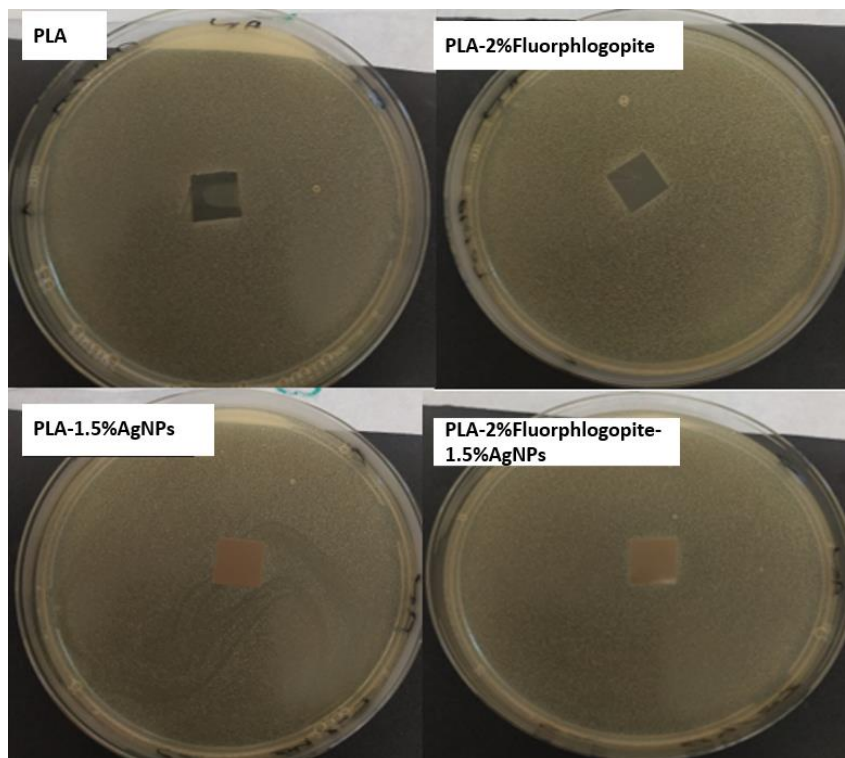


Figure III.SI-4: Results of disc diffusion test on S.aureus of PLA and PLA Fluorphlogopite-AgNPs composites

Reference

- [1] R.L. Scharff, Health-Related Costs from Foodborne Illness in the United States, (2010).
- [2] J. Gustavsson, C. Cederberg, U. Sonesson, R.V. Otterdijk, A. Meybeck, Global food losses and food waste: extent, causes and prevention, Undefined. (2011). <https://www.semanticscholar.org/paper/Global-food-losses-and-food-waste%3A-extent%2C-causes-Gustavsson-Cederberg/19c0065b1ad3f83f5ce7b0b16742d137d0f2125e> (accessed March 8, 2022).
- [3] T. Huang, Y. Qian, J. Wei, C. Zhou, Polymeric Antimicrobial Food Packaging and Its Applications, *Polymers*. 11 (2019) 560. <https://doi.org/10.3390/polym11030560>.
- [4] J.-W. Han, L. Ruiz-Garcia, J.-P. Qian, X.-T. Yang, Food Packaging: A Comprehensive Review and Future Trends, *Compr. Rev. Food Sci. Food Saf.* 17 (2018) 860–877. <https://doi.org/10.1111/1541-4337.12343>.
- [5] M. Asgher, S.A. Qamar, M. Bilal, H.M.N. Iqbal, Bio-based active food packaging materials: Sustainable alternative to conventional petrochemical-based packaging materials, *Food Res. Int.* 137 (2020) 109625. <https://doi.org/10.1016/j.foodres.2020.109625>.
- [6] R. Jain, A. Tiwari, Biosynthesis of planet friendly bioplastics using renewable carbon source, *J. Environ. Health Sci. Eng.* 13 (2015) 11. <https://doi.org/10.1186/s40201-015-0165-3>.
- [7] D. Valerini, L. Tammaro, F. Villani, A. Rizzo, I. Caputo, G. Paolella, G. Vigliotta, Antibacterial Al-doped ZnO coatings on PLA films, *J. Mater. Sci.* 55 (2020) 4830–4847. <https://doi.org/10.1007/s10853-019-04311-z>.
- [8] A.H. Mohsen, N.A. Ali, Mechanical, Color and Barrier, Properties of Biodegradable Nanocomposites Polylactic Acid/Nanoclay, *J. Bioremediation Biodegrad.* 09 (2018). <https://doi.org/10.4172/2155-6199.1000455>.
- [9] V. Siracusa, P. Rocculi, S. Romani, M.D. Rosa, Biodegradable polymers for food packaging: a review, *Trends Food Sci. Technol.* 19 (2008) 634–643. <https://doi.org/10.1016/j.tifs.2008.07.003>.
- [10] G. Colomines, V. Ducruet, C. Courgneau, A. GUINAULT, S. Domenek, Barrier properties of poly(lactic acid) and its morphological changes induced by aroma compound sorption, *Polym. Int.* 59 (2010) 818–826. <https://doi.org/10.1002/pi.2793>.
- [11] S. Sinha Ray, K. Yamada, M. Okamoto, Y. Fujimoto, A. Ogami, K. Ueda, New polylactide/layered silicate nanocomposites. 5. Designing of materials with desired properties, *Polymer*. 44 (2003) 6633–6646. <https://doi.org/10.1016/j.polymer.2003.08.021>.
- [12] E. Picard, E. Espuche, R. Fulchiron, Effect of an organo-modified montmorillonite on PLA crystallization and gas barrier properties, *Appl. Clay Sci.* 53 (2011) 58–65. <https://doi.org/10.1016/j.clay.2011.04.023>.
- [13] J.-W. Rhim, S.-I. Hong, C.-S. Ha, Tensile, water vapor barrier and antimicrobial properties of PLA/nanoclay composite films, *LWT - Food Sci. Technol.* 42 (2009) 612–617. <https://doi.org/10.1016/j.lwt.2008.02.015>.
- [14] F. Li, C. Zhang, Y. Weng, Improvement of the Gas Barrier Properties of PLA/OMMT Films by Regulating the Interlayer Spacing of OMMT and the Crystallinity of PLA, *ACS Omega*. 5 (2020) 18675–18684. <https://doi.org/10.1021/acsomega.0c01405>.

- [15] P. Maiti, K. Yamada, M. Okamoto, K. Ueda, K. Okamoto, New Polylactide/Layered Silicate Nanocomposites: Role of Organoclays, *Chem. Mater.* 14 (2002) 4654–4661. <https://doi.org/10.1021/cm020391b>.
- [16] K. Kabiri, H. Mirzadeh, M.J. Zohuriaan-Mehr, Chitosan modified MMT-poly(AMPS) nanocomposite hydrogel: Heating effect on swelling and rheological behavior, *J. Appl. Polym. Sci.* 116 (2010) 2548–2556. <https://doi.org/10.1002/app.31727>.
- [17] L. Martino, N. Guigo, J.G. van Berkel, N. Sbirrazzuoli, Influence of organically modified montmorillonite and sepiolite clays on the physical properties of bio-based poly(ethylene 2,5-furandicarboxylate), *Compos. Part B Eng.* 110 (2017) 96–105. <https://doi.org/10.1016/j.compositesb.2016.11.008>.
- [18] M. del R. Moreira, S.I. Roura, A. Ponce, Effectiveness of chitosan edible coatings to improve microbiological and sensory quality of fresh cut broccoli, *LWT - Food Sci. Technol.* 44 (2011) 2335–2341. <https://doi.org/10.1016/j.lwt.2011.04.009>.
- [19] S. Kumar, V. Deepak, M. Kumari, P.K. Dutta, Antibacterial activity of diisocyanate-modified chitosan for biomedical applications, *Int. J. Biol. Macromol.* 84 (2016) 349–353. <https://doi.org/10.1016/j.ijbiomac.2015.12.027>.
- [20] W. Wang, W. Zhen, S. Bian, X. Xi, Structure and properties of quaternary fulvic acid–intercalated saponite/poly(lactic acid) nanocomposites, *Appl. Clay Sci.* 109–110 (2015) 136–142. <https://doi.org/10.1016/j.clay.2015.02.033>.
- [21] Y. Lei, L. Mao, J. Yao, Z. Li, Efficient Gas Barrier and Antibacterial Properties of Poly(lactic acid) Nanocomposites: Functionalization with Phytic Acid–Cu(II) Loaded Layered Clay, *Materials.* 13 (2020) 2033. <https://doi.org/10.3390/ma13092033>.
- [22] A. Nabgui, T. El Assimi, A. El Meziane, G.A. Luinstra, M. Raihane, G. Gouhier, P. Thébault, K. Draoui, M. Lahcini, Synthesis and antibacterial behavior of bio-composite materials-based on poly(ϵ -caprolactone)/bentonite, *Eur. Polym. J.* 156 (2021) 110602. <https://doi.org/10.1016/j.eurpolymj.2021.110602>.
- [23] S. Kumar, B. Krishnakumar, A.J.F.N. Sobral, J. Koh, Bio-based (chitosan/PVA/ZnO) nanocomposites film: Thermally stable and photoluminescence material for removal of organic dye, *Carbohydr. Polym.* 205 (2019) 559–564. <https://doi.org/10.1016/j.carbpol.2018.10.108>.
- [24] M.E. El-Naggar, M. Hasanin, A.H. Hashem, Eco-Friendly Synthesis of Superhydrophobic Antimicrobial Film Based on Cellulose Acetate/Polycaprolactone Loaded with the Green Biosynthesized Copper Nanoparticles for Food Packaging Application, *J. Polym. Environ.* 30 (2022) 1820–1832. <https://doi.org/10.1007/s10924-021-02318-9>.
- [25] S. Murali, S. Kumar, J. Koh, S. Seenaa, P. Singh, A. Ramalho, A.J.F.N. Sobral, Bio-based chitosan/gelatin/Ag@ZnO bionanocomposites: synthesis and mechanical and antibacterial properties, *Cellulose.* 26 (2019) 5347–5361. <https://doi.org/10.1007/s10570-019-02457-2>.
- [26] I. Zorraquín-Peña, C. Cueva, B. Bartolomé, M.V. Moreno-Arribas, Silver Nanoparticles against Foodborne Bacteria. Effects at Intestinal Level and Health Limitations, *Microorganisms.* 8 (2020) 132. <https://doi.org/10.3390/microorganisms8010132>.
- [27] Y.-G. Yuan, Q.-L. Peng, S. Gurunathan, Effects of Silver Nanoparticles on Multiple Drug-Resistant Strains of *Staphylococcus aureus* and *Pseudomonas aeruginosa* from Mastitis-

Infected Goats: An Alternative Approach for Antimicrobial Therapy, *Int. J. Mol. Sci.* 18 (2017) 569. <https://doi.org/10.3390/ijms18030569>.

[28] K. Kraśniewska, S. Galus, M. Gniewosz, Biopolymers-Based Materials Containing Silver Nanoparticles as Active Packaging for Food Applications—A Review, *Int. J. Mol. Sci.* 21 (2020) 698. <https://doi.org/10.3390/ijms21030698>.

[29] R.K. Dhall, Advances in Edible Coatings for Fresh Fruits and Vegetables: A Review, *Crit. Rev. Food Sci. Nutr.* 53 (2013) 435–450. <https://doi.org/10.1080/10408398.2010.541568>.

[30] J. Cheng, X. Lin, X. Wu, Q. Liu, S. Wan, Y. Zhang, Preparation of a multifunctional silver nanoparticles polylactic acid food packaging film using mango peel extract, *Int. J. Biol. Macromol.* 188 (2021) 678–688. <https://doi.org/10.1016/j.ijbiomac.2021.07.161>.

[31] J.A. Prince, G. Singh, D. Rana, T. Matsuura, V. Anbharasi, T.S. Shanmugasundaram, Preparation and characterization of highly hydrophobic poly(vinylidene fluoride) – Clay nanocomposite nanofiber membranes (PVDF–clay NNMs) for desalination using direct contact membrane distillation, *J. Membr. Sci.* 397–398 (2012) 80–86. <https://doi.org/10.1016/j.memsci.2012.01.012>.

[32] S. Snigdha, K. Nandakumar, T. Sabu, E.K. Radhakrishnan, CLOISITE 10A AS AN EFFECTIVE ANTIBACTERIAL AGENT IN POLYMER MATRICES: ROLE OF NANOSCALE ROUGHNESS AND INTERFACIAL INTERACTIONS, *Clays Clay Miner.* 69 (2021) 289–298. <https://doi.org/10.1007/s42860-021-00122-z>.

[33] Y. Yuan, M. P. Hays, P. R. Hardwidge, J. Kim, Surface characteristics influencing bacterial adhesion to polymeric substrates, *RSC Adv.* 7 (2017) 14254–14261. <https://doi.org/10.1039/C7RA01571B>.

[34] I.S. Bayer, Thermomechanical Properties of Polylactic Acid-Graphene Composites: A State-of-the-Art Review for Biomedical Applications, *Materials.* 10 (2017) 748. <https://doi.org/10.3390/ma10070748>.

[35] N.K. Dhiman, S. Agnihotri, R. Shukla, Silver-Based Polymeric Nanocomposites as Antimicrobial Coatings for Biomedical Applications, in: S. Singh, P.K. Maurya (Eds.), *Nanotechnol. Mod. Anim. Biotechnol.*, Springer Singapore, Singapore, 2019: pp. 115–171. https://doi.org/10.1007/978-981-13-6004-6_4.

[36] C. Liu, J. Shen, K.W.K. Yeung, S.C. Tjong, Development and Antibacterial Performance of Novel Polylactic Acid-Graphene Oxide-Silver Nanoparticle Hybrid Nanocomposite Mats Prepared By Electrospinning, *ACS Biomater. Sci. Eng.* 3 (2017) 471–486. <https://doi.org/10.1021/acsbiomaterials.6b00766>.

[37] B.S. Munteanu, Z. Aytac, G.M. Pricope, T. Uyar, C. Vasile, Polylactic acid (PLA)/Silver-NP/VitaminE bionanocomposite electrospun nanofibers with antibacterial and antioxidant activity, *J. Nanoparticle Res.* 16 (2014) 2643. <https://doi.org/10.1007/s11051-014-2643-4>.

[38] F. Mohanty, S.K. Swain, Silver Nanoparticles Decorated Polyethylmethacrylate/Graphene Oxide Composite: As Packaging Material, *Polym. Compos.* 40 (2019) E1199–E1207. <https://doi.org/10.1002/pc.24944>.

[39] S. Cheng, K. Lau, T. Liu, Y. Zhao, P.-M. Lam, Y. Yin, Mechanical and thermal properties of chicken feather fiber/PLA green composites, *Compos. Part B Eng.* 40 (2009) 650–654. <https://doi.org/10.1016/j.compositesb.2009.04.011>.

- [40] M. Métayer, M. Labbé, S. Marais, D. Langevin, C. Chappey, F. Dreux, M. Brainville, P. Belliard, Diffusion of water through various polymer films: a new high performance method of characterization, *Polym. Test.* 18 (1999) 533–549. [https://doi.org/10.1016/S0142-9418\(98\)00052-X](https://doi.org/10.1016/S0142-9418(98)00052-X).
- [41] S. Marais, M. Metayer, M. Labbe, Water diffusion and permeability in unsaturated polyester resin films characterized by measurements performed with a water-specific permeameter: Analysis of the transient permeation, *J. Appl. Polym. Sci.* 74 (1999) 3380–3395. [https://doi.org/10.1002/\(SICI\)1097-4628\(19991227\)74:14<3380::AID-APP12>3.0.CO;2-F](https://doi.org/10.1002/(SICI)1097-4628(19991227)74:14<3380::AID-APP12>3.0.CO;2-F).
- [42] S. Marais, M. Métayer, Q.T. Nguyen, M. Labbé, D. Langevin, New methods for the determination of the parameters of a concentration-dependent diffusion law for molecular penetrants from transient permeation or sorption data, *Macromol. Theory Simul.* 9 (2000) 207–214. [https://doi.org/10.1002/\(SICI\)1521-3919\(20000401\)9:4<207::AID-MATS207>3.0.CO;2-Q](https://doi.org/10.1002/(SICI)1521-3919(20000401)9:4<207::AID-MATS207>3.0.CO;2-Q).
- [43] S. Marais, Q.T. Nguyen, C. Devallencourt, M. Metayer, T.U. Nguyen, P. Schaezel, Permeation of water through polar and nonpolar polymers and copolymers: Determination of the concentration-dependent diffusion coefficient, *J. Polym. Sci. Part B Polym. Phys.* 38 (2000) 1998–2008. [https://doi.org/10.1002/1099-0488\(20000801\)38:15<1998::AID-POLB50>3.0.CO;2-A](https://doi.org/10.1002/1099-0488(20000801)38:15<1998::AID-POLB50>3.0.CO;2-A).
- [44] N. Follain, J.-M. Valleton, L. Lebrun, B. Alexandre, P. Schaezel, M. Metayer, S. Marais, Simulation of kinetic curves in mass transfer phenomena for a concentration-dependent diffusion coefficient in polymer membranes, *J. Membr. Sci.* 349 (2010) 195–207. <https://doi.org/10.1016/j.memsci.2009.11.044>.
- [45] P.C. Singh, R.K. Singh, Application of Gab Model for Water Sorption Isotherms of Food Products1, *J. Food Process. Preserv.* 20 (1996) 203–220. <https://doi.org/10.1111/j.1745-4549.1996.tb00743.x>.
- [46] N. Tenn, N. Follain, J. Soulestin, R. Crétois, S. Bourbigot, S. Marais, Effect of Nanoclay Hydration on Barrier Properties of PLA/Montmorillonite Based Nanocomposites, *J. Phys. Chem. C.* 117 (2013) 12117–12135. <https://doi.org/10.1021/jp401546t>.
- [47] G. Peng, X. Chen, W. Wu, X. Jiang, Modeling of water sorption isotherm for corn starch, *J. Food Eng.* 80 (2007) 562–567. <https://doi.org/10.1016/j.jfoodeng.2006.04.063>.
- [48] C. Lomauro, A. Bakshi, T. Labuza, Evaluation of food moisture sorption isotherm equations. Part I: Fruit, vegetable and meat products, *LWT - Food Sci. Technol.* 18 (1985) 111–117.
- [49] C. Joly, D. Le Cerf, C. Chappey, D. Langevin, G. Muller, Residual solvent effect on the permeation properties of fluorinated polyimide films, *Sep. Purif. Technol.* 16 (1999) 47–54. [https://doi.org/10.1016/S1383-5866\(98\)00118-X](https://doi.org/10.1016/S1383-5866(98)00118-X).
- [50] B. Diawara, K. Fatyeyeva, J. Ortiz, S. Marais, Polycarbonate/mica extrusion using mixing elements: Improvement of transparency and thermal, mechanical and water and gas barrier properties, *Polymer.* 230 (2021) 124030. <https://doi.org/10.1016/j.polymer.2021.124030>.
- [51] H. Baniasadi, J. Trifol, A. Ranta, J. Seppälä, Exfoliated clay nanocomposites of renewable long-chain aliphatic polyamide through in-situ polymerization, *Compos. Part B Eng.* 211 (2021) 108655. <https://doi.org/10.1016/j.compositesb.2021.108655>.

- [52] Y. Dong, J. Marshall, H.J. Haroosh, S. Mohammadzadehmoghadam, D. Liu, X. Qi, K.-T. Lau, Poly(lactic acid) (PLA)/halloysite nanotube (HNT) composite mats: Influence of HNT content and modification, *Compos. Part Appl. Sci. Manuf.* 76 (2015) 28–36. <https://doi.org/10.1016/j.compositesa.2015.05.011>.
- [53] H.M. Cele, V. Ojijo, H. Chen, S. Kumar, K. Land, T. Joubert, M.F.R. de Villiers, S.S. Ray, Effect of nanoclay on optical properties of PLA/clay composite films, *Polym. Test.* 36 (2014) 24–31. <https://doi.org/10.1016/j.polymertesting.2014.03.010>.
- [54] V. Demchenko, S. Kobylinskyi, M. Iurzenko, S. Riabov, A. Vashchuk, N. Rybalchenko, S. Zahorodnia, K. Naumenko, O. Demchenko, G. Adamus, M. Kowalczyk, Nanocomposites based on polylactide and silver nanoparticles and their antimicrobial and antiviral applications, *React. Funct. Polym.* 170 (2022) 105096. <https://doi.org/10.1016/j.reactfunctpolym.2021.105096>.
- [55] J.-W. Rhim, L.-F. Wang, Preparation and characterization of carrageenan-based nanocomposite films reinforced with clay mineral and silver nanoparticles, *Appl. Clay Sci.* 97–98 (2014) 174–181. <https://doi.org/10.1016/j.clay.2014.05.025>.
- [56] N. Asim, M. Badiei, M. Mohammad, Recent advances in cellulose-based hydrophobic food packaging, *Emergent Mater.* (2021). <https://doi.org/10.1007/s42247-021-00314-2>.
- [57] M. Martin-Polo, C. Mauguin, A. Voilley, Hydrophobic films and their efficiency against moisture transfer. 1. Influence of the film preparation technique, *J. Agric. Food Chem.* 40 (1992) 407–412. <https://doi.org/10.1021/jf00015a009>.
- [58] I. Armentano, E. Fortunati, L. Latterini, S. Rinaldi, E. Saino, L. Visai, F. Elisei, J. Kenny, Biodegradable PLGA matrix nanocomposite with silver nanoparticles: Material properties and bacteria activity, *J. Nanostructured Polym. Nanocomposites.* 6 (2010) 110–117.
- [59] Z. Wang, Z. Yao, J. Zhou, M. He, Q. Jiang, A. Li, S. Li, M. Liu, S. Luo, D. Zhang, Improvement of poly(lactic acid) film properties through the addition of cellulose nanocrystals isolated from waste cotton cloth, *Int. J. Biol. Macromol.* 129 (2019) 878–886. <https://doi.org/10.1016/j.ijbiomac.2019.02.021>.
- [60] EFFECT OF NUCLEATING AGENTS ON PHYSICAL-MECHANICAL PROPERTIES, in: *Handb. Nucleating Agents*, Elsevier, 2016: pp. 205–215. <https://doi.org/10.1016/B978-1-895198-93-5.50014-9>.
- [61] S.-M. Lai, S.-H. Wu, G.-G. Lin, T.-M. Don, Unusual mechanical properties of melt-blended poly(lactic acid) (PLA)/clay nanocomposites, *Eur. Polym. J.* 52 (2014) 193–206. <https://doi.org/10.1016/j.eurpolymj.2013.12.012>.
- [62] E. Vidović, F. Faraguna, A. Jukić, Influence of inorganic fillers on PLA crystallinity and thermal properties, *J. Therm. Anal. Calorim.* 127 (2017) 371–380. <https://doi.org/10.1007/s10973-016-5750-x>.
- [63] H. Rezaei, S. Seifi, E. Moeinifar, I. Hejazi, J. Seyfi, H.A. Khonakdar, Effect of nanoparticle type and content on morphology, rheology, and crystallinity of poly(lactic acid) using titanium dioxide and polyhedral oligomeric silsesquioxane nanoparticles, *Polym. Compos.* 41 (2020) 1551–1560. <https://doi.org/10.1002/pc.25477>.
- [64] M. Ramos, E. Fortunati, M. Peltzer, F. Dominici, A. Jiménez, M. del C. Garrigós, J.M. Kenny, Influence of thymol and silver nanoparticles on the degradation of poly(lactic acid)

based nanocomposites: Thermal and morphological properties, *Polym. Degrad. Stab.* 108 (2014) 158–165. <https://doi.org/10.1016/j.polymdegradstab.2014.02.011>.

[65] M.M. Jamel, P. Khoshnoud, S. Gunashekar, N. Abu-Zahra, Mechanical Properties and Dimensional Stability of Rigid PVC Foam Composites Filled with High Aspect Ratio Phlogopite Mica, *J. Miner. Mater. Charact. Eng.* 3 (2015) 237–247. <https://doi.org/10.4236/jmmce.2015.34026>.

[66] N. Follain, B. Alexandre, C. Chappey, L. Colasse, P. Médéric, S. Marais, Barrier properties of polyamide 12/montmorillonite nanocomposites: Effect of clay structure and mixing conditions, *Compos. Sci. Technol.* 136 (2016) 18–28. <https://doi.org/10.1016/j.compscitech.2016.09.023>.

[67] C. Dombre, S. Marais, C. Chappey, C. Lixon-Buquet, P. Chalier, The behaviour of wine aroma compounds related to structure and barrier properties of virgin, recycled and active PET membranes, *J. Membr. Sci.* 463 (2014) 215–225. <https://doi.org/10.1016/j.memsci.2014.03.066>.

[68] G.S. Park, Transport Principles—Solution, Diffusion and Permeation in Polymer Membranes, in: P.M. Bungay, H.K. Lonsdale, M.N. de Pinho (Eds.), *Synth. Membr. Sci. Eng. Appl.*, Springer Netherlands, Dordrecht, 1986: pp. 57–107. https://doi.org/10.1007/978-94-009-4712-2_3.

[69] P.E.R. Rouse Jr, Diffusion of Vapors in Films, *ACS Publ.* (2002). <https://doi.org/10.1021/ja01197a029>.

[70] R.W. Baker, J.G. Wijmans, Membrane Separation of Organic Vapors from Gas Streams, in: *Polym. Gas Sep. Membr.*, CRC Press, 1994.

[71] Van Krevelen, Properties of Polymers - 3rd Edition, (n.d.). <https://www.elsevier.com/books/properties-of-polymers/van-krevelen/978-0-444-82877-4> (accessed March 11, 2022).

[72] Y. Wang, Q. Liu, Z.-C. Zhen, J.-L. Liu, R.-M. Qiao, W.-Q. He, Effects of mica modification with ethylene-vinyl acetate wax on the water vapor barrier and mechanical properties of poly-(butylene adipate-co-terephthalate) nanocomposite films, *J. Appl. Polym. Sci.* 138 (2021) 50610. <https://doi.org/10.1002/app.50610>.

[73] S. Zheng, M. Bawazir, A. Dhall, H.-E. Kim, L. He, J. Heo, G. Hwang, Implication of Surface Properties, Bacterial Motility, and Hydrodynamic Conditions on Bacterial Surface Sensing and Their Initial Adhesion, *Front. Bioeng. Biotechnol.* 9 (2021). <https://www.frontiersin.org/article/10.3389/fbioe.2021.643722> (accessed March 11, 2022).

[74] J.K. Oh, Y. Yegin, F. Yang, M. Zhang, J. Li, S. Huang, S.V. Verkhoturov, E.A. Schweikert, K. Perez-Lewis, E.A. Scholar, T.M. Taylor, A. Castillo, L. Cisneros-Zevallos, Y. Min, M. Akbulut, The influence of surface chemistry on the kinetics and thermodynamics of bacterial adhesion, *Sci. Rep.* 8 (2018) 17247. <https://doi.org/10.1038/s41598-018-35343-1>.

[75] K.K. Sadasivuni, S. Rattan, S. Waseem, S.K. Brahme, S.B. Kondawar, S. Ghosh, A.P. Das, P.K. Chakraborty, J. Adhikari, P. Saha, P. Mazumdar, Silver Nanoparticles and Its Polymer Nanocomposites—Synthesis, Optimization, Biomedical Usage, and Its Various Applications, in: K.K. Sadasivuni, D. Ponnamma, M. Rajan, B. Ahmed, M.A.S.A. Al-Maadeed (Eds.), *Polym. Nanocomposites Biomed. Eng.*, Springer International Publishing, Cham, 2019: pp. 331–373. https://doi.org/10.1007/978-3-030-04741-2_11.

- [76] S. Cai, B. Pourdeyhimi, E.G. Lobo, High-Throughput Fabrication Method for Producing a Silver-Nanoparticles-Doped Nanoclay Polymer Composite with Novel Synergistic Antibacterial Effects at the Material Interface, *ACS Appl. Mater. Interfaces*. 9 (2017) 21105–21115. <https://doi.org/10.1021/acsami.7b03793>.
- [77] K. Vasilev, J. Cook, H.J. Griesser, Antibacterial surfaces for biomedical devices, *Expert Rev. Med. Devices*. 6 (2009) 553–567. <https://doi.org/10.1586/erd.09.36>.
- [78] M. Bartel, H. Remde, A. Bohn, J. Ganster, Barrier properties of poly(lactic acid)/cloisite 30B composites and their relation between oxygen permeability and relative humidity, *J. Appl. Polym. Sci.* 134 (2017). <https://doi.org/10.1002/app.44424>.
- [79] K. Taleb, I. Pillin, Y. Grohens, S. Saidi-Besbes, Polylactic acid/Gemini surfactant modified clay bio-nanocomposites: Morphological, thermal, mechanical and barrier properties, *Int. J. Biol. Macromol.* 177 (2021) 505–516. <https://doi.org/10.1016/j.ijbiomac.2021.02.135>.
- [80] Y. Huang, T. Wang, X. Zhao, X. Wang, L. Zhou, Y. Yang, F. Liao, Y. Ju, Poly(lactic acid)/graphene oxide–ZnO nanocomposite films with good mechanical, dynamic mechanical, anti-UV and antibacterial properties, *J. Chem. Technol. Biotechnol.* 90 (2015) 1677–1684. <https://doi.org/10.1002/jctb.4476>.
- [81] F. Benhacine, A.S. Hadj-Hamou, A. Habi, Y. Grohens, Development of Antimicrobial Poly(ϵ -caprolactone)/Poly(lactic acid)/Silver Exchanged Montmorillonite Nanoblend Films with Silver Ion Release Property for Active Packaging Use, *Int. Polym. Process.* 30 (2015) 511–521. <https://doi.org/10.3139/217.3087>.
- [SI-1] M. Bartel, H. Remde, A. Bohn, J. Ganster, Barrier properties of poly(lactic acid)/cloisite 30B composites and their relation between oxygen permeability and relative humidity, *J. Appl. Polym. Sci.* 134 (2017). <https://doi.org/10.1002/app.44424>.
- [SI-2] K. Taleb, I. Pillin, Y. Grohens, S. Saidi-Besbes, Polylactic acid/Gemini surfactant modified clay bio-nanocomposites: Morphological, thermal, mechanical and barrier properties, *Int. J. Biol. Macromol.* 177 (2021) 505–516. <https://doi.org/10.1016/j.ijbiomac.2021.02.135>.
- [SI-3] Y. Huang, T. Wang, X. Zhao, X. Wang, L. Zhou, Y. Yang, F. Liao, Y. Ju, Poly(lactic acid)/graphene oxide–ZnO nanocomposite films with good mechanical, dynamic mechanical, anti-UV and antibacterial properties, *J. Chem. Technol. Biotechnol.* 90 (2015) 1677–1684. <https://doi.org/10.1002/jctb.4476>.
- [SI-4] F. Benhacine, A.S. Hadj-Hamou, A. Habi, Y. Grohens, Development of Antimicrobial Poly(ϵ -caprolactone)/Poly(lactic acid)/Silver Exchanged Montmorillonite Nanoblend Films with Silver Ion Release Property for Active Packaging Use, *Int. Polym. Process.* 30 (2015) 511–521. <https://doi.org/10.3139/217.3087>.

Chapter V:

**Chitosan/Green Silver nanoparticles
nanobiocomposites: an efficient dual functionality
as antibacterial materials and 4-Nitroaniline
reduction catalysts**

Chapter overview

The result of the previous chapter highlights the potential use of PLA-fluorophlogopite-AgNPs nanocomposites in active food packaging. Indeed, the targeted objectives were attained by enhancing PLA properties as well as providing an important antibacterial activity through contact by using AgNPs as nanofillers. The AgNPs used in that work are commercial and were prepared using a chemical approach. Such approaches involve the use of chemical reducing and stabilizing agents that are harmful to the environment.

Indeed, AgNPs are prepared using 3 pathways: physical, chemical, or biological. However, the first two pathways present many drawbacks such as the use of toxic chemicals as discussed above, the necessity of specific equipment, or the excessive use of energy in the case of physical methods (laser ablation, mechanical milling). Consequently, biological methods using biological entities such as bacteria, fungi, and plants are considered an alternative and promising route to circumvent these issues.

AgNPs properties, including the antibacterial activity are size-dependent. Thus, their size and stability (which affect their size), are important parameters that need to be finely optimized. Indeed, the first choice that need to be made is the plant. Aromatic and medicinal plants are considered an ideal choice due to their high content in secondary metabolites, which are known for their excellent reducing and stabilizing potential. For that reason, rosemary (*Salvia rosmarinus* Spenn) was chosen. Other parameters such as reaction time, temperature, concentration, and post-synthesis stabilization are also need to be optimized in order to obtain a viable alternative to chemical AgNPs.

This chapter is thus, dedicated to the synthesis of silver nanoparticles (AgNPs) via a biological pathway using an aqueous rosemary extract and to the study of their stability.

The results of this chapter are presented in form of a paper entitled « Long term impact of surfactants on colloidal stability and antibacterial properties of biogenic silver nanoparticle » submitted on 10th of October, 2021 on “*Surfaces and Interfaces*”.

Moreover, the experiments that were not shown on this paper are presented and briefly discussed on the “supplementary information” section below.

Long term impact of surfactants on colloidal stability and antibacterial properties of biogenic silver nanoparticle

Abderrahmane Nabgui^{1,2,3}, Abdelmalik Brik^{3,4}, Khalid Agayr³, Géraldine Gouhier⁴, Redouane Beniazza⁵, Elvira Vidović⁶, Jamal El Haskouri⁷, Béatrice Labat⁸, Mohamed Lahcini^{3,5}, Pascal Thébault^{2*} & Abdellatif El Meziane^{1**}

¹ Centre of Agrobiotechnology and Bioengineering, AgroBiotech Center, URL-CNRST-05, Faculty of Sciences and Techniques, Cadi-Ayyad University, 40000, Marrakech, Morocco.

² Normandie Univ, UNIROUEN, INSA Rouen, CNRS, PBS UMR6270, Bd Maurice de Broglie, 76821 Mont Saint Aignan Cedex, France

³ IMED-Lab, Faculty of Sciences and Techniques, Cadi-Ayyad University, 40000, Marrakech, Morocco.

⁴ Normandie Univ, COBRA UMR 6014, FR 3038, INSA Rouen, CNRS, IRCOF, 76821 Mont-Saint-Aignan, France.

⁵ Mohammed VI Polytechnic University, 43150 Ben Guerir, Morocco.

⁶ University of Zagreb, Faculty of Chemical Engineering and Technology, HR-10000, Croatia

⁷ Instituto de ciencias de los materiales de la universidad de valencia, Calle catedrático José beltrán, 2, C.P 46980 Paterna Valencia Spain

⁸ Normandie Univ, UNIROUEN, INSA Rouen, CNRS, PBS UMR6270, 55 rue Saint-Germain, 27000 Évreux, France

* Corresponding author at : Normandie Univ, UNIROUEN, INSA Rouen, CNRS, PBS UMR6270, Bd Maurice de Broglie, 76821 Mont Saint Aignan Cedex, France. pascal.thebault@univ-rouen.fr

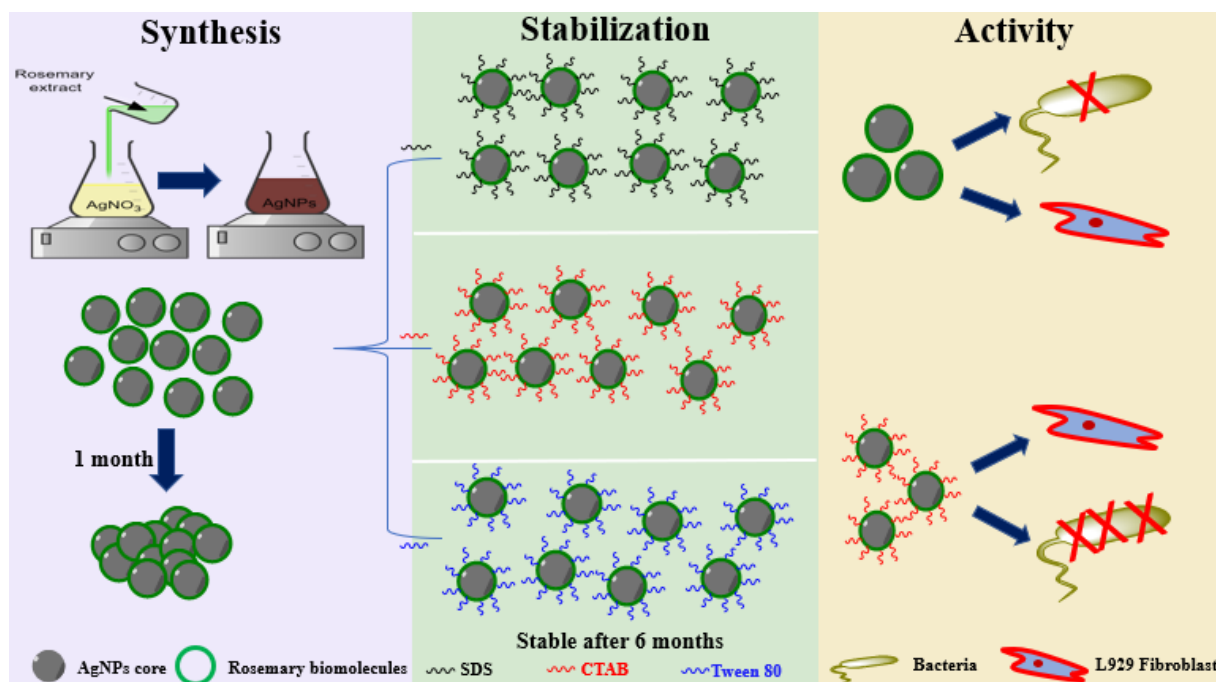
** Corresponding author at: Centre of Agrobiotechnology and Bioengineering, AgroBiotech Center, URL-CNRST-05, Faculty of Sciences and Techniques, Cadi-Ayyad University, 40000, Marrakech, Morocco. a.elmeziane@uca.ma

Abstract

Green synthesis of silver nanoparticles (AgNPs) using diverse plant species has gained a lot of attention in nanotechnology due to its simplicity, low cost, and eco-friendliness compared to the chemical and physical approaches. Plant extracts act both as reducing and capping agents making a one-pot synthesis possible. However, one of the main drawbacks of Plant-mediated AgNPs synthesis is nanoparticles aggregation and agglomeration during storage. Additional capping of AgNPs with stable surfactants will be probably required for their long-term stability. In this study, biogenic AgNPs were capped with surfactants and tested for long-term stability. R-AgNPs were synthesized using *Salvia rosmarinus* leaf extract at first, then their physico-chemical properties were determined using UV-Vis spectroscopy, X-ray diffraction (XRD), Dynamic light scattering (DLS), Transmission electron microscopy (TEM), Fourier transform infrared spectroscopy (FTIR) and Thermogravimetric analysis (TGA). TEM images of R-AgNPs display a quasi-spherical shape with an average size of 31 nm (TEM), whereas the hydrodynamic size (DLS) is only equivalent to 9 nm. The FTIR and TGA analysis showed the binding of rosemary biomolecules to R-AgNPs. Indeed, these biomolecules represent approximately 50% of the R-AgNPs weight. As the R-AgNPs stability decreases significantly after only one month of storage, the R-AgNPs were further stabilized by three surfactants differing in charge: CTAB (Cationic surfactant), SDS (anionic surfactant), and Tween 80 (non-ionic surfactant). All surfactants were effective in stabilizing R-AgNPs. The R-AgNPs capping with as low as 3 μ M CTAB showed higher stability and smaller size compared to R-AgNPs without surfactant, SDS-R-AgNPs, and Tween 80-R-AgNPs. As the addition of surfactants to R-AgNPs might reduce their antibacterial activities and cause toxicity to mammalian cells, surfactant-stabilized R-AgNPs were tested against pathogenic bacteria and mouse cell line. The R-AgNPs showed significant antibacterial activities against *E. coli*, *P. aeruginosa*, *S. aureus*, and *E. faecalis* with Minimum Inhibitory Concentration (MIC) values of 37.5, 37.5, 75, and 18.74 μ g/mL respectively. Moreover, an 8-fold enhancement in the bacterial activity against *S. aureus* was achieved using only 3 μ M of CTAB. Finally, both the surfactant-capped and pristine R-AgNPs have shown no cytotoxic effect against L929 mouse fibroblast at concentrations effective against all the tested above-mentioned bacteria.

Keywords: Silver nanoparticles, Antibacterial activity, Surfactant stabilization.

Graphical abstract



V.1) Introduction

Metal nanoparticles (MeNPs) have gained considerable attention among scientists in recent years, owing to their broad range of applications in medical and pharmaceutical fields, agriculture, food processing, cosmetics, environmental, and renewable energy technologies [1–3]. The MeNPs are used mainly in antimicrobial coatings, catalysis, water filtration, and sensors [4]. The beneficial activities of MeNPs depend on their physicochemical properties, therefore the preparation of stabilized MeNPs with the desired size and shape are needed to reach and retain their valuable activities. The synthesis of MeNPs has been carried out for several decades using physical or chemical methods [4–7]. However, physical methods such as laser ablation or mechanical milling require expensive equipment, whereas chemical methods such as chemical reduction and photochemical methods are cost-effective but cannot avoid the use of toxic chemicals [8,9]. In response to these drawbacks, the biological method has been developed for MeNPs preparation. This alternative approach uses microorganisms, plant extracts, and purified cellular constituents (polysaccharides, proteins, and enzymes) as eco-friendly bioreactors and capping compounds for the synthesis and stabilization of MeNPs [10–17]. The use of such natural resources aims to reduce energy consumption, production costs, and adverse environmental impacts of toxic chemicals. In

this eco-friendly method, molecules with reactive functional groups such as reducing sugars or heterocyclic compounds, and proteins of the biological systems play a key role in the reduction of metals and the capping and functionalization of synthesized nanoparticles [16,18–21]. Furthermore, plant extracts are shown to be more efficient in metal reduction than fungi and bacteria [22]. Therefore, plants are considered the most cost-effective alternative material for synthesizing small-sized MeNPs.

In view of the prospects and promises of plant-mediated nanoparticle synthesis, extracts of diverse plant species have been used for MeNPs synthesis, with a special emphasis on aromatic and medicinal plant species [23–26]. These plants are rich in several secondary metabolites, including polyphenols and alkaloids, which can act as electron donors in the reduction reaction of the metal ions [27,28]. At the present moment, Rosemary is among the most exploited medicinal plants for MeNPs synthesis. Indeed, Rosemary extract has been used for the synthesis of several MeNPs: Ag, AgS, Au, Co, Cu, Fe, Mg, Ni, NiFe, Pb, Pd, S, Zn, Zr. Among these metals, silver is well-known for its high antimicrobial activities [29].

Comparison studies on the plant-mediated synthesis of silver nanoparticles (AgNPs) have shown that Rosemary extracts display highly significant antioxidant potential, which is significantly correlated with its reducing capacity, and therefore its capacity in AgNPs synthesis [30]. Rosemary (*Salvia rosmarinus* Spenn., syn. *Rosmarinus officinalis* L.), is a well-known Mediterranean woody herb with valuable therapeutic effects and preservative properties. It possesses antioxidant, antibacterial, antifungal, antidiabetic, anticarcinogenic, anticancer, and anti-inflammatory activities [31–35]. Its beneficial properties are probably due to its richness in phenolic compounds (30 ± 1 mg/g), which include mainly Rosmarinic acid (6.9 ± 0.2 mg/g), Yunnaneic acid (5.6 ± 0.2 mg/g), and Luteolin-O-glucuronide (3.9 ± 0.1 mg/g) [36].

AgNPs showed higher antibacterial activities compared to bulk silver and are also proved to possess antifungal, anti-plasmodial, and anti-larvicidal [37–40]. Due to these properties; AgNPs find many applications in medicine, cosmetics, agriculture, and different industries. Many studies have reported Rosemary mediated AgNPs synthesis (R-AgNPs). The optimized protocols generally produce small-sized quasi-spherical R-AgNPs, with a fairly narrow size distribution. Exceptionally rod-like shapes were observed when Rosemary essential oil was used to reduce silver acetate instead of silver nitrate [12]. The R-AgNPs have shown significant antimicrobial activities and antioxidant properties [19,30,41–46]. The R-AgNPs antibacterial activity was reported to be higher than the commercialized

antibiotics such as Gentamicin [19] and efficient against many pathogenic species, even the multi-resistant strains [45,46]. Since R-AgNPs act in synergy with several antibiotics and extracts from other plants [41,47], the R-AgNPs combination with other compounds and antibiotics will reduce the prescribed antibiotics doses and the emergence of multi-resistant strains. As shown above, R-AgNPs contain remarkable activities but more importantly, the beneficial properties of R-AgNPs need to be repeatable and preserved during scale-up and storage, respectively.

Physicochemical characteristics of AgNPs are known to affect their chemical and biological activities. In practice, nanoparticles size, shape, dispersion, and stability depend on the preparation protocols. Therefore, most of the R-AgNPs studies have focused on standardizing synthesis parameters (Temperature, Incubation time, AgNO₃ concentration, and extract amounts) in order to increase the production of small-sized nanoparticles. Although the optimized protocols produce a high yield of uniformly small-sized R-AgNPs, the plant-mediated AgNPs synthesis has two main drawbacks: variability in AgNPs synthesis between plant batches and AgNPs aggregation during storage. Hadi Soltanabad *et al.*, (2018) [43] have carried out R-AgNPs synthesis using extracts from Rosemary leaves, which are sampled every month for a whole year. Even though the R-AgNPs yield fluctuates slightly over the whole year, R-AgNPs yield is significantly correlated to protein contents and total reducing capacity of rosemary extracts, on the one hand, and to total tannin and flavonoid contents, on the other [43,48]. Accordingly, the output of the reduction reaction may be predicted from the extract parameters. Nevertheless, the stability of Plant-mediated nanoparticles has not been well studied. The Plant-mediated synthesis of AgNPs produces monodispersed nanoparticles but also fast aggregating nanoparticles that accumulate during storage [49–51]. The AgNPs aggregations could be extensive as shown in *Dillenia indica*-mediated AgNPs synthesis [52]. It was reported that reaction parameters such as high concentrations of plant extract increase the aggregation of plant-mediated AgNPs [53,54]. Therefore, the AgNPs aggregations could be controlled by fine-tuning the bioprocess parameters. Optimal quantities of plant compounds create electrostatic interactions and form a negative layer on the surface of nanoparticles. These negatively charged capping molecules produce electrostatic repulsion forces providing more stable AgNPs. However, the aggregation phenomenon of AgNPs also occurs during storage reducing significantly the concentration and properties of AgNPs over time. Tripathy *et al.*, (2010) [54] have observed an increase of both aggregation and shape anisotropy (ellipsoidal, polyhedral, and capsular)

of Neem-AgNPs after 2 months in colloidal solution as evidenced by a red shift in UV-Vis result from 440 to 462 nm and TEM result. Vanaja & Annadurai (2013) [49] suggested that the secondary metabolites of plant extracts may contribute to AgNPs aggregation. Therefore, stabilizers such as surfactants are required to prevent nanoparticles instability and aggregation during long-term storage.

The stability of silver nanoparticles can be increased using two mechanisms, (i) steric repulsion using polymers and non-ionic surfactants such as Tween 80 and (ii) electrostatic repulsion using ionic surfactants such as Sodium dodecyl sulfate (SDS) and cetyltrimethylammonium chloride or bromide (CTAC, CTAB) [55]. However, only a few papers have reported the potential use of ionic surfactants as stabilizers of biogenic AgNPs. Therefore, it will be essential to further assess the role of both ionic and non-ionic surfactants on the stability of green-prepared silver nanoparticles.

This study aims to analyze the stability of R-AgNPs during storage and the effect of surfactants as additional capping agents on R-AgNPs long-term stability. As the addition of surfactants may reduce the antibacterial properties of R-AgNPs and even cause toxicity to mammalian cells, the new stabilized R-AgNPs were evaluated for their antimicrobial activity against pathogenic bacteria and their biocompatibility using mouse cell lines. To the best of our knowledge, this is the first comparative report on the impact of non-ionic and ionic surfactants on plant-mediated AgNPs long-term stability. The results of this study will improve the stabilization of nanoparticles and their potential use in different applications.

V.2) Materials and Methods

V.2.1) Materials

Fresh Rosemary (*Salvia rosmarinus* Spenn., syn. *Rosmarinus officinalis* L.) leaves were collected from the region of Marrakech (Morocco). Silver nitrate (AgNO_3) was purchased from Fluka Chemika (Switzerland). Cetrimonium bromide, sodium dodecyl sulfate, and Tween 80 were purchased from Amresco chemicals Co. (USA). EDTA, alpha MEM medium, PBS buffer, and Penicillin-Streptomycin were purchased from Sigma Aldrich (USA) Foetal bovine serum was purchased from Invitrogen (USA). All the chemicals were used as received.

V.2.2) Rosemary extract preparation

Rosemary leaves were washed with tap water and milliQ water, respectively, and then dried in darkness at room temperature until no variation of the leaf weight was observed. The extraction of 10 g dried cut leaves was carried out in 100 mL of milliQ water at 80°C for 30 min. The Rosemary leaves extract was then filtered using Whatman paper No. 1 and stored at 4°C until further use.

V.2.3) Silver nanoparticles preparation and purification

In order to prepare silver nanoparticles, 10 mL of AgNO₃ aqueous solution (10 mM) was added to 80 mL of milliQ water and heated to reach different temperatures: 25°C, 40°C, 60°C, and 80°C. Then, 10 mL of a 2-fold diluted solution of the rosemary extract was added dropwise and samples were collected regularly for the UV-Vis spectroscopy measurement.

Silver nanoparticles (R-AgNPs) were then purified by centrifugation at 9300 g for 15 min and were washed thrice with milliQ water to remove all unreacted silver ions and plant extract.

V.2.4) Silver nanoparticles characterization

UV-vis absorption spectroscopy was performed in the range of 200-800 nm using MilliQ water as blank using a Shimadzu UV-2600 spectrophotometer in order to confirm R-AgNPs synthesis and determine their theoretical Size using the Mie theory. The Mie calculations of R-AgNPs diameter were performed using the computer simulation program “MiePlot v. 3.4”. The hydrodynamic size and Zeta potential were investigated by dynamic light scattering using a Malvern ZetaSizer NanoZS instrument. Biofunctionalization of R-AgNPs was studied by Fourier Transformed InfraRed spectroscopy (FTIR) using a Thermo Scientific™ Nicolet™ iS™ 50 in attenuated total reflection (ATR) mode on a dried sample and spectra were recorded in the range of 400-4000 cm⁻¹ with a spectral resolution of 4 cm⁻¹. TGA analysis was performed using a TA analysis TGA 55 instrument in the range of 30-1000 °C. X-Ray diffraction was performed using a Rigaku smartlab device at 2θ in the range of 5-90° with a 0.02° resolution. To determine their morphology and their size, R-AgNPs were examined by transmission electron microscopy (TEM) using a Hitachi HT7800 operating at an accelerating voltage of 100Kv.

V.2.5) Stabilization of Silver nanoparticles using surfactants

The surface stabilization of silver nanoparticles was assessed using three surfactants: R-AgNPs solution was uniformly mixed with CTAB, SDS or Tween 80 (1:1, v/v), to reach a final surfactant concentration of 0.001, 0.003, 0.005, 0.007, 0.01, 0.05 and 0.1 mM. The mixture was stirred in an agitator (200 rpm) for 12 h at room temperature. UV-Vis spectroscopy was performed to assess the stability of silver nanoparticles.

V.2.6) Assessment of silver nanoparticles antibacterial activity

V.2.6.1) Bacterial strains

Four bacterial strains, Two Gram+, *Staphylococcus aureus* (ATCC 29213) and *Enterococcus faecalis* (ATCC 29212), and two Gram-, *Escherichia coli* (K12 MG1655) and *Pseudomonas aeruginosa* (PA14) were used to evaluate the antibacterial activity of silver nanoparticles. All materials were previously autoclaved at 121°C for 15 min. Bacteria were maintained at -20°C in 30% glycerol. All strains were precultured under aerobic conditions in “Brain Heart Infusion” nutritive medium (BHI, Bacto™) at 37°C and 140 rpm for 16 h. Optical density was then adjusted to 0.05, using BHI solution, at 600 nm corresponding to a bacterial concentration around $5 \cdot 10^6$ Colony Forming Units CFU. mL⁻¹

V.2.6.2) Minimum Inhibitory Concentrations (MICs) and Minimum Bactericidal Concentrations (MBCs) assay

MICs and MBCs of rosemary extract and R-AgNPs were determined using the standard broth dilution method. Two-fold serial dilutions of the prepared rosemary extracts and silver nanoparticles in the range from 300 to 0.58 µg.mL⁻¹ were performed in a 96-wells microplate. Two controls were used, a negative control without the inoculum and a positive control without silver nanoparticles or rosemary extract. MIC is defined as the lowest concentration which inhibits visible bacterial growth after 24 h (no turbidity). Then 50 µl of each well without visible bacterial growth was spread onto BHI agar plates in order to determine MBC. MBC is defined as the lowest concentration that eradicates bacteria after 24-48h.

V.2.7) Assessment of silver nanoparticles cytotoxicity

V.2.7.1) Cell culture

L929 mouse fibroblast cells (ATCC® CCL-1) were used to assess the cytotoxicity of R-AgNPs. The cells were collected and washed using PBS buffer (Sigma) and detached using trypsin 0.25%-EDTA (Sigma), then centrifuged at 300 g for 3 min and resuspended in an alpha-MEM medium (Sigma) supplemented with 10% of foetal bovine serum (Invitrogen),

1% of antibiotics Penicillin-Streptomycin (Sigma) and, 1% of L-Glutamine (Sigma). They were routinely maintained at 37°C in a 5% CO₂ humidified atmosphere.

V.2.7.2) Cytotoxicity assay

Alamar Blue[®] (AB[®] - Biorad) assay was used to assess the viability of L929 cells in contact with R-AgNPs. AB[®] is an oxidation-reduction indicator of the mitochondrial activity of viable cells. Cells were seeded at a density of 10 x 10³ cells.cm⁻² into 48 well-plates, and then R-AgNPs (pristine R-AgNPs or stabilized with surfactant) were added at a final concentration of 18.75, 37.5, or 75 µg. mL⁻¹. Untreated cells were used as a negative control while 10 % DMSO (Sigma) was used as a positive control. The plates were incubated at 37°C for 24 hours. Then, the R-AgNPs-containing culture medium was discarded and replaced by 10% (v/v) AB[®]-containing culture medium for each well and let in contact time for 2.5 hours. The plates were then read at 570 and 600 nm and the percentage of reduction of AB[®] was calculated in accordance with the manufacturer's instructions. Each experiment was performed in triplicate. Optical images of cells were also taken 24 hours after being in contact with R-AgNPs.

V.2.7.3) Statistical analysis

Statistical analysis was carried out using SPSS version 25.0 software (IBM SPSS Statistics for Windows, Armonk, NY). The statistical significance of the antibacterial activity of different R-AgNPs was evaluated using the analysis of variance (ANOVA). The data of the cytotoxicity test were compared using the Mann-Whitney Wilcoxon test. Statistical differences were considered significant at $p < 0.05$.

V.3) Results and discussion

V.3.1) Silver nanoparticles preparation using Rosemary extracts.

Silver nanoparticles were prepared in a one-pot biosynthesis using biomolecules present in rosemary leaves extract as reducing and capping agents. Fig. IV.1 represents a schematic illustration of the experimental setup followed in this study. The addition of Rosemary extract to silver nitrate solution at 80°C turned out gradually the colourless solution to yellow and then to reddish or reddish-brown (Figure IV.SI-1), indicative of the formation of R-AgNPs. The change of colour was due to the combined oscillations of electrons in silver nanoparticles that were stimulated by incident light [56]. This phenomenon, known as surface plasmon resonance (SPR), causes strong light scattering only when the frequency of incident light photons matches the natural frequency of nanoparticles surface electrons [57].

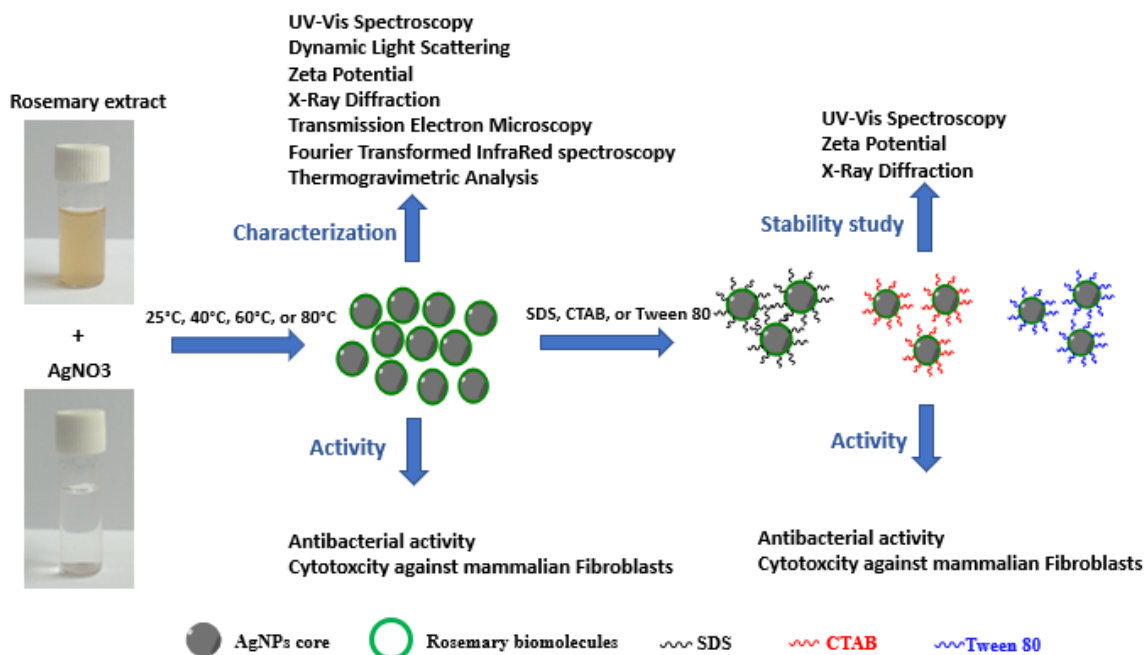


Figure IV.21: Schematic representation outlining the experimental setup used in this study

The prepared R-AgNPs were further studied using UV-Vis spectroscopy. The extinction spectra of the synthesized R-AgNPs (yellowish and reddish solutions) display an SPR band in the range between 350 nm and 550 nm with λ_{max} at 430-460nm (Figure IV.SI-2). The SPR band shape, range, and λ_{max} values are in concordance with typical spectra of spherical silver nanoparticles [58].

Interestingly, a minor resonance band of R-AgNPs was induced at 350 nm, beside the main SPR at 430 nm (Figure IV.SI-3) appeared as a weak shoulder of the main SPR band. The weak SPR might be misinterpreted as a very low small-sized AgNPs, but the 350 nm extinction band is not red-shifted enough to account for the smallest silver nanoparticles as experimentally, AgNPs as small as 5nm exhibited the main extinction band at 393 nm wavelength [59]. Moreover, the weak SPR bands are also noticed when using simulation by the Mie Theory of 35 nm spherical AgNPs (Figure IV.SI-4). Earlier studies have explained the main and weak SPR bands of AgNPs by dipole and quadrupole resonance, respectively [60]. The dipole resonance band appears as a consequence of sign reversion between the opposite sides of the spherical nanoparticles. More precisely, the dipole moment reverses signs at the same frequency as the incident light and induces the main AgNPs SPR. The weak quadrupole resonance band at 350-370 nm is characterized by two parallel dipoles of opposite sign charges, which result from energy losses that make the incident light non-uniform across the spherical nanoparticles [60]. Accordingly, the minor and main SPR bands

in R-AgNPs extinction spectra are produced in R-AgNPs extinction spectra from the same spherical nanoparticles.

V.3.2) Effect of temperature on R-AgNPs production and sizes.

The optimization of silver nanoparticles (R-AgNPs) biosynthesis using rosemary extract was performed by studying the kinetics of the synthesis at different temperatures (25°C, 40°C, 60°C, and 80°C). The R-AgNPs formation increased with time, at all tested temperatures except at 25°C. Indeed, the intensity of the SPR band increased up to 60 min at 25°C, and then it decreased with time only to increase again to about the same level at 24h analysis (Figure IV.SI-2A). As these experiments were repeated at least 3 times at different periods during the last 3 years, this discrepancy in reaction proceeding could not be the result of an experimental artefact. Similar results were found by Elemike *et al.*, (2017) [61].

In order to understand the effect of the reaction temperature on the size of R-AgNPs, UV-Vis results at a reaction time of 15 min were compared (Figure IV.2A). The SPR intensity at a reaction time of 15 min reaches an absorbance value of 0.31, 0.48, and 0.61 at 40°C, 60°C, and 80°C, respectively, whereas the R-AgNPs synthesis reaction produces only an intensity of 0.27 at 25°C after 30 min. Although the R-AgNPs formation was faster at 80°C with a maximum reached in less than 8 min, the R-AgNPs synthesis at 60°C produced slightly the highest yield (after 120 min).

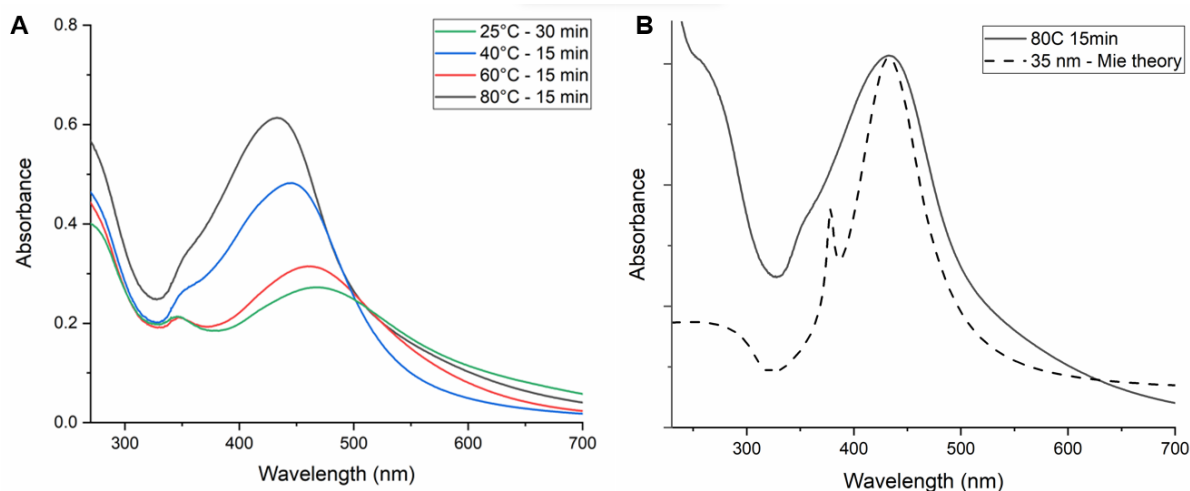


Figure IV.2: UV-Vis Extinction spectra of biosynthesized silver nanoparticles R-AgNPs and simulated 35 nm AgNPs A) UV-vis spectra of biosynthesized silver nanoparticles at different temperatures depicting blue shift in λ_{max} as the temperature is increased and B) UV-Vis spectrum of R-AgNPs prepared at 80°C and theoretical extinction curve calculated using the Mie Theory of AgNPs of 35 nm

Figure IV.2A depicts clearly the effect of temperature on R-AgNPs sizes and dispersity. Indeed, all the extinction spectra revealed a major SPR band with a different position from 468 nm at 25°C to 433 nm at 80°C. This blue shift in λ_{\max} corresponds to a decrease in the size of R-AgNPs. Indeed, from the UV-Vis spectrum of R-AgNPs, we can estimate the size of nanoparticles by comparing the experimental curve with the theoretical ones using Mie theory. Based on the Mie theory, the following size values were obtained: 47 nm at 25°C, 44 nm at 40°C, 39 nm at 60°C, and 35 nm at 80°C. Several works have studied the effect of temperature on the size of silver nanoparticles and reported a decrease in size as the temperature is increased as evidenced by a blueshift in UV-Vis spectra. This result is explained by the generation of a higher number of nuclei when the temperature is higher, and subsequently, their growth produces a large number of small-sized nanoparticles [62–64].

Furthermore, with the increase in temperature a narrower band was observed which indicates a lower R-AgNPs polydispersity. The broadening and redshift are attributed to agglomeration or an increase in the size of the particles.

The fastest R-AgNPs preparation that produced the less broad SPR band used the following conditions: reaction temperature of 80°C, reaction time of 15 min, and 20-fold dilution of Rosemary extract. These optimized conditions were therefore chosen for all subsequent experiments.

V.3.3) Determination of R-AgNPs size using direct measures and approximations

Table IV.1: The size of R-AgNPs prepared at 80°C for 15 min determined using different techniques.

Technique	Size (nm)
UV-Vis spectroscopy	35
TEM analysis	31.1±6.5
DLS	9
XRD	9.5

The R-AgNPs size synthesized at 80°C was determined directly from TEM images and DLS analysis or using either Mie scattering theory or Scherrer formula, results are summarized in Table IV.1. Figure IV.2B shows the best fit between the UV-Vis curve and the theoretical extinction curve based on Mie calculations of nanoparticles with an approximate size of 35

nm using a 20% standard deviation. The slight difference between the predicted and the experimental data could be explained by the difference in polydispersity of the real sample and the polydispersity of the approximation fixed at 20%.

From TEM images of nanoparticles (Figure IV.3A) the average size of the synthesized R-AgNPs at 80°C was 31.1±6.5 nm as calculated using the size distribution histogram (Figure IV.3B). The calculation of the R-AgNPs average size from TEM images ignored the large population of small-sized nanoparticles. The R-AgNPs size from TEM images correlates with those calculated using Mie Theory. Although TEM images provide a direct estimation of the projected area diameter of the nanoparticles, the size measurement does not take into account the organic coating layer due to its poor contrast [65]. Therefore, the R-AgNPs average size is underestimated because the coating layer is generally missing in TEM images.

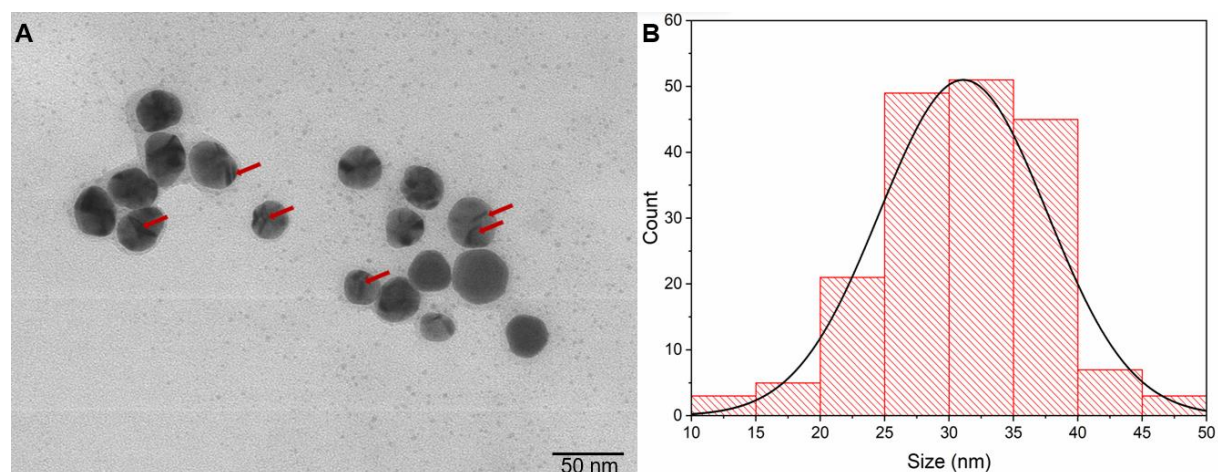


Figure IV.3: A) TEM Image of R-AgNPs and B) The size distribution (nm) of R-AgNPs prepared at 80°C determined using TEM

Then DLS analysis was carried out to measure the hydrodynamic diameter of the spherical AgNPs, including the silver core and the molecules tightly adsorbed to the surface such as capping agents and solvent layers [65,66]. The DLS analysis of R-AgNPs has shown a large population of small-sized nanoparticles (>99%) with a size of 9 nm.

Furthermore, R-AgNPs size was also determined using the XRD spectrum and applying the following Scherrer's formula:

$$D = \frac{k\lambda}{\beta \cos \theta} \quad \text{eq (1)}$$

Where D is the crystallite size, K is the Scherrer constant, λ is the X-ray wavelength, β is the full width at half maximum of each diffraction peak and θ is the Bragg diffraction angle. The

K factor depends on the crystallite shape, crystallite size distribution, and the definition of the FWHM [67]. The R-AgNPs size is calculated on the basis of the (111) peak in the XRD pattern, and K value of 0.94 for FWHM of spherical crystals with cubic symmetry [68,69]. From XRD pattern of R-AgNPs (Figure IV.4), the crystallite size was approximately equal to 9.5 nm, which is in agreement with the hydrodynamic values obtained by DLS.

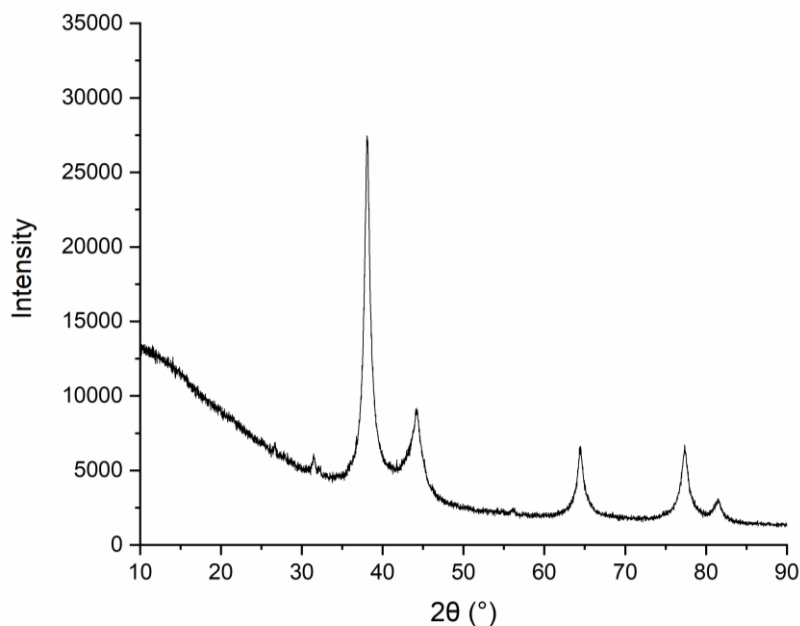


Figure IV.4: XRD spectrum of biosynthesized silver nanoparticles at 80°C for 15min

X-ray diffraction was also used in the range of 5-90° at 2θ in order to assess the crystallinity nature of the prepared R-AgNPs. The XRD pattern of lyophilized AgNPs depicts 5 peaks at 38.19°, 44.37°, 64.56°, 77.47°, and 81.46° corresponding to the (111), (200), (220), (311), and (222) crystallographic planes, respectively. These data indicate a face-centered cubic (fcc) structure of metallic silver confirming the crystalline nature of the prepared R-AgNPs [70,71].

The size of R-AgNPs was determined using different techniques that gave different values. These differences could be due to multiple factors, The Mie calculations of R-AgNPs diameter and the hydrodynamic approximation assume that the nanoparticles are spherical. Additionally, these calculated sizes will be approximate to the theoretical ones if only the nanoparticles were fully crystalline (crystalline size) and monodisperse in an ideal viscous medium (hydrodynamic size and Mie calculations). Therefore, any deviation from such assumptions will lead to discrepancies in the calculated sizes, as determined in this study. Since TEM reproduced only the core R-AgNPs, the real size of R-AgNPs had to be higher

than the average size of 31.1 ± 6.5 nm as determined from R-AgNPs TEM images. Only the Mie calculations of silver nanoparticles with 35 nm achieved the best fit to the expected R-AgNPs size. One may ask why the Nanoparticles with hydrodynamic or crystalline size were missing in TEM images. Firstly, nanoparticles with hydrodynamic of 9 nm will appear smaller than 9 nm in TEM images because the capping molecules will be missing in TEM images. If we suppose that two spherical nanoparticles with sizes of 9.5 and 31.1 nm have proportionally the same composition, the 9.5 nm nanoparticles will come out 11 times less dense than the 31.1 nm ones. Consequently, these small-sized nanoparticles might not appear in TEM images if the apparatus is not sensitive enough to detect them. Secondly, if nanoparticles with hydrodynamic of 9 nm may contain mainly organic components or may not be silver ones, they will not be revealed in TEM images. But, the crystalline size revealed the presence of 9 nm silver nanoparticles. This latter data could be explained by partly crystalline R-AgNPs samples. It is known that Scherrer's formula calculates a crystal size different from the primary particle size in the partly crystalline samples due to the amorphous fraction [72]. Interestingly, the R-AgNPs contain some dense spots or lines, as indicated by arrows in TEM images (Figure IV.3A). These observations might be explained by the capping of nanoparticles at the same time as silver reduction (one-pot nanoparticles synthesis), therefore the growth of nanoparticles will be mainly limited to small nuclei and mixed with organic extracts. We suppose that the spherical R-AgNPs contain mainly a homogenous blend of organic compounds from Rosemary extract and silver nuclei, with limited small-sized silver nanoparticles in some heterogeneous R-AgNPs.

V.3.4) Silver nanoparticles-Rosemary extract interaction and characterization

In order to identify the nature of rosemary molecules involved in the silver nanoparticles capping, FTIR analysis was carried out. Figure IV.5 shows the FTIR spectra of freeze-dried rosemary leaf extract and the prepared R-AgNPs at 80°C. The FTIR spectrum of purified R-AgNPs showed similar bands to the rosemary leaf extract spectrum which are associated with functional groups such as esters C-O stretching (1165 cm^{-1}), Alkane C-H bending (1381 & 1453 cm^{-1}), and Alkane C-H stretching (2839 , 2914 & 2949 cm^{-1}) respectively [73] suggesting that only molecules with those groups were implicated in the capping of silver nanoparticles. It is worth mentioning that other functional groups that are absent in the spectrum of lyophilized R-AgNPs but present in the leaf extract spectrum (O-H and N-H) could be responsible only for the reduction of Ag^+ to Ag^0 [43,74].

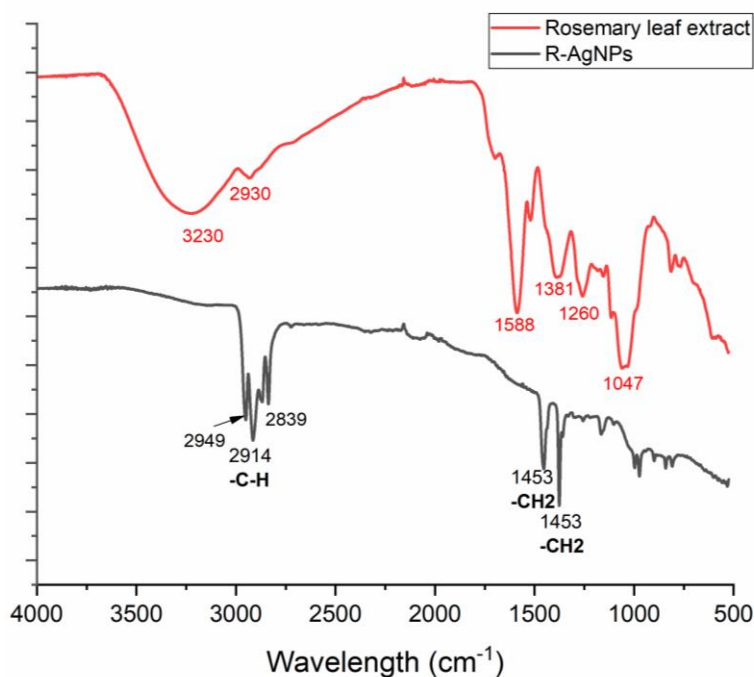


Figure IV.5: FTIR spectra of Rosemary leaf Extract and Biosynthesized silver nanoparticles at 80°C for 15 min.

To determine the weight proportion of biomolecules stabilizing the prepared R-AgNPs, thermogravimetric analysis was carried out in the range of 30-1000°C. The TGA results (Figure IV.SI-5) show 3 phases of weight loss. The first loss before 100°C corresponds to water residue, and a second of around 40% before 400°C. The weight loss continued at a slower rate to reach approximately 50% at 1000°C. This weight loss profile is also found by other studies on the plant-mediated AgNPs synthesis which was attributed to the multitude of bioorganic molecules coating AgNPs [75]. Indeed, this result is also supported by FTIR results discussed above.

V.3.5) Stabilization of silver nanoparticles using surfactants

As discussed in the introduction, the stability of AgNPs is of primordial importance in order to maintain the expected properties. First, the stability of R-AgNPs was tested in deionized water at 25°C for 78 days as depicted with the black line (*i.e.*, Control) in Figure IV.6. After 7 days, a slight decrease of their absorbance was observed with a slight red-shift of the SPR position, which indicates an increase in R-AgNPs size or aggregation. But after 28 days, a high decrease in their absorbance by about 40% was observed. These variations in the intensity of the SPR band at λ_{max} show decreases in the quantity of silver nanoparticles, which clearly implies R-AgNPs instability during storage at room temperature suggesting that even in the presence of rosemary extract, the R-AgNPs are not stable over time.

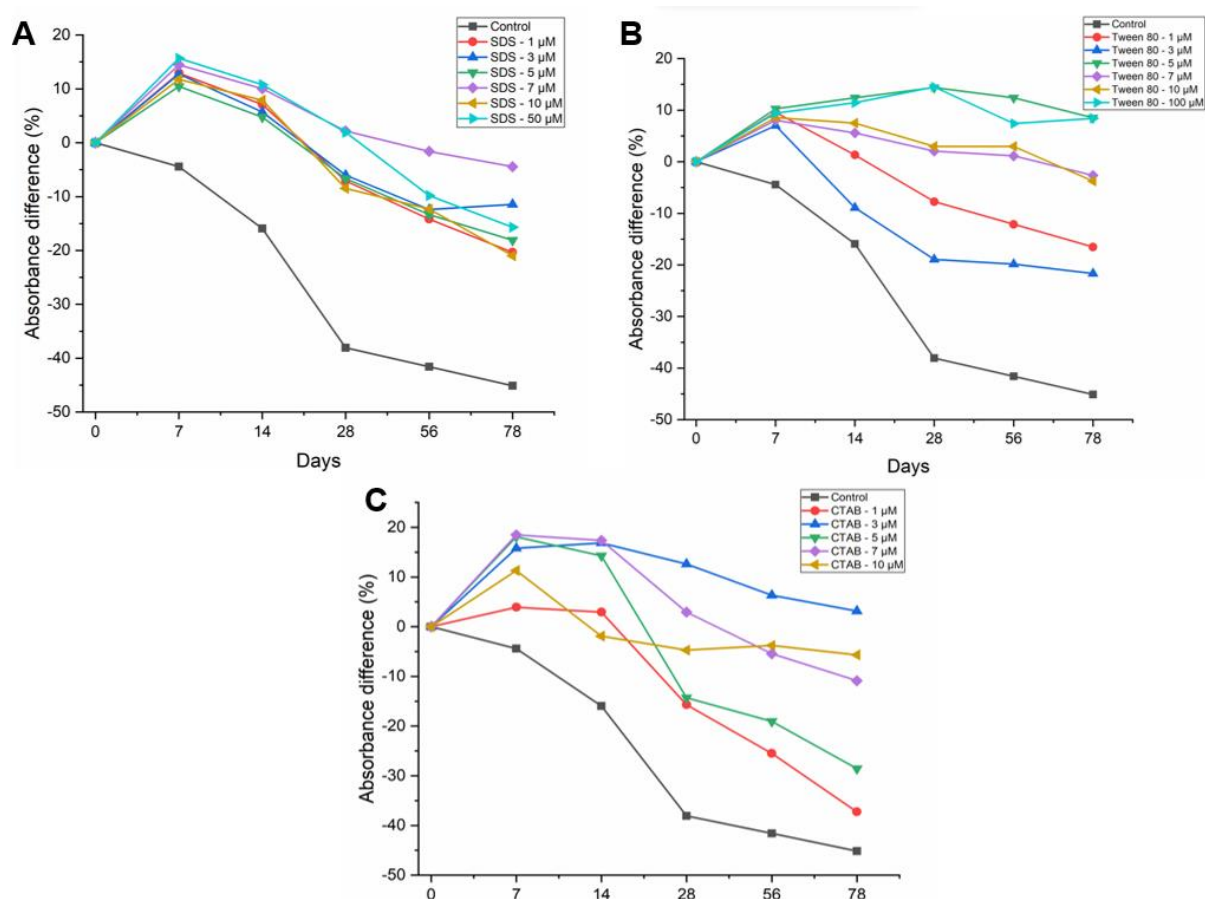


Figure IV.6: The absorbance difference at λ_{max} (%) of non-stabilized and surfactant stabilized silver nanoparticles in function of days. A: SDS stabilized R-AgNPs, B: Tween 80 stabilized R-AgNPs, and C: CTAB stabilized R-AgNPs. The non-stabilized group is depicted in all figures as control (Black line)

In this study, three surfactants differing in their charge were used to assess their potential role in enhancing the stability of silver nanoparticles: Tween 80, a non-ionic surfactant, Sodium dodecyl sulfate (SDS), an anionic surfactant, and cetyltrimethylammonium chloride (CTAB) a cationic surfactant. The evolution of R-AgNPs stability over time was monitored using UV-Vis spectroscopy (Figure IV.6A, B, and C). Figure IV.6 showed the results of the difference in absorbance at λ_{max} compared to day 0 in function of time at different concentrations of surfactants.

In the presence of surfactant, for the first 7 days, the absorbance level was not only maintained but also increased which could be due to an immediate effect of surfactant on the dispersion of R-AgNPs. Another possibility is a continuous AgNPs synthesis in the presence of surfactants. Indeed, Liz-Marazan et Lado Tourino (1996) [76] have reported the preparation of AgNPs using surfactants. Interestingly, a mixture of silver nitrate and Tween 80, SDS, or CTAB with the same ratios as in our stabilization experiment, did not induce AgNPs synthesis (data not shown), suggesting a complementary role of rosemary extract

and surfactants in the synthesis and stabilization of R-AgNPs respectively. In the case of SDS, an anionic surfactant, the absorbance peaks increased to day 7 and then decreased continuously and slightly over time for all tested concentrations. However, at a concentration of 7 μM , after 78 days, the absorbance peak decreased only by 4.4% showing much higher stability than the control (-45.13%).

Similarly, Tween 80 at the various tested concentration have induced a substantial increase in stability over time, especially for very low concentration such as 5 and 7 μM for which the absorbance difference has increased to 8% and decreased to only 2.6% respectively compared to the drop of 45.13% for the control after 78 days. Moreover, at a concentration as low as 7 μM , the Zeta potential dropped from -34.45 to -26.26 mV confirming the adsorption of non-ionic Tween 80 molecules onto the surface of silver nanoparticles.

On the other hand, using CTAB, a cationic surfactant, a higher increase in absorbance difference was noticed on day 7 and maintained until day 14. Then a slight decrease over time was observed. However, even after 78 days, all tested concentrations remained significantly more stable than the control. Moreover, a blue shift of λ_{max} was also noticed (423 to 414 nm after 78 days), suggesting a substantial decrease in R-AgNPs mean size. The Same as SDS and Tween 80, the best enhancement in stability was obtained with very low concentration (3 to 7 μM). Moreover, an increase of Zeta potential from -34.45 to -9.15 mV was noticed evidencing partial CTAB adsorption onto the surface of AgNPs.

Interestingly, testing higher concentrations for all the surfactants (data not shown) resulted in an apparent aggregation of R-AgNPs which could be due to the increase of the interaction between surfactant-capped R-AgNPs when the surfactant concentration used is high. Indeed, in a study by Kurrey *et al.*, (2019) [77], silver nanoparticles were used as a colorimetric probe for the detection of quaternary ammonium surfactants, including CTAB. The result showed that quaternary ammonium surfactants induced AgNPs aggregation, which was attributed to the increase of hydrophobic and electrostatic interactions between the surfactants and the molecules capping AgNPs. This could explain the aggregation behavior of R-AgNPs at higher surfactant concentrations and also the decrease in stabilization efficiency above a certain concentration.

The measurements of stability were continued up until 198 days. As shown in Figure IV.7, the stability of non-stabilized R-AgNPs as well as their surfactant-stabilized counterparts continued to drop over time at different rates. After 198 days, the absorbance of the control

(non-stabilized R-AgNPs) dropped by 84.07% while the stabilized R-AgNPs showed a relatively greater stability as 3 μ M CTAB R-AgNPs dropped by 41.05%, 5 μ M Tween 80 R-AgNPs dropped by 41.34% and 7 μ M SDS R-AgNPs dropped by 37.55%.

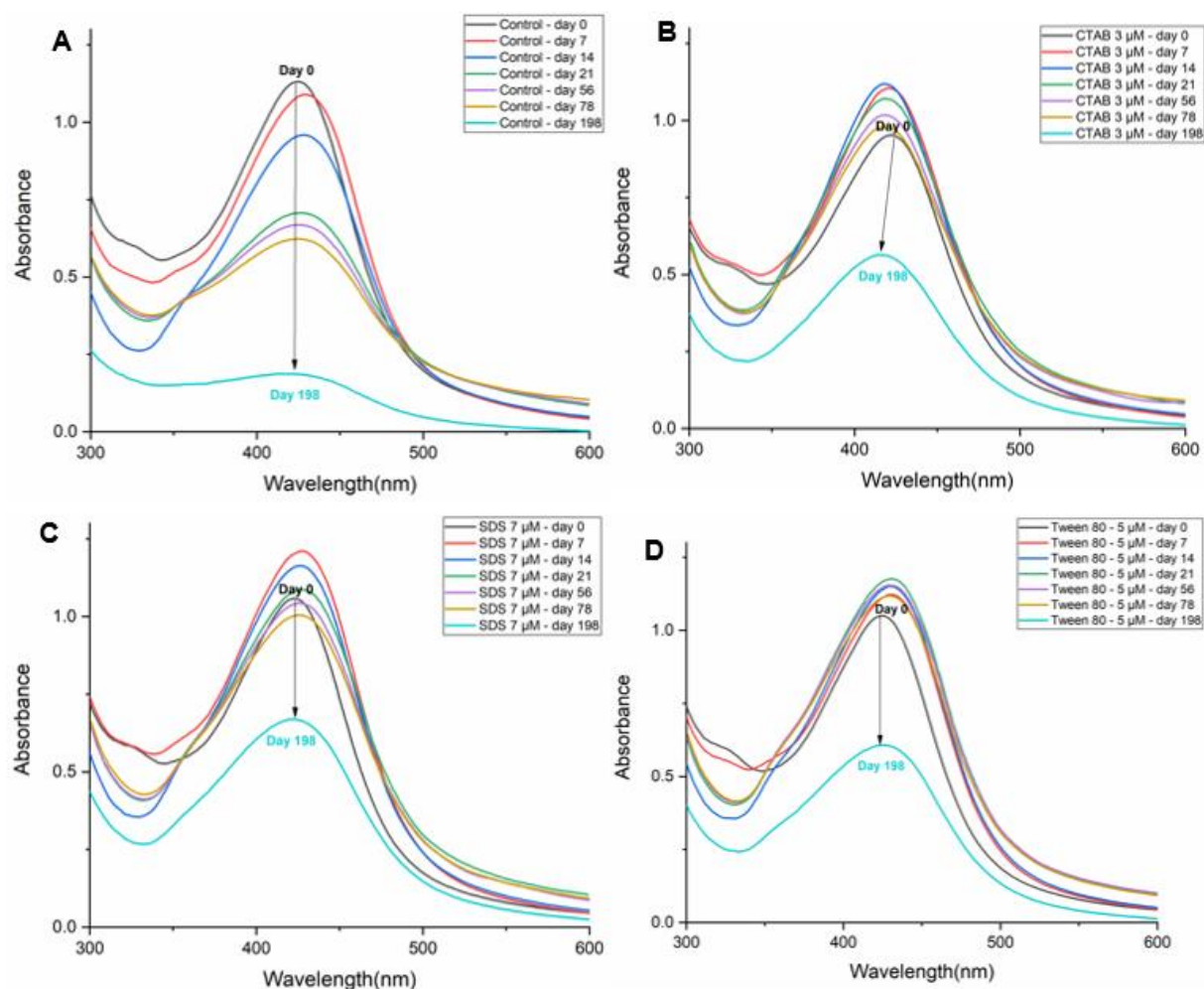


Figure IV.7: UV-Vis spectra of A: pristine R-AgNPs (Control), B: 3 μ M CTAB R-AgNPs, C: 7 μ M SDS R-AgNPs and, D: 5 μ M Tween 80 R-AgNPs over time

The three tested surfactants showed similar results with a slightly better stabilization using SDS. The stabilization of silver nanoparticles could be achieved either sterically, electrostatically or both (Electrosterically) [78]. In the case of ionic surfactants (SDS and CTAB), both mechanisms could be involved especially for molecules with relatively higher molecular weight. However, for CTAB, it is more likely that the enhancement of stabilization was rather the result of a steric repulsion because Zeta potential values were decreased. While in the case of non-ionic surfactants (Tween 80), the stabilization could only be achieved by steric repulsion. The fact that the best enhancement results were obtained by SDS, the anionic surfactant, emphasizes the role of surface charge on the stability of AgNPs given that SDS has the lowest molecular weight among the three tested

surfactants. Thus, in this study, we shed the light on the instability of biosynthesized AgNPs and proved that a post-synthesis, long-term stabilization of silver nanoparticles could be achieved with very low concentrations of surfactants ($\approx 3\text{-}7\mu\text{M}$) and that negatively-charged and relatively bigger molecules favor a high stabilization of negatively-charged AgNPs.

The effect of $7\mu\text{M}$ surfactant capping on the crystalline structure of R-AgNPs was studied using XRD. As shown in Figure IV.SI-6, All R-AgNPs, whether surfactants-capped or not showed 5 peaks corresponding to the (111), (200), (220), (311), and (222) crystallographic planes indicating a face-centered cubic (fcc) structure of metallic silver [70]. Moreover, the crystallite size ($D_{\text{W-H}}$) and microstrain ε were calculated using the Williamson-Hall (W-H) method using the following equation [79].

$$\beta \cos\theta = \frac{K\lambda}{D} + 4 \varepsilon \sin\theta \quad \text{eq. (2)}$$

Where D is the crystallite size, K is the Scherrer constant, λ is the X-ray wavelength, β is the full width at half maximum of each diffraction peak, θ is the Bragg diffraction angle, and ε is the microstrain. Thus, by plotting $\beta \cos\theta$ against $4 \sin\theta$ we could calculate the crystallite size $D_{\text{W-H}}$ from the intercept of the linear fit of W-H plot and the microstrain ε from its slope. Results are shown in Figure IV.SI-7 in table IV.SI-1. Moreover, the lattice constant (a) values were found to be 4.089, 4.089, 4.080, and 4.069 Å for R-AgNPs, CTAB-capped R-AgNPs, Tween 80-capped R-AgNPs, and SDS-capped R-AgNPs, respectively, which is consistent with the value reported in the JCPDS Card No. 04-0783 [80]. These results indicate that none of the 3 surfactants used in this study has induced changes in the crystalline structure of pristine R-AgNPs.

V.3.6) Evaluation of the antibacterial activity of silver nanoparticles

The biosynthesized R-AgNPs antibacterial activity was studied against four pathogenic bacterial species, two Gram-negative (*E. coli* and *P. aeruginosa*) and two Gram-positive (*S. aureus* and *E. faecalis*). These bacteria are of great interest in the medical and food packaging fields due to their pathogenicity and ability to cause food spoilage and food poisoning [81,82]. First, the antibacterial activity of biosynthesized R-AgNPs without surfactant capping was evaluated by MIC and MBC measurements through the microdilution method and compared to commercial silver nanoparticles (size = 50-60 nm) (Table IV.2).

Table IV.2: MICs and MBCs results of biosynthesized silver nanoparticles at 80°C for 15 min (size using TEM = 31nm) and commercial nanoparticles (size = 50-60nm)

Bacterial species	MICs ($\mu\text{g.mL}^{-1}$)	MBCs ($\mu\text{g.mL}^{-1}$)	MICs ($\mu\text{g.mL}^{-1}$)
	R-AgNPs	R-AgNPs	Commercial AgNPs
<i>S. aureus</i>	75	150	150
<i>E. faecalis</i>	18.75	75	75
<i>E. coli</i>	37.5	150	150
<i>P. aeruginosa</i>	37.5	150	300

Biosynthesized R-AgNPs exhibited good antibacterial activity against all tested bacteria ($\text{CMI} < 75 \mu\text{g.mL}^{-1}$) and a much higher activity compared to the commercial AgNPs (Table IV.1). This difference could be mainly attributed to the much smaller size of the prepared nanoparticles (31 nm) compared to the commercial ones (50-60nm). Indeed, many studies have reported a size-dependent antibacterial activity of AgNPs, owing to the higher surface area of small nanoparticles compared to bigger ones [83,84].

The obtained results show no correlation between the antibacterial activity of R-AgNPs and the Gram classification. Other studies have observed higher antibacterial activity of silver nanoparticles against Gram-negative bacteria than Gram-positive, but many of them have realized their study against only two bacteria: *E. coli* and *S. aureus* [85–87]. The antibacterial activity of R-AgNPs may be due to either the release of silver ions or the direct interaction between silver nanoparticles and bacteria which cause cell membrane disruption, DNA damage and sulphur and phosphorous-containing compounds damages via free radical generations [88,89]. Furthermore, in our case, biomolecules on the surface of silver nanoparticles could enhance AgNPs antibacterial activity. Indeed, many studies have used biofunctionalization to increase the antibacterial activity of AgNPs [55].

Figure IV.8 shows the effect of surfactant stabilization of silver nanoparticles on their antibacterial activity against two bacteria, *E. coli* and *S. aureus*. Three surfactant concentrations were chosen, 3, 5, and 7 μM based on their stabilization potency, and the experiment was performed using a concentration of 37.5 mg. L^{-1} of either surfactant capped or pristine R-AgNPs which corresponds to MIC value in the case of *E. coli* for pristine R-AgNPs. Compared to the pristine R-AgNPs, none of the surfactants-capped R-AgNPs showed any significant improvement in the antibacterial activity against *E. coli*. On the

contrary, in the case of SDS, a slight decrease in the antibacterial activity was noticed that could be due to the delayed release of silver ions from silver nanoparticles as evidenced by the increase of R-AgNPs stability. The non-improvement of antibacterial activity by CTAB and Tween 80 could be due to the very low concentrations used for R-AgNPs stabilization. Indeed, the reported MIC of CTAB, while it varies significantly, it is much higher than the used concentration. Sun *et al.*, (2019) [90] have evaluated the MIC of CTAB on 510 isolates of *E. coli*. The smallest reported MIC value is 87 nM of CTAB against one *E. coli* isolate, while for most isolates (405 isolates), the MIC of CTAB was 256 mg. L⁻¹ (702 μM). Similar results were reported by Kvitek *et al.*, (2008) [55] where Tween 80 and SDS stabilized silver nanoparticles were tested against *E. coli* and no enhancement of bacterial activity was observed.

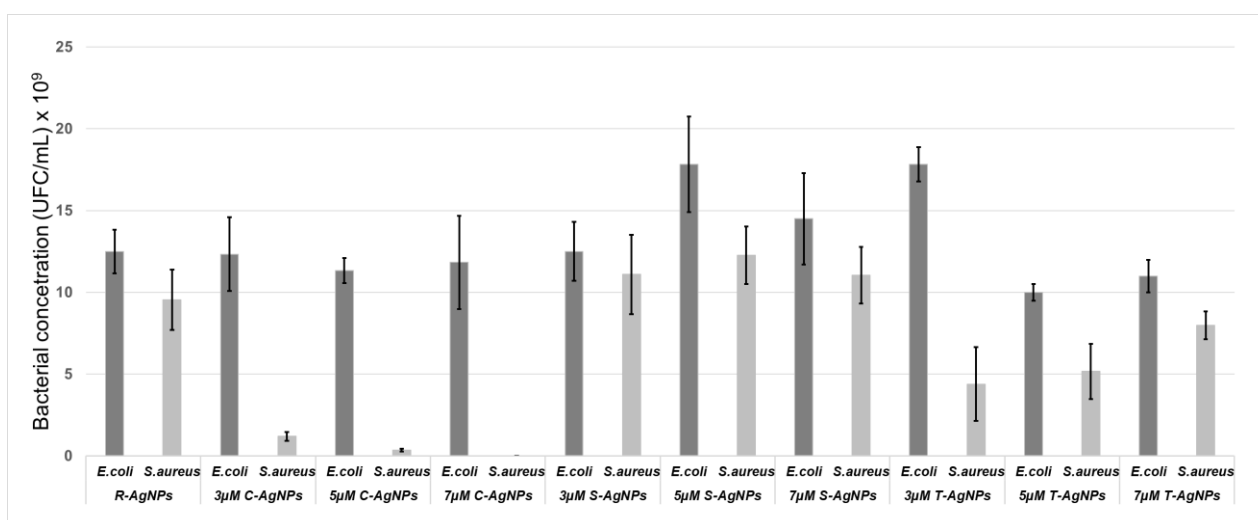


Figure IV.8: The effect of surfactant capping on the antibacterial activity of R-AgNPs against *E. coli* (dark grey) and *S. aureus* (light grey). C-AgNPs: CTAB-capped R-AgNPs, S-AgNPs: SDS-capped R-AgNPs, and T-AgNPs: Tween 80- capped R-AgNPs.

As for *S. aureus*, CTAB-stabilized AgNPs have shown a remarkable increase in the antibacterial activity with all the tested concentrations (an 8-fold increase in antibacterial activity using only 3 μM CTAB-capped AgNPs), while SDS-capped silver nanoparticles haven't shown any effect. Similar results were found by Jang *et al.*, (2015) [91] against multiple strains of *S. aureus* where the MIC of AgNPs passed from (>125 mg. mL⁻¹) to 32mg. mL⁻¹ while the MIC of SDS-capped AgNPs remained unchanged compared to the pristine AgNPs. However, they have used much higher concentrations of surfactants in order to stabilize their AgNPs (0.125 and 0.25 mM for CTAB and SDS, respectively). The enhancement of the antibacterial activity using CTAB could be due to numerous factors. As proven by Zeta potential results, the surface charge of CTAB-capped R-AgNPs shifted to

more positive values which could increase their interaction with the negatively charged bacteria. Also, the decrease in size of CTAB-capped R-AgNPs as evidenced by the blue shift in UV-Vis spectroscopy could be a contributor to the enhanced activity. However, the magnitude of the enhancement is more likely to be induced synergistically by the intrinsic antibacterial activity of the CTAB and R-AgNPs. The difference between *E. coli* and *S. aureus* is probably due to the higher antibacterial activity of quaternary ammonium compounds such as CTAB against Gram-positive bacteria (*S. aureus*) compared to Gram-negative bacteria (*E. coli*) [92]. To the best of our knowledge, this is the first study reporting the enhancement of the antibacterial activity of silver nanoparticles using such low amounts of stabilizing CTAB ($\approx 3\text{-}7\mu\text{M}$).

V.3.7) Cytotoxicity of pristine and surfactants-capped R-AgNPs

Figure IV.9 shows the Alamar Blue[®] assay for L929 cells in contact with three concentrations of either surfactant-capped or pristine silver nanoparticles, corresponding to the MIC values of the tested bacteria reported above *i.e.*, 18.75, 27.5, or 75 $\mu\text{g. mL}^{-1}$. Based on the direct contact cytotoxicity test of the standard ISO 10993-5:2009 [93], the results show that none of the tested samples exhibited any cytotoxic effect upon L929 cells for each tested concentration as cell viability was $>70\%$. Interestingly, the pristine R-AgNPs rather showed a proliferative activity while the chemically-prepared AgNPs exerted a dose-dependent slight cytotoxicity even though their size is higher. Moreover, none of the surfactant-capped AgNPs showed any cytotoxic effect even with the higher concentration (75 $\mu\text{g. mL}^{-1}$). Figure IV.SI-8 shows L929 cells under an optical microscope after contacting AgNPs for 24 hours. These results indicate that the prepared R-AgNPs are safe for usage in applications where they could be exposed to human cells at concentrations that were demonstrated to be effective against bacteria.

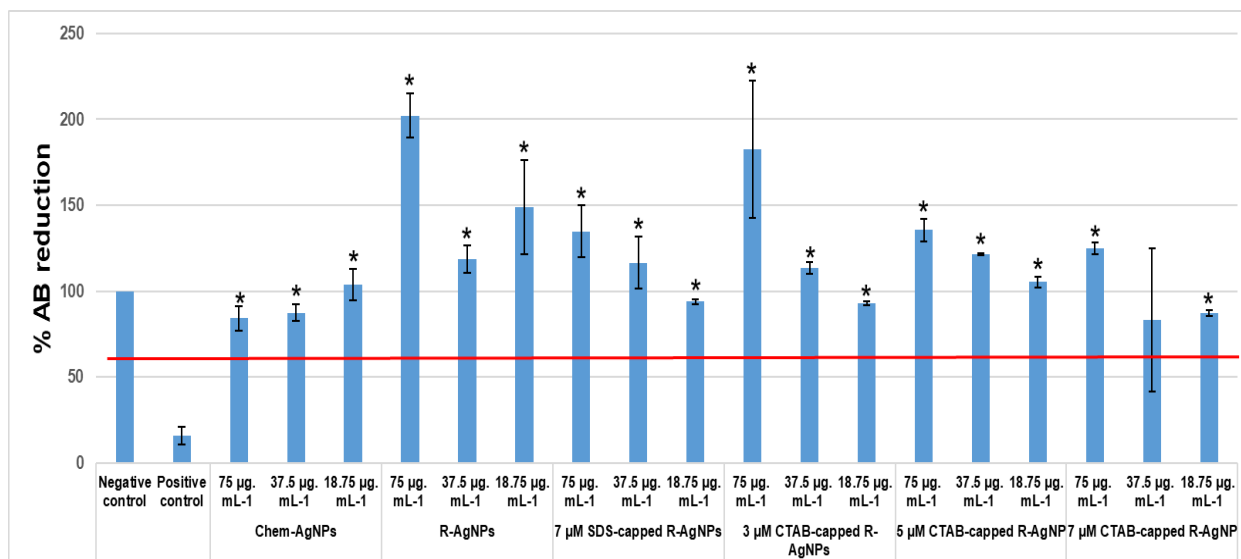


Figure IV.9: The effect of surfactant capping on the cytotoxic of AgNPs in contact with L929 fibroblasts for 24 hours. The horizontal red line corresponds to the threshold of cell viability set at 70%. Results are presented as mean \pm SD. * correspond to $p < 0.05$ compared to cytotoxicity positive control.

V.4) Conclusion

In conclusion, around 32 nm sized silver nanoparticles were successfully prepared using rosemary leaves extract as a green approach, these R-AgNPs were characterized using various techniques such as UV-Vis spectroscopy, DLS, FTIR, XRD, TEM, and TGA. The prepared R-AgNPs were tested and found effective against four pathogenic bacterial strains, two Gram-negative (*E.coli* and *P.aeruginosa*) and two Gram-positive (*S.aureus* and *E.faecalis*). The stability of AgNPs was assessed over time and improved substantially by the use of three surfactants, the anionic surfactant SDS, the cationic surfactant CTAB and the non-ionic surfactant Tween 80 at very low concentrations $\approx 3-7\mu\text{M}$. The use of CTAB to stabilize R-AgNPs has also enhanced remarkably the bacterial activity against *S. aureus*. The cytotoxicity against L929 mouse fibroblast was also assessed and none of the prepared R-AgNPs, either surfactant-capped or not have shown any significant cytotoxic effect against mammalian cells.

Acknowledgment

This project was financially supported by French-Morocco bilateral programs by CAMPUS FRANCE: PHC TOUBKAL/18/71 and APUR 2019.

This work was also performed with the support of the Erasmus+ programme of the European Union (Mobility at the university of Zagreb (HRZAGREB01) and Moroccan CNRST grant (Projet prioritaire PPR1/2015/73).

Conflict of interest

The authors declare no conflict of interest.

CRedit authorship contribution statement

A.Nabgui: Conceptualization, Methodology, Validation, Investigation, Writing – original draft, **A. Brik:** Investigation. **K. Agayr:** Investigation. **G. Gouhier:** supervision. **R. Beniazza:** Resources, **E. Vidović:** Resources, **J. El Haskouri:** Resources, Investigation, **B. Labat:** Resources, Investigation. **M. Lahcini:** Conceptualization, Resources, Writing - Review & Editing, Supervision, Funding acquisition **P. Thébault:** Conceptualization, Resources, Writing - Review & Editing, Supervision, Funding acquisition **A. El Meziane:** Conceptualization, Resources, Writing - Review & Editing, Supervision, Funding acquisition.

V.5) Supporting information

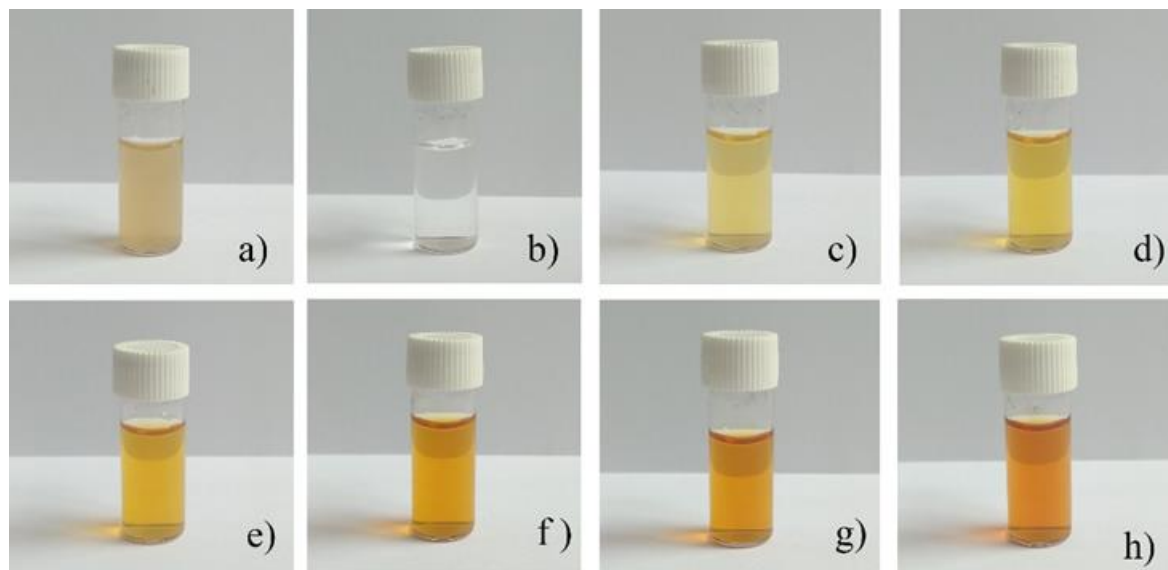


Figure IV.SI-1 : a) Rosemary leaves extract, b) 2 mM Silver nitrate , c-h) R-AgNPs prepared at 80°C at different reaction time c: 0.5 min, d: 1 min, e: 3 min, f: 5 min, g: 7 min, h: 9 min.

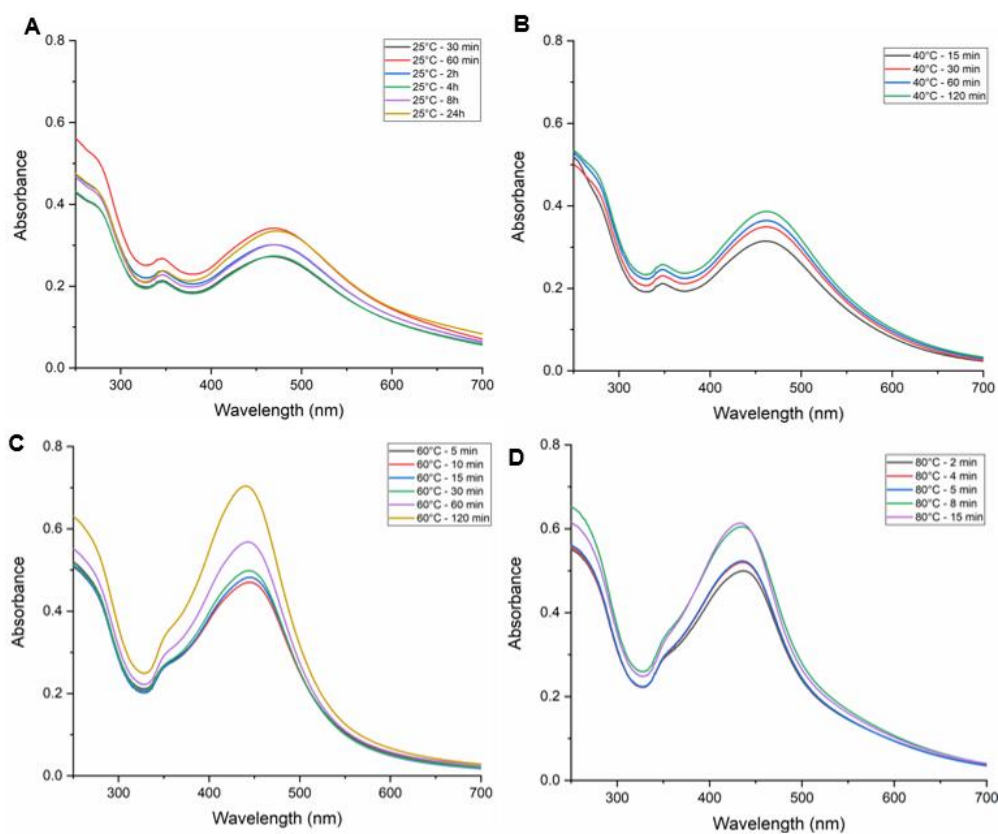


Figure IV.SI-2: UV-vis spectra of biosynthesized silver nanoparticles at, A: 25°C, B: 40°C, C: 60°C and D: 80°C.

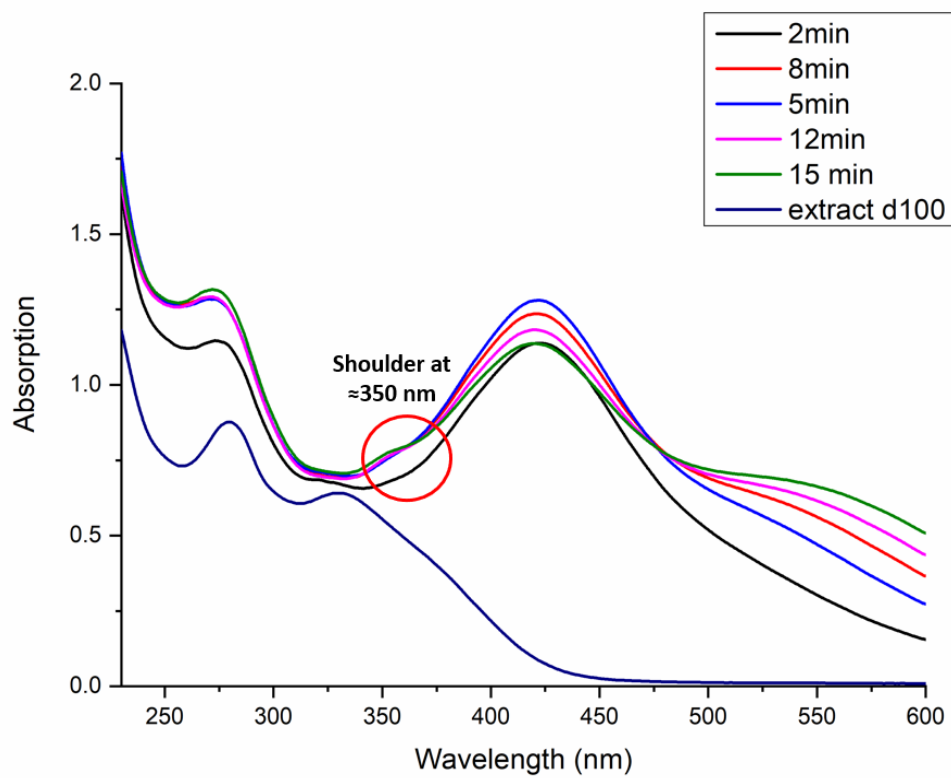


Figure IV.SI-3: UV-Vis spectra of R-AgNPs prepared at 80°C for different times.

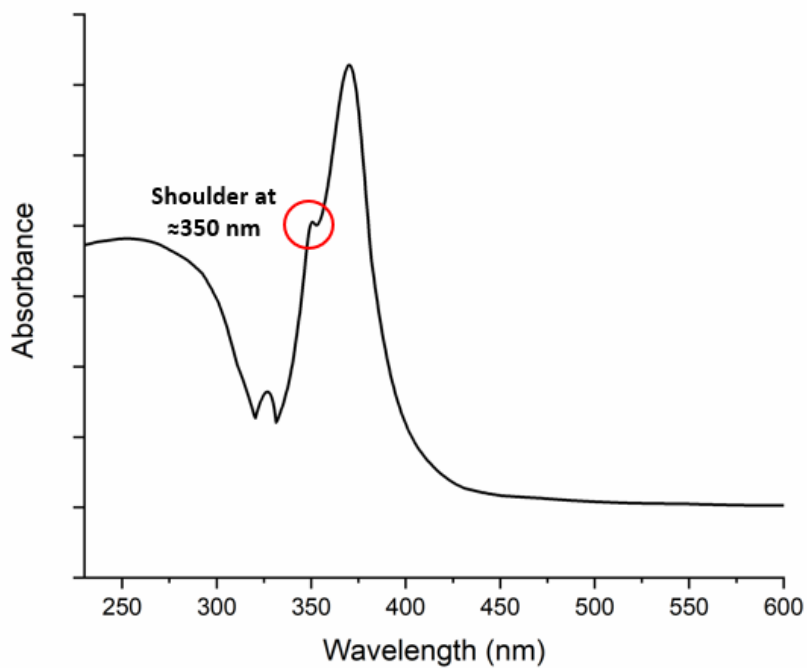


Figure IV.SI-4: Theoretical calculation of absorption spectrum of spherical AgNPs of theoretical size of 35 nm using the Mie theory.

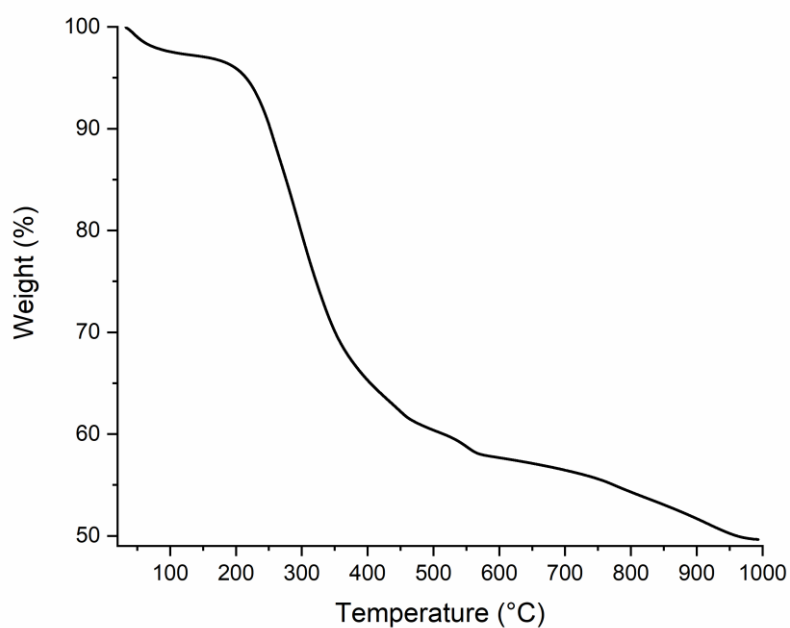


Figure IV.SI-5: Thermogravimetric analysis (TGA) profile of R-AgNPs prepared at 80°C.

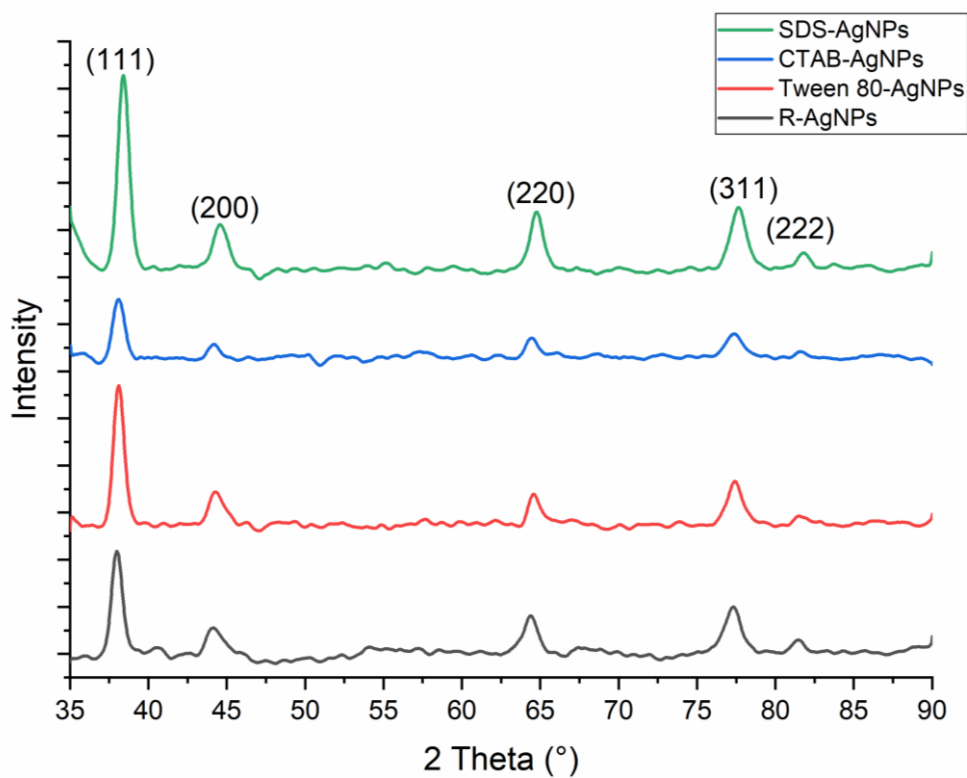


Figure IV.SI-6: XRD Spectra of biosynthesized silver nanoparticles at 80°C for 15min before (R-AgNPs) and after surfactants capping

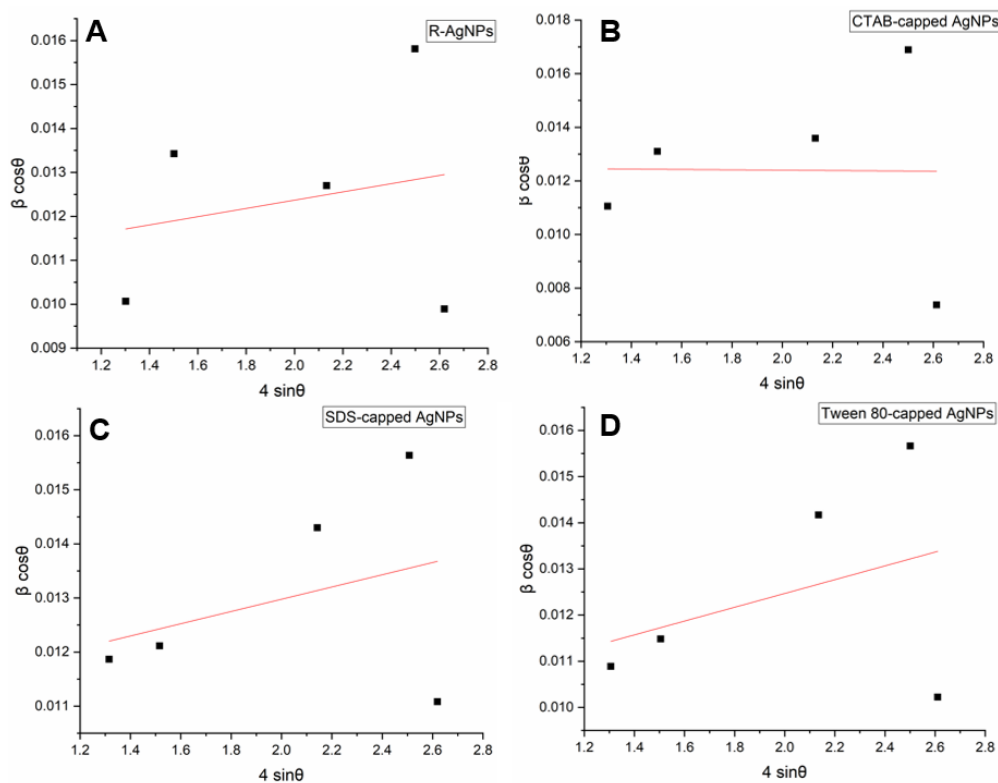


Figure IV.SI-7: Williamson-Hall plot of A) Pristine R-AgNPs, B: 7 μM CTAB R-AgNPs, C: 7 μM SDS R-AgNPs and, D: 7 μM Tween 80 R-AgNPs

Table IV.SI-1: Crystallite size (D), Microstrain (ϵ) obtained from Williamson-Hall plot, and Lattice constant (a) of Pristine and capped R-AgNPs

	Crystallite size D (nm)	Microstrain ϵ (10^{-3})	Lattice constant a (\AA)
Pristine R-AgNPs	13.8	0.93	4.0890
CTAB-capped AgNPs	12.1	0.65	4.0891
SDS-capped AgNPs	13.5	1.13	4.0690
Tween 80-capped AgNPs	15.3	1.4	4.0805

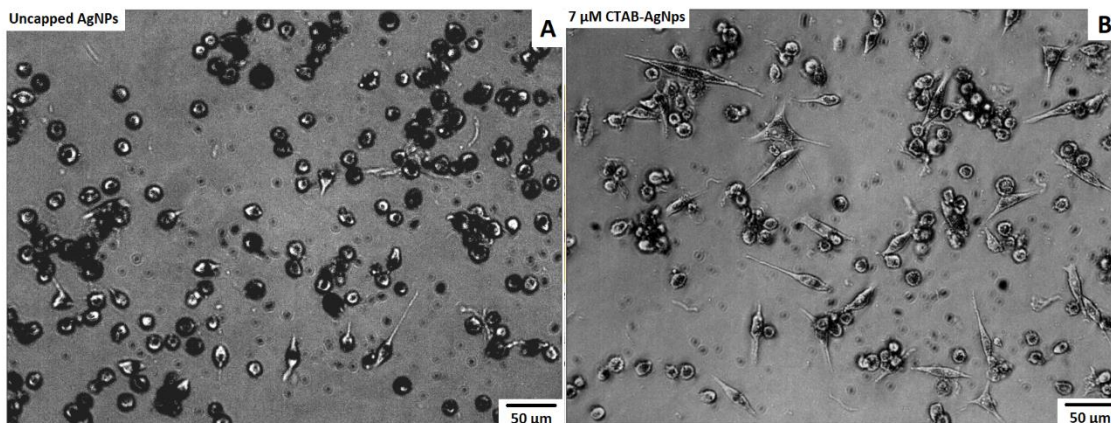


Figure IV.SI-8: Optical images of L929 cells at magnification X20. A) Cells treated with pristine R-AgNPs and, B) cells treated with 7 μM CTAB-AgNPs. Scale bar: 50 μm .

V.6) Supplementary information

Before choosing *Salvia rosmarinus* (Rosemary) extract as the reducing and capping agent for the synthesis of AgNPs. Two plants were subject to preliminary testing, Rosemary and *Thymus vulgaris* (Thyme). These two aromatic and medicinal plants were chosen due to their composition rich in secondary metabolites which are highly implicated in the synthesis and stabilization of silver nanoparticles as previously discussed. The same protocols as described in sections IV.2.2 and IV.2.3 were followed and the UV-Vis spectroscopy and DLS results are depicted in Fig IV.S1 and IV.S2 and summarized in Table IV.S1.

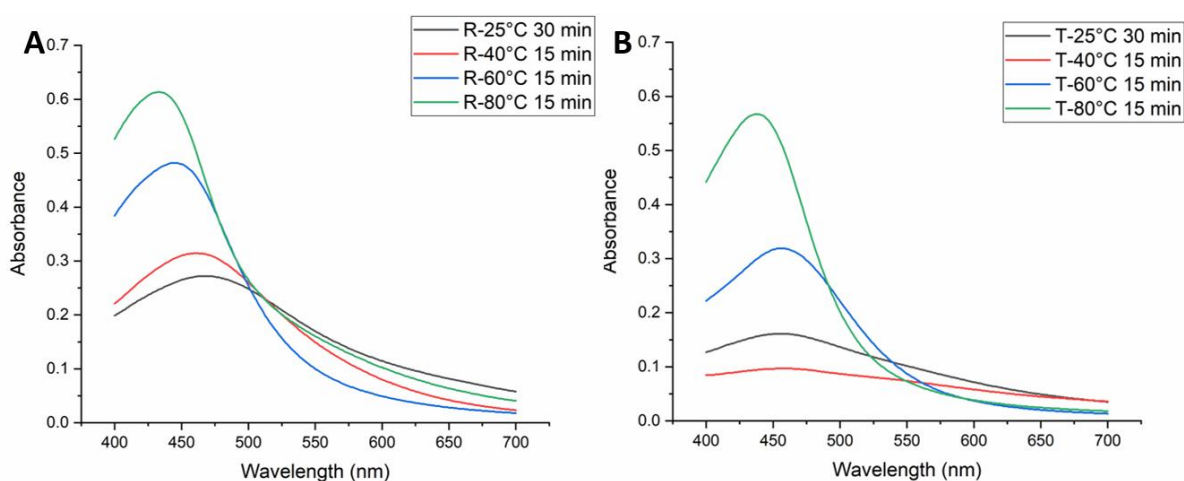


Figure IV.S1: UV-Vis spectra of synthesized AgNPs at different temperatures and times using A: Rosemary extract and B: Thyme extract

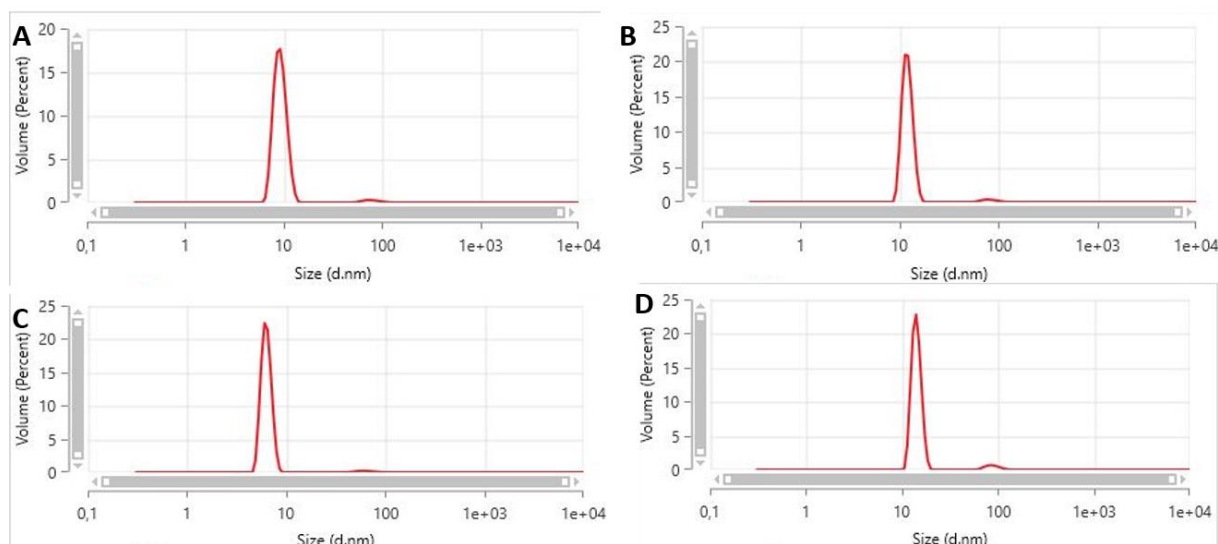


Figure IV.S2: Size distribution by volume measured using DLS of A: R-AgNPs prepared at 80°C, B: R-AgNPs prepared at 60°C, C: T-AgNPs prepared at 80°C, and D: T-AgNPs prepared at 60°C.

The results show a high similarity between AgNPs prepared using rosemary and thyme. However, it is apparent that rosemary induced a higher SPR intensity at all tested temperatures, while the hydrodynamic size obtained from DLS measurements remained almost identical. As rosemary extract showed a higher AgNPs synthesis rate at all tested temperatures with no significant change in the hydrodynamic size for AgNPs prepared at 80°C, it was chosen for the remainder of this work and R-AgNPs prepared at 80°C were fully characterized as shown in chapter IV.

Table IV.S1: The approximative hydrodynamic size obtained using DLS of AgNPs prepared using rosemary extract (R-AgNPs) and thyme extract (T-AgNPs) at different temperatures

	Hydrodynamic size (nm)
R-AgNPs 80°C	9
R-AgNPs 60°C	11
T-AgNPs 80°C	8
T-AgNPs 60°C	13

As AgNPs stability is primordial for their properties, R-AgNPs prepared at 80°C were found to aggregate after months. In the literature, multiple approaches are used to increase AgNPs stability. In this study, 3 surfactants were chosen and the results are discussed in length in IV.3.5. The Choice of the nature of the surfactants was based on their surface charge, but before choosing the range of concentrations of each surfactant, a preliminary test was performed using

0.1, 1, and 5mM of surfactants. Fig IV.SI-S3 shows results of the effect of surfactants at 0.1 mM and 1 mM on the AgNPs stability after 24 h.

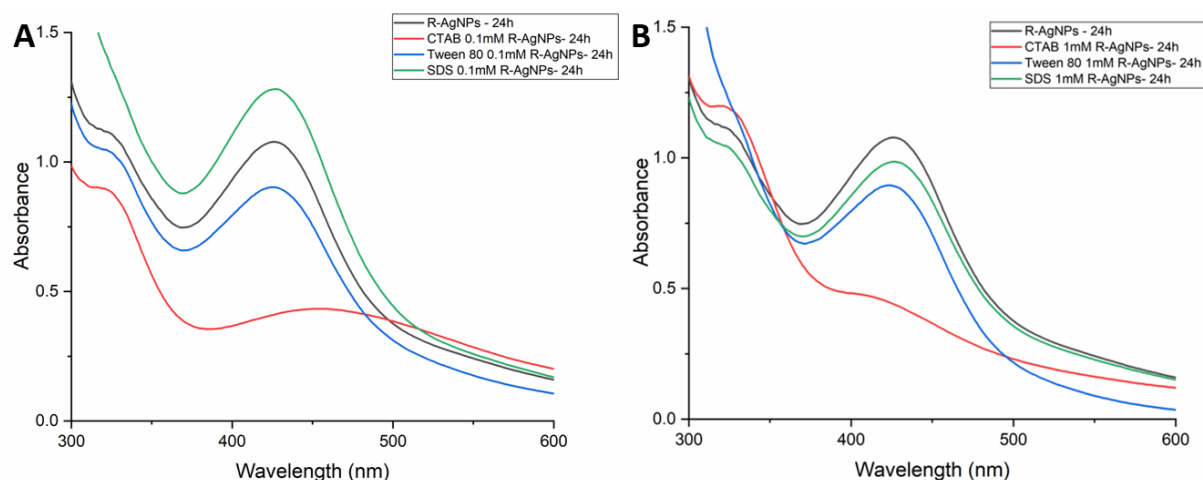


Figure IV.S3: The effect of CTAB, SDS, and Tween 80 on the stability of R-AgNPs after 24 h at A: 0.1 mM and B: 1 mM.

Results have shown that using a concentration of 1mM or higher (Fig. IV.S3-B) induced a rapid decline in R-AgNPs SPR band, especially using CTAB where the aggregation was also apparent visually while for SDS and Tween 80 the effect was much lower. The same thing was found using a concentration of 5 mM. When surfactants concentration was decreased to 0.1 mM, a slight decline of the SPR band was observed in the case of Tween while a higher absorbance than non-stabilized AgNPs was obtained for AgNPs with SDS. In the case of CTAB, always an apparent and rapid aggregation was observed, although to a much lesser extent than for 1 or 5 mM. In light of these results, concentrations between 1 μ M and 100 μ M were chosen for the study of the effect of surfactants on the stability of R-AgNPs.

Reference

- [1] F. Carrouel, S. Viennot, L. Ottolenghi, C. Gaillard, D. Bourgeois, Nanoparticles as Anti-Microbial, Anti-Inflammatory, and Remineralizing Agents in Oral Care Cosmetics: A Review of the Current Situation, *Nanomaterials*. 10 (2020) 140. <https://doi.org/10.3390/nano10010140>.
- [2] M. Shirzadi-Ahodashti, S. Mortazavi-Derazkola, M.A. Ebrahimzadeh, Biosynthesis of noble metal nanoparticles using crataegus monogyna leaf extract (CML@X-NPs, X= Ag, Au): Antibacterial and cytotoxic activities against breast and gastric cancer cell lines, *Surf. Interfaces*. 21 (2020) 100697. <https://doi.org/10.1016/j.surfin.2020.100697>.
- [3] B. Kumar, Green Synthesis of Gold, Silver, and Iron Nanoparticles for the Degradation of Organic Pollutants in Wastewater, *J. Compos. Sci.* 5 (2021) 219. <https://doi.org/10.3390/jcs5080219>.
- [4] A. Haider, I.-K. Kang, Preparation of Silver Nanoparticles and Their Industrial and Biomedical Applications: A Comprehensive Review, *Adv. Mater. Sci. Eng.* 2015 (2015) e165257. <https://doi.org/10.1155/2015/165257>.
- [5] M.A. Zakaria, A.A. Menazea, A.M. Mostafa, E.A. Al-Ashkar, Ultra-thin silver nanoparticles film prepared via pulsed laser deposition: Synthesis, characterization, and its catalytic activity on reduction of 4-nitrophenol, *Surf. Interfaces*. 19 (2020) 100438. <https://doi.org/10.1016/j.surfin.2020.100438>.
- [6] P.P. Gan, S.F.Y. Li, Potential of plant as a biological factory to synthesize gold and silver nanoparticles and their applications, *Rev. Environ. Sci. Biotechnol.* 11 (2012) 169–206. <https://doi.org/10.1007/s11157-012-9278-7>.
- [7] S.B. Yaqoob, R. Adnan, R.M. Rameez Khan, M. Rashid, Gold, Silver, and Palladium Nanoparticles: A Chemical Tool for Biomedical Applications, *Front. Chem.* 8 (2020). <https://www.frontiersin.org/article/10.3389/fchem.2020.00376> (accessed April 25, 2022).
- [8] S.O. Aisida, K. Ugwu, P.A. Akpa, A.C. Nwanya, U. Nwankwo, S.S. Botha, P.M. Ejikeme, I. Ahmad, M. Maaza, F.I. Ezema, Biosynthesis of silver nanoparticles using bitter leave (*Veronica amygdalina*) for antibacterial activities, *Surf. Interfaces*. 17 (2019) 100359. <https://doi.org/10.1016/j.surfin.2019.100359>.
- [9] T.D. Dat, N.D. Viet, N.M. Dat, P.L.T. My, D.B. Thinh, L.T.M. Thy, L.M. Huong, P.T. Khang, N.D. Hai, H.M. Nam, M.T. Phong, N.H. Hieu, Characterization and bioactivities of silver nanoparticles green synthesized from Vietnamese *Ganoderma lucidum*, *Surf. Interfaces*. 27 (2021) 101453. <https://doi.org/10.1016/j.surfin.2021.101453>.
- [10] M. Darroudi, M.B. Ahmad, A.H. Abdullah, N.A. Ibrahim, Green synthesis and characterization of gelatin-based and sugar-reduced silver nanoparticles, *Int. J. Nanomedicine*. 6 (2011) 569–574. <https://doi.org/10.2147/IJN.S16867>.
- [11] S. Davidović, V. Lazić, I. Vukoje, J. Papan, S.P. Anhrenkiel, S. Dimitrijević, J.M. Nedeljković, Dextran coated silver nanoparticles — Chemical sensor for selective cysteine detection, *Colloids Surf. B Biointerfaces*. 160 (2017) 184–191. <https://doi.org/10.1016/j.colsurfb.2017.09.031>.
- [12] J. González-Rivera, C. Duce, V. Ierardi, I. Longo, A. Spepi, M.R. Tiné, C. Ferrari, Fast and Eco-friendly Microwave-Assisted Synthesis of Silver Nanoparticles using Rosemary Essential Oil as Renewable Reducing Agent., *ChemistrySelect*. 2 (2017) 2131–2138. <https://doi.org/10.1002/slct.201700244>.
- [13] K. Jyoti, P. Pattnaik, T. Singh, Green Synthesis of Silver Nanoparticles Using Sustainable Resources and their Use as Antibacterial Agents: A Review, *Curr. Mater. Sci.* 14 (n.d.) 40–52.

- [14] I. Ijaz, E. Gilani, A. Nazir, A. Bukhari, Detail review on chemical, physical and green synthesis, classification, characterizations and applications of nanoparticles, *Green Chem. Lett. Rev.* 13 (2020) 223–245. <https://doi.org/10.1080/17518253.2020.1802517>.
- [15] M. Khatami, S. Iravani, Green and Eco-Friendly Synthesis of Nanophotocatalysts: An Overview, *Comments Inorg. Chem.* 41 (2021) 133–187. <https://doi.org/10.1080/02603594.2021.1895127>.
- [16] M. Nasiriboroumand, M. Montazer, H. Barani, Preparation and characterization of biocompatible silver nanoparticles using pomegranate peel extract, *J. Photochem. Photobiol. B.* 179 (2018) 98–104. <https://doi.org/10.1016/j.jphotobiol.2018.01.006>.
- [17] Y.-K. Twu, Y.-W. Chen, C.-M. Shih, Preparation of silver nanoparticles using chitosan suspensions, *Powder Technol.* 185 (2008) 251–257. <https://doi.org/10.1016/j.powtec.2007.10.025>.
- [18] J. Das, P. Velusamy, Antibacterial effects of biosynthesized silver nanoparticles using aqueous leaf extract of *Rosmarinus officinalis* L., *Mater. Res. Bull.* 48 (2013) 4531–4537. <https://doi.org/10.1016/j.materresbull.2013.07.049>.
- [19] M.J. Firdhouse, P. Lalitha, Biogenic silver nanoparticles – Synthesis, characterization and its potential against cancer inducing bacteria, *J. Mol. Liq.* 222 (2016) 1041–1050. <https://doi.org/10.1016/j.molliq.2016.07.141>.
- [20] M. Ghaedi, M. Yousefinejad, M. Safarpour, H.Z. Khafri, M.K. Purkait, *Rosmarinus officinalis* leaf extract mediated green synthesis of silver nanoparticles and investigation of its antimicrobial properties, *J. Ind. Eng. Chem.* 31 (2015) 167–172. <https://doi.org/10.1016/j.jiec.2015.06.020>.
- [21] J. Singh, T. Dutta, K.-H. Kim, M. Rawat, P. Samddar, P. Kumar, ‘Green’ synthesis of metals and their oxide nanoparticles: applications for environmental remediation, *J. Nanobiotechnology.* 16 (2018) 84. <https://doi.org/10.1186/s12951-018-0408-4>.
- [22] Y. Bao, J. He, K. Song, J. Guo, X. Zhou, S. Liu, Plant-Extract-Mediated Synthesis of Metal Nanoparticles, *J. Chem.* 2021 (2021) e6562687. <https://doi.org/10.1155/2021/6562687>.
- [23] H. Chandra, P. Kumari, E. Bontempi, S. Yadav, Medicinal plants: Treasure trove for green synthesis of metallic nanoparticles and their biomedical applications, *Biocatal. Agric. Biotechnol.* 24 (2020) 101518. <https://doi.org/10.1016/j.bcab.2020.101518>.
- [24] S. Jadoun, R. Arif, N.K. Jangid, R.K. Meena, Green synthesis of nanoparticles using plant extracts: a review, *Environ. Chem. Lett.* 19 (2021) 355–374. <https://doi.org/10.1007/s10311-020-01074-x>.
- [25] T. My-Thao Nguyen, T. Anh-Thu Nguyen, N. Tuong-Van Pham, Q.-V. Ly, T. Thuy-Quynh Tran, T.-D. Thach, C.-L. Nguyen, K.-S. Banh, V.-D. Le, L.-P. Nguyen, D.-T. Nguyen, C.-H. Dang, T.-D. Nguyen, Biosynthesis of metallic nanoparticles from waste *Passiflora edulis* peels for their antibacterial effect and catalytic activity, *Arab. J. Chem.* 14 (2021) 103096. <https://doi.org/10.1016/j.arabjc.2021.103096>.
- [26] A. Rana, K. Yadav, S. Jagadevan, A comprehensive review on green synthesis of nature-inspired metal nanoparticles: Mechanism, application and toxicity, *J. Clean. Prod.* 272 (2020) 122880. <https://doi.org/10.1016/j.jclepro.2020.122880>.
- [27] G. Marslin, K. Siram, Q. Maqbool, R.K. Selvakesavan, D. Kruszka, P. Kachlicki, G. Franklin, Secondary Metabolites in the Green Synthesis of Metallic Nanoparticles, *Materials.* 11 (2018) 940. <https://doi.org/10.3390/ma11060940>.
- [28] M. Ovais, A.T. Khalil, N.U. Islam, I. Ahmad, M. Ayaz, M. Saravanan, Z.K. Shinwari, S. Mukherjee, Role of plant phytochemicals and microbial enzymes in biosynthesis of metallic nanoparticles, *Appl. Microbiol. Biotechnol.* 102 (2018) 6799–6814. <https://doi.org/10.1007/s00253-018-9146-7>.

- [29] T.M. Aminabhavi, S.P. Dharupaneedi, U.A. More, 1 - The role of nanotechnology and chitosan-based biomaterials for tissue engineering and therapeutic delivery, in: J.A. Jennings, J.D. Bumgardner (Eds.), *Chitosan Based Biomater.* Vol. 2, Woodhead Publishing, 2017: pp. 1–29. <https://doi.org/10.1016/B978-0-08-100228-5.00001-8>.
- [30] V. Goodarzi, H. Zamani, L. Bajuli, A. Moradshahi, Evaluation of antioxidant potential and reduction capacity of some plant extracts in silver nanoparticles' synthesis, *Mol. Biol. Res. Commun.* 3 (2014) 165–174.
- [31] T. Bakırel, U. Bakırel, O.Ü. Keleş, S.G. Ülgen, H. Yardibi, In vivo assessment of antidiabetic and antioxidant activities of rosemary (*Rosmarinus officinalis*) in alloxan-diabetic rabbits, *J. Ethnopharmacol.* 116 (2008) 64–73. <https://doi.org/10.1016/j.jep.2007.10.039>.
- [32] S. Cheung, J. Tai, Anti-proliferative and antioxidant properties of rosemary *Rosmarinus officinalis*, *Oncol. Rep.* 17 (2007) 1525–1531.
- [33] J. Rocha, M. Eduardo-Figueira, A. Barateiro, A. Fernandes, D. Brites, R. Bronze, C.M. Duarte, A.T. Serra, R. Pinto, M. Freitas, E. Fernandes, B. Silva-Lima, H. Mota-Filipe, B. Sepodes, Anti-inflammatory Effect of Rosmarinic Acid and an Extract of *Rosmarinus officinalis* in Rat Models of Local and Systemic Inflammation, *Basic Clin. Pharmacol. Toxicol.* 116 (2015) 398–413. <https://doi.org/10.1111/bcpt.12335>.
- [34] G. Nieto, G. Ros, J. Castillo, Antioxidant and Antimicrobial Properties of Rosemary (*Rosmarinus officinalis*, L.): A Review, *Medicines.* 5 (2018) 98. <https://doi.org/10.3390/medicines5030098>.
- [35] R. Ribeiro-Santos, D. Carvalho-Costa, C. Cavaleiro, H.S. Costa, T.G. Albuquerque, M.C. Castilho, F. Ramos, N.R. Melo, A. Sanches-Silva, A novel insight on an ancient aromatic plant: The rosemary (*Rosmarinus officinalis* L.), *Trends Food Sci. Technol.* 45 (2015) 355–368. <https://doi.org/10.1016/j.tifs.2015.07.015>.
- [36] G.A. Gonçalves, R.C.G. Corrêa, L. Barros, M.I. Dias, R.C. Calhelha, V.G. Correa, A. Bracht, R.M. Peralta, I.C.F.R. Ferreira, Effects of in vitro gastrointestinal digestion and colonic fermentation on a rosemary (*Rosmarinus officinalis* L) extract rich in rosmarinic acid, *Food Chem.* 271 (2019) 393–400. <https://doi.org/10.1016/j.foodchem.2018.07.132>.
- [37] G. Mishra, B. Dash, S. Pandey, P.P. Mohanty, Antibacterial actions of silver nanoparticles incorporated Zn–Al layered double hydroxide and its spinel, *J. Environ. Chem. Eng.* 1 (2013) 1124–1130. <https://doi.org/10.1016/j.jece.2013.08.031>.
- [38] E. Parthiban, N. Manivannan, R. Ramanibai, N. Mathivanan, Green synthesis of silver-nanoparticles from *Annona reticulata* leaves aqueous extract and its mosquito larvicidal and anti-microbial activity on human pathogens, *Biotechnol. Rep.* 21 (2019) e00297. <https://doi.org/10.1016/j.btre.2018.e00297>.
- [39] M. Rai, K. Kon, A. Ingle, N. Duran, S. Galdiero, M. Galdiero, Broad-spectrum bioactivities of silver nanoparticles: the emerging trends and future prospects, *Appl. Microbiol. Biotechnol.* 98 (2014) 1951–1961. <https://doi.org/10.1007/s00253-013-5473-x>.
- [40] C. Vanlalveni, S. Lallianrawna, A. Biswas, M. Selvaraj, B. Changmai, S.L. Rokhum, Green synthesis of silver nanoparticles using plant extracts and their antimicrobial activities: a review of recent literature, *RSC Adv.* 11 (2021) 2804–2837. <https://doi.org/10.1039/D0RA09941D>.
- [41] A.K.S.H. Mohamed, M.F. Qayyum, A.M. Abdel-Hadi, R.A. Rehman, S. Ali, M. Rizwan, Interactive effect of salinity and silver nanoparticles on photosynthetic and biochemical parameters of wheat, *Arch. Agron. Soil Sci.* 63 (2017) 1736–1747. <https://doi.org/10.1080/03650340.2017.1300256>.
- [42] S. Saeidi, F. Javadian, Z. Sepehri, Z. Shahi, R. Farazmand, M. Anbari, Antibacterial activity of silver Nanoparticles produced by *Rosmarinus officinalis* L leaf extract against

- some human pathogenic bacteria, *Int. J. Adv. Biol. Biomed. Res.* 4 (2016) 108–111. <https://doi.org/10.26655/ijabbr.2016.2.15>.
- [43] M. Hadi Soltanabad, M.B. Bagherieh-Najjar, E. Kohan Baghkheirati, M. Mianabadi, Ag-Conjugated Nanoparticle Biosynthesis Mediated by Rosemary Leaf Extracts Correlates with Plant Antioxidant Activity and Protein Content, *Int. J. Nanosci. Nanotechnol.* 14 (2018) 319–325.
- [44] R.C. Fierascu, I.R. Bunghez, R. Somoghi, I. Fierascu, R.M. Ion, CHARACTERIZATION OF SILVER NANOPARTICLES OBTAINED BY USING ROSMARINUS OFFICINALIS EXTRACT AND THEIR ANTIOXIDANT ACTIVITY, *Silver Nanoparticles*. (n.d.) 6.
- [45] A.A. Abu-Zaid, M.H.E.- Sehwawy, M. H, A.H. Nemari, Biosynthesis of silver nanoparticles by plants extract and their antimicrobial activities, *Adv. Environ. Biol.* 10 (2016) 114–128.
- [46] A.A. Abu-Zaid, Antibacterial effect of green synthesis silver nanoparticles against *Escherichia coli*, *Res. J. Fish. Hydrobiol.* 11 (2016) 7–14.
- [47] M. Safarpour, M. Ghaedi, A. Asfaram, M. Yousefi-Nejad, H. Javadian, H. Zare Khafri, M. Bagherinasab, Ultrasound-assisted extraction of antimicrobial compounds from *Thymus daenensis* and *Silybum marianum*: Antimicrobial activity with and without the presence of natural silver nanoparticles, *Ultrason. Sonochem.* 42 (2018) 76–83. <https://doi.org/10.1016/j.ultsonch.2017.11.001>.
- [48] R.L. Olteanu, C.M. Nicolescu, M. Bumbac, Influence of Phytochemical Reductive Capacity on Ultraviolet–visible Spectroscopic Behavior of Silver Nanoparticles, *Anal. Lett.* 50 (2017) 2786–2801. <https://doi.org/10.1080/00032719.2017.1298119>.
- [49] M. Vanaja, G. Annadurai, *Coleus aromaticus* leaf extract mediated synthesis of silver nanoparticles and its bactericidal activity, *Appl. Nanosci.* 3 (2013) 217–223. <https://doi.org/10.1007/s13204-012-0121-9>.
- [50] F.E. Meva, J.O.A. Mbeng, C.O. Ebongue, C. Schlüsener, Ü. Kökçam-Demir, A.A. Ntomba, P.B.E. Kedi, E. Elanga, E.-R.N. Loudang, M.H.J. Nko’o, E. Tchoumbi, V. Deli, C.C. Nanga, E.A.M. Mpondo, C. Janiak, *Stachytarpheta cayennensis* Aqueous Extract, a New Bioreactor towards Silver Nanoparticles for Biomedical Applications, *J. Biomater. Nanobiotechnology.* 10 (2019) 102–119. <https://doi.org/10.4236/jbnb.2019.102006>.
- [51] H. Muthukumar, S.K. Palanirajan, M.K. Shanmugam, S.N. Gummadi, Plant extract mediated synthesis enhanced the functional properties of silver ferrite nanoparticles over chemical mediated synthesis, *Biotechnol. Rep.* 26 (2020) e00469. <https://doi.org/10.1016/j.btre.2020.e00469>.
- [52] S. Nayak, M.P. Bhat, A. c. Udayashankar, T. r. Lakshmeesha, N. Geetha, S. Jogaiyah, Biosynthesis and characterization of *Dillenia indica*-mediated silver nanoparticles and their biological activity, *Appl. Organomet. Chem.* 34 (2020) e5567. <https://doi.org/10.1002/aoc.5567>.
- [53] V. Kumar, S.K. Yadav, Characterisation of gold nanoparticles synthesised by leaf and seed extract of *Syzygium cumini* L., *J. Exp. Nanosci.* 7 (2012) 440–451. <https://doi.org/10.1080/17458080.2010.543989>.
- [54] A. Tripathy, A.M. Raichur, N. Chandrasekaran, T.C. Prathna, A. Mukherjee, Process variables in biomimetic synthesis of silver nanoparticles by aqueous extract of *Azadirachta indica* (Neem) leaves, *J. Nanoparticle Res.* 12 (2010) 237–246. <https://doi.org/10.1007/s11051-009-9602-5>.
- [55] L. Kvítek, A. Panáček, J. Soukupová, M. Kolář, R. Večeřová, R. Prucek, M. Holecová, R. Zbořil, Effect of Surfactants and Polymers on Stability and Antibacterial Activity of

- Silver Nanoparticles (NPs), *J. Phys. Chem. C.* 112 (2008) 5825–5834. <https://doi.org/10.1021/jp711616v>.
- [56] J.S. Pawar, R.H. Patil, Green synthesis of silver nanoparticles using *Eulophia herbacea* (Lindl.) tuber extract and evaluation of its biological and catalytic activity, *SN Appl. Sci.* 2 (2019) 52. <https://doi.org/10.1007/s42452-019-1846-9>.
- [57] S. Kumar, S.K. Sardana, Optical properties of silver nanoparticles deposited on glass and silicon substrates, *AIP Conf. Proc.* 2220 (2020) 050013. <https://doi.org/10.1063/5.0001530>.
- [58] M. Ndikau, N.M. Noah, D.M. Andala, E. Masika, Green Synthesis and Characterization of Silver Nanoparticles Using *Citrullus lanatus* Fruit Rind Extract, *Int. J. Anal. Chem.* 2017 (2017) e8108504. <https://doi.org/10.1155/2017/8108504>.
- [59] S. Agnihotri, S. Mukherji, S. Mukherji, Size-controlled silver nanoparticles synthesized over the range 5–100 nm using the same protocol and their antibacterial efficacy, *RSC Adv.* 4 (2013) 3974–3983. <https://doi.org/10.1039/C3RA44507K>.
- [60] B.J. Wiley, S.H. Im, Z.-Y. Li, J. McLellan, A. Siekkinen, Y. Xia, Maneuvering the Surface Plasmon Resonance of Silver Nanostructures through Shape-Controlled Synthesis, *J. Phys. Chem. B.* 110 (2006) 15666–15675. <https://doi.org/10.1021/jp0608628>.
- [61] E.E. Elemike, O.E. Fayemi, A.C. Ekennia, D.C. Onwudiwe, E.E. Ebenso, Silver Nanoparticles Mediated by *Costus afer* Leaf Extract: Synthesis, Antibacterial, Antioxidant and Electrochemical Properties, *Molecules.* 22 (2017) 701. <https://doi.org/10.3390/molecules22050701>.
- [62] A. Mohammed Fayaz, K. Balaji, P.T. Kalaichelvan, R. Venkatesan, Fungal based synthesis of silver nanoparticles—An effect of temperature on the size of particles, *Colloids Surf. B Biointerfaces.* 74 (2009) 123–126. <https://doi.org/10.1016/j.colsurfb.2009.07.002>.
- [63] J. Singh, A.S. Dhaliwal, Novel Green Synthesis and Characterization of the Antioxidant Activity of Silver Nanoparticles Prepared from *Nepeta leucophylla* Root Extract, *Anal. Lett.* 52 (2019) 213–230. <https://doi.org/10.1080/00032719.2018.1454936>.
- [64] M. Mosaviniya, T. Kikhavani, M. Tanzifi, M. Tavakkoli Yaraki, P. Tajbakhsh, A. Lajevardi, Facile green synthesis of silver nanoparticles using *Crocus Haussknechtii* Bois bulb extract: Catalytic activity and antibacterial properties, *Colloid Interface Sci. Commun.* 33 (2019) 100211. <https://doi.org/10.1016/j.colcom.2019.100211>.
- [65] C.M. Maguire, M. Rösslein, P. Wick, A. Prina-Mello, Characterisation of particles in solution – a perspective on light scattering and comparative technologies, *Sci. Technol. Adv. Mater.* 19 (2018) 732–745. <https://doi.org/10.1080/14686996.2018.1517587>.
- [66] R.I. MacCuspie, K. Rogers, M. Patra, Z. Suo, A.J. Allen, M.N. Martin, V.A. Hackley, Challenges for physical characterization of silver nanoparticles under pristine and environmentally relevant conditions, *J. Environ. Monit.* 13 (2011) 1212–1226. <https://doi.org/10.1039/C1EM10024F>.
- [67] J.I. Langford, A.J.C. Wilson, Scherrer after sixty years: A survey and some new results in the determination of crystallite size, *J. Appl. Crystallogr.* 11 (1978) 102–113. <https://doi.org/10.1107/S0021889878012844>.
- [68] D.E. Diaz-Droguett, R. Espinoza, V.M. Fuenzalida, Copper nanoparticles grown under hydrogen: Study of the surface oxide, *Appl. Surf. Sci.* 257 (2011) 4597–4602. <https://doi.org/10.1016/j.apsusc.2010.12.082>.
- [69] J.C. Rhoda, M. Giruba, S. Chellammal, Role of capping agents on size variation of cadmium oxide nanocrystallites, *AIP Conf. Proc.* 2115 (2019) 030184. <https://doi.org/10.1063/1.5113023>.

- [70] M. Zargar, A.A. Hamid, F.A. Bakar, M.N. Shamsudin, K. Shameli, F. Jahanshiri, F. Farahani, Green Synthesis and Antibacterial Effect of Silver Nanoparticles Using Vitex Negundo L., *Molecules*. 16 (2011) 6667–6676. <https://doi.org/10.3390/molecules16086667>.
- [71] S. Dehghanizade, J. Arasteh, A. Mirzaie, Green synthesis of silver nanoparticles using Anthemis atropatana extract: characterization and in vitro biological activities, *Artif. Cells Nanomedicine Biotechnol.* 46 (2018) 160–168. <https://doi.org/10.1080/21691401.2017.1304402>.
- [72] H. Jensen, K.D. Joensen, J.-E. Jørgensen, J.S. Pedersen, G. Søggaard, Characterization of nanosized partly crystalline photocatalysts, *J. Nanoparticle Res.* 6 (2004) 519–526. <https://doi.org/10.1007/s11051-004-1714-3>.
- [73] J. Coates, Interpretation of infrared spectra, a practical approach, (2000).
- [74] G.A. Otunola, A.J. Afolayan, In vitro antibacterial, antioxidant and toxicity profile of silver nanoparticles green-synthesized and characterized from aqueous extract of a spice blend formulation, *Biotechnol. Equip.* 32 (2018) 724–733. <https://doi.org/10.1080/13102818.2018.1448301>.
- [75] A.K. Mittal, J. Bhaumik, S. Kumar, U.C. Banerjee, Biosynthesis of silver nanoparticles: Elucidation of prospective mechanism and therapeutic potential, *J. Colloid Interface Sci.* 415 (2014) 39–47. <https://doi.org/10.1016/j.jcis.2013.10.018>.
- [76] L.M. Liz-Marzán, I. Lado-Touriño, Reduction and Stabilization of Silver Nanoparticles in Ethanol by Nonionic Surfactants, *Langmuir*. 12 (1996) 3585–3589. <https://doi.org/10.1021/la951501e>.
- [77] R. Kurrey, M.K. Deb, K. Shrivastava, Surface enhanced infra-red spectroscopy with modified silver nanoparticles (AgNPs) for detection of quaternary ammonium cationic surfactants, *New J. Chem.* 43 (2019) 8109–8121. <https://doi.org/10.1039/C9NJ01795J>.
- [78] I. De Leersnyder, L. De Gelder, I. Van Driessche, P. Vermeir, Revealing the Importance of Aging, Environment, Size and Stabilization Mechanisms on the Stability of Metal Nanoparticles: A Case Study for Silver Nanoparticles in a Minimally Defined and Complex Undefined Bacterial Growth Medium, *Nanomaterials*. 9 (2019) 1684. <https://doi.org/10.3390/nano9121684>.
- [79] M.K. Ahmed, M.E. El-Naggar, A. Aldalbahi, M.H. El-Newehy, A.A. Menazea, Methylene blue degradation under visible light of metallic nanoparticles scattered into graphene oxide using laser ablation technique in aqueous solutions, *J. Mol. Liq.* 315 (2020) 113794. <https://doi.org/10.1016/j.molliq.2020.113794>.
- [80] H.S. Al-Ghamdi, W.E. Mahmoud, One pot synthesis of multi-plasmonic shapes of silver nanoparticles, *Mater. Lett.* 105 (2013) 62–64. <https://doi.org/10.1016/j.matlet.2013.04.086>.
- [81] L. Gram, L. Ravn, M. Rasch, J.B. Bruhn, A.B. Christensen, M. Givskov, Food spoilage—interactions between food spoilage bacteria, *Int. J. Food Microbiol.* 78 (2002) 79–97. [https://doi.org/10.1016/S0168-1605\(02\)00233-7](https://doi.org/10.1016/S0168-1605(02)00233-7).
- [82] D.-H. Kim, D. Jeong, H. Kim, I.-B. Kang, J.-W. Chon, K.-Y. Song, K.-H. Seo, Antimicrobial Activity of Kefir against Various Food Pathogens and Spoilage Bacteria, *Food Sci. Anim. Resour.* 36 (2016) 787–790. <https://doi.org/10.5851/kosfa.2016.36.6.787>.
- [83] P. Korshed, L. Li, Z. Liu, A. Mironov, T. Wang, Size-dependent antibacterial activity for laser-generated silver nanoparticles, *J. Interdiscip. Nanomedicine*. 4 (2019) 24–33. <https://doi.org/10.1002/jin2.54>.
- [84] M.A. Raza, Z. Kanwal, A. Rauf, A.N. Sabri, S. Riaz, S. Naseem, Size- and Shape-Dependent Antibacterial Studies of Silver Nanoparticles Synthesized by Wet Chemical Routes, *Nanomaterials*. 6 (2016) 74. <https://doi.org/10.3390/nano6040074>.

- [85] S. Kaviya, J. Santhanalakshmi, B. Viswanathan, J. Muthumary, K. Srinivasan, Biosynthesis of silver nanoparticles using citrus sinensis peel extract and its antibacterial activity, *Spectrochim. Acta. A. Mol. Biomol. Spectrosc.* 79 (2011) 594–598. <https://doi.org/10.1016/j.saa.2011.03.040>.
- [86] M.S. Riaz Rajoka, H.M. Mehwish, H. Zhang, M. Ashraf, H. Fang, X. Zeng, Y. Wu, M. Khurshid, L. Zhao, Z. He, Antibacterial and antioxidant activity of exopolysaccharide mediated silver nanoparticle synthesized by *Lactobacillus brevis* isolated from Chinese koumiss, *Colloids Surf. B Biointerfaces.* 186 (2020) 110734. <https://doi.org/10.1016/j.colsurfb.2019.110734>.
- [87] J.S. Kim, E. Kuk, K.N. Yu, J.-H. Kim, S.J. Park, H.J. Lee, S.H. Kim, Y.K. Park, Y.H. Park, C.-Y. Hwang, Y.-K. Kim, Y.-S. Lee, D.H. Jeong, M.-H. Cho, Antimicrobial effects of silver nanoparticles, *Nanomedicine Nanotechnol. Biol. Med.* 3 (2007) 95–101. <https://doi.org/10.1016/j.nano.2006.12.001>.
- [88] P. Das, K. Ghosal, N.K. Jana, A. Mukherjee, P. Basak, Green synthesis and characterization of silver nanoparticles using belladonna mother tincture and its efficacy as a potential antibacterial and anti-inflammatory agent, *Mater. Chem. Phys.* 228 (2019) 310–317. <https://doi.org/10.1016/j.matchemphys.2019.02.064>.
- [89] N. Durán, M. Durán, M.B. de Jesus, A.B. Seabra, W.J. Fávaro, G. Nakazato, Silver nanoparticles: A new view on mechanistic aspects on antimicrobial activity, *Nanomedicine Nanotechnol. Biol. Med.* 12 (2016) 789–799. <https://doi.org/10.1016/j.nano.2015.11.016>.
- [90] Y. Sun, X. Hu, D. Guo, C. Shi, C. Zhang, X. Peng, H. Yang, X. Xia, Disinfectant Resistance Profiles and Biofilm Formation Capacity of *Escherichia coli* Isolated from Retail Chicken, *Microb. Drug Resist.* 25 (2019) 703–711. <https://doi.org/10.1089/mdr.2018.0175>.
- [91] H. Jang, S.H. Lim, J.S. Choi, Y. Park, Antibacterial properties of cetyltrimethylammonium bromide-stabilized green silver nanoparticles against methicillin-resistant *Staphylococcus aureus*, *Arch. Pharm. Res.* 38 (2015) 1906–1912. <https://doi.org/10.1007/s12272-015-0605-8>.
- [92] A.N. Vereshchagin, N.A. Frolov, K.S. Egorova, M.M. Seitkalieva, V.P. Ananikov, Quaternary Ammonium Compounds (QACs) and Ionic Liquids (ILs) as Biocides: From Simple Antiseptics to Tunable Antimicrobials, *Int. J. Mol. Sci.* 22 (2021) 6793. <https://doi.org/10.3390/ijms22136793>.
- [93] 14:00-17:00, ISO 10993-5:2009, ISO. (n.d.). <https://www.iso.org/cms/render/live/en/sites/isoorg/contents/data/standard/03/64/36406.html> (accessed April 25, 2022).

Chapter V:

**Chitosan/Green Silver nanoparticles
nanobiocomposites: an efficient dual functionality
as antibacterial materials and 4-Nitroaniline
reduction catalysts**

Chapter overview

In the previous chapter, we optimized the biosynthesis of R-AgNPs *via* an eco-friendly pathway in terms of size and production. These R-AgNPs showed a much higher antibacterial activity against Gram-positive and Gram-negative bacteria compared to commercial AgNPs used in chapter III.

In this chapter, we aimed to evaluate the antibacterial potential of these R-AgNPs when incorporated into a polymeric matrix. In that regard, chitosan (CS) was used as a matrix for the preparation of CS-AgNPs nanocomposites. CS differs from PCL and PLA in its polysaccharidic nature as well as its inherent bacteriostatic activity. These properties make CS an ideal candidate for applications in food packaging. However, unlike PCL and PLA, polysaccharides such as CS cannot be melted as they degrade before melting, therefore techniques like melt extrusion cannot be used for these types of polymers. As an alternative, the solution mixing/solvent casting method is a simple and eco-friendly approach in the case of hydro-soluble polymers-based nanocomposites.

Using solution mixing, CS-Metallic nanoparticles (MeNPs) nanocomposites are usually prepared using an *in-situ* approach in which MeNPs are prepared inside the CS matrix via the reduction of Me^+ using CS itself. Alternatively, an *ex-situ* approach could be used in which AgNPs are prepared beforehand, and then dispersed in the CS matrix. This technique allows more control over NPs characteristics (size, surface charge, and stability). For these reasons, we adopted the *ex-situ* approach using R-AgNPs as nanofillers.

The results of this chapter are presented in the form of a paper ready for submission under the title «Chitosan/Green Silver nanoparticles nanobiocomposites: an efficient dual functionality as antibacterial materials and 4-Nitroaniline reduction catalysts».

Chitosan/Green Silver nanoparticles nanobiocomposites: an efficient dual functionality as antibacterial materials and 4-Nitroaniline reduction catalysts

Abderrahmane Nabgui^{1,2,3}, Abdelmalik Brik^{3,4}, Khalid Agayr³, Géraldine Gouhier⁴, Elvira Vidović⁵, Jamal El Haskouri⁶, Abdellatif El Meziane^{2*}, Pascal Thébault^{1**} & Mohammed Lahcini^{3,7**}

¹ Normandie Univ, UNIROUEN, INSA Rouen, CNRS, PBS UMR6270, Bd Maurice de Broglie, 76821 Mont Saint Aignan Cedex, France

² Laboratory of Agrobiotechnology and Bio-engineering, Department of Biology. Faculty of Sciences and Techniques, Cadi-Ayyad University, 40000, Marrakech, Morocco.

³ IMED-Lab, Faculty of Sciences and Techniques, Cadi-Ayyad University, 40000, Marrakech, Morocco.

⁴ Normandie Université, COBRA UMR 6014, FR 3038, INSA Rouen, CNRS, IRCOF, 76821 Mont-Saint-Aignan, France.

⁵ University of Zagreb, Faculty of Chemical Engineering and Technology, HR-10000, Croatia

⁶ Instituto de ciencias de los materiales de la universidad de valencia, Calle catedrático José Beltrán, 2, C.P 46980 Paterna Valencia Spain

⁷ Mohammed VI Polytechnic University, 43150 Ben Guerir, Morocco.

* Corresponding author at: Laboratory of Agrobiotechnology and Bio-engineering, Department of Biology. Faculty of Sciences and Techniques, Cadi-Ayyad University, 40000, Marrakech, Morocco. a.elmeziane@uca.ma

** Corresponding author at : Normandie Univ, UNIROUEN, INSA Rouen, CNRS, PBS UMR6270, Bd Maurice de Broglie, 76821 Mont Saint Aignan Cedex, France. pascal.thebault@univ-rouen.fr

*** Corresponding author at: IMED-Lab, Faculty of Sciences and Techniques, Cadi-Ayyad University, 40000, Marrakech, Morocco. m.lahcini@uca.ac.ma

Abstract

Chitosan (CS) is a natural biocompatible, biodegradable, and non-toxic polysaccharide with a high potential in various applications in medicine, food packaging, and catalysis. Similarly, Silver nanoparticles (AgNPs) are known for their excellent antimicrobial properties, catalytic activity, and their high compatibility with Cs. These AgNPs are usually prepared through expensive and non-ecofriendly chemical or physical approaches. Alternatively, plant-mediated synthesis of AgNPs is regarded as the ecofriendly, low-cost, and simplest approach for AgNPs preparation. In this work, we aimed to combine CS with Rosemary-mediated AgNPs to prepare CS/R-AgNPs films through a simple *ex-situ* solution mixing approach for potential applications in antimicrobial food packaging due to the antibacterial activity of both CS and AgNPs, and in heterogeneous catalysis of reduction of aromatic nitro-compounds to their corresponding anilines using CS as a support and R-AgNPs as metal catalysts for the hydrogenation of 4-Nitroaniline (4-NA). CS/R-AgNPs films were characterized using UV-Vis spectroscopy, X-ray diffraction (XRD), Transmission electron microscopy (TEM), Fourier transform infrared spectroscopy (FTIR), and Thermogravimetric analysis (TGA). TEM images showed well-distributed R-AgNPs in the CS matrix and FTIR proved the existence of electrostatic interactions between R-AgNPs and CS. Finally, their antibacterial and catalytic activities were tested. CS/R-AgNPs showed excellent antibacterial activity against both Gram-positive bacterium *Staphylococcus aureus* and Gram-negative bacterium *Escherichia coli* at very low R-AgNPs loading *i.e.*, 0.5%. Furthermore, we reported the successful use of CS/R-AgNPs as a heterogenous catalysis system for the dehydrogenation of 4-Nitroaniline in the presence of Sodium Borohydride (NaBH₄). The reaction followed a pseudo-first order kinetic with an R-AgNPs dose-dependent rate constant K as follow: 0.09 min⁻¹ for CS/1% R-AgNPs, 0.11 min⁻¹ for CS/2% R-AgNPs, and 0.20 min⁻¹ for CS/3% R-AgNPs. The catalyst recyclability showed that even after 10 consecutive cycles, CS/R-AgNPs retained a 96% conversion. Thus, CS/R-AgNPs films could find potential applications in active food packaging as well as water treatment.

Keywords: Chitosan nanocomposites, Silver nanoparticles, Antibacterial activity, Heterogenous catalysis, Water treatment.

VI.1) Introduction

Chitosan (CS), a cationic polysaccharide prepared by deacetylation of chitin, is a byproduct of the fishing industry and the second most abundant polysaccharide in nature after cellulose [1]. In addition to its low cost, biocompatibility, biodegradability, and nontoxicity, CS is rich in -OH and -NH₂ functional groups allowing its functionalization [2,3]. Furthermore, the CS amino groups are also known to be responsible for its antibacterial behavior [4]. Consequently, CS has been used in a variety of applications such as medicine [5], active food packaging [6], and catalysis [7]. Indeed, CS has gained a lot of attention as an antimicrobial food packaging material. Thus, the use of CS in food coating inhibits for example the bacterial growth of Broccoli [8] and increased significantly the shelf life of meat products [9]. However, as CS films tend to disintegrate in contact with water due to their primary ammonium groups, the deprotonation of these groups is an essential step to limit this degradation. Nevertheless, this step results in the reduction of the CS antibacterial efficacy due to the decrease of the electrostatic interactions between CS and microorganisms [10]. Moreover, the qualitative and quantitative antibacterial activity of CS are very limited mainly at neutral pH. Indeed, CS is rather considered bacteriostatic than bactericidal [11]. Therefore, to maintain, enhance, and/or enlarge the antibacterial activity of CS-based food packaging, additives such as essential oils have been added [12,13]. But, as the diffusion of these additives may compromise the organoleptic properties of the packaged food [14], it is necessary to find an alternative. For this purpose, silver nanoparticles (AgNPs) appear as good candidates due to their high antibacterial activity against a wide range of bacteria [15], their non-interference with organoleptic properties of food [16], and also due to the good affinity between silver nanoparticles and CS [17]. The synthesis of AgNPs is usually carried out by chemical or physical methods, which require the use of environmentally hazardous substances and excessive use of energy, respectively [18,19]. Alternatively, AgNPs can be prepared *via* a more friendly pathway, for example using biological extracts. Indeed, plant extracts are rich in biological molecules such as polyphenols, polysaccharides, proteins which can be exploited for the reduction of silver ions, and the subsequent capping of the produced AgNPs [20].

Thus, we prepared AgNPs by this green process and incorporate them into chitosan films to prepare CS/AgNPs bio nanocomposites. Then, we studied their innovative properties for two applications such as antimicrobial food packaging and water remediation.

Indeed, water pollution is one of the biggest worldwide challenges in this century. Among the groundwater contaminants, nitro-aromatic compounds are known as the most intractable

organic pollutants in industrial and agricultural wastewaters [21]. These are highly toxic to humans, animals, and plants, and they may pose a serious threat to human life and the environment, even at low concentrations [22]. Over the last few years, several methods have been reported for degradation, transformation, or removal of nitro-aromatics compounds from wastewater, including for example, electrochemical and photochemical degradation, ozonation, and adsorption [23]. Among all these methods, catalytic hydrogenation has been proved to be an impressive and environmentally benign approach. Indeed, this available and efficient technology reduces harmful pollutants and can simultaneously generate high value-added products. In this context, the CS/AgNPs nanocomposites could also be considered an excellent candidate as heterogeneous catalysts for the controlled and selective hydrogenation of nitroarenes. Indeed, the CS chemical functionalities are known to have a high affinity with transition metals, and CS has been used as support in a wide variety of heterogeneous catalytic systems [24,25]. Indeed, the use of CS as solid support for metal nanoparticles (MNPs) increases their stability, reactivity, selectivity, and reusability. Such nano-composites [MNPs-CS] have been widely employed in various catalytic protocols [26] and were obtained using either an *in-situ* or an *ex-situ* approach. In the *in-situ* approach, MNPs were prepared inside the CS matrix either by exploiting the reducing and capping power of CS [27] or by adding other toxic reducing agents to produce small MNPs [28]. On the other hand, in the *ex-situ* approach, the already prepared MNPs are only mixed with CS allowing the formation of MNPs with tuned characteristics before their incorporation into CS and, better control of important features such as the size [29]. Moreover, the *ex-situ* approach is more scaled-up [30].

In the present study, we prepared Rosemary extract mediated AgNPs (R-AgNPs) via a simple biological pathway. These AgNPs were embedded into CS to form CS/R-AgNPs nanocomposites via a simple solution mixing technique. The prepared CS/R-AgNPs were characterized using Thermogravimetric Analysis (TGA), Fourier Transform InfraRed spectroscopy (FTIR), and Transmission Electron microscopy (TEM). Afterward, the nanocomposites were tested for the two potential applications i) as antimicrobial food packaging by assessing their antibacterial activity against a Gram-negative bacterium, *Escherichia coli*, and a Gram-positive bacterium, *Staphylococcus aureus*, two bacteria highly associated with food contaminations and widely used as model bacteria and ii) in water treatment by the evaluation of their heterogeneous catalytic activity in the reduction of 4 nitroaniline (4-NA) as a model of industrial contaminant.

VI.2) Material and methods

VI.2.1) Materials

Chitosan powder (Molecular weight = 310000 - 375000 Da, Degree of deacetylation > 75%) was obtained from Sigma Aldrich (USA). Silver nitrate was purchased from Fluka Chemika (France). BHI and BHI agar were purchased from Fischer Chemical (France) and PBS was purchased from Sigma Aldrich (France). All chemicals were used as received.

VI.2.2) Silver nanoparticles preparation

Green silver nanoparticles (R-AgNPs) were prepared following an optimized protocol using rosemary leaves extract as a reducing and stabilizing agent (Nabgui *et al.*, submitted). Briefly, rosemary leaves extract was prepared using 10 g of dried leaves in 100 mL of milliQ water. 10 mL of the prepared extract was then added to 90 mL of an aqueous solution of silver nitrate (AgNO_3) with a final concentration of 1 mM. and the mixture was stirred at 80°C for 15 min. The prepared R-AgNPs were washed and purified three times using centrifugation at 9300 g for 15 min.

VI.2.3) Chitosan-AgNPs films preparation

Four grams of Chitosan (CS) were dissolved in 100 mL of 1% (v/v) acetic acid at room temperature. Afterwards, 1 g of CS/R-AgNPs films were prepared by mixing the appropriate amount of the previous CS solution and the green AgNPs to have 0.5 wt%, 1 wt%, 1.5 wt%, 2 wt%, and 3 wt% of R-AgNPs with regard to CS (the films were noted respectively CS/0.5% R-AgNPs, CS/1% R-AgNPs, CS/1.5% R-AgNPs, CS/2% R-AgNPs, and CS/3% R-AgNPs). The solution was kept under stirring for 2 h and then was ultrasonicated for 15 min. The solution was then cast onto Petri dishes (78.5 cm²) and allowed to dry at room temperature. Films were peeled off and immersed in a 2 M NaOH solution.

Finally, the antibacterial activity of CS, CS/0.5% R-AgNPs, CS/1%R-AgNPs, and CS/1.5% R-AgNPs was tested. As preliminary results showed that a higher R-AgNPs content might be needed for the catalytic activity, CS, CS/1% R-AgNPs, CS/2% R-AgNPs, and CS/3% R-AgNPs films were chosen to assess the heterogeneous catalytic activity of CS/R-AgNPs nanocomposites.

VI.2.4) Characterization of Silver nanoparticles

UV-vis spectroscopy was used to confirm the synthesis of silver nanoparticles using a Shimadzu UV-2600 spectrophotometer. The Zeta Potential was determined using a Malvern

ZetaSizer NanoZS device. Transmission electronic microscopy (TEM) was used to determine the size and distribution of silver nanoparticles using a Hitachi HT7800 device operating at an accelerating voltage of 100 Kv.

VI.2.5) Characterization of CS/R-AgNPs films

The prepared CS/AgNPs were characterized using multiple techniques. Thermogravimetric analysis (TGA) was performed using a TGA 55 Discovery device at a rate of $20^{\circ}\text{C min}^{-1}$ under nitrogen in the range of 25°C to 800°C . FTIR analysis was performed using a Thermo Scientific™ Nicolet™ iS™ 50 instrument in attenuated total reflection (ATR) mode. Spectra were recorded in the range of $400\text{-}4000\text{ cm}^{-1}$ with a spectral resolution of 4 cm^{-1} . The distribution and aggregation state of R-AgNPs in the CS matrix was assessed with TEM using a Hitachi HT7800 device operating at an accelerating voltage of 100 Kv.

VI.2.6) Assessment of antibacterial activity of CS and CS/R-AgNPs films

VI.2.6.1) Bacterial strains

Two bacterial strains, a Gram-positive strain, *Staphylococcus aureus* (ATCC 29213), and a Gram-negative strain, *Escherichia coli* (K12 MG1655) were used to evaluate the antibacterial activity of neat CS and CS/R-AgNPs films. Bacterial strains were maintained at -20°C in 30% glycerol. All strains were precultured in Brain Heart Infusion nutritive medium (BHI, Bacto™) at 37°C and 140 rpm for 16 h under aerobic conditions. The bacterial suspension was diluted in a BHI medium to obtain an approximated bacterial concentration of either 4.10^5 Colony Forming Units (CFU). mL^{-1} or 5.10^9 CFU. mL^{-1} estimated through the optical density measurement at 595 nm. The exact bacterial concentration was determined by counting on BHI-agar (Difco™).

VI.2.6.2) Antibacterial activity of CS and CS/R-AgNPs films

Native CS and CS/R-AgNPs films antibacterial activity was assessed by counting the adhered *S. aureus* and *E. coli* on the surface of nanocomposites discs ($d=0.8\text{mm}$). The discs were immersed in 3 mL of the previously prepared bacterial suspensions and were incubated at 37°C for 18 h at 140 rpm. The films were then gently washed using sterile PBS and allowed to dry under sterile conditions. Then they were immersed in a 3 mL sterile PBS solution and were sonicated for 3 min to remove the adhered bacteria from the surface. Decimal dilutions, *i.e.*, 10^{-1} , 10^{-2} , 10^{-3} , and 10^{-4} of the bacterial suspension were spread onto BHI agar plates. After incubation for 24 h at 37°C , the colonies were enumerated and

expressed as CFU.cm⁻². Three independent enumerations were carried out for each assay. The inhibition values were expressed as percentages compared to the number of adhered bacteria on native CS film as a control.

VI.2.6.3) Catalytic reduction of 4-NA

The catalytic reduction of 4-NA using CS/R-AgNPs films was assessed using NaBH₄ as a reducing agent. Briefly, 0.5 mL of NaBH₄ (1 M) was mixed with 2.5 mL of an aqueous solution of 4-NA (1 mM) at room temperature under constant stirring. 7.2 mg of CS/R-AgNPs films with different percentages of R-AgNPs (1, 2, or 3 wt%) were introduced into the reaction medium, and samples were taken at regular times for UV-Vis spectroscopy measurements. The reaction was performed without catalyst as a negative control and with 3 µl of a 2.5 wt% R-AgNPs solution as a positive control. In order to test the recyclability of the catalytic system, after each experiment, the CS/R-AgNPs film was removed from the reaction medium, washed with distilled water for 10 min under gentle mixing, then dried at room temperature, and reused for another 4-NA reduction reaction following the same procedure.

VI.3) Results and discussion

VI.3.1) Synthesis and Characterization of silver nanoparticles

Silver nanoparticles used for the preparation of Chitosan (CS)/Silver nanoparticles (R-AgNPs) blends were prepared using an *ex-situ* biosynthesis approach. As described in the introduction section, this approach allows more control over nanoparticles characteristics such as the size and it is easily scaled up compared to the *in-situ* approach [29,30].

R-AgNPs were prepared using Rosemary extract as a reducing and capping agent at 80°C for 15 min. The UV-vis spectrum confirmed the synthesis of narrowly distributed R-AgNPs as depicted in Fig. V.1. TEM analysis (Fig. V.2) showed also a narrow distribution of spherical R-AgNPs with an average size of 31.11±6.49 nm. Finally, the stability of the R-AgNPs was evaluated using Zeta potential measurement. Indeed, AgNPs are considered stable when the absolute value of their Zeta potential is higher than 30 mV [32]. For the prepared R-AgNPs, Zeta potential measurements revealed a value of -34.45mV indicating a stable dispersion due to the negatively charged rosemary extract molecules adsorbed onto the surface of nanoparticles.

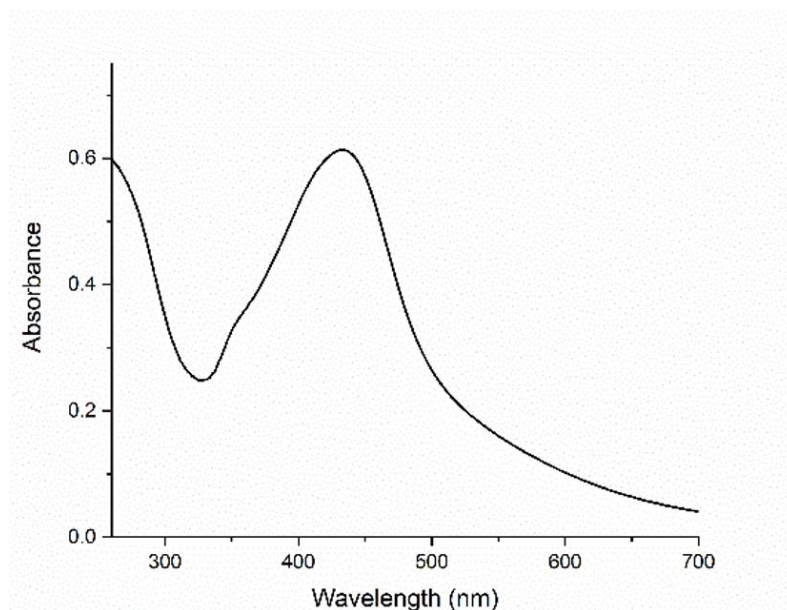


Figure V.1: UV-Vis Spectrum of Rosemary extract mediated R-AgNPs prepared at 80°C.

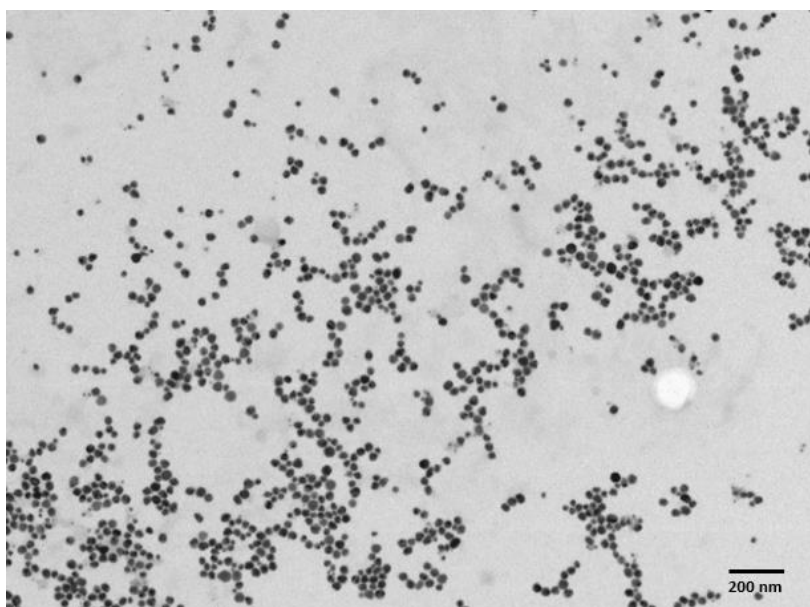


Figure V.2: TEM result of R-AgNPs prepared at 80°C.

VI.3.2) Preparation and Characterization of CS/AgNPs films

The effect of R-AgNPs loading ratio in CS/R-AgNPs films was studied using different AgNPs percentages, 0.5%, 1%, 1.5%, 2%, and 3% (w/w). Solvent casting method by mixing a 2.5% (w/v) CS solution in 1% acetic acid with the corresponding quantity of AgNPs was used as illustrated in Fig. V.3. After being peeled off, the films were immersed in a 2 M NaOH solution to prevent their disintegration as discussed in the introduction section.

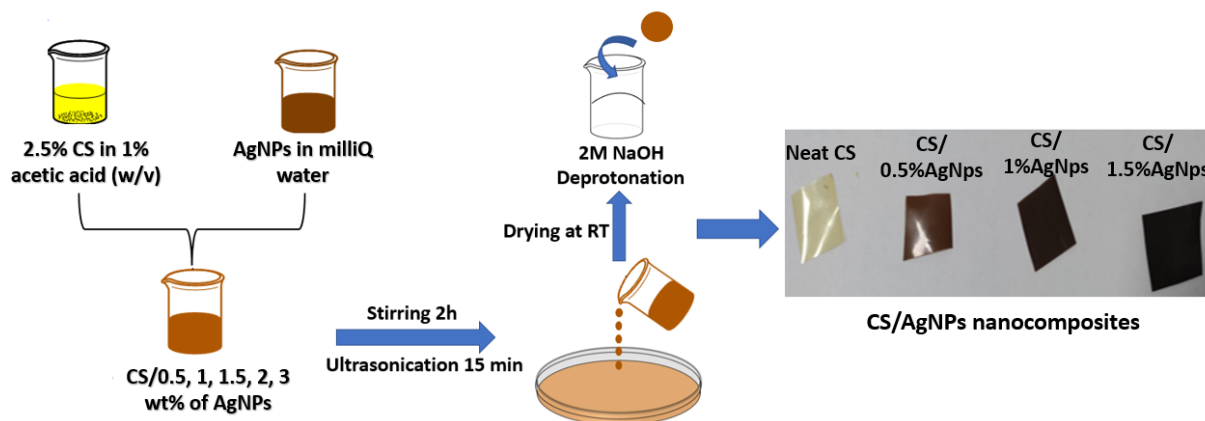


Figure V.3: Protocol of the preparation of CS and CS/AgNPs nanocomposites at different AgNPs loadings.

FTIR analysis is an effective tool to study the interaction between multiple-component materials via the identification of changes in the binding of the functional groups. Fig. V.4 shows FTIR spectra of native CS film and CS/AgNPs nanocomposites for the highest AgNPs concentration (*i.e.*, 3%) in order to better visualize the effect of the incorporation of AgNPs into CS on the signals of the different functions of CS especially acetamide (NHCOCH_3) and amine (NH_2). Moreover, expected the intensity of some bands, whatever the AgNPs amounts the spectra were similar (data not shown)

The slight shift observed in the resonance of the acetamide NHCOCH_3 at 1641 cm^{-1} to 1635 cm^{-1} demonstrates a significant interplay of these functional groups with the metal nanoparticles and its surrounding outer-sphere by acid-base donation (mainly by $-\text{C}=\text{O}-\text{AgNPs}$) highlighting the stabilization of AgNPs by CS as reported by Affes *et al.*, (2021) [26,31].

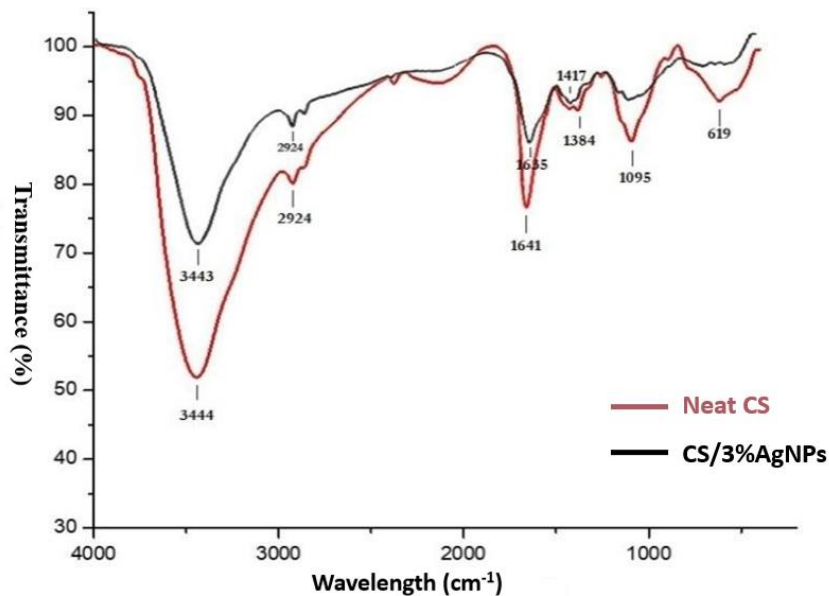


Figure V.4: FTIR spectra of native CS and CS/3% R-AgNPs films.

TGA analysis was used to measure the thermal stability of CS and CS/AgNPs films (Fig. V.5). All materials had a similar degradation profile with only a slight difference at 150°C, probably due to the residual water molecules in the films entrapped in the CS chains. Above 150°C, all films followed a classic CS thermal degradation curve corresponding to the dehydration, depolymerization, and pyrolytic decomposition of the chitosan backbone [31]. However, the presence of R-AgNPs in the CS matrix increased slightly the thermal stability of CS, which could probably be explained by the restriction of CS chains mobility [32]. Other studies have reported a similar slight increase in thermal stability using similar AgNPs loadings prepared using an *in-situ* approach [27,33].

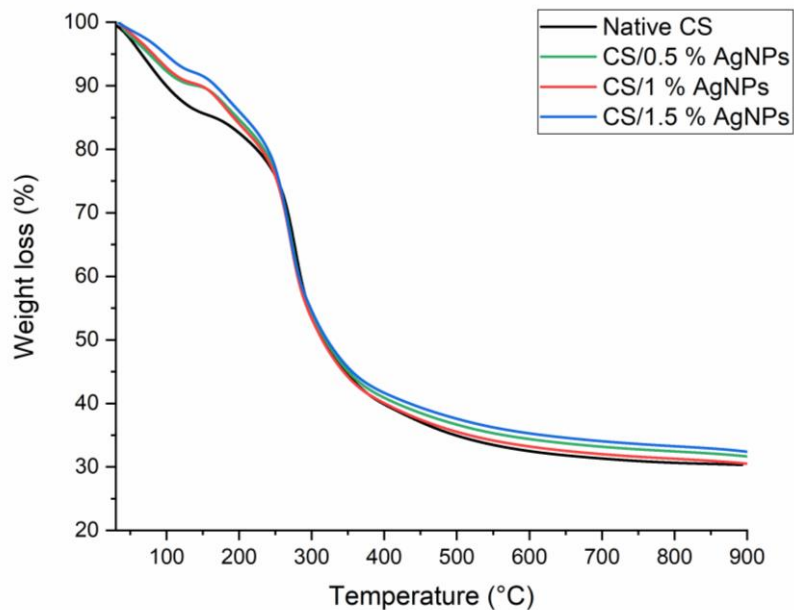


Figure V.5: TGA curves of native CS and CS/R-AgNPs films.

The morphological study using TEM analysis was carried out to measure the distribution of AgNPs in the CS matrix as well as its aggregation state. The TEM images of neat CS (Fig. V.6A) and CS/1.5% AgNPs (Fig. V.6B) showed good distribution of AgNPs within the CS matrix. However, as demonstrated by TEM size calculations, R-AgNPs in the CS matrix have aggregated as evidenced by an increase of AgNPs size from 31.11 ± 6.49 nm to 169 ± 70 nm for free R-AgNPs and R-AgNPs in CS, respectively. Very few studies have compared the size of AgNPs before and after their introduction in a CS matrix and the majority of reported works have used an *in-situ* approach for the synthesis of CS/AgNPs nanocomposites. In a study using an *ex-situ* approach, You *et al.*, (2017) [34] described similar results with about a 4-fold increase of AgNPs size in Collagen/Chitosan scaffolds compared to the free AgNPs.

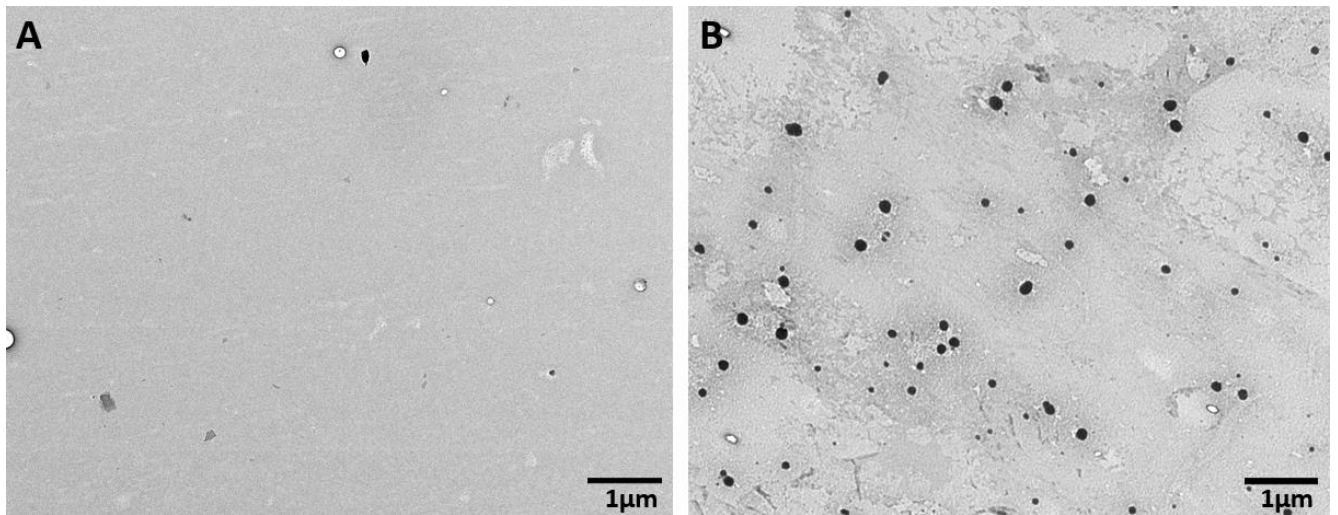


Figure V.6: TEM images of A) Neat CS and B) CS/1.5%R-AgNPs nanocomposites.

VI.3.3) Antibacterial activity of CS and CS/R-AgNPs films

Antibacterial activity of CS and CS nanocomposites was assessed against both Gram-positive bacteria *S. aureus* and Gram-negative bacteria *E. coli* by counting the number of adhered bacteria on the surface of the films after 18 hours.

First, an initial concentration of around 4×10^5 CFU.mL⁻¹ of bacteria was used (Table V.1. Neat CS films showed a bacterial concentration on their surface of 4.2×10^4 CFU. cm⁻² and 1.7×10^4 CFU. cm⁻² for *E. coli* and *S. aureus*, respectively. The introduction of R-AgNPs for all tested loadings (*i.e.*, 0.5%, 1, and 1.5%) exhibited a total inhibition of the bacterial adhesion on the surface of the films. Even if an initial bacterial concentration of 10^5 CFU.mL⁻¹ is already higher than the concentrations found in real life, in order to test the effect of R-AgNPs concentration, the initial concentration of bacteria was increased to about 5×10^9 CFU. mL⁻¹ and the experiment was repeated following the same procedure as used previously. At this bacterial concentration, a higher number of adhered bacteria on the neat CS films was observed (*i.e.*, 1.45×10^6 CFU. cm⁻² for *E.coli* and 2.17×10^6 CFU. cm⁻² for *S. aureus*) compared to the lower initial bacterial concentration. As shown in Table V.1, CS/R-AgNPs films exhibited a significant inhibition in the bacterial adhesion on their surface compared to native CS films for all tested R-AgNPs concentrations. The inhibition reached about 82% and 85% against *E. coli* and *S. aureus* respectively, with only 0.5% R-AgNPs loaded films. We noticed that the inhibition increased with the percentage of R-AgNPs to about 95% against both tested bacteria for 1.5% of R-AgNPs.

Table V.1: The inhibition percentage of *E. coli* (Light grey) and *S. aureus* (Dark grey) adhesion on CS/R-AgNPs nanocomposites compared to native CS films (n=3).

Sample	Adhesion inhibition percentage Bacterial initial concentration 4×10^5 CFU.mL ⁻¹		Adhesion inhibition percentage Bacterial initial concentration 5×10^9 CFU.mL ⁻¹	
	<i>E. coli</i>	<i>S. aureus</i>	<i>E. coli</i>	<i>S. aureus</i>
	CS/0.5% R-AgNPs	> 99.99	> 99.99	82.45±2.38
CS/1% R-AgNPs	> 99.99	> 99.99	89.80±5.24	93.14±1.32
CS/1.5% R-AgNPs	> 99.99	> 99.99	94.70±1.65	95.97±1.93

These results showed that CS films loaded with a very low concentration of R-AgNPs could exhibit high antibacterial activity against both Gram-positive and Gram-negative bacteria even when these films were deprotonated. To study if the modified CS films have antiadhesive or antibacterial properties, R-AgNPs used for the preparation of CS/AgNPs films were tested in solution in a previous work against both *E. coli* and *S. aureus* and showed minimal inhibitory concentration (MIC) of 37.5 and 75 $\mu\text{g. mL}^{-1}$, respectively, and a minimal bactericidal concentration (MBC) of 150 $\mu\text{g. mL}^{-1}$ against both bacteria (Nabgui *et al.*, submitted). Indeed, AgNPs are considered excellent antibacterial agents against both Gram-positive and Gram-negative bacteria by affecting the bacterial cells directly or through the release of silver ions. Both AgNPs and silver ions interact with membranes, proteins, and nucleic acids leading to the disruption of their functioning [35]. Moreover, AgNPs produce bacterial death through the generation of Reactive Oxygen Species (ROS), which generate cell lipid peroxidation and DNA damage leading to the apoptosis of the cells [35,36].

1.1. Catalytic activity of CS/R-AgNPs

As mentioned above, AgNPs present, in addition to their antibacterial activity, a catalytic effect on different chemical reactions. The catalytic property of the prepared CS/R-AgNPs catalysts in the reduction of nitro-aromatics compounds to their corresponding anilines was performed in an aqueous medium at room temperature by using NaBH₄ as a hydrogen generator. The reaction was monitored by using UV-Vis spectroscopy at 380 nm (Fig. V.7). As can be seen in Fig. V.7A, in the absence of R-AgNPs and the presence of NaBH₄, there is no change in the 4-NA absorbance peak, however, when only 3 μl of 2.5% (w/v) R-AgNPs are added (Fig. V.7B), a total conversion of 4-NA to 4-phenylenediamine (4-PD) was achieved within 40 seconds as evidenced by the disappearance of the 380 nm peak (λ_{max} of 4-NA) and the appearance of 240 nm absorbance peak corresponding to 4-PD. Fig. V.7C shows the conversion result of CS/3% R-AgNPs over time. We observed the decrease of the absorbance peak of 4-NA with time to reach a complete conversion within 15 min. In another experiment (Fig. V.7D), the films were

removed after 7 min and the reaction was stopped almost immediately proving the absence of R-AgNPs residue released in medium.

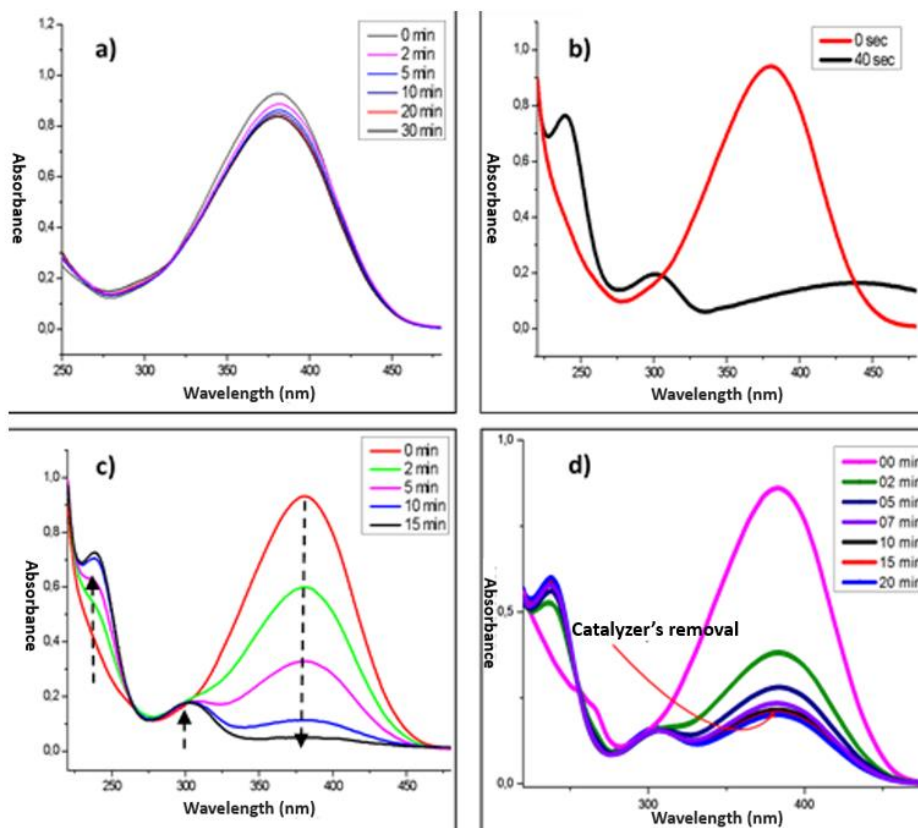


Figure V.7: UV-Vis result for the reduction of 4-NA to 4-PD: A) Without catalysts, B) Free 3 μl of 2.5% R-AgNPs as catalysts, C) CS/3% R-AgNPs film as catalysts, D) The elimination of the catalyst after 7 min.

To compare the effect of R-AgNPs concentration on the 4-NA reduction reaction, films with different loading of R-AgNPs were tested containing 1%, 2%, or 3% of R-AgNPs (w/w). As the NaBH₄ concentration used in the experiment was in excess, the reaction is probably a pseudo first-order reaction with a rate law equation corresponding to:

$$-K \cdot t = \ln \left(\frac{A_t}{A_0} \right)$$

Where A_t is the absorbance at a giving time t and A_0 is the initial absorbance.

The rate reaction K was calculated from the slope of plotting $\ln(A_t/A_0)$ versus time. As shown in Fig. V.8. the linear fit confirms a pseudo first-order kinetic. Moreover, it is apparent that the

catalytic reaction rate increases with the increase of R-AgNPs loading: 0.09 min^{-1} for CS/1% R-AgNPs, 0.11 min^{-1} for CS/2% R-AgNPs, and 0.20 min^{-1} for CS/3% R-AgNPs, respectively.

NaBH_4 , even though a powerful reducing agent, requires the presence of a metal catalyst to achieve the successful hydrogenation of 4-NA. The reduction of 4-NA to 4-PD by NaBH_4 in the presence of R-AgNPs is based on the Langmuir-Hinshelwood mechanism in which R-AgNPs facilitate electrons transfer from BH_4^- to 4-NA. BH_4^- molecules adsorbed onto the surface of R-AgNPs provide electrons useful to reduce 4-NA, also adsorbed on the surface. The product of the reaction 4-PD is then desorbed from the surface of R-AgNPs [37,38]. CS films act as a supporting material allowing the easy recovery of the catalyst and its immobilization, thus preventing its aggregation.

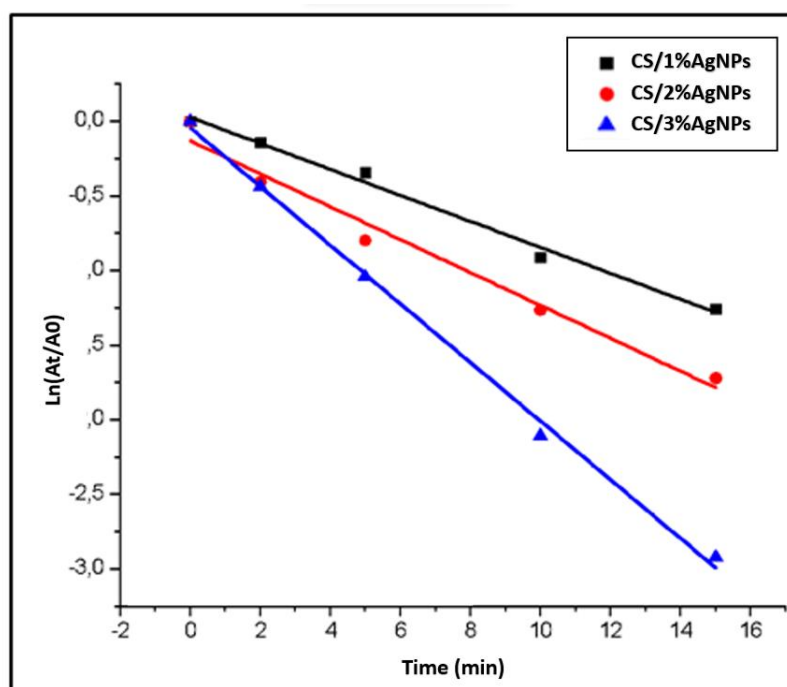


Figure V.8: The plot of $\ln(A_t/A_0)$ vs time for 4-NA reduction using CS nanocomposites with different R-AgNPs loadings.

VI.3.4) Recyclability of the CS/R-AgNPs catalyst

The stability and the reusability of the catalyst are the main factors that defined its efficiency and are essential for industrial and large scales applications. To evaluate this recyclability, the CS/R-AgNPs catalyst was reused in several consecutive reaction cycles (Fig. V.9). The graph shows the conversion (%) obtained with CS/3% R-AgNPs film plotted against the number of cycles, after each cycle, the film was washed once with distilled water. After 10 consecutive cycles, the film kept a very high conversion of 96%. The slight decrease after the 10th cycle was

probably due to the physical loss of a small portion of the catalyst during the washing steps [39]. The result proves that the CS/3% R-AgNPs films can be used as excellent catalysts for the hydrogenation of 4-NA. Similar systems were tested in the literature and found similar results [40,41]. Indeed, Alshehri *et al.*, (2016) prepared CS-AgNPs-multiwalled carbon nanotubes nanocomposites using an *in-situ* approach which were applied in the reduction of 4-nitrophenol. In this work, the author used a much higher AgNPs loading (6.4 wt%) obtaining a significantly smaller rate constant ($0.13 \times 10^{-3} \text{ min}^{-1}$) [41].

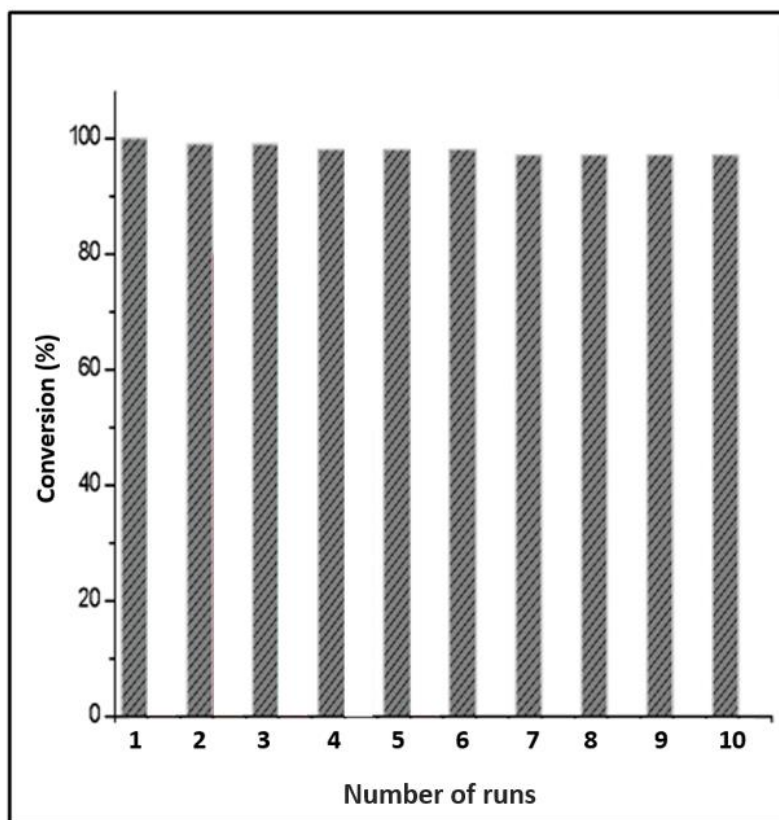


Figure V.9: The recyclability of CS/3% R-AgNPs film for the 4-NA reduction.

VI.4) Conclusion

In this work, small-sized silver nanoparticles (R-AgNPs) were prepared using rosemary extract as a reducing and stabilizing agent. These R-AgNPs were used in a simple *ex-situ* preparation with Chitosan (CS) to form CS/R-AgNPs nanocomposites films with different loadings of R-AgNPs. CS/R-AgNPs were characterized using multiple techniques such as FTIR, TGA, and TEM demonstrating a well distributed R-AgNPs inside the CS matrix and also evidencing the interaction between AR-AgNPs and CS.

CS/R-AgNPs films showed an excellent antibacterial activity against both bacteria inhibiting their growth on the surface of films at all tested R-AgNPs loadings (*i.e.*, 0.5%, 1%, and 1.5%). Indeed, even at the lowest R-AgNPs loading (*i.e.*, 0.5%), complete inhibition of bacterial growth on the films surfaces was observed at an initial bacterial concentration of $4 \cdot 10^5$ CFU.mL⁻¹. The deprotonation of CS films is necessary to maintain the stability and integrity of CS films in contact with water. However, it also compromises the antibacterial activity of CS. Therefore, the use of R-AgNPs is an effective strategy to obtain CS-based films with excellent antibacterial activity, even when deprotonated.

CS/R-AgNPs nanocomposites have also proven to be an efficient heterogeneous catalytic system for the dehydrogenation of toxic 4-Nitroaniline in presence of NaBH₄. The reaction followed a pseudo-first order kinetics with a R-AgNPs dose-dependent rate constant K as follow: 0.09 min⁻¹ for CS/1% R-AgNPs, 0.11 min⁻¹ for CS/2% R-AgNPs, and 0.20 min⁻¹ for CS/3% R-AgNPs. Moreover, the recyclability study showed that even after 10 consecutive cycles, the film kept a very high conversion of 96%.

This work demonstrated that CS/R-AgNPs films are good candidates for applications in active food packaging as well as water treatment.

Acknowledgment

This project was financially supported by French-Morocco bilateral programs by CAMPUS FRANCE: PHC TOUBKAL/18/71 and APUR 2019. This work was also performed with the support of the Erasmus+ program of the European Union (Mobility at the university of Zagreb HRZAGREB01) and Projet prioritaire (PPR1/2015/73).

Conflict of interest

The authors declare no conflict of interest.

Reference

- [1] B.E. Abdelmalek, A. Sila, A. Haddar, A. Bougatef, M.A. Ayadi, β -Chitin and chitosan from squid gladius: Biological activities of chitosan and its application as clarifying agent for apple juice, *Int. J. Biol. Macromol.* 104 (2017) 953–962. <https://doi.org/10.1016/j.ijbiomac.2017.06.107>.
- [2] L. Xu, Y.-A. Huang, Q.-J. Zhu, C. Ye, Chitosan in Molecularly-Imprinted Polymers: Current and Future Prospects, *Int. J. Mol. Sci.* 16 (2015) 18328–18347. <https://doi.org/10.3390/ijms160818328>.
- [3] S. Pokhrel, P.N. Yadav, Functionalization of chitosan polymer and their applications, *J. Macromol. Sci. Part A.* 56 (2019) 450–475. <https://doi.org/10.1080/10601325.2019.1581576>.
- [4] B.S. Inbaraj, T.-Y. Tsai, B.-H. Chen, Synthesis, characterization and antibacterial activity of superparamagnetic nanoparticles modified with glycol chitosan, *Sci. Technol. Adv. Mater.* 13 (2012) 015002. <https://doi.org/10.1088/1468-6996/13/1/015002>.
- [5] B. Sultankulov, D. Berillo, K. Sultankulova, T. Tokay, A. Saparov, Progress in the Development of Chitosan-Based Biomaterials for Tissue Engineering and Regenerative Medicine, *Biomolecules.* 9 (2019) 470. <https://doi.org/10.3390/biom9090470>.
- [6] S. Yadav, G.K. Mehrotra, P.K. Dutta, Chitosan based ZnO nanoparticles loaded gallic-acid films for active food packaging, *Food Chem.* 334 (2021) 127605. <https://doi.org/10.1016/j.foodchem.2020.127605>.
- [7] J. Zhu, X. Zhang, Z. Qin, L. Zhang, Y. Ye, M. Cao, L. Gao, T. Jiao, Preparation of PdNPs doped chitosan-based composite hydrogels as highly efficient catalysts for reduction of 4-nitrophenol, *Colloids Surf. Physicochem. Eng. Asp.* 611 (2021) 125889. <https://doi.org/10.1016/j.colsurfa.2020.125889>.
- [8] M. del R. Moreira, S.I. Roura, A. Ponce, Effectiveness of chitosan edible coatings to improve microbiological and sensory quality of fresh cut broccoli, *LWT - Food Sci. Technol.* 44 (2011) 2335–2341. <https://doi.org/10.1016/j.lwt.2011.04.009>.
- [9] S.R. Kanatt, M.S. Rao, S.P. Chawla, A. Sharma, Effects of chitosan coating on shelf-life of ready-to-cook meat products during chilled storage, *LWT - Food Sci. Technol.* 53 (2013) 321–326. <https://doi.org/10.1016/j.lwt.2013.01.019>.
- [10] J. Li, S. Zhuang, Antibacterial activity of chitosan and its derivatives and their interaction mechanism with bacteria: Current state and perspectives, *Eur. Polym. J.* 138 (2020) 109984. <https://doi.org/10.1016/j.eurpolymj.2020.109984>.
- [11] R.C. Goy, D. de Britto, O.B.G. Assis, A review of the antimicrobial activity of chitosan, *Polímeros.* 19 (2009) 241–247. <https://doi.org/10.1590/S0104-14282009000300013>.
- [12] S.M. Ojagh, M. Rezaei, S.H. Razavi, S.M.H. Hosseini, Effect of chitosan coatings enriched with cinnamon oil on the quality of refrigerated rainbow trout, *Food Chem.* 120 (2010) 193–198. <https://doi.org/10.1016/j.foodchem.2009.10.006>.
- [13] S. Shankar, D. Khodaei, M. Lacroix, Effect of chitosan/essential oils/silver nanoparticles composite films packaging and gamma irradiation on shelf life of strawberries, *Food Hydrocoll.* 117 (2021) 106750. <https://doi.org/10.1016/j.foodhyd.2021.106750>.
- [14] J. Krisch, R. Tserennadmid, C. Vágvölgyi, Essential oils against yeast and moulds causing food spoilage, *Sci. Microb. Pathog. Commun. Curr. Res. Technol. Adv. Microbiol.* (2011).
- [15] M. k. Rai, S. d. Deshmukh, A. p. Ingle, A. k. Gade, Silver nanoparticles: the powerful nanoweapon against multidrug-resistant bacteria, *J. Appl. Microbiol.* 112 (2012) 841–852. <https://doi.org/10.1111/j.1365-2672.2012.05253.x>.

- [16] F. Ortega, L. Giannuzzi, V.B. Arce, M.A. García, Active composite starch films containing green synthesized silver nanoparticles, *Food Hydrocoll.* 70 (2017) 152–162. <https://doi.org/10.1016/j.foodhyd.2017.03.036>.
- [17] R.E. Morsi, A.M. Alsabagh, S.A. Nasr, M.M. Zaki, Multifunctional nanocomposites of chitosan, silver nanoparticles, copper nanoparticles and carbon nanotubes for water treatment: Antimicrobial characteristics, *Int. J. Biol. Macromol.* 97 (2017) 264–269. <https://doi.org/10.1016/j.ijbiomac.2017.01.032>.
- [18] M. Khan, M.R. Shaik, S.F. Adil, S.T. Khan, A. Al-Warthan, M.R.H. Siddiqui, M.N. Tahir, W. Tremel, Plant extracts as green reductants for the synthesis of silver nanoparticles: lessons from chemical synthesis, *Dalton Trans.* 47 (2018) 11988–12010. <https://doi.org/10.1039/C8DT01152D>.
- [19] O. Pryshchepa, P. Pomastowski, B. Buszewski, Silver nanoparticles: Synthesis, investigation techniques, and properties, *Adv. Colloid Interface Sci.* 284 (2020) 102246. <https://doi.org/10.1016/j.cis.2020.102246>.
- [20] S. Kumar, I.B. Basumatary, H.P.K. Sudhani, V.K. Bajpai, L. Chen, S. Shukla, A. Mukherjee, Plant extract mediated silver nanoparticles and their applications as antimicrobials and in sustainable food packaging: A state-of-the-art review, *Trends Food Sci. Technol.* 112 (2021) 651–666. <https://doi.org/10.1016/j.tifs.2021.04.031>.
- [21] A.K. Sasmal, S. Dutta, T. Pal, A ternary Cu₂O–Cu–CuO nanocomposite: a catalyst with intriguing activity, *Dalton Trans.* 45 (2016) 3139–3150. <https://doi.org/10.1039/C5DT03859F>.
- [22] D.H. Blakey, K.L. Maus, R. Bell, J. Bayley, G.R. Douglas, E.R. Nestmann, Mutagenic activity of 3 industrial chemicals in a battery of in vitro and in vivo tests, *Mutat. Res. Toxicol.* 320 (1994) 273–283. [https://doi.org/10.1016/0165-1218\(94\)90080-9](https://doi.org/10.1016/0165-1218(94)90080-9).
- [23] Z. Wu, X. Yuan, H. Zhong, H. Wang, G. Zeng, X. Chen, H. Wang, L. Zhang, J. Shao, Enhanced adsorptive removal of p-nitrophenol from water by aluminum metal–organic framework/reduced graphene oxide composite, *Sci. Rep.* 6 (2016) 25638. <https://doi.org/10.1038/srep25638>.
- [24] E. Guibal, Heterogeneous catalysis on chitosan-based materials: a review, *Prog. Polym. Sci.* 30 (2005) 71–109. <https://doi.org/10.1016/j.progpolymsci.2004.12.001>.
- [25] M.S.J. Khan, S.B. Khan, T. Kamal, A.M. Asiri, Catalytic Application of Silver Nanoparticles in Chitosan Hydrogel Prepared by a Facile Method, *J. Polym. Environ.* 28 (2020) 962–972. <https://doi.org/10.1007/s10924-020-01657-3>.
- [26] S. Frindy, A. el Kadib, M. Lahcini, A. Primo, H. García, Copper Nanoparticles Stabilized in a Porous Chitosan Aerogel as a Heterogeneous Catalyst for C–S Cross-coupling, *ChemCatChem*. 7 (2015) 3307–3315. <https://doi.org/10.1002/cctc.201500565>.
- [27] G. López-Carballo, L. Higuera, R. Gavara, P. Hernández-Muñoz, Silver Ions Release from Antibacterial Chitosan Films Containing in Situ Generated Silver Nanoparticles, *J. Agric. Food Chem.* 61 (2013) 260–267. <https://doi.org/10.1021/jf304006y>.
- [28] A. Shah, I. Hussain, G. Murtaza, Chemical synthesis and characterization of chitosan/silver nanocomposites films and their potential antibacterial activity, *Int. J. Biol. Macromol.* 116 (2018) 520–529. <https://doi.org/10.1016/j.ijbiomac.2018.05.057>.
- [29] S. Briceño, E.A. Chavez-Chico, G. González, Diatoms decorated with gold nanoparticles by In-situ and Ex-situ methods for in vitro gentamicin release, *Mater. Sci. Eng. C*. 123 (2021) 112018. <https://doi.org/10.1016/j.msec.2021.112018>.
- [30] M. Zahran, A.H. Marei, Innovative natural polymer metal nanocomposites and their antimicrobial activity, *Int. J. Biol. Macromol.* 136 (2019) 586–596. <https://doi.org/10.1016/j.ijbiomac.2019.06.114>.
- [31] S. Affes, H. Maalej, I. Aranaz, H. Kchaou, N. Acosta, Á. Heras, M. Nasri, Controlled size green synthesis of bioactive silver nanoparticles assisted by chitosan and its

- derivatives and their application in biofilm preparation, *Carbohydr. Polym.* 236 (2020) 116063. <https://doi.org/10.1016/j.carbpol.2020.116063>.
- [32] C.-W. Chou, S. Hsu, H. Chang, S.-M. Tseng, H.-R. Lin, Enhanced thermal and mechanical properties and biostability of polyurethane containing silver nanoparticles, *Polym. Degrad. Stab.* 91 (2006) 1017–1024. <https://doi.org/10.1016/j.polymdegradstab.2005.08.001>.
- [33] G.O. Akalin, O. Oztuna Taner, T. Taner, The preparation, characterization and antibacterial properties of chitosan/pectin silver nanoparticle films, *Polym. Bull.* (2021). <https://doi.org/10.1007/s00289-021-03667-0>.
- [34] C. You, Q. Li, X. Wang, P. Wu, J.K. Ho, R. Jin, L. Zhang, H. Shao, C. Han, Silver nanoparticle loaded collagen/chitosan scaffolds promote wound healing via regulating fibroblast migration and macrophage activation, *Sci. Rep.* 7 (2017) 10489. <https://doi.org/10.1038/s41598-017-10481-0>.
- [35] I.X. Yin, J. Zhang, I.S. Zhao, M.L. Mei, Q. Li, C.H. Chu, The Antibacterial Mechanism of Silver Nanoparticles and Its Application in Dentistry, *Int. J. Nanomedicine.* 15 (2020) 2555–2562. <https://doi.org/10.2147/IJN.S246764>.
- [36] M.A. Quinteros, V. Cano Aristizábal, P.R. Dalmaso, M.G. Paraje, P.L. Páez, Oxidative stress generation of silver nanoparticles in three bacterial genera and its relationship with the antimicrobial activity, *Toxicol. In Vitro.* 36 (2016) 216–223. <https://doi.org/10.1016/j.tiv.2016.08.007>.
- [37] S.G. Jiji, K.G. Gopchandran, Shape dependent catalytic activity of unsupported gold nanostructures for the fast reduction of 4-nitroaniline, *Colloid Interface Sci. Commun.* 29 (2019) 9–16. <https://doi.org/10.1016/j.colcom.2018.12.003>.
- [38] Z.H. Farooqi, R. Khalid, R. Begum, U. Farooq, Q. Wu, W. Wu, M. Ajmal, A. Irfan, K. Naseem, Facile synthesis of silver nanoparticles in a crosslinked polymeric system by in situ reduction method for catalytic reduction of 4-nitroaniline, *Environ. Technol.* 40 (2019) 2027–2036. <https://doi.org/10.1080/09593330.2018.1435737>.
- [39] N. Alhokbany, T. Ahama, Ruksana, M. Naushad, S.M. Alshehri, AgNPs embedded N-doped highly porous carbon derived from chitosan based hydrogel as catalysts for the reduction of 4-nitrophenol, *Compos. Part B Eng.* 173 (2019) 106950. <https://doi.org/10.1016/j.compositesb.2019.106950>.
- [40] I. Ahmad, T. Kamal, S.B. Khan, A.M. Asiri, An efficient and easily retrievable dip catalyst based on silver nanoparticles/chitosan-coated cellulose filter paper, *Cellulose.* 23 (2016) 3577–3588. <https://doi.org/10.1007/s10570-016-1053-4>.
- [41] S.M. Alshehri, T. Almuqati, N. Almuqati, E. Al-Farraj, N. Alhokbany, T. Ahamad, Chitosan based polymer matrix with silver nanoparticles decorated multiwalled carbon nanotubes for catalytic reduction of 4-nitrophenol, *Carbohydr. Polym.* 151 (2016) 135–143. <https://doi.org/10.1016/j.carbpol.2016.05.018>.

General conclusion and future works

General conclusion and future works

Conventional food packaging systems using petroleum-based plastics are widely used to extend the shelf life of food. However, these polymers are non-biodegradable, thus, they constitute an environmental problem. Moreover, they do not provide active antimicrobial protection. Thus, the need to develop new sustainable eco-friendly, and antimicrobial active materials is of utmost importance. In that regard, my thesis entitled “Development of composites based on biodegradable polymers and natural fillers for potential applications in food packaging” is carried out in a collaboration between Cadi Ayyad University in Marrakesh, Morocco, and the University of Rouen Normandie in Rouen, France.

At first, PCL-OBnt nanocomposites (Chapter II) were prepared using a “*Grafted from*” ROP approach in open air and under solvent-free conditions. The used bentonite (Bnt) is a Moroccan natural clay of the smectite group was chosen due to its sheet-like structure and its high surface area. However, its hydrophilicity raises a compatibility problem between Bnt and the hydrophobic PCL. In order to solve this problem, Bnt was organo-modified using CTAB, a quaternary ammonium with a long alkyl chain (16-Carbon chain). The organomodification using CTAB increases both the hydrophobicity of Bnt and its interlamellar spacing (d); thus, allowing Bnt to enhance the physical properties of PCL (Mechanical and thermal properties). Moreover, CTAB is a surfactant with an inherent antibacterial activity, therefore it can render the resulting nanocomposites bioactive. Indeed, the incorporation of OBnt (1wt%, 5wt%, and 10wt%) enhanced the thermal stability of PCL and increased its hydrophobicity, a parameter that is highly sought-after in materials applied in food packaging as it limits the transfer of moisture from the external environment to the food and vice-versa. PCL-OBnt nanocomposites have also shown an enhanced tensile strength compared to pristine PCL (*i.e.*, 66 MPa for PCL-5%Obnt vs 46 MPa for neat PCL). Finally, the antibacterial activity of PCL-OBnt nanocomposites showed an inhibition of more than 96% of the bacterial growth against both *S. aureus* and *S. epidermidis* using only 1wt% of OBnt. When the OBnt loading was increased to 5%, the bacterial growth was inhibited by more than 99%. These results show the potential of CTAB-modified Bnt to enhance the physical properties of PCL as well as to provide a high antibacterial activity to the resulting nanocomposites. As a result, these PCL-Obnt nanocomposites are good candidates for potential application in active food packaging.

Always in the pursuit of the same objective, nanocomposites of PLA-Fluorophlogopite-AgNPs (Chapter III) were developed using melt extrusion. This approach is preferable as it is the most

used in the thermoplastic polymers industry. Fluorophlogopite is a modified Mica in which -OH groups were substituted with F groups, making it more hydrophobic which increases the compatibility between the polymer and the filler, allowing us to skip the organomodification step. As for AgNPs, they were chosen in order to provide the antibacterial activity to the resulting composites. This choice was based on i) the high antibacterial activity of AgNPs against a wide range of pathogens and ii) their low migration from the nanocomposites to food, allowing thus preserving the organoleptic properties of food. The incorporation of fluorophlogopite enhanced substantially the thermal stability of neat PLA. Indeed, the addition of 2wt% of fluorophlogopite increased T_{Onset} of PLA from 315°C to 338°C and $T_{50\%}$ from 342°C to 360°C. Moreover, the incorporated fillers did not affect the barrier properties (Water vapor sorption, water permeability, and Gas permeability to O₂, CO₂, and N₂) of neat PLA, comparable already to the barrier properties of conventional plastics. Finally, PLA-2%fluorophlogopite-1.5% AgNPs showed excellent inhibition of bacterial adhesion after 16 h of contact (*i.e.*, 89%, 92%, and 76% against *S. aureus*, *E. faecalis*, and *E. coli*, respectively). These results show that these nanocomposites could be used as excellent active food packaging materials.

The results of chapter III have shown the important potential of AgNPs as antibacterial additives for the preparation of active packaging materials. Moreover, most of AgNPs available on the market today are prepared chemically using toxic reducing agents such as NABH₄ or hydrazine. Among the other methods, the biological pathway using plant extracts is an ideal choice as its ecofriendly as well as cost-effective. In chapter IV, one of the objectives was to optimize the biosynthesis of AgNPs using an aqueous extract of rosemary (*Salvia rosmarinus* Spenn). Rosemary was chosen because it is an aromatic and medicinal plant rich in secondary metabolites that are highly implicated in the reduction and stabilization of AgNPs. At first, the biosynthesis of AgNPs was optimized in terms of temperature and reaction time leading to choosing 80 °C for 15 min as reaction parameters. Small-sized and uniformly distributed AgNPs (31.1±6.5 nm using TEM) were thus produced and characterized using multiple techniques. FTIR and ATG results also showed the implication of rosemary biomolecules in the synthesis and stabilization of AgNPs. Subsequently, the assessment of the antibacterial activity of AgNPs showed MICs values of 18.75 µg.ml⁻¹ against *E. faecalis*, 75 µg.ml⁻¹ against *S. aureus*, and 37.5 µg.ml⁻¹ against *E. coli* and *P. aeruginosa*. These AgNPs showed a much higher antibacterial activity compared to the commercial AgNPs used in the preparation of PLA nanocomposites (Chapter III).

The stability of AgNPs is another important parameter, but not as well studied as the other parameters such as the size or surface charge. Indeed, all AgNPs properties are highly dependent on their size, and consequently, on their stability. For that reason, we evaluated the stability of the prepared AgNPs in function of time which showed an aggregation after 1 month. Consequently, enhancing their stability is a must. In that pursuit, three surfactants differing by their charge were used, CTAB (a cationic surfactant), SDS (an anionic surfactant), and Tween 80 (a non-ionic surfactant). After 6 months, all these surfactants enhanced substantially the stability of AgNPs using very low concentrations (3-7 μM). Then, we studied the effect of surfactants on the antibacterial activity and the cytotoxicity of AgNPs. A substantial enhancement of the antibacterial activity was obtained using 3 μM of CTAB against *S. aureus* but not against *E. coli*. Finally, none of the prepared AgNPs, surfactants-capped or not, have shown any cytotoxicity against L929 mammalian fibroblasts.

In order to validate the use of AgNPs prepared in the work presented in chapter IV, we used these AgNPs as a nanofiller for the preparation of chitosan-AgNPs films via a simple technique of solution mixing/solvent casting (Chapter V). Chitosan (CS) is a natural and biodegradable polysaccharide with an inherent bacteriostatic activity which makes it an ideal candidate for applications in food packaging. However, in contact with water, CS disintegrates unless its amine groups are deprotonated, but then again, the deprotonation of these groups deprives CS of its bacteriostatic activity. Therefore, in order to restore, broaden, and enhance the antibacterial CS films, AgNPs were used. FTIR results showed the interaction between CS functional groups and AgNPs ($-\text{C}=\text{O}-\text{AgNPs}$). Subsequently, the antibacterial activity of these films was evaluated against two model bacteria: *E. coli* and *S. aureus*. These nanocomposites showed an important inhibition of the bacterial adhesion on their surface. Indeed, using only 0.5 wt% of AgNPs, we obtained an inhibition of 82% against *E. coli* and 85% against *S. aureus* compared to neat CS. Finally, due to the potential of metal nanoparticles in the hydrogenation of nitroarenes, we tested CS-AgNPs films as heterogeneous catalytic systems in the hydrogenation of 4-nitroaniline. The films showed an important catalytic activity with a rate constant K of 0.09 min^{-1} , 0.11 min^{-1} , and 0.20 min^{-1} for CS-1%AgNPs, CS-2%AgNPs, and CS-3%AgNPs films, respectively. Moreover, CS-AgNPs were recyclable, and even after 10 consecutive runs, these films maintained 96% of their catalytic activity. These results prove that these films could be used in potential applications in food packaging and water remediation.

In a summary, during this thesis, we prepared multiple antibacterial nanocomposites for potential application in antibacterial food packaging. We used different preparation techniques

(*i.e.*, ROP, melt extrusion, and solution mixing). These nanocomposites were characterized while focusing on their thermal, barrier, and antibacterial properties. All these nanocomposites showed a great potential for applications in antibacterial food packaging particularly, PLA-Fluorophlogopite-AgNPs. These films, in addition to their excellent physical properties (Thermal, mechanical, and barrier properties), have shown an important antibacterial activity by contact and not by diffusion, indicating a low migration of the antibacterial agent. As a continuity of this work, multiple perspectives could be explored.

Regarding the elaboration of nanocomposites:

- A real-life application of the prepared nanocomposites using food (*e.g.*, meat). The effectiveness of these materials could be tested by comparing the total bacterial growth on food packaged by the antibacterial nanocomposites to food packaged by a conventional plastic (*e.g.*, PE). Finally, the shelf life of food could be compared and a migration test for the antibacterial agent could be performed.
- The polymers we used in this work are all biodegradable (PCL, PLA, and chitosan). However, the introduction of nanofillers, especially antibacterial nanofillers could affect their biodegradability by inhibiting microorganisms' growth. Thus, it would be interesting to study the effect of the incorporation of nanofillers on the biodegradation of these nanocomposites compared to the native form of their polymers.
- Based on our results, other applications could be explored such as in the medical field. More precisely, these nanocomposites could be used in the coating of implantable medical devices (*e.g.*, vascular grafts, catheters, *etc.*). These devices are a favorite target for bacterial colonization, hence, the necessity for antibacterial and antiadhesive coating. The results shown by PLA-Fluorophlogopite-AgNPs (antibacterial activity by contact), make these nanocomposites an ideal candidate for such an application.

Regarding the biosynthesis of AgNPs:

- During this thesis, we noticed major issues regarding the reproducibility of the biosynthesis of AgNPs using plant extracts. These issues are caused primarily by the variability of the chemical composition of the extract which could have many sources that are very hard to control (Variability between plant species, varietal variability within the same species, seasonal variability within the same variety, *etc.*). Given that reproducibility is essential, solving this problem is a must. In that regard, characterizing the plant extract using one or more measurable parameters could solve this issue.

Thereby, using the “redox potential” of the plant extract as such a parameter seems interesting. In that regard, everything else being equal, one could plot the result of the biosynthesis of AgNPs (size, SPR band, *etc*) in function of the redox potential of plant extracts and see if a relationship (linear or not) could be found. Finally, the coefficient of determination R^2 could be determined.

Résumé étendu en Français:

Développement de composites à base de polymères biodégradables et de charges naturelles pour une potentielle application en emballage alimentaire

Résumé étendu

I. Introduction générale

Les contaminations alimentaires par les micro-organismes pathogènes constituent l'un des problèmes majeurs de l'industrie alimentaire à cause des pertes énormes qu'elles posent tant sur le plan sanitaire que sur le plan économique. Selon l'Organisation Mondiale de la Santé (l'OMS), les pathogènes alimentaires causent approximativement 600 millions de cas de maladie et 420 milles décès chaque année dans le monde. Economiquement, ces pathogènes causent des pertes d'environ 152 milliards de dollars chaque année aux États-Unis [1]. De plus, environ 1,3 milliards de tonnes des pertes annuelles des aliments sont attribuées aux contaminations par des pathogènes [2]. Afin de lutter contre ces contaminations, plusieurs méthodes sont utilisées tels que la congélation, la réfrigération, les traitements thermiques, l'utilisation d'additifs et l'utilisation des emballages alimentaires [3]. D'autre part, l'utilisation des emballages alimentaires est essentielle pour protéger les aliments des facteurs de l'environnement extérieur tels que la poussière, les gaz et l'humidité [4].

Les matériaux utilisés dans l'emballage alimentaire sont généralement des plastiques d'origine pétrolière comme le polyéthylène (PE), le polyamide (PA) et le polystyrène (PS) [5] car ils présentent de bonnes propriétés mécaniques et barrières. Cependant, leur origine fossile et leur non-biodégradabilité posent des problèmes environnementaux majeurs [5]. De plus, ces polymères ne présentent pas une activité antibactérienne intrinsèque et par conséquent, ils n'offrent pas une protection active contre les bactéries [6]. L'enjeu est donc le développement de matériaux d'emballage actif pouvant limiter les contaminations microbiennes et par conséquent, prolonger la durée de stockage des aliments. Selon le règlement de la Commission N° 450/2009, un emballage alimentaire actif est défini comme un emballage qui offre une protection au-delà de la protection barrières vis-à-vis de l'environnement extérieur [7]. Ceci concerne, par exemple, des matériaux avec une activité antimicrobienne capable de réduire, inhiber ou retarder la croissance des microorganismes [8].

L'utilisation de matériaux antimicrobiens biodégradables respectueux de l'environnement pour l'emballage alimentaire actif est par conséquent, indispensable pour un développement durable. Pour cela, des polymères avec une activité antimicrobienne intrinsèque peuvent être utilisés comme le chitosane [9]. L'incorporation d'agents antibactériens au sein des polymères ou des composites constitue également un moyen de développement de matériau d'emballage actif. En

effet, des acides organiques [10], des enzymes [11], des huiles essentielles [12] et des nanoparticules métalliques [13,14] ont été utilisés comme additifs antibactériens aux matériaux d'emballage. Parmi les nanoparticules métalliques utilisées, les nanoparticules d'argent (AgNPs) sont considérées comme des additifs antibactériens prometteurs à cause de leur activité antibactérienne importante contre une large gamme de bactéries pathogènes, notamment *Escherichia coli*, *Pseudomonas aeruginosa*, *Staphylococcus aureus*, *Listeria monocytogenes* et *Salmonella spp.* [15–18]. De plus, les AgNPs n'ont quasiment aucun effet sur les propriétés organoleptiques des aliments contrairement aux extraits des plantes (*e.g.*, les huiles essentielles) [19].

L'emballage actif doit avoir également de bonnes propriétés mécaniques et barrières à l'oxygène et à l'humidité [3]. Cependant, ces propriétés sont relativement faibles dans les polymères biodégradables tels que le polycaprolactone (PCL), le polylactide (PLA) et les polysaccharides comme le chitosane (CS). Afin de pouvoir améliorer ces propriétés, plusieurs techniques sont développées tels que la copolymérisation [20], la préparation de micro- ou de nanocomposites *via* l'incorporation de charges telles les argiles [21,22]. La préparation de nanocomposites reste la méthode de choix car elle offre une meilleure amélioration des propriétés physiques des polymères avec une quantité de charges plus faible que dans le cas de microcomposites [23] et elle permet un meilleur contrôle des propriétés finales des matériaux par rapport à la copolymérisation.

Dans ce contexte, le présent travail de thèse explore la préparation de nanocomposites à base d'une matrice des polymères biodégradables et de différentes charges naturelles afin d'élaborer des emballages alimentaires actifs.

Ce manuscrit de thèse est rédigé en anglais et il est constitué de 5 chapitres : le premier représente une synthèse bibliographique sur les matériaux utilisés dans l'emballage alimentaire et les méthodes de préparation d'emballage actifs à base de polymères biodégradables et de charges naturels ; les chapitres II à V décrivent et discutent les différents matériaux élaborés dans le cadre de cette thèse, à savoir l'élaboration des nanocomposites de PCL/Bentonite organo-modifiée (OBnt) *via* la polymérisation par ouverture de cycle (POC) (chapitre II), de PLA/Fluorophlogopite/AgNPs par extrusion à l'état fondu (Chapitre III), la synthèse d'AgNPs par voie biologique (Chapitre IV) et la préparation de nanocomposites à base de chitosane et des AgNPs synthétisées par voie biologique.

II. Synthèse bibliographique sur la synthèse des matériaux d'emballage alimentaire antibactérien

Les plastiques d'origine pétrolière présentent actuellement la majorité des emballages alimentaires utilisés dans la vie quotidienne. Cependant, comme discuté dans l'introduction, ils posent des problèmes majeurs liés à leur non biodégradabilité ainsi qu'à leur inaptitude à inhiber la croissance des bactéries d'origine alimentaire. Parmi les solutions proposées afin de lutter contre ces problèmes est l'utilisation des nanocomposites à base de polymères biodégradables.

Ainsi, le PCL, le PLA et le chitosane sont des polymères biodégradable et biocompatible avec un potentiel important pour des applications en emballage alimentaire. Cependant, ceci est conditionné par l'amélioration de leur propriétés thermique, mécanique, barrières et antibactériennes [24–27]. Afin d'améliorer ces propriétés, on a généralement recours à plusieurs techniques, dont la préparation des nanocomposites par incorporation des nanocharges [28]. Les nanocomposites à base de polymères sont définis comme étant des matériaux formés de deux ou plusieurs phases dont au moins une phase est nanométrique [29]. Ceci permet d'avoir de nouveaux matériaux avec des propriétés améliorées ou même nouvelles. Le tableau I.1 (**page 13**) résume les études portant sur la synthèse des matériaux antibactériens à base de PCL, PLA et de chitosane.

Plusieurs types de charges sont utilisées pour la préparation des nanocomposites et elles peuvent être distinguées par leurs dimensions en : i) des nanocharges 1D (*e.g.*, nanotubes de carbone) ; ii) des nanocharges 2D (*e.g.*, nanofeuillets comme les phyllosilicates) et iii) des nanocharges 0D (*e.g.*, les nanoparticules) [30]. Parmi ces charges, les argiles 2D comme la montmorillonite, la bentonite et le mica, ont reçu le plus d'attention à cause de leur origine naturelle, leur abondance et leur potentiel énorme d'améliorer les propriétés thermiques, barrières et mécaniques des polymères grâce à leur structure feuilletée et leur surface spécifique très élevée. Ce type de nanocharges agissent généralement en limitant le transfert des gaz et des produits de dégradation thermique grâce à l'augmentation de la tortuosité et la formation d'une couche de char [31].

Le deuxième type de nanocharges d'intérêt pour le développement des nanocomposites antibactérien s'agit de nanocharges pourvues d'une activité antibactérienne. Généralement, l'introduction du caractère antibactérien est achevée par l'utilisation des molécules organiques qui peuvent être toxiques et peuvent migrer du matériau d'emballage vers les aliments, et par conséquent, les contaminer ou affecter leurs propriétés organoleptiques. Alternativement, des

nanoparticules d'argent peuvent être utilisées comme excellent agents antibactériens contre une large gamme de pathogènes avec une migration des AgNPs de l'emballage vers les aliments qui se retrouve généralement au-dessous de la limite autorisée (0,01 mg/kg de nourriture) par le règlement de la commission (CE) N° 450/2009 [7,32].

Ces nanoparticules d'argent (AgNPs) sont préparées en utilisant des méthodes physiques, chimiques ou biologiques [33–35]. Les deux premiers types utilisent généralement des molécules organiques toxiques (méthodes chimiques) ou nécessite un usage excessif d'énergie (méthodes physiques). Comme alternative respectueux de l'environnement, des méthodes biologiques peuvent être employées. Dans ces méthodes, généralement les extrait de plantes sont utilisées comme des agents réducteurs et stabilisateurs des AgNPs.

III. Nanocomposites antibactériens de PCL-Bentonite

Le polycaprolactone (PCL) est un polyester biodégradable. Il est synthétisé généralement par deux méthodes (i) la polycondensation de l'acide hydroxycarboxylique et (ii) la POC de l' ϵ -CL. La polycondensation génère des PCLs avec un faible poids moléculaire, entraînant ainsi des propriétés mécaniques faibles et une dispersité importante. Pour ces raisons, la POC est préférable pour l'application visée car elle permet l'obtention d'un polymère avec un poids moléculaire important et une faible dispersité. Cependant, le PCL présente des propriétés mécaniques et thermiques faibles, ce qui limite ces applications. Pour faire face à ces problèmes, la préparation des nanocomposites par incorporation de nanocharges semble être une voie prometteuse. Mais, l'incompatibilité entre l'argile hydrophile et le PCL hydrophobe limite le renforcement des propriétés du PCL, d'où la nécessité d'amélioration de la compatibilité entre ces deux phases. Dans ce travail, nous avons utilisé une POC *in-situ* via une approche « *grafting from* » pour associer le PCL à la bentonite (Bnt) de manière covalente. La bentonite naturelle a été choisie comme nanocharge grâce à sa structure lamellaire et à sa grande surface spécifique. Pour améliorer la compatibilité entre le PCL et la Bnt, cette dernière a été rendue hydrophobe par modification par du bromure de cetyltriméthylammonium (OBnt) (**Fig. II.1, page 67**). En parallèle, le catalyseur $\text{Sn}(\text{C}\equiv\text{CPh})_4$ a été préparé selon le protocole expérimental décrit par Jousseume et *al.*, (2002) [36]. Pour la préparation des nanocomposites de PCL-OBnt, 1%, 5% ou 10% de Obnt (p/p) a été mélangé à d' ϵ -CL dans un erlenmeyer de 50ml et dispersé sous ultrason pendant 10min. Ensuite, le catalyseur $\text{Sn}(\text{C}\equiv\text{CPh})_4$ préparé selon le protocole expérimental décrit par Jousseume *et al.*, (2002) [36], a été injecté au mélange Obnt/ ϵ -CL à un ratio (ϵ -CL/ $(\text{Sn}(\text{C}\equiv\text{CPh})_4 = 500)$), et l'ensemble a été mis sous agitation pendant

2h à température ambiante. Afin d'obtenir la conversion totale, le mélange a été placé à 120°C pendant 15 min (**Fig. II.1, page 67**).

Pour préparer les films, les nanocomposites ont été dissous dans 2ml de dichlorométhane pendant 1h jusqu'à dissolution totale. La solution a ensuite été coulée dans des moules en Teflon et laissée sécher pendant 24h à température ambiante. Les films séchés ont été décollés des moules et pressés à l'aide d'une presse hydraulique à chaud (**Fig. II.2, page 68**).

Dans ce processus de préparation des nanocomposites de PCL-Bnt, l'organomodification de la Bnt est une étape nécessaire pour deux raisons, premièrement pour améliorer la compatibilité entre le PCL et la Bnt en augmentant son hydrophobicité et deuxièmement pour augmenter l'espace interlamellaire (d). Effectivement, les résultats de la diffraction des rayons X (DRX) de la Bnt, avant et après l'organomodification, montrent un décalage du pic du plan cristallographique (001) vers une valeur plus basse à 2θ , montrant une augmentation de l'espace interlamellaire (d) de 7,34 Å à 11,32 Å. De plus, après la POC, le pic du plan cristallographique (001) a passé de 4° à presque 1° (2θ) montrant ainsi l'intercalation des chaînes de PCL entre les feuillets de l'OBnt. Effectivement, l'OBnt présente sur sa surface des groupes hydroxyles qui agissent comme des co-initiateurs de la polymérisation. Ces groupes sont plus accessibles après l'organomodification pour réagir avec le catalyseur pour former des centres actifs -Sn-O-OBnt. La POC commence après le chauffage à 120°C par un mécanisme de coordination insertion (Fig. VI.1) où l' ϵ -CL se coordine au centre réactif par sa fonction carbonyle, suivi par l'insertion du monomère dans le centre actif via une attaque nucléophile menant à l'ouverture du monomère au niveau de la liaison O-acyl.

Plusieurs techniques ont été effectuées afin de caractériser les biocomposites de PCL-OBnt. Les résultats de la chromatographie d'exclusion stérique (SEC) (**Tableau II.1, page 73**) montrent le succès de la POC *in situ* en utilisant l'OBnt. Quand on augmente le pourcentage d'OBnt de 1% à 5% ou à 10%, on observe une diminution des valeurs de M_n de 65973 g.mol⁻¹ à 33556 et 20092 g.mol⁻¹ respectivement. Ce résultat est attendu car une teneur plus élevée de la OBnt augmente le nombre des centres actifs Sn-O-OBnt et par conséquent, la synthèse des chaînes polymériques plus courtes. De plus, la faible dispersité D observée dans ces expériences montrent que la polymérisation se produit au moins en partie par un mécanisme contrôlé et des réactions de transestérification limitées.

Ensuite, l'analyse thermogravimétrique (ATG) des biocomposites a été effectuée afin d'évaluer leur stabilité thermique. Les thermogrammes affichés dans la figure II.6 (**page 76**) montre que

la dégradation du PCL natif commence à 315°C alors que la dégradation des biocomposites de PCL-OBnt commence à 320°C. Ces résultats montrent une augmentation légère de la stabilité thermique quand les nanocharges d'argile sont ajoutées. Ces résultats sont dus au fait que les feuillets d'argile forment des couches protectrices limitant la diffusion des gaz et des composés volatiles de la dégradation [37,38].

L'analyse des propriétés mécaniques du PCL natif et des biocomposites de PCL-OBnt a été effectuée. La figure II.8 (**page 78**) montre les résultats de la résistance à la traction et l'allongement à la rupture. Le PCL natif montre l'allongement à la rupture le plus élevé ($\approx 18\%$) alors que tous les biocomposites de PCL-OBnt montrent des valeurs inférieures à 5%. Cette différence est causée par la réduction de la mobilité des chaînes du PCL induites par l'incorporation de nanocharges ce qui conduit à des tensions locales plus élevées et entraîne la rupture des liaisons chimiques. Finalement, les résultats de la résistance à la traction montrent que les films de PCL et PCL-OBnt ont une résistance à la traction proportionnelle à leurs masses molaires moyennes.

L'activité antibactérienne des films de PCL et PCL-OBnt a été évaluée par diffusion (**Figure II.10, page 80**) et en suspension (**Tableau II.2, page 80**) contre *Staphylococcus epidermidis* et *S. aureus*. Pour le test de diffusion sur Agar, des disques du PCL et du PCL-OBnt ($d=2,6\text{cm}$) ont été placés sur des boîtes de Petri de BHI-Agar inoculées par une concentration de 10^6 UFC/ml de *S. aureus* ou *S. epidermidis*. Les films de PCL natif n'ont pas montré une zone d'inhibition contre les deux bactéries testées alors que les biocomposites PCL-OBnt ont montré une zone d'inhibition proportionnelle à leur teneur en OBnt. De plus, les zones d'inhibition contre *S. aureus* sont légèrement inférieures à celles contre *S. epidermidis*.

Ensuite, le pourcentage d'inhibition des bactéries par les films du PCL natif et des biocomposites a été calculé dans du milieu liquide (tableau VI.2). Les films ont montré une activité importante contre les deux bactéries testées. En fait, une inhibition quasiment totale des bactéries *S. epidermidis* et *S. aureus* a été obtenue par les films de PCL-1%OBnt : 96,3% contre *S. epidermidis* et 97,9% contre *S. aureus*. Ces résultats sont expliqués par l'organomodification de la bentonite en utilisant le CTAB, un surfactant cationique bactéricide. Cette explication est supportée par l'augmentation de l'activité antibactérienne (par diffusion et en suspension) quand la teneur de la bentonite est augmentée.

Ces résultats montrent qu'avec seulement 1% de Bnt organo-modifiée par le CTAB, on peut préparer des biocomposites de PCL-OBnt par une POC *in situ* en utilisant une approche

« *Grafted from* ». Ces biocomposites montrent des masses molaires moyennes élevées, une stabilité thermique et une résistance à la traction supérieure à celle du PCL natif. Du plus, les composites PCL-1%OBnt révèlent une activité antibactérienne importante contre *S. epidermidis* et *S. aureus*. Ainsi, ces films peuvent être utilisés comme des emballages alimentaires actifs. Cependant, les résultats de l'activité antibactérienne montrent qu'il y a une diffusion de l'agent antibactérien des films vers le milieu de culture. Ceci peut engendrer des problèmes de contaminations des aliments par l'agent antibactérien d'une part et de perte progressive de l'activité antibactérienne des films.

IV. Nanocomposites antibactériens de PLA-Fluorphlogopite-Nanoparticules d'argents (AgNPs)

Les problématiques soulevées lors de la dernière section ainsi que la nature pétrolière du PCL nous ont poussé à explorer une nouvelle voie plus respectueuse de l'environnement et qui peut générer des matériaux avec une activité antibactérienne par contact et non par diffusion. Pour cela, nous avons choisi un autre polymère biodégradable mais cette fois d'origine naturelle, le polylactide (PLA) ainsi qu'un autre type de nanocharges antibactériennes (*i.e.*, les nanoparticules d'argent).

Ainsi, dans cette section, la conception de nanocomposites de PLA-Fluorphlogopite-Nanoparticules d'argent par un processus simple d'extrusion à l'état fondu a été développée. Le choix du fluorphlogopite pour améliorer les propriétés intrinsèques du PLA (*i.e.*, propriétés thermiques, barrières et mécaniques), réside dans sa structure lamellaire similaire à celle de la Bnt et à son caractère hydrophobe dû à la substitution des groupements OH, présent dans le mica naturel, par des groupements F⁻. Ce caractère hydrophobe doit permettre d'augmenter la compatibilité entre le PLA et la nanocharge.

Les nanoparticules d'argents (AgNPs) ont été choisies pour leur activité antibactérienne [39]. Elles présentent de nombreux avantages par rapport aux molécules organiques (*e.g.*, CTAB), notamment leur faible migration une fois piégées dans les composites. D'autre part, elles n'affectent pas les propriétés organoleptiques des aliments, paramètre important dans les applications en emballage alimentaire actif. La figure (**Graphical abstract, page 90**) résume la méthodologie de synthèse des films de PLA-Fluorphlogopite-AgNPs et présente un aperçu sur les résultats obtenus.

En premier, différents pourcentages de fluorphlogopite (*i.e.*, 2%, 5% et 10% (p/p)) ont été utilisés pour préparer des nanocomposites binaires PLA-Fluorphlogopite par extrusion à l'état

fondu. Les films de ces matériaux ont été produits par une presse hydraulique. La caractérisation des films par la microscopie électronique à balayage (MEB) et l'ATG montrent une bonne dispersion de la charge au sein de la matrice polymérique avec une augmentation de la rugosité et une amélioration de la stabilité thermique de PLA par l'ajout de la nanocharge. En effet, le $T_{50\%}$ passe de 334°C pour les films de PLA natif à 365°C pour les films de PLA-2%Fluorphlogopite (**Figure III.SI-1, page 127**). Ces résultats sont probablement dus à la structure lamellaire de la fluorphlogopite dont les feuillets peuvent agir comme une barrière qui réduit le transfert des gaz et des produits volatiles de la dégradation (isolation thermique). Cependant, l'augmentation de fluorphlogopite à 5% diminue la stabilité thermique des films. Cette diminution peut être attribuée à l'agrégation des particules d'argile au-delà de certain pourcentage ($\leq 5\%$). Or, l'augmentation du pourcentage de fluorphlogopite à 10% augmente la stabilité thermique des films. Cette amélioration de stabilité peut être expliquée par la taille des agrégats qui devient assez grande pour pouvoir agir comme une barrière des gaz et des produits volatiles [40]. En tenant compte des résultats d'ATG et de MEB, 2% de fluorphlogopite a été choisi pour préparer les films tertiaires de PLA-fluorphlogopite-AgNPs.

En utilisant la même approche que celle décrite au-dessus, des films tertiaires de PLA-2%Fluorphlogopite ont été préparés en incorporant différents pourcentages massiques des AgNPs (*i.e.*, 0,5, 1 et 1,5%). L'analyse morphologique par microscopie électronique à transmission (MET) a été effectuée et les micrographes des films sont présentés dans la figure III.2 (**page 103**) Ces micrographes montrent une bonne dispersion des deux charges utilisées, les particules de la fluorphlogopite (Cercles en vert) et les AgNPs (Cercles en rouge). De plus, les résultats de la DRX montrent également un décalage de pic du plan cristallographique (001) vers la gauche indiquant une augmentation de l'espace interlamellaire (d) et alors, une intercalation des chaînes de PLA dans la charge d'argile. Ensuite, les résultats d'angle de contact de l'eau de ces films montrent une augmentation de l'hydrophobicité dans les films contenant de la fluorphlogopite.

Les paramètres thermiques de fusion et de cristallisation du PLA natif et des nanocomposites ont été évalués par la calorimétrie différentielle à balayage (DSC). Les résultats calculés de la première montée sont résumés dans le tableau III.1 (**page 107**). Ces résultats montrent que l'addition des charges, seules ou combinées, induisent une augmentation de la température de fusion (T_m) indiquant que ces charges se comportent comme des agents de nucléation. De plus, l'ajout des charges a induit une diminution du taux de cristallinité. Ces résultats pourront

apparaître contradictoires (*i.e.*, les charges comportant comme des agents de nucléation et la diminution de χ_c), sont expliqués par une possible exfoliation partielle [41].

Ensuite, les propriétés mécaniques et barrières à l'eau et aux gaz ont été évaluées à cause de leur importance dans les applications en emballage alimentaire. L'analyse des propriétés mécaniques montre qu'il n'y a pas de changement significatif entre les films de PLA natif et les nanocomposites préparés que ce soit pour le module de Young que pour l'allongement à la rupture.

Pour les propriétés barrières, les résultats du flux d'eau réduit expérimental ($J \cdot L$) et normalisé (J/J_{st}) en fonction du temps réduit (t/L^2) sont montrés dans la figure III.11 (**page 117**). Ces résultats montrent que l'incorporation (fluorophlogopite et AgNPs) n'a aucun effet significatif sur la perméabilité à l'eau. Ceci peut être attribué à leur faible teneur au sein de la matrice de PLA. Ces résultats sont en accord avec les valeurs de la sorption à la vapeur d'eau.

De plus, la perméabilité aux N_2 , O_2 et CO_2 , un autre facteur important pour des applications en emballage alimentaire a été testé (**Figure III.12, page 120**) a suit la même tendance dans tous les films testés : $P(N_2) < P(O_2) < P(CO_2)$. Ces résultats sont expliqués par les différences des températures critiques de ces gaz (*i.e.*, CO_2 ayant une température critique élevée : $31,15^\circ C$ et N_2 ayant une température critique très basse : $-146,94^\circ C$). En comparant les différents films, l'introduction des charges (Fluorophlogopite et AgNPs) n'a pas induit un grand changement de la perméabilité aux trois gaz indiquant que peu ces charges n'ont pas induit de tortuosité importante. En résumé, les propriétés barrières, déjà excellente de PLA et comparables aux polymères d'emballage classique, ont été maintenues après l'ajout des charges.

L'activité antibactérienne des films du PLA et des nanocomposites a été évaluée en testant l'adhésion de 3 bactéries sur la surface des films (**Figure III.13, page 122**), tous les nanocomposites ont inhibé l'adhésion de *S. aureus*, *Escherichia coli* et *Enterococcus faecalis* par rapport au PLA natif. Cette inhibition est plus importante dans les films contenant les nanoparticules d'argent. Les films de PLA-2% Fluorophlogopite-1,5% AgNPs ont montré une inhibition d'adhésion de 89%, 92% et 76% contre *S. aureus*, *E. faecalis* et *E. coli*, respectivement. Ces résultats sont dus principalement à l'activité antibactérienne des AgNPs. En outre, Les films de PLA-2%Fluorophlogopite ont inhibé l'adhésion des trois bactéries d'une façon assez importante. Ce résultat non attendu, peut-être dû à l'effet de la fluorophlogopite sur la surface du PLA (rugosité) et sur son hydrophobicité, deux facteurs qui peuvent affecter l'adhésion des bactéries sur les surfaces [42,43].

En résumé, les films nanocomposites à base de PLA ont été préparés via un simple processus d'extrusion à l'état fondu. Ils ont montré des bonnes propriétés thermiques, mécaniques et barrières et ont inhibé significativement l'adhésion de trois bactéries à Gram-positif et à Gram-négatif. Ces films peuvent être considérés dans des applications potentielles en emballage alimentaire.

V. L'effet des surfactants sur la stabilité colloïdale des nanoparticules d'argent préparées par voie biologique

Dans le chapitre III, les AgNPs ont été incorporées comme agents antibactériens dans les nanocomposites actifs. Cependant, ces nanoparticules commercialisées ont été préparées par la méthode chimique. Afin de rendre le processus encore plus respectueux de l'environnement, nous avons consacré ce chapitre à la synthèse biologique des AgNPs.

Les AgNPs peuvent être préparées selon 3 voies : physique, chimique ou biologique. Les deux premières voies possèdent des inconvénients majeurs à savoir la nécessité d'équipements particuliers et la consommation d'énergie excessive dans le cas des méthodes physiques (Moulin à billes, l'Ablation laser) et l'utilisation de produits chimiques toxiques dans les méthodes chimiques. Récemment, la voie biologique a été développée en utilisant des entités biologiques comme les bactéries, les champignons et les plantes. Cette méthode biologique représente une alternative prometteuse pour éviter tous les problèmes des autres méthodes. D'autre part, les extraits des plantes sont préférables par rapport aux autres systèmes biologiques car leur méthode de préparation est simple et moins coûteuse et ne nécessite ni de milieux de culture ni de purification post-synthèse. Parmi les plantes utilisées, le romarin (*Salvia rosmarinus* Spenn), possède une importante concentration en biomolécules réductrices (métabolites secondaires), qui permettent la réduction des ions Ag^+ ainsi que la stabilisation des AgNPs formées.

Dans notre étude, la synthèse des AgNPs par l'extrait aqueux de romarin a été optimisée en termes de température, de temps de réaction et de stabilisation. La figure IV.1 (**page 148**) est un résumé graphique de cette étude.

Dans un premier temps, la synthèse des AgNPs a été optimisée en testant quatre températures différentes : 20°C, 40°C, 60°C et 80°C. Les résultats de la spectroscopie UV-Vis des AgNPs (**Figure IV.2A, page 149**) montrent que les meilleurs résultats en termes de production et de taille des AgNPs ont été obtenus à 80°C pendant 15 min. Ceci est par l'intensité et le décalage de la bande de résonance plasmon de surface (SPR) vers la gauche [44]. De plus, les spectres

de SPR montrent deux pics, un pic principal entre 430-460 nm et un pic secondaire (épaulement) indiquant que ces AgNPs ont une forme sphérique.

Les nanoparticules préparées à 80°C pendant 15 min (R-AgNPs) ont été caractérisées par plusieurs techniques : DRX, FTIR, TEM et l'ATG. La DRX montre que les R-AgNPs présentent une structure cristalline cubique à faces centrées (fcc). La taille des R-AgNPs mesurée par la microscopie électronique à transmission (**figure IV.3, page 151**) montre une taille de $31,1 \pm 6,5$ nm.

En outre, l'analyse de l'ATG a montré plusieurs phases de dégradation dont la principale correspond à la dégradation des molécules organiques attachées aux R-AgNPs. Ces molécules occupent autour de 50% de poids des R-AgNPs. L'analyse de la spectroscopie infrarouge à transformée de Fourier (IRTF) a pu démontrer que ces molécules attachées aux R-AgNPs contiennent des groupements esters et des alcanes.

Les propriétés des AgNPs (*e.g.*, activité antibactérienne) sont étroitement dépendantes de leur taille et leur forme. Ainsi, la stabilité des AgNPs est primordiale pour toutes application potentielle. Dans notre étude, nous avons suivi la stabilité des R-AgNPs au cours du temps en analysant l'intensité de leur bande SPR principal (430 – 460 nm) par la spectroscopie UV-Vis. Après un mois, l'intensité de la bande SPR a diminué de plus de 40%. Ce résultat indique que les R-AgNPs sont instables. En général, les AgNPs peuvent être stabilisées en agissant sur les interactions électrostatiques, stériques ou électro-stériques [31]. Afin d'améliorer la stabilité des R-AgNPs, trois tensioactifs de charges différentes ont été utilisés : CTAB comme surfactant cationique, dodecylsulfate de sodium comme surfactant anionique et Tween 80 comme surfactant non-ionique. Les résultats présentés dans la figure IV.6 (**page 155**) montrent que l'utilisation des concentrations très faibles de tensioactifs (3-5 μ M) améliorent très significativement la stabilité des R-AgNPs. Les valeurs du potentiel Zeta avant et après le capping par les tensioactifs prouvent l'adsorption de ces derniers sur la surface des R-AgNPs. Effectivement, ces valeurs ont changé de -34,45 à -26,26 mV pour le Tween 80, de -34,45 à -9,15 mV pour le CTAB alors que pour le SDS, aucun changement significatif n'a été observé. Ces résultats suggèrent que le mécanisme d'amélioration de la stabilité pour le Tween 80 et le CTAB est surtout stérique alors que pour le SDS, est probablement électro-stérique. Effectivement, après six mois de mesure, le SDS a montré une stabilisation supérieure par rapport aux autres tensioactifs.

L'activité antibactérienne est une propriété très exploitée des AgNPs dans plusieurs domaines dont l'emballage alimentaire actif. Dans notre étude, nous l'avons testé contre quatre bactéries, deux à Gram-positif (*S. aureus* et *E. faecalis*) et deux à Gram-négatif (*E. coli* et *P. aeruginosa*). Les R-AgNPs (31 nm) ont montré une meilleure activité antibactérienne contre les quatre bactéries par rapport aux AgNPs commerciales (50-60 nm) (**Tableau IV.2, page 159**). Cette différence peut être attribuée à la taille des nanoparticules. Korshed *et al.*, (2019) [45] ont montré que l'activité antibactérienne des AgNPs est inversement proportionnelle à la taille des nanoparticules. Ces résultats sont expliqués par la différence au niveau de la surface spécifique des AgNPs. En effet, les AgNPs de petite taille ont une surface spécifique plus grande que les AgNPs de grande taille [45].

L'activité antibactérienne des AgNPs est due à plusieurs mécanismes. Ces AgNPs agissent soit par interaction directe avec la bactérie soit par le relargage des ions d'argent. L'interaction entre les AgNPs ou les ions Ag⁺ avec la bactérie induit une perturbation de la membrane cellulaire, endommagement de l'ADN et les composés contenant du soufre et du phosphore via la génération des radicaux libres [16,46]. Également, l'activité antibactérienne des R-AgNPs stabilisées par les tensioactifs a été testée sur les bactéries *E. coli* et *S. aureus*. En comparaison avec les R-AgNPs, les nanoparticules stabilisées par le CTAB (3-5 µM) montrent une amélioration très significative de l'activité antibactérienne contre *S. aureus*. Ce résultat peut être expliqué par l'effet antibactérien de CTAB contre les bactéries à Gram-positif.

Dans la dernière partie, la cytotoxicité des AgNPs commerciales et des R-AgNPs stabilisées ou non contre les fibroblastes de souris L929 a été évaluée par le test Alamar Blue. Les résultats n'ont pas montré de cytotoxicité en utilisant trois concentrations différentes de R-AgNPs. Ces concentrations ont été choisies sur la base des valeurs de CMI : 18,75, 37,5 ou 75 µg. ml⁻¹. Les résultats montrent que les R-AgNPs stabilisées par les tensioactifs peuvent être utilisées comme des agents antibactériens à des concentrations qui ne sont pas toxiques contre les cellules mammaliennes.

VI. Nanobiocomposites antibactériens de Chitosane-AgNPs

Dans l'objectif d'élaborer un matériau d'emballage actif, les AgNPs synthétisées par une voie biologique simple (chapitre IV) ont été incorporées dans une matrice de chitosane. Le chitosane (CS) diffère du PCL et du PLA, utilisés dans le chapitre II et III, par sa nature polysaccharidique naturelle et de son activité bactériostatique intrinsèque, faisant de lui un polymère idéal pour des applications en emballage alimentaire.

De plus, les nanobiocomposites de CS/AgNPs peuvent être utilisées comme des systèmes de catalyse hétérogène dans l'hydrogénation des nitroarènes toxiques en utilisant le CS comme support qui facilite, l'enlèvement des films et par conséquent, le recyclage du catalyseur (R-AgNPs).

En général, les nanobiocomposites CS/AgNPs sont préparés en utilisant une approche *in-situ*, dans laquelle la synthèse des nanoparticules se fait au sein de la matrice du CS en exploitant le pouvoir réducteur du CS pour la réduction des ions Ag^+ . Dans l'approche *ex-situ*, les AgNPs sont préparées au préalable avant leur dispersion dans la matrice de CS. Cette dernière approche permet ainsi, un meilleur contrôle des caractéristiques des NPs, notamment la taille et la stabilité colloïdale.

Pour ces raisons, les films de nanobiocomposites de CS/AgNPs ont été préparés par une approche *ex-situ*. Le CS a été dissous dans l'acide acétique à 1% jusqu'à dissolution complète, puis les R-AgNPs ont été ajoutées selon les pourcentages suivants : 0,5, 1, 1,5, 2 ou 3% (p/p). L'ensemble a été laissé sous agitation pendant 2h suivi par une ultrasonication pendant 15min. Les films ont été préparés par évaporation de solvant (**Figure V.3, page 188**).

L'interaction entre les R-AgNPs et le CS a été étudiée par l'IRTF (**Figure V.4, page 189**). Cette analyse montre un décalage de la bande de résonance d'acétamide NHCOCH_3 de 1641 cm^{-1} à 1635 cm^{-1} révélant une probable interaction entre ces groupes fonctionnels et les molécules stabilisantes des AgNPs ($-\text{C}=\text{O}-\text{AgNPs}$) [47,48].

La dispersion des R-AgNPs au sein de la matrice du chitosane a été étudiée en utilisant la MET. Les micrographes du CS/AgNPs (**Figure V.6, page 191**) montrent une bonne dispersion des R-AgNPs avec quelques agglomérations.

Dans la deuxième partie de ce travail sur les films de Cs/AgNPs, l'inhibition de l'adhésion bactérienne a été étudiée contre deux bactéries : *E. coli* (Gram-négatif) et *S. aureus* (Gram-positif) (**Tableau V.1, page 192**). Les résultats montrent une inhibition totale de la croissance bactérienne sur la surface des films en utilisant une concentration initiale des bactéries de 4×10^5 CFU/ml après incubation à 37°C pendant 18h. Afin de pouvoir visualiser l'effet de la teneur en R-AgNPs, la concentration initiale des bactéries a été augmenté à 5×10^9 CFU/ml. Les résultats montrent des pourcentages d'inhibition similaires contre les deux bactéries et que seulement avec 0,5% des R-AgNPs l'inhibition a atteint 82% et 85% contre *E. coli* et *S. aureus* respectivement. L'inhibition de l'adhésion des bactéries sur la surface des films est

proportionnelle à la teneur en R-AgNPs. Ces résultats prouvent que les films de CS-AgNPs peuvent être considérés dans des applications en emballage alimentaire.

VII. Conclusion générale et perspectives

L'objectif principal de cette thèse est l'élaboration des matériaux antibactériens pour des applications potentielles en emballage alimentaire actif. A cette fin, nous avons développé plusieurs nanocomposites antibactériens en utilisant différentes techniques de préparation (*i.e.*, POC, l'extrusion à l'état fondu et le mélange en solution). Ces nanocomposites ont été caractérisés en se focalisant sur les propriétés thermiques, mécaniques, barrières et antibactériennes.

Les polymères choisis dans cette étude sont biodégradables et biocompatibles mais leur utilisation dans l'emballage alimentaire actif à leur état natif est limitée d'une part à cause de leur propriétés thermiques et mécaniques faibles et d'une autre part, à cause de l'absence de l'activité antibactérienne sauf pour le chitosane qui a un effet bactériostatique. Par conséquent, il est indispensable de i) améliorer leur propriétés thermiques, mécaniques et barrières et ii) de leur apporter une activité antibactérienne.

Pour atteindre ces objectifs, de nombreuses charges ont été utilisées. Premièrement, la bentonite modifiée par le CTAB a été utilisée afin d'initier la POC d' ϵ -Cl et par conséquent, préparer des nanocomposites de PCL-Obnt. L'incorporation de la Obnt a pu améliorer les propriétés thermiques et mécaniques du PCL ainsi qu'apporter l'activité antibactérienne des nanocomposites grâce à la modification par le CTAB. Cependant, l'activité antibactérienne par diffusion montrée par les nanocomposites de PCL-Obnt peut être problématique pour les applications visées. Effectivement, la diffusion de l'agent antibactérien peut contaminer les aliments emballés. Afin de résoudre ce problème, Nous avons essayé de préparer de nouveaux matériaux avec une activité antibactérienne par contact. Pour cela, nous avons préparé des nanocomposites tertiaires de PLA-fluorophlogopite-AgNPs en exploitant l'activité antibactérienne des AgNPs. La fluorophlogopite, un mica synthétique dont les groupements hydroxyles sont substitués par des groupements F⁻, a été choisie grâce à sa structure lamellaire similaire à celle de la OBnt mais contrairement à celle-ci, la fluorophlogopite est hydrophobe et ne nécessite pas une étape d'organomodification. Cependant, à cause de l'absence des groupements -OH, qui agissent comme des co-initiateurs de la POC *in-situ*, nous avons choisi le PLA commerciales pour la préparation des nanocomposites par l'extrusion à l'état fondu au lieu de la POC. Le choix du PLA au lieu du PCL réside sur son origine naturelle contrairement

au PLC qui est d'origine pétrochimique. Ces nanocomposites de PLA-fluorophlogopite-AgNPs ont des propriétés thermiques supérieures à celles du PLA natif ainsi que des propriétés mécaniques et barrières excellentes. De plus, ils ont montré une activité antibactérienne importante par contact contre des bactéries à Gram-positif et à Gram-négatif.

Les résultats de l'activité antibactérienne des films de PLA-fluorophlogopite-AgNPs ont montré un potentiel important des AgNPs comme agent antibactérien. Par conséquent, nous avons dédié un chapitre à l'optimisation de leur synthèse par voie biologique. Ainsi, la synthèse des AgNPs par l'extrait aqueux du romarin a été optimisée en termes de taille et de production. Ensuite, leur stabilité a été étudiée à long-terme (six mois) et améliorée substantiellement en utilisant des quantités très faibles de tensioactifs (3-7 μM). Ces AgNPs ont été ensuite incorporées dans des films de chitosane par une technique de mélange en solution afin de confirmer leur activité antibactérienne une fois piégées dans des films. Le choix du chitosane réside sur sa nature polysaccharidique ainsi que sur sa propriété bactériostatique. Ces nanocomposites CS-AgNPs ont également montré une excellente activité antibactérienne.

Les résultats présentés dans cette thèse montrent un bon potentiel des trois nanocomposites préparées pour des applications en emballage alimentaire antibactérien. Particulièrement, les films de PLA-Fluorophlogopite-AgNPs ont montré des propriétés thermiques, mécaniques et barrières élevées, ainsi qu'une activité antibactérienne importante sans diffusion. Comme continuité de ce travail, plusieurs perspectives pourraient être envisagées.

Concernant le développement des matériaux nanocomposites :

- Une application réelle des nanocomposites qu'on a développé en utilisant des aliments (*e.g.*, les produits carnés). L'efficacité de ces matériaux peut être testée en comparant la croissance des bactéries totales sur les aliments emballés par les nanocomposites antibactériens et ceux emballés par les plastiques conventionnelles (PE). Finalement, leur durée de conservation peut être comparée et le taux de migration des agents antibactériens vers l'aliment peut être mesuré.
- Les polymères utilisés pour préparer les nanocomposites durant cette thèse (PCL, PLA et Chitosane) sont bien biodégradable. Cependant, l'introduction des charges peut affecter cette biodégradabilité en affectant les microorganismes qui peuvent contribuer à cette biodégradation. Ainsi, ça serait intéressant comme continuité, d'étudier l'effet des nanocharges sur la biodégradation des nanocomposites préparés par rapport à leur polymère natif.

- D'autres applications peuvent être envisagées en se basant sur nos résultats, notamment dans le domaine médical. Plus précisément, dans l'enrobage des dispositifs médicaux implantables (e.g., greffes vasculaires, cathéters...). Ces dispositifs sont des cibles favorables pour les colonisations bactériennes, d'où la nécessité d'enrobage par des matériaux antibactériens et antiadhésifs. Les résultats démontrés par les films de PLA-Fluorhlogopite-AgNPs (activité antibactérienne par contact) rendent ces nanocomposites un candidat idéal pour une telle application.

Concernant la synthèse biologique des AgNPs :

- Durant cette thèse, on a remarqué des problèmes de reproductibilité majeurs liés à la synthèse des AgNPs par les extraits des plantes causée principalement par la variation de la composition chimique de l'extrait. Cette variation pouvant avoir plusieurs origines, elle est extrêmement difficile à contrôler (variation entre les espèces des plantes, variation variétale au sein de la même espèce, variation saisonnière au sein de la même variété etc.). Étant donné que la reproductibilité est une composante indispensable, trouver des solutions pour ce problème est une nécessité. Pour cela, la caractérisation de l'extrait de plantes par un ou plusieurs paramètres mesurables pourrait résoudre ce problème.

Références

- [1] R.L. Scharff, Health-Related Costs from Foodborne Illness in the United States, (2010).
- [2] J. Gustavsson, C. Cederberg, U. Sonesson, R.V. Otterdijk, A. Meybeck, Global food losses and food waste: extent, causes and prevention, Undefined. (2011). <https://www.semanticscholar.org/paper/Global-food-losses-and-food-waste%3A-extent%2C-causes-Gustavsson-Cederberg/19c0065b1ad3f83f5ce7b0b16742d137d0f2125e> (accessed March 8, 2022).
- [3] T. Huang, Y. Qian, J. Wei, C. Zhou, Polymeric Antimicrobial Food Packaging and Its Applications, *Polymers*. 11 (2019) 560. <https://doi.org/10.3390/polym11030560>.
- [4] N.A. Al-Tayyar, A.M. Youssef, R. Al-hindi, Antimicrobial food packaging based on sustainable Bio-based materials for reducing foodborne Pathogens: A review, *Food Chem.* 310 (2020) 125915. <https://doi.org/10.1016/j.foodchem.2019.125915>.
- [5] F. Luzi, L. Torre, J.M. Kenny, D. Puglia, Bio- and Fossil-Based Polymeric Blends and Nanocomposites for Packaging: Structure–Property Relationship, *Materials*. 12 (2019) 471. <https://doi.org/10.3390/ma12030471>.
- [6] E. Drago, R. Campardelli, M. Pettinato, P. Perego, Innovations in Smart Packaging Concepts for Food: An Extensive Review, *Foods*. 9 (2020) 1628. <https://doi.org/10.3390/foods9111628>.
- [7] Commission Regulation (EC) No 450/2009 of 29 May 2009 on act... - EUR-Lex, (n.d.). <https://eur-lex.europa.eu/legal-content/en/LSU/?uri=CELEX%3A32009R0450> (accessed April 3, 2022).
- [8] R. Chawla, S. Sivakumar, H. Kaur, Antimicrobial edible films in food packaging: Current scenario and recent nanotechnological advancements- a review, *Carbohydr. Polym. Technol. Appl.* 2 (2021) 100024. <https://doi.org/10.1016/j.carpta.2020.100024>.
- [9] M. del R. Moreira, S.I. Roura, A. Ponce, Effectiveness of chitosan edible coatings to improve microbiological and sensory quality of fresh cut broccoli, *LWT - Food Sci. Technol.* 44 (2011) 2335–2341. <https://doi.org/10.1016/j.lwt.2011.04.009>.
- [10] M.C. Cruz-Romero, T. Murphy, M. Morris, E. Cummins, J.P. Kerry, Antimicrobial activity of chitosan, organic acids and nano-sized solubilisates for potential use in smart antimicrobially-active packaging for potential food applications, *Food Control*. 34 (2013) 393–397. <https://doi.org/10.1016/j.foodcont.2013.04.042>.
- [11] R. Irkin, O.K. Esmer, Novel food packaging systems with natural antimicrobial agents, *J. Food Sci. Technol.* 52 (2015) 6095–6111. <https://doi.org/10.1007/s13197-015-1780-9>.
- [12] R. Priyadarshi, Sauraj, B. Kumar, F. Deeba, A. Kulshreshtha, Y.S. Negi, Chitosan films incorporated with Apricot (*Prunus armeniaca*) kernel essential oil as active food packaging material, *Food Hydrocoll.* 85 (2018) 158–166. <https://doi.org/10.1016/j.foodhyd.2018.07.003>.
- [13] F. Li, C. Zhang, Y. Weng, Improvement of the Gas Barrier Properties of PLA/OMMT Films by Regulating the Interlayer Spacing of OMMT and the Crystallinity of PLA, *ACS Omega*. 5 (2020) 18675–18684. <https://doi.org/10.1021/acsomega.0c01405>.
- [14] H. de V. Pina, A.J.A. de Farias, F.C. Barbosa, J.W. de L. Souza, A.B. de S. Barros, M.J.B. Cardoso, M.V.L. Fook, R.M.R. Wellen, Microbiological and cytotoxic perspectives of active PCL/ZnO film for food packaging, *Mater. Res. Express*. 7 (2020) 025312. <https://doi.org/10.1088/2053-1591/ab7569>.
- [15] A. Roy, O. Bulut, S. Some, A.K. Mandal, M.D. Yilmaz, Green synthesis of silver nanoparticles: biomolecule-nanoparticle organizations targeting antimicrobial activity, *RSC Adv*. 9 (2019) 2673–2702. <https://doi.org/10.1039/C8RA08982E>.

- [16] N. Durán, M. Durán, M.B. de Jesus, A.B. Seabra, W.J. Fávaro, G. Nakazato, Silver nanoparticles: A new view on mechanistic aspects on antimicrobial activity, *Nanomedicine Nanotechnol. Biol. Med.* 12 (2016) 789–799. <https://doi.org/10.1016/j.nano.2015.11.016>.
- [17] S. Belluco, C. Losasso, I. Patuzzi, L. Rigo, D. Conficoni, F. Gallochio, V. Cibin, P. Catellani, S. Segato, A. Ricci, Silver As Antibacterial toward *Listeria monocytogenes*, *Front. Microbiol.* 7 (2016). <https://www.frontiersin.org/article/10.3389/fmicb.2016.00307> (accessed April 3, 2022).
- [18] C. Losasso, S. Belluco, V. Cibin, P. Zavagnin, I. Mičetić, F. Gallochio, M. Zanella, L. Bregoli, G. Biancotto, A. Ricci, Antibacterial activity of silver nanoparticles: sensitivity of different *Salmonella* serovars, *Front. Microbiol.* 5 (2014). <https://www.frontiersin.org/article/10.3389/fmicb.2014.00227> (accessed April 3, 2022).
- [19] R.K. Dhall, Advances in Edible Coatings for Fresh Fruits and Vegetables: A Review, *Crit. Rev. Food Sci. Nutr.* 53 (2013) 435–450. <https://doi.org/10.1080/10408398.2010.541568>.
- [20] L. Genovese, M. Soccio, N. Lotti, M. Gazzano, V. Siracusa, E. Salatelli, F. Balestra, A. Munari, Design of biobased PLLA triblock copolymers for sustainable food packaging: Thermo-mechanical properties, gas barrier ability and compostability, *Eur. Polym. J.* 95 (2017) 289–303. <https://doi.org/10.1016/j.eurpolymj.2017.08.001>.
- [21] N. Rasana, K. Jayanarayanan, Polypropylene/short glass fiber/nanosilica hybrid composites: evaluation of morphology, mechanical, thermal, and transport properties, *Polym. Bull.* 75 (2018) 2587–2605. <https://doi.org/10.1007/s00289-017-2173-1>.
- [22] A. Arora, G. w. Padua, Review: Nanocomposites in Food Packaging, *J. Food Sci.* 75 (2010) R43–R49. <https://doi.org/10.1111/j.1750-3841.2009.01456.x>.
- [23] K. Müller, E. Bugnicourt, M. Latorre, M. Jorda, Y. Echegoyen Sanz, J.M. Lagaron, O. Miesbauer, A. Bianchin, S. Hankin, U. Bölz, G. Pérez, M. Jesdinszki, M. Lindner, Z. Scheuerer, S. Castelló, M. Schmid, Review on the Processing and Properties of Polymer Nanocomposites and Nanocoatings and Their Applications in the Packaging, Automotive and Solar Energy Fields, *Nanomaterials.* 7 (2017) 74. <https://doi.org/10.3390/nano7040074>.
- [24] K. Wang, P.N. Lim, S.Y. Tong, E.S. Thian, Development of grapefruit seed extract-loaded poly(ϵ -caprolactone)/chitosan films for antimicrobial food packaging, *Food Packag. Shelf Life.* 22 (2019) 100396. <https://doi.org/10.1016/j.fpsl.2019.100396>.
- [25] T. Jin, J. b. Gurtler, Inactivation of *Salmonella* in liquid egg albumen by antimicrobial bottle coatings infused with allyl isothiocyanate, nisin and zinc oxide nanoparticles, *J. Appl. Microbiol.* 110 (2011) 704–712. <https://doi.org/10.1111/j.1365-2672.2011.04938.x>.
- [26] S.R. Kanatt, M.S. Rao, S.P. Chawla, A. Sharma, Effects of chitosan coating on shelf-life of ready-to-cook meat products during chilled storage, *LWT - Food Sci. Technol.* 53 (2013) 321–326. <https://doi.org/10.1016/j.lwt.2013.01.019>.
- [27] R. Umamaheswara Rao, B. Venkatanarayana, K.N.S. Suman, Enhancement of Mechanical Properties of PLA/PCL (80/20) Blend by Reinforcing with MMT Nanoclay, *Mater. Today Proc.* 18 (2019) 85–97. <https://doi.org/10.1016/j.matpr.2019.06.280>.
- [28] J.-M. Raquez, Y. Habibi, M. Murariu, P. Dubois, Polylactide (PLA)-based nanocomposites, *Prog. Polym. Sci.* 38 (2013) 1504–1542. <https://doi.org/10.1016/j.progpolymsci.2013.05.014>.
- [29] E. Omanović-Miklićanin, A. Badnjević, A. Kazlagic, M. Hajlovac, Nanocomposites: a brief review, *Health Technol.* 10 (2020) 51–59. <https://doi.org/10.1007/s12553-019-00380-x>.

- [30] S. Fu, Z. Sun, P. Huang, Y. Li, N. Hu, Some basic aspects of polymer nanocomposites: A critical review, *Nano Mater. Sci.* 1 (2019) 2–30. <https://doi.org/10.1016/j.nanoms.2019.02.006>.
- [31] D.E. Abulyazied, A. Ene, An Investigative Study on the Progress of Nanoclay-Reinforced Polymers: Preparation, Properties, and Applications: A Review, *Polymers*. 13 (2021) 4401. <https://doi.org/10.3390/polym13244401>.
- [32] M. Gangarapu, S. Sarangapany, K.K. Veerabhali, S.P. Devipriya, V.B.R. Arava, A High-Performance Catalytic and Recyclability of Phyto-Synthesized Silver Nanoparticles Embedded in Natural Polymer, *J. Clust. Sci.* 28 (2017) 3127–3138. <https://doi.org/10.1007/s10876-017-1280-3>.
- [33] S. Iravani, H. Korbekandi, S.V. Mirmohammadi, B. Zolfaghari, Synthesis of silver nanoparticles: chemical, physical and biological methods, *Res. Pharm. Sci.* 9 (2014) 385.
- [34] M.G. Guzmán, J. Dille, S. Godet, Synthesis of Silver Nanoparticles by Chemical Reduction Method and Their Antibacterial Activity, (2008). <https://doi.org/10.5281/zenodo.1062628>.
- [35] G. Arya, N. Sharma, R. Mankamna, S. Nimesh, Antimicrobial Silver Nanoparticles: Future of Nanomaterials, in: R. Prasad (Ed.), *Microb. Nanobionics Vol. 2 Basic Res. Appl.*, Springer International Publishing, Cham, 2019: pp. 89–119. https://doi.org/10.1007/978-3-030-16534-5_6.
- [36] B. Jousseume, H. Riague, T. Toupance, M. Lahcini, P. Mountford, B.R. Tyrrell, A General Route to Alkylene-, Arylene-, or Benzylene-Bridged Ditin Hexachlorides and Hexaalkynides, *Organometallics*. 21 (2002) 4590–4594. <https://doi.org/10.1021/om0202468>.
- [37] T. El Assimi, Roko Blažic, A. El Kadib, M. Raihane, R. Beniazza, G.A. Luinstra, E. Vidović, M. Lahcini, Synthesis of poly(ϵ -caprolactone)-grafted guar gum by surface-initiated ring-opening polymerization, *Carbohydr. Polym.* 220 (2019) 95–102. <https://doi.org/10.1016/j.carbpol.2019.05.049>.
- [38] M. Lahcini, S. Elhakioui, D. Szopinski, B. Neuer, A. El Kadib, F. Scheliga, M. Raihane, F.J. Baltá Calleja, G.A. Luinstra, Harnessing synergies in tin-clay catalyst for the preparation of poly(ϵ -caprolactone)/halloysite nanocomposites, *Eur. Polym. J.* 81 (2016) 1–11. <https://doi.org/10.1016/j.eurpolymj.2016.05.014>.
- [39] I.X. Yin, J. Zhang, I.S. Zhao, M.L. Mei, Q. Li, C.H. Chu, The Antibacterial Mechanism of Silver Nanoparticles and Its Application in Dentistry, *Int. J. Nanomedicine*. 15 (2020) 2555–2562. <https://doi.org/10.2147/IJN.S246764>.
- [40] H. Baniyadi, J. Trifol, A. Ranta, J. Seppälä, Exfoliated clay nanocomposites of renewable long-chain aliphatic polyamide through in-situ polymerization, *Compos. Part B Eng.* 211 (2021) 108655. <https://doi.org/10.1016/j.compositesb.2021.108655>.
- [41] S.-M. Lai, S.-H. Wu, G.-G. Lin, T.-M. Don, Unusual mechanical properties of melt-blended poly(lactic acid) (PLA)/clay nanocomposites, *Eur. Polym. J.* 52 (2014) 193–206. <https://doi.org/10.1016/j.eurpolymj.2013.12.012>.
- [42] S. Zheng, M. Bawazir, A. Dhall, H.-E. Kim, L. He, J. Heo, G. Hwang, Implication of Surface Properties, Bacterial Motility, and Hydrodynamic Conditions on Bacterial Surface Sensing and Their Initial Adhesion, *Front. Bioeng. Biotechnol.* 9 (2021). <https://www.frontiersin.org/article/10.3389/fbioe.2021.643722> (accessed March 11, 2022).
- [43] J.K. Oh, Y. Yegin, F. Yang, M. Zhang, J. Li, S. Huang, S.V. Verkhoturov, E.A. Schweikert, K. Perez-Lewis, E.A. Scholar, T.M. Taylor, A. Castillo, L. Cisneros-Zevallos, Y. Min, M. Akbulut, The influence of surface chemistry on the kinetics and thermodynamics of bacterial adhesion, *Sci. Rep.* 8 (2018) 17247. <https://doi.org/10.1038/s41598-018-35343-1>.

- [44] A. Mohammed Fayaz, K. Balaji, P.T. Kalaichelvan, R. Venkatesan, Fungal based synthesis of silver nanoparticles—An effect of temperature on the size of particles, *Colloids Surf. B Biointerfaces*. 74 (2009) 123–126. <https://doi.org/10.1016/j.colsurfb.2009.07.002>.
- [45] P. Korshed, L. Li, Z. Liu, A. Mironov, T. Wang, Size-dependent antibacterial activity for laser-generated silver nanoparticles, *J. Interdiscip. Nanomedicine*. 4 (2019) 24–33. <https://doi.org/10.1002/jin2.54>.
- [46] P. Das, K. Ghosal, N.K. Jana, A. Mukherjee, P. Basak, Green synthesis and characterization of silver nanoparticles using belladonna mother tincture and its efficacy as a potential antibacterial and anti-inflammatory agent, *Mater. Chem. Phys.* 228 (2019) 310–317. <https://doi.org/10.1016/j.matchemphys.2019.02.064>.
- [47] S. Affes, H. Maalej, I. Aranaz, H. Kchaou, N. Acosta, Á. Heras, M. Nasri, Controlled size green synthesis of bioactive silver nanoparticles assisted by chitosan and its derivatives and their application in biofilm preparation, *Carbohydr. Polym.* 236 (2020) 116063. <https://doi.org/10.1016/j.carbpol.2020.116063>.
- [48] S. Frindy, A. el Kadib, M. Lahcini, A. Primo, H. García, Copper Nanoparticles Stabilized in a Porous Chitosan Aerogel as a Heterogeneous Catalyst for C–S Cross-coupling, *ChemCatChem*. 7 (2015) 3307–3315. <https://doi.org/10.1002/cctc.201500565>.